Dissertation

submitted to the

Combined Faculties for the Natural Sciences and for Mathematics

of the Ruperto-Carola University of Heidelberg, Germany

for the degree of

Doctor of Natural Sciences

presented by

Diplom-Biochemikerin Sophia Maria Ungelenk

born in Ochsenfurt

Oral examination: 07.05.2015

Structural features and interactions of substrates complexed with molecular chaperones

Referees:

Prof. Dr. Bernd Bukau

Dr. Marius Lemberg

Für Jan

Abstract

Protein misfolding and aggregation perturbs cellular functions and is involved in aging and numerous medical disorders. In cells, the first line of defense is the association of deleterious aggregating proteins with small Heat shock proteins (sHsp). These oligomeric, ATP-independent chaperones sequester misfolded proteins into complexes and facilitate subsequent substrate solubilization and refolding by ATP-dependent chaperones. The cytosol of *S. cerevisiae* contains two sHsps: Hsp42 is constitutively active, while Hsp26 is activated at elevated temperatures. In my thesis, I wanted to elucidate how sHsps change the structure of aggregates, facilitating substrate reactivation. To this end, I studied the impact of Hsp26 and Hsp42 incorporation on the architecture of heat-induced aggregates by amide hydrogen exchange (HX). I established the experimental conditions for HX of heat-induced protein aggregates using thermolabile malate dehydrogenase (MDH) as model substrate. My data show that the formation of heat-induced Hsp26/MDH or Hsp42/MDH complexes has profound impact on the MDH structure. In the aggregated state formed in absence of sHsps, almost the entire MDH polypeptide becomes accessible to HX, reflecting global, large misfolding. In contrast, a more protected form of MDH is detected when complexed with Hsp26 or Hsp42. I observed that the mass spectra of many MDH peptides derived from sHsp/MDH complexes exist as a mixture of two populations after HX: a native-like and an aggregate-like population. Higher excess of sHsps promoted the native-like state. Single-molecule experiments confirmed the binding of sHsps to near native substrate folds. Furthermore, FRET experiments showed that sHsps increase the spacing between MDH molecules in sHsp/MDH complexes, preventing intermolecular contacts of misfolded MDH species. Finally, crosslinking approaches identified peripheral, surface-exposed MDH sites showing high HX as major sHsp binding sites. Summarized, these findings indicate that sHsps capture early unfolding intermediates of substrates and keep parts of the protein in a native-like state. This activity of sHsps might facilitate chaperone-dependent disaggregation.

I then investigated how the two sHsps of yeast interact with their substrates. The N-terminal extensions (NTE) of both yeast sHsps were found to be the major substrate interaction sites. Compared to all known sHsps, the NTE of Hsp42 is unusually elongated and it was shown to be involved in the organized deposition of misfolded proteins at CytoQ (cytosolic quality control compartment). Hsp42 NTE harbors the two prototypes of intrinsically disordered domains (IDD): a prion-like and an unstructured subdomain. IDDs play important roles in the formation of membrane-free compartments due to their ability to self-associate and to coalesce into

inclusions. In this study, the roles of both NTE subdomains in CytoQ formation and Hsp42 chaperone activity were investigated. We found that the prion-like domain of Hsp42 has a dual function: It binds misfolded substrate proteins and triggers CytoQ formation. The unstructured domain is dispensable for CytoQ formation, but it has a regulatory function, controlling Hsp42 localization and CytoQ numbers. Deletion of the unstructured domain increases Hsp42 substrate interaction and holdase activity, i.e. the prevention of tight contacts between misfolded species.
Together, the presented data show that the prion-like domain of Hsp42 is essential for CytoQ formation, extending the role of prion-like domains in inclusion formation from RNA granules to protein aggregates and emphasizing their crucial contributions to protein phase transitions.

In a second part of my thesis I studied how the Hsp70 chaperone system interacts with RepE, a dimeric replication initiation protein in *E. coli*. The disassembly of RepE seems mechanistically related to the disaggregation process. As a dimer RepE represses its own transcription, as a monomer it initiates the replication of the mini-F plasmid. Monomerization is mediated by the DnaK chaperone system. So far, it remained elusive, how components of the DnaK chaperone system interact with RepE and how they change its structure, leading to the disassembly of the RepE dimer. In this study the binding of DnaK and DnaJ to dimeric RepE wt and to RepE54, a constitutively monomeric variant, was studied by HX. HX analysis of RepE wt revealed a putative DnaK binding site and conformational changes induced by chaperones. Only dimeric RepE wt, but not monomeric RepE54, interacts with DnaJ. In contrast, both oligomeric states of RepE were able to bind DnaK – at least in absence of DNA. In presence of their respective DNA-binding elements, the binding of DnaK was prevented, most likely due to sterical hindrance as the DNA and the putative DnaK binding sites in RepE are in close proximity. The binding of DnaJ probably occurs in aa 96-116, and it destabilized parts of the DNA binding region in RepE, indicating conformational changes. Although interaction with DnaJ was shown to enhance the binding affinity of RepE to DNA, the DnaJ-induced conformational change might enable DnaK to access its binding site. Crosslinking experiments, however, showed that DnaJ binding is not sufficient to allow for interaction of DnaK with DNA-complexed RepE wt. Only concomitant presence of DnaJ and GrpE enabled DnaK to interact with DNA-bound RepE wt. HX revealed, that concerted binding of DnaJ and DnaK causes substantial conformational changes in RepE: Destabilization of the C-terminal region and stabilization in helix α4 near the dimer interface. The latter might be implicated in the monomerization of RepE wt.
In summary, my results provide major contributions to elucidate the chaperone-mediated RepE monomerization process.

Zusammenfassung

Fehlfaltung und Aggregation von Proteinen stören Zellfunktionen und sind wesentlich am Alterungsprozess und an zahlreichen Krankheiten beteiligt. Die erste Abwehrstrategie der Zelle ist die Assoziation von schädlichen, aggregierenden Proteinen mit kleinen Hitzeschockproteinen (small heat shock proteins, sHsp). Diese oligomeren, ATP-unabhängigen Chaperone binden fehlgefaltete Proteine und bilden Komplexe, aus denen Substrate effizienter durch ATP-abhängige Chaperone herausgelöst und zurückgefaltet werden. Das Zytosol von *S. cerevisiae* enthält zwei sHsps: Hsp42 is konstitutiv aktiv, wohingegen Hsp26 durch Hitzestress aktiviert wird. In meiner Doktorarbeit wollte ich herausfinden, wie sHsps die Aggregatstruktur ändern und so die Reaktivierung von Substraten erleichtern. Hierfür habe ich den Einfluss von Hsp26 und Hsp42 auf die Struktur von hitzeinduzierten Aggregaten mittels Wasserstoff/Deuterium-Austausch (HX) untersucht. Zunächst habe ich die experimentellen Bedingungen für HX von hitzeinduzierten Proteinaggregaten ermittelt, wofür ich thermolabile Malatdehydrogenase (MDH) als Modellsubstrat verwendet habe. Meine Daten zeigen, dass die Bildung von hitzeinduzierten Hsp26/MDH- oder Hsp42/MDH-Komplexen tiefgreifende Auswirkung auf die MDH-Struktur hat. Im aggregierten Zustand, der in Abwesenheit von sHsps gebildet wurde, wird beinahe das gesamte MDH-Polypeptid zugänglich für HX, was eine globale, starke Fehlfaltung widerspiegelt. Im Gegensatz dazu befindet sich MDH in einem geschützteren Zustand, wenn sie sich im Komplex mit Hsp26 oder Hsp42 befindet. Ich habe festgestellt, dass die Massenspektren vieler Peptide, die von sHsp/MDH-Komplexen stammen, nach dem HX eine Mischung aus zwei Populationen darstellen: eine nativ-ähnliche und eine Aggregat-ähnliche Population. Höherer Überschuss an sHsps begünstigt den nativ-ähnlichen Zustand. Einzelmolekül-Experimente bestätigten, dass sich die Struktur sHsp-gebundener Proteine nahe am nativen Zustand befindet. Zudem zeigten FRET Experimente, dass sHsps den Abstand zwischen MDH Molekülen in sHsp/MDH-Komplexen vergrößern, wodurch intermolekulare Kontakte von fehlgefalteter MDH verringert werden. Schließlich habe ich in Quervernetzungsexperimenten herausgefunden, dass periphere, Oberflächen-exponierte MDH-Bereiche, die hohen HX zeigten, die Hauptbindestellen für sHsps sind. Zusammengenommen zeigen diese Ergebnisse, dass sHsps frühe Entfaltungsintermediate der Substrate binden und Teile des Proteins in einem nativ-ähnlichen Zustand halten. Diese Aktivität von sHsps könnte die Chaperon-vermittelte Disaggregation erleichtern.

Dann habe die Interaktion beider Hefe-sHsps mit ihren Substraten untersucht. Es zeigte sich, dass vorwiegend die N-terminalen Domänen (N-terminal extension, NTE) beider Hefe-sHsps mit Substraten interagieren. Im Vergleich zu allen anderen bekannten sHsps, ist die NTE von Hsp42 verlängert, und wird für die Ablagerung missgefalteter Proteine an CytoQ (cytosolic quality control compartment) Einschlüssen benötigt. Die NTE von Hsp42 enthält zwei Prototypen von intrinsisch ungeordneten Domänen (intrinsically disordered domains, IDD): Eine Prionen-ähnliche und eine unstrukturierte Subdomäne. Durch ihre Fähigkeit zur Selbst-Assoziation und zur Vereinigung in Einschlüssen, spielen IDDs bei der Bildung von membranfreien Kompartimenten eine wichtige Rolle. In dieser Arbeit wurden die Rollen beider NTE Subdomänen für die Bildung von CytoQ und Hsp42 Chaperonaktivität untersucht. Es wurde gezeigt, dass die Prionen-ähnliche Domäne von Hsp42 eine duale Funktion besitzt: Sie bindet fehlgefaltete Substratproteine und löst deren Ablagerung an CytoQs aus. Die unstrukturierte Domäne wird für die CytoQ Bildung nicht benötigt. Sie hat vielmehr eine regulatorische Funktion, indem sie die Hsp42 Lokalisierung und die CytoQ Anzahl kontrolliert. Die Deletion der unstrukturierten Domäne führt zu einer erhöhten Substratinteraktion von Hsp42, welche mit einer erhöhten Chaperoneaktivität einhergeht.
Zusammengefasst zeigen die Daten, dass die Prionen-ähnliche Domäne von Hsp42 essentiell für die Ausbildung von CytoQs ist. Die Rolle von Prionen-ähnlichen Domänen bei der Bildung von Einschlusskörpern kann somit von RNA granules auf Proteinaggregate erweitert werden und unterstreicht ihre Bedeutung bei Phasenübergängen von Proteinen.

In einem zweiten Teil meiner Doktorarbeit untersuchte ich die Interaktion zwischen dem Hsp70 Chaperon-System und RepE, einem dimeren Replikation-Initiations-Protein in *E. coli*. Die Disassemblierung des DnaK-Substrats RepE scheint dem Disaggregations-Prozess mechanistisch ähnlich zu sein. Als Dimer unterdrückt RepE seine eigene Transkription, als Monomer initiiert es die Replikation des mini-F Plasmids. Die Monomerisierung erfolgt durch das DnaK Chaperon-System. Bislang blieb unerforscht, wie Komponenten des DnaK Chaperon-Systems mit RepE interagieren und wie sie dessen Struktur ändern, sodass die Disassemblierung des RepE Dimers erfolgt. In dieser Studie wurde die Bindung von DnaK und DnaJ an dimeres RepE wt und an RepE54, einer konstitutiv monomeren Variante, mittels HX untersucht. Durch HX Analyse von RepE wt konnte die mutmaßliche DnaK-Bindestelle identifiziert, und Chaperon-induzierte Konformationsänderungen beobachtet werden. Dimeres RepE wt jedoch nicht monomeres RepE54 konnte mit DnaJ interagieren. Im Gegensatz dazu konnten beide oligomeren Zustände von RepE DnaK binden – zumindest in Abwesenheit von DNA. In Gegenwart ihrer entsprechenden DNA-Bindeelemente wurde die Bindung von DnaK verhindert, sehr

wahrscheinlich aus sterischen Gründen, da die DNA- und die mutmaßliche DnaK-Bindestelle in RepE eng beieinander liegen. Die Bindung von DnaJ erfolgt wahrscheinlich an aa 96-116 und führt zur Destabilisierung in Teilen der DNA-Binderegion in RepE, was auf Konformationsänderungen hindeutet. Quervernetzungsexperimente zeigten jedoch, dass DnaJ-Bindung nicht ausreicht um die Interaktion von DnaK mit DNA-komplexiertem RepE wt zu ermöglichen. Nur die gleichzeitige Anwesenheit von DnaK und GrpE erlaubte DnaK mit DNA-gebundenem RepE wt zu interagieren. HX zeigte, dass die gleichzeitige Bindung von DnaJ und DnaK erhebliche Konformationsänderungen verursacht: Destabilisierung in der C-terminalen Region von RepE und Stabilisierung in Helix α4 nahe der Dimerisierungsgrenzfläche. Letzteres könnte bei der Monomerisierung von RepE wt eine Rolle spielen.

Ergebnisse dieser Arbeit leisten einen bedeutenden Beitrag zur Aufklärung des Chaperon-vermittelten RepE Monomerisierungsprozesses.

Contents

1 Introduction

Proteins are the most abundant and diverse class of biomolecules found in living cells. They function either alone or by forming complexes with other proteins or different cellular components. Proteins are involved in virtually all biochemical processes, including the transport and storage of molecules, the control of development and cell differentiation, the immune response, the enzymatic catalysis of thousands of reactions, and many further tasks. Therefore, the efficient functioning and regulation of the proteome (i.e. all proteins expressed by a genome) is of central importance to cellular health and impacts the lifespan of all organisms.

1.1 Protein aggregation

1.1.1 General relevance of protein aggregation

Protein aggregation is a process during which identical polypeptides self-associate, forming insoluble, high-molecular assemblies that can finally precipitate. In recent years, this self-assembly of misfolded proteins has increasingly gained importance since aggregates cause the perturbation of cellular functions, which is associated with the process of aging and a variety of severe human disorders (e.g. Alzheimer's disease, Parkinson's disease and diabetes type II) (Dobson, 2003; Kelly, 2005; Selkoe, 2003). Moreover, protein aggregation is a major issue in the biotechnological production. The massive recombinant overexpression of proteins generates high protein concentrations, favoring aggregation and reducing the yields of protein-based pharmaceutical products (Ventura, 2005; Ventura and Villaverde, 2006).

In cells, the vast majority of vital processes is performed by proteins. The synthesis of proteins occurs at ribosomes, initially generating a linear chain of amino acids (primary structure) that exists as an unfolded polypeptide or random coil structure. In order to be functional, these amino acid chains have to fold into a well-defined three-dimensional structure, referred to as 'native state' (Figure 1). Although the proper fold is essential for protein activity, in some cases parts of functional proteins may remain unfolded (Dunker et al., 2008). Occasionally, polypeptide chains fail to assume the native structure and end up as misfolded species that are trapped in free energy minima (Tyedmers et al., 2010). Misfolding might, however, also affect properly folded polypeptides. In diluted solutions proteins usually exist as soluble conformers and are able to circumvent aggregation. Yet, the native conformation of proteins is in general only marginally stable, even at physiological conditions. Within

the cell, an extremely high concentration of total protein (300 g/l) causes excluded-volume effects (macromolecular crowding), increasing the probability of proteins to misfold and to form aggregated species (Ellis and Minton, 2006). Therefore, native proteins are at permanent risk of unfolding, and already small perturbations in protein homeostasis may produce inactive conformers that have modified or toxic properties (Dobson, 2003; Jaenicke, 1998; Jahn and Radford, 2005).

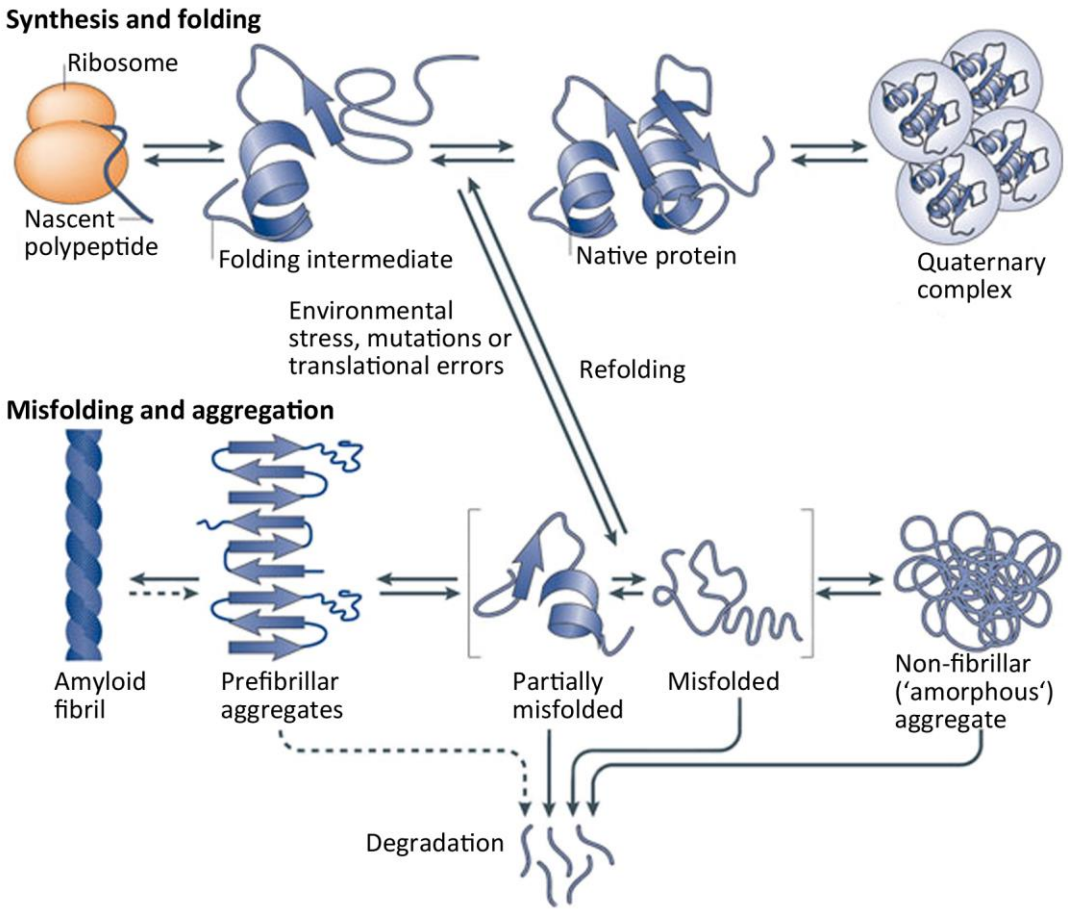

Figure 1: *Overview of cellular protein aggregation. Translational errors, mutations or environmental stress can lead to the unfolding or misfolding of polypeptide chains. Components of the protein quality control system are able to refold or degrade non-native proteins. However, if its capacity is exceeded, misfolded species accumulate and assemble into protein aggregates. In general, two types of aggregates are distinguished: Amyloidogenic aggregates with highly ordered β-sheet structure and aggregates with disordered parts and varying degree of β-sheet content (Tyedmers et al., 2010).*

The failure of proteins to assume or keep their properly folded native structure might occur as a consequence of various different circumstances or events:

False amino acid incorporation during ribosomal translation might lead to partial unfolding or misfolding and thereby to impaired assembly of protein complexes. Together, this increases the tendency of proteins to aggregate (Drummond and Wilke, 2008; Pierre, 2005).

Furthermore, mutations in genes, usually encoding soluble proteins, can result in the destabilization of their native conformation and thus promote aggregation (Canet et al., 2002). Many such mutations are associated with numerous medical disorders,

including Huntington's, Parkinson's or Alzheimer's disease. Here, the misfolding of proteins disrupts their function and leads to the formation of high-molecular, insoluble depositions (see below). Accordingly, they are termed as 'conformational diseases' (Chiti and Dobson, 2006; Powers et al., 2009; Ross and Poirier, 2004).
Finally, environmental stress conditions, such as heat or oxidative stress, can cause enhanced protein aggregation. Exposure of cells to unphysiologically high temperatures can result in the excessive unfolding and aggregation of numerous proteins. A fraction of those heat-induced aggregates can be reactivated (see below) (Parsell et al., 1994). In contrast, oxidative stress often results in irreversible protein modifications. So called 'reactive oxygen species' (ROS) cause the oxidation of amino acid side chains, the formation of undesired protein-crosslinks and the oxidation of the polypeptide backbone, leading to protein fragmentation. Carbonyl groups are produced by the direct oxidation of side chains (especially of Arg, Pro, Lys, and Thr), and by reactions with aldehydes generated during lipid peroxidation or with reactive carbonyl derivatives (Berlett and Stadtman, 1997). Oxidative damage can then result in protein misfolding and subsequent aggregation.
Advanced age or high stress levels increase the probability of protein aggregation. Here, one reason is the enhanced production of misfolded protein conformers leading to a high burden on components of the cellular protein quality machinery (see chapter 1.2). A capacity overload results in the accumulation of non-native polypeptides, which might form aggregates (David et al., 2010; Koga et al., 2011; Reis-Rodrigues et al., 2012).
The aggregation tendency of a specific protein is determined by the chemical nature of its amino acid sequence, the stability of its natively folded conformation, and its cellular concentration (Chiti and Dobson, 2006; Ciryam et al., 2013). Interestingly, high expression levels are observed preferentially for proteins that are less prone to aggregation (Tartaglia et al., 2007).

1.1.2 Types of protein aggregates

Protein aggregates can be defined as any assembly of two or more protein molecules exhibiting a non-native conformation. In general, two classes of protein aggregates are distinguished: The first class comprises amyloidogenic aggregates. Amyloids form large, highly ordered, fibrillar assemblies that are characterized by so called 'cross-β' structures (see below) and they are associated with numerous neurodegenerative diseases (Lührs et al., 2005; Nelson et al., 2005; Ritter et al., 2005; Sawaya et al., 2007; Tanaka et al., 2006; Wasmer et al., 2008). The term 'amyloid' means 'starch-like', since fibrillar deposits that were observed in patients suffering from amyloid-related disorders produce a purple color when reacting with iodine, comparable to effects

caused by starch (Buxbaum and Linke, 2012; Sipe and Cohen, 2000). The second class contains non-fibrillar aggregates lacking any long-range order. They are therefore traditionally termed as 'amorphous' aggregates (Bowden et al., 1991). This type includes precipitates and bacterial inclusion bodies, which cause major concerns in the biotechnological production (Fink, 1998; Rousseau et al., 2006; Ventura and Villaverde, 2006).

1.1.3 Fibrillar, amyloidogenic aggregates

Amyloid fibrils are unbranched filamentous structures, consisting of several protofilaments that are twisted around each other. Fibrils made from different proteins appear to be very similar in size (with diameters between 5 and 25 nm and with a length of several micrometers) (Chiti and Dobson, 2006; Cohen, 1969; Sunde et al., 1997). X-ray analysis revealed that amyloid fibrils generally contain a 'cross-β' structure, i.e. an extended β-sheet conformation, in which the β-strands are oriented perpendicularly to the main fibril axis (Eisenberg and Jucker, 2012; Fitzpatrick et al., 2013; Sawaya et al., 2007). This highly ordered and closely packed organization confers very robust properties to amyloids, including resistance to denaturants and proteases as well as mechanical stability (Chiti and Dobson, 2006; Vendruscolo, 2011).

The exact process of amyloid fibril formation is still under debate. However, many biophysical studies (microscopy, mass spectrometry and single-molecule optical methods) suggested that a heterogeneous ensemble of oligomers is involved in initial steps of fibril formation (Bernstein et al., 2009; Cremades et al., 2012; Nettleton et al., 2000; Smith et al., 2010). For some proteins, including α-synuclein and yeast prions, conformational transitions of those oligomers have been reported, starting from a rather disordered state to more organized structures that are able to assemble into fibrils (Serio et al., 2000; Walsh et al., 2002). During 'secondary nucleation' fibrils act as a template: When monomers are attached to the fibril ends, they convert to the cross-β conformation, enlarging the extended β-sheet structure (Nelson et al., 2005; Serio et al., 2000).

A special subclass of amyloids is spreading within and between cells. These self-perpetuating and infectious features were initially discovered for prions (proteinaceous infectious particles) (Collinge, 2007; Krishnan and Lindquist, 2005). However, recent studies revealed the spreading of amyloids for further disease-related proteins, such as α-synuclein, tau and amyloid-β (Jucker and Walker, 2013; Walker et al., 2013).

1.1.4 Non-fibrillar ('amorphous') aggregates

The formation of non-fibrillar aggregates is typically promoted by high temperature, extreme pH values, high protein concentration and by heterologous protein overexpression in bacteria (Jahn and Radford, 2005; Jahn and Radford, 2008). In the latter case, the aggregates are deposited as 'inclusion bodies'. Using electron microscopy or atomic force microscopy this aggregate type often appears as very heterogeneous in its overall structure. Thus, such aggregates were assumed to be random-coil-like structures that stick to each other through nonspecific interactions. They were therefore termed as 'amorphous' aggregates (Fink, 1998; Rousseau et al., 2006; Ventura and Villaverde, 2006). Meanwhile, however, many studies using dye binding (Congo red, Thioflavin T), X-ray diffraction, CD and IR spectroscopy or other techniques have demonstrated that amorphous aggregates are significantly structured (Christopeit et al., 2005; Fink, 1998; Fändrich et al., 2003; Fändrich et al., 2006; Jackson and Mantsch, 1991). In fact, those non-fibrillar aggregates show extensively higher contents of β-sheet structure than the soluble conformation of the same polypeptide (Chang et al., 2009; Kendrick et al., 1998; Okuno et al., 2007). Inclusion bodies even contain some amyloid-like segments coexisting with disordered and remaining folded parts (García-Fruitós et al., 2005; Sambashivan et al., 2005; Wang et al., 2008). Despite common structural features of inclusion bodies and amyloid fibrils, inclusion bodies are not toxic to its host *E. coli* and they are even thought to counteract the cytotoxicity of misfolded proteins (Gonzalez-Montalban et al., 2005). However, the described structural similarities explain the observation that non-fibrillar aggregates can accelerate amyloid formation by acting as nuclei during fibril assembly (Chiti and Dobson, 2006; Dobson, 2001; Fändrich et al., 2006; Goldsbury et al., 2005; Serio et al., 2000).
Taken together, intramolecular β-sheets seem to be a common structural feature of amorphous and amyloidogenic aggregates. However, the level of their structural organization is much more pronounced in highly ordered amyloid fibrils (Chiti and Dobson, 2006; Fändrich, 2007; Maji and Riek, 2009; Nelson and Eisenberg, 2006).

1.1.5 A single protein can adapt different types of aggregates

In recent years, it became increasingly evident that the ability to adopt amyloid structures is more general than previously assumed. Amyloid formation is not restricted to a few disease-related proteins. Rather, it represents an alternative conformational state that can be formed by a multitude of polypeptides (Chiti and Dobson, 2006; Dobson, 1999-Dobson, 2001; Eisenberg and Jucker, 2012; Fändrich and Dobson, 2002). For instance, *in vitro* experiments revealed that myoglobin, which is predominantly α-helical in its globular state, can form non-fibrillar aggregates or

amyloid fibrils, both containing high β-sheet content (Fändrich et al., 2001; Smeller et al., 1999). In a recent study, five different aggregate types of the protein HypF were generated by using distinct denaturing conditions, which cause different unfolding/aggregation processes (Ben-Zvi and Goloubinoff, 2002; Wang and Riek, 2010). The aggregates differed in morphology, stability, toxicity and further properties. Structural investigation showed that all five forms contained cross-β sheet structure, which, however, involved different segments of the protein sequence (Heise et al., 2005; Petkova et al., 2005; van derWel et al., 2007).
Unlike the native state, the basic amyloid structure is not sequence-dependent (Dobson, 1999; Dobson, 2003), although it is favored by continuous glutamine and asparagine stretches (Michelitsch and Weissman, 2000). It is therefore in principle accessible to most proteins. Interestingly, cells have developed mechanisms to avoid the conversion of proteins into the non-functional amyloid conformation. During evolution, polypepetide sequences that promote amyloid formation are commonly selected against (Broome and Hecht, 2000; Tartaglia et al., 2008), or residues are inserted which interrupt the interactions between such amino acid stretches (termed as 'gatekeepers') (Otzen and Oliveberg, 1999; Tartaglia et al., 2008).

1.1.6 Deleterious effects of protein aggregates

Non-native protein conformers are deleterious to cells as they are unable to perform their designated functions. Furthermore, folding intermediates and misfolded conformers expose hydrophobic segments that are usually embedded in the core of the natively folded protein (Bolognesi et al., 2010; Campioni et al., 2010; Cheon et al., 2007; Olzscha et al., 2011). These hydrophobic patches are now accessible to the cellular environment and can initiate the aggregation process. Predominantly, a single protein accumulates within aggregates. However, the aggregation of different proteins can be triggered (Ben-Zvi and Goloubinoff, 2002), and exposed hydrophobic surfaces can interact inappropriately with various functional cellular components, including other proteins, lipid membranes and nucleic acids (Narayan et al., 2013; Olzscha et al., 2011). In association with amyloid disorders there were no correlations observed between the levels of fibrillar aggregates and the state of disease advancement (Cohen et al., 2013; Haass and Selkoe, 2007; Karran and De Strooper, 2011). These findings and further evidence suggest that pre-fibrillar oligomers, rather than mature amyloid fibrils, seem to be the primary toxic species (Chiti and Dobson, 2006; Eisenberg and Jucker, 2012; Haass and Selkoe, 2007). The trapping of cellular components by those intermediates were found to be generically damaging to cells (Cremades et al., 2012; Lesné et al., 2006; Walsh et al., 2002). Interestingly, cell

viability studies using Aβ40 and Aβ42 oligomers indicated that toxicity increases with decreasing oligomer size (Kayed et al., 2003; Kayed et al., 2009).
Consequently, the appearance of aggregation-prone misfolded species is a permanent danger for cell homeostasis. Initial aggregation events might activate a cascade of pathological reactions and might accelerate the aging process.

1.2 Interaction of chaperones with protein assemblies and aggregates

In the living cell, protein aggregation is modified by components of the protein quality control network consisting of molecular chaperones and proteases (Tyedmers et al., 2010). Molecular chaperones assist in the *de novo* synthesis of proteins, minimizing misfolding, and prevent or even reverse protein aggregation (see chapter 1.2.2). Proteins that cannot be rescued are targeted for protease-mediated degradation. Most chaperones use ATP binding and hydrolysis to switch between states with low or high binding affinities for their polypeptide substrates (Beissinger and Buchner, 1998; Bukau and Horwich, 1998; Walter and Buchner, 2002). In contrast, the small Heat shock proteins (sHsps) work in an ATP-independent manner. In fact, this class of chaperones acts as the first line of defense during unfolding stress as they associate fast with misfolded polypeptides and form stable complexes (Cashikar et al., 2005; Haslbeck et al., 1999; Mogk et al., 2003). In this way, misfolded proteins are sequestered, reducing the probability for severe protein aggregation and lowering the burden on other components of the protein quality system.

1.2.1 Influence of sHsps on protein aggregation

1.2.1.1 The sHsp family

The sHsp family comprises a group of ubiquitous, diverse intracellular chaperones, ranging from 12 to 43 kDa in monomeric size. Many of them can form oligomeric states. sHsps were first discovered due to their strongly induced expression at high temperatures. However, other environmental or pathological stresses were similarly found to increase sHsp expression, and some sHsps are constitutively expressed (Haslbeck et al., 2005; McHaourab et al., 2009; Walter and Buchner, 2002). sHsps exist in all kingdoms of life, and, unlike many other chaperone families, they show extensive sequence variation and evolutionary divergence (Basha et al., 2012). In humans ten paralogous sHsps were found, termed HspB1-HspB10, with HspB4 (αA-crystallin) and HspB5 (αB-crystallin) being the best characterized members (Kampinga et al., 2009; Vos et al., 2008).

Some sHsps are located to distinct tissues, and expression levels might considerably vary within different cell types. However, organelle-specific sHsps have only been observed in plants, with the exception of a mitochondrion-located sHsp in *Drosophila melanogaster*. In addition, sHsp levels increase during the stationary phase in numerous microorganisms and in quiescent cells of many invertebrates (Wadhwa et al., 2010).

1.2.1.2 Roles of sHsps and sHsp-associated diseases

In contrast to many other molecular chaperones, sHsps themselves do not actively refold target proteins. Instead, sHsps specifically interact with misfolded polypeptides thereby preventing or attenuating irreversible aggregation (Gobbo et al., 2011; Horwitz, 1992; Kim et al., 1998). sHsps and the bound polypeptides form large, stable, globular complexes (Basha et al., 2004; Haslbeck et al., 1999; Lee et al., 1997), in which the non-native substrate proteins are maintained in a refolding-competent state (Ehrnsperger et al., 1997; Lee et al., 1997; Stromer et al., 2003). Subsequently, ATP-dependent Hsp70 and Hsp100 chaperones are able to refold the bound substrate protein (Haslbeck et al., 2005; McHaourab et al., 2009; Mogk et al., 2003) (see chapter 1.2.2). Many sHsps have a substantial binding capacity and bind up to an equal weight of misfolded polypeptides (Haslbeck et al., 2005; McHaourab et al., 2009; van Montfort et al., 2001a). With increasing amounts of sHsps being present during aggregation, sHsp-substrate complexes become smaller and more soluble. Concomitantly, the reactivation of sequestered proteins by ATP-dependent chaperones is facilitated (Stengel et al., 2010). Typically, sHsps are less efficient with larger proteins, reflecting the need for direct interactions between sHsps and non-native substrates (Basha et al., 2013).

Within the protein homeostasis network there must be a coordinated interaction between chaperones and components of the protein degradation machinery. So far, little is known about the mechanisms, deciding if misfolded proteins are refolded or subjected to proteolysis. However, some human sHsps have been shown to interact with the proteasome (directly or indirectly) and to be part of an ubiquitin ligase complex (Lanneau et al., 2007). For instance, human HspB1 (Hsp27) interacts with HDM2, an ubiquitin ligase (E3) that target the tumor protein p53 for degradation (O'Callaghan-Sunol et al., 2007). In addition, specific sHsps are involved in directing native or aggregated proteins toward autophagy (Carra et al., 2010).

These important functions in protein quality control explain the cytoprotective effects of sHsps (Bruey et al., 2000; Charette et al., 2001; Paul et al., 2002). Furthermore, some sHsps can interact with key apoptotic proteins thereby preventing apoptotic cell death (Garridoa et al., 2012).

Beyond their role in protein quality control, sHsps were reported to influence the redox metabolism of cells thereby modifying their ability to respond to oxidative stress (Préville et al., 1999). Moreover, some sHsps assist during cytoskeleton assembly: They associate with the main cytoskeletal constituents (microtubules, intermediate filaments and microfilaments) and control interactions between filaments thereby inhibiting their aggregation (Launay et al., 2006; Perng et al., 1999; Tessier et al., 2003).

According to their multiple important roles described above, the dysfunction of sHsps is linked to a broad spectrum of pathological disorders. Various inherited diseases were discovered to result from defects (e.g. amino acid changes) in sHsps (Clark and Muchowski, 2000). In association with their anti-aggregating function, mutations in the vertebrate eye lens sHsps (α-crystallins) lead to the formation of cataracts (Brady et al., 1997; Graw, 2009; Horwitz, 2003) and mutated sHsps in muscle tissues cause cardio-, skeletal- and neuro-myopathies (Goldfarb and Dalakas, 2009; Goldfarb et al., 2008; Rajasekaran et al., 2007). Malfunctions of sHsps are also involved in the development of a variety of neurodegenerative disorders that are linked to protein misfolding, e.g. Alzheimer's, Huntington's and Creutzfeldt-Jakob disease or multiple sclerosis (Laskowska et al., 2010; Lowe et al., 1992; van Noort et al., 2010). Accordingly, some sHsps were shown to suppress the aggregation of polyQ proteins (Carra et al., 2010; Robertson et al., 2010; Vos et al., 2010) and to prevent the formation of amyloid fibrils (Ecroyd and Carver, 2009; Shammas et al., 2011; Waudby et al., 2010). With respect to their function in cytoskeleton assembly, sHsps are implicated in renal or pulmonary fibrosis (Garridoa et al., 2012). Moreover, due to their anti-apoptotic activities, sHsps are connected to cancer, and several cancers show characteristic changes in their sHsp expression pattern (Deng et al., 2010; Kamada et al., 2007). Their implication in diverse devastating diseases let sHsps appear as promising therapeutic targets.

1.2.1.3 Structure and organization of sHsps

The common feature of sHsps is the highly conserved α-crystallin domain (ACD) (around 90 aa), which is named after the vertebrate eye lens sHsp α-crystallin (Ecroyd and Carver, 2009; Horwitz, 1992). It is flanked by flexible N- and C-terminal extensions (NTE and CTE), that are variable in sequence and length (on average: NTE 55 aa; CTE < 20 aa) (Kriehuber et al., 2010; Poulain et al., 2010). Despite low overall sequence similarities, the CTE contains a conserved I/L/V-X-I/L/V motif (Haslbeck et al., 2005; McHaourab et al., 2009; van Montfort et al., 2001a) (Figure 2a and b).

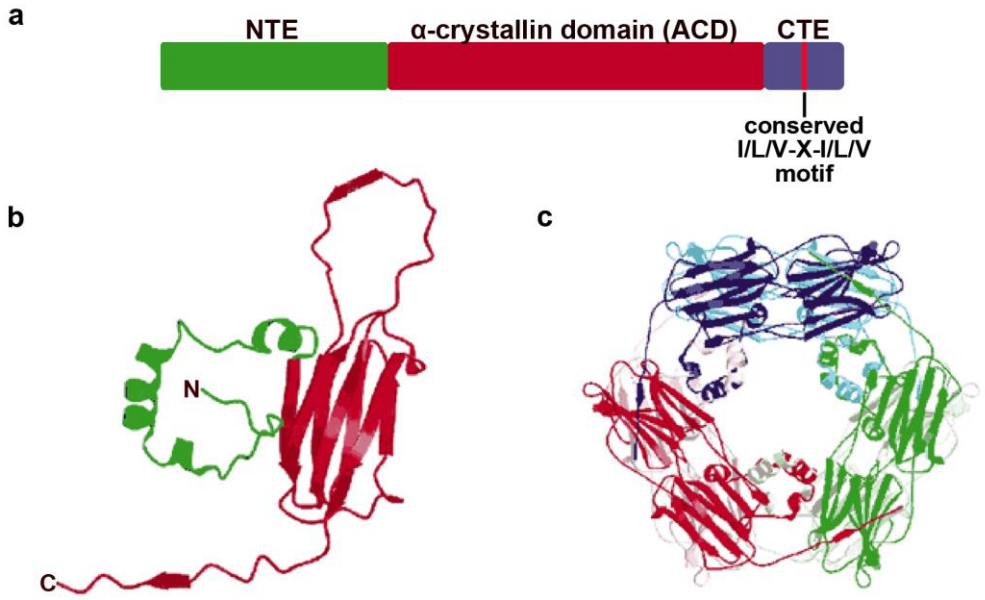

Figure 2**: Structural organization of sHsps.* ***(a) *Domain organization of sHsps. NTE: N-terminal extension, CTE: C-terminal extension.* ***(b)-(c)*** *Assembly and fold of the wheat sHsp Hsp16.9 are shown.* ***(b)*** *Ribbon diagram of the monomer with the NTE shown in green, and the alpha-crystallin domain and CTE in red.* ***(c)*** *In the Hsp16.9 dodecamer dimeric subunits are arranged as two disks with a central hole. Dimers of the top disk are colored red, green and blue, dimers of the bottom disk pink, sage and turquoise (van Montfort et al., 2001b).*

Most sHsps form oligomeric structures frequently consisting of 12 or 24 monomers (Kennaway et al., 2005; Stamler et al., 2005; White et al., 2006) (Figure 2c). But even larger complexes with up to 50 monomers were reported for α-crystallin or other sHsps (Haslbeck et al., 2005; van Montfort et al., 2001b). Despite these variations, the common building block of oligomer assemblies is a dimeric subunit (Ecroyd and Carver, 2009; Haslbeck et al., 2005; McHaourab et al., 2009). This was demonstrated in biochemical and structural studies (Haslbeck et al., 2008; Kim et al., 1998; Peschek et al., 2009; van Montfort et al., 2001b). Some sHsp oligomers were shown to dissociate into dimers and monomers at elevated temperatures (Benesch et al., 2003; Giese and Vierling, 2002; Haslbeck et al., 1999; van Montfort et al., 2001b).

Many members of the sHsp family are extremely dynamic and heterogeneous in size and form. Therefore, the structure of sHsps remained poorly understood for a long time. But due to technical improvements in electron microscopy and X-ray crystallography increasing structural information was obtained during the last years. Often, sHsp oligomers form sphere- or barrel-shaped assemblies (Kim et al., 1998; van Montfort et al., 2001b). Atomic structures showed that the α-crystallin domain consists of seven or eight anti-parallel β-strands forming a β-sandwich (Kriehuber et al., 2010; Poulain et al., 2010) and that it is involved in dimerization of monomers. Two different dimer interfaces have been observed, depending on presence of a loop that contains β-strand β6. Many bacterial, yeast and plant sHsps contain this β6-loop structure (e.g. *Methanocaldococcus* Hsp16.5 or wheat Hsp16.9). Here, dimerization is mediated through strand swapping: β6 of one monomer is incorporated at the end of

the β-sheet, comprising β2, β3, β8 and β9, in the α-crystallin domain of the other monomer. Many metazoan sHsps (e.g. HspB4, HspB5 and HspB6) do not possess this β6-loop. Instead, β7 of one monomer positions in antiparallel orientation next to β7 of the second monomer, forming a continuous β-sheet and connecting both monomers (Bagnéris et al., 2009; Jehle et al., 2009a). While dimerization of sHsps is mediated by the α-crystallin domain, both N- and C-terminal extensions have been shown to contribute to oligomer formation. The partial or complete deletion of either of these domains or certain amino acid changes have been reported to disrupt oligomerization. This often results in the formation of stable dimeric subunits or leads to the appearance of amorphous aggregates (Basha et al., 2012; Giese and Vierling, 2004; Lindner et al., 2000). Crystal structures of *Methanocaldococcus* Hsp16.5 and wheat Hsp16.9 revealed for the first time a widespread mechanism for establishing oligomers: The conserved C-terminal I/L/V-X-I/L/V motif in one dimer interacts with a hydrophobic groove formed by β4 and β8 in the α-crystallin domain of the adjacent dimer (Kim et al., 1998; van Montfort et al., 2001b). Due to the high flexibility that has been observed for N- and C-terminal domains, dimers can associate in different geometries (Baldwin et al., 2011; Jehle et al., 2009a; Jehle et al., 2009b; Laganowsky et al., 2010). Moreover, the large variability in the length of the N-terminal extension seems to be the reason for the formation of significantly differently sized oligomers (Narberhaus, 2002).

1.2.1.4 Dynamics of sHsps

sHsps form highly dynamic structures, which continuously exchange dimeric subunits between oligomers (Aquilina et al., 2005; Franzmann et al., 2005; Painter et al., 2008; Sobott et al., 2002). The rate limiting step during this process seems to be the dissociation of dimers from the oligomers, whereas the association is very rapid (Basha et al., 2012; Bova et al., 2000). The dynamic of subunit exchange increases with elevated temperature, and it is sensitive to other environmental conditions (e.g. ionic strength) (Basha et al., 2012). In addition, phosphorylation patterns have been found to influence subunit association (Bova et al., 2002; Giese and Vierling, 2002; Haslbeck et al., 1999; van Montfort et al., 2001a). This dynamic exchange of subunits seems to be a common feature among sHsps. Yet, its biological significance and functional importance remain unclear (Bova et al., 1997; Haslbeck et al., 1999; Sobott et al., 2002). There have been speculations that subunit exchange might be implicated in the chaperone mechanism by uncovering substrate binding sites (Basha et al., 2012; Stengel et al., 2010). However, several studies demonstrated that subunit exchange does not necessarily correlate with the activity of sHsps (Aquilina et al., 2005; Franzmann et al., 2005).

1.2.1.5 Substrate interaction and activation of sHsps

sHsps tightly bind non-native, aggregation-prone substrate proteins and keep them in a refolding-competent state. How sHsps recognize their substrates and which extent of unfolding is required remains unclear. Many sHsps, especially from bacteria and yeast, have a broad substrate spectrum, lacking substrate specificity (Basha et al., 2004; Haslbeck et al., 2004). More specific binding has been demonstrated for some mammalian sHsps (van Montfort et al., 2001a; Vos et al., 2008).

So far, the identity of substrate binding sites within sHsps is unknown. Studies analyzing deletion mutants, crosslinking approaches and peptide library scanning were performed in order to identify interaction sites (Ahrman et al., 2007; Ghosh et al., 2007). Overall, the findings suggest that multiple sites belonging to each of the three domains contribute to substrate binding (Jaya et al., 2009; McHaourab et al., 2009). Though, the N-terminal region seems to play a major role in the recognition of substrates (Giese et al., 2005; Haslbeck et al., 2004).

Some sHsps are constitutively active (i.e. they bind misfolded polypeptides). Others are activated by heat, phosphorylation or different modifications (Ecroyd et al., 2007; Haslbeck et al., 1999; Shashidharamurthy et al., 2005).

The emerging picture is that activation occurs via improved substrate binding due to an increase in accessible hydrophobic surfaces on the sHsps (Figure 3). This is reached in different ways. The dissociation of subunits or the formation of smaller oligomeric species could reveal buried, hydrophobic sites which are able to interact with non-native proteins. In this case higher oligomers would act as a storage form, preserving binding sites until they are needed (Haslbeck et al., 2005; McHaourab et al., 2009; van Montfort et al., 2001a). Consistently, for several sHsps, including α-crystallin and Hsp16.2 from *Caenorhabditis elegans*, it was suggested that the N-terminal regions, which are often involved in substrate binding, are buried inside the oligomers (Kim et al., 1998). However, a few studies demonstrated that oligomer dissociation does not necessarily correlate with sHsp activity (Franzmann et al., 2005). Rather, for many sHsps structural plasticity seems to be the decisive factor during substrate recognition and binding (Aquilina et al., 2004; Bepperling et al., 2012; Franzmann et al., 2008). For instance, in αB-crystallin it has been shown that enhanced substrate binding is based on increased flexibility of the NTE (Peschek et al., 2013). High structural plasticity of the NTE also explains the ability to bind a variety of substrate proteins differing in sequence and structure (Bardwell and Jakob, 2012; Tompa and Csermely, 2004; Uversky, 2011). This order-to-disorder transition during activation has also been reported for other chaperones (Chen et al., 2011; Reichmann et al., 2012; Tapley et al., 2009).

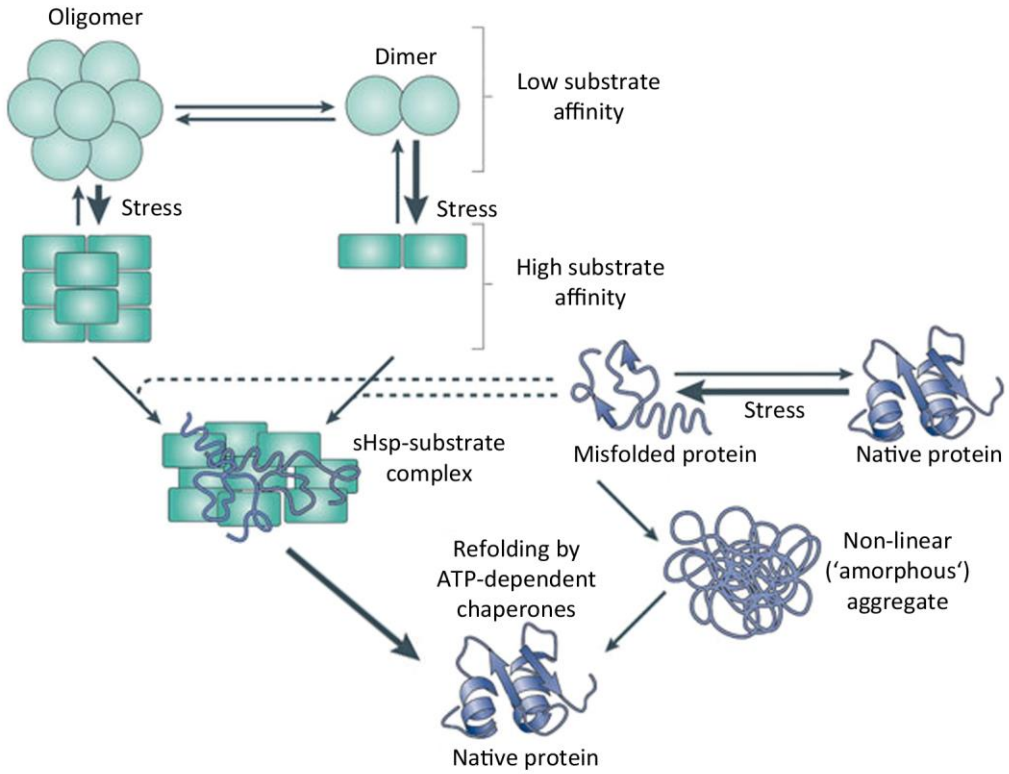

Figure 3: *Function of sHsps during protein aggregation. sHsps often form oligomeric complexes, which dynamically exchange dimeric subunits between each other. Upon stress, many sHsps can convert from a state with low substrate affinity to a state with high substrate affinity. In this activated state sHsps co-aggregate with misfolded polypeptides and prevent the formation of large aggregates. The resulting sHsp-substrate complexes can be disaggregated and refolded more efficiently by ATP-dependent chaperones (adapted from Tyedmers et al. 2010).*

Regarding the findings described above, it becomes increasingly obvious that there is no general mechanism which could explain the activation of chaperone function for all sHsps.

1.2.1.6 Post-translational phosphorylation of sHsps

The properties of sHsps are frequently altered by post-translational phosphorylation. Many sHsps possess serine or threonine residues that can be reversibly phosphorylated in response to multiple kinds of stresses including heat, mitogens or oxidants (Butt et al., 2001; Rogalla et al., 1999; Shemetov et al., 2008). Often, phosphorylation promotes oligomer dissociation and activates the sHsp (Aquilina et al., 2004; Parcellier et al., 2005). In addition, the interactions with some cytoskeletal components require the phosphorylation of the respective sHsps (Launay et al., 2006). Phosphorylation has also been reported to influence the cellular distribution of sHsps, inducing their translocation into the nucleus (Brunet Simioni et al., 2009; den Engelsman et al., 2004).

1.2.1.7 sHsps in *Saccharomyces cerevisiae*

The cytosol of *S. cerevisiae* contains two chaperones of the sHsp family, sharing 46% identity and 66% similarity (Wotton et al., 1996): Hsp26 and Hsp42. Hsp26 was found to be activated at elevated temperature (Haslbeck et al., 1999), whereas Hsp42 displays chaperone activity under physiological and heat shock conditions (Haslbeck et al., 2004). The expression of both yeast sHsps is increased by various stress conditions (e.g. heat, high salt and starvation). However, unlike Hsp26, Hsp42 is also expressed in unstressed cells (Kurtz et al., 1986; Varela et al., 1992). Under physiological conditions Hsp42 is five times more abundant (0.15% Hsp42 and only around 0.03% of Hsp26 of total cytosolic protein). After exposure to heat, up to ten times more Hsp42 is present compared to Hsp26 (Haslbeck et al., 2004).
The overexpression of several sHsps was shown to confer thermoresistance (Haslbeck, 2003). Yet, with the exception of Hsp16.6 from *Synechocystis sp.*, the deletion of those chaperones does usually not lead to defects in thermotolerance (Giese and Vierling, 2002). According to this, cells deleted for Hsp26, Hsp42 or both are able to survive after a severe heat shock (Haslbeck et al., 2004; Petko and Lindquist, 1986; Susek and Lindquist, 1989). Although the deletion strains did not exhibit pronounced phenotypic effects at first glance, scanning electron microscopy revealed dramatic changes in cell morphology at elevated temperature (Haslbeck et al., 2004), indicating a protective influence of Hsp26 and Hsp42 on the general status of the cell. The different appearance of the cells might be the consequence of massive protein aggregation upon deletion of either sHsp during heat stress (Haslbeck et al., 2004). In yeast cell lysates, both sHsps were shown to suppress the aggregation of one third of the cytosolic proteins during heat treatment (Haslbeck et al., 2004). 90% of Hsp26 and Hsp42 substrates are similar, suggesting at least partially overlapping functions. The substrate proteins comprise molecular masses from 10 to 100 kDa belonging to different biochemical pathways. This indicates nonspecific binding properties and a general protective role of Hsp26 and Hsp42 for proteome stability in yeast (Haslbeck et al., 2004). After heat shock, large fractions of both sHsps become insoluble as well. For Hsp26 it was demonstrated that it is subsequently solubilized by the chaperone Hsp104, an ATP-driven disaggregase, which dissolves protein aggregates and is crucial for mediating thermoresistance in yeast (Bosl et al., 2006; Parsell et al., 1994). Although the deletion of Hsp26 does not affect thermotolerance, the double deletion of Hsp26 and Hsp104 decreases the survival rate of yeast cells during heat stress five-fold, suggesting a functional link between both chaperones. In contrast, Hsp42 does not show this effect. This might indicate differences in the line of action of Hsp26 and Hsp42 (Cashikar et al., 2006).

Hsp26

As mentioned above, Hsp26 belongs to the group of temperature-regulated sHsps. Only upon heat shock mediated activation Hsp26 interacts with non-native polypeptides (Franzmann et al., 2008; Franzmann et al., 2005; Haslbeck et al., 1999; Stromer et al., 2003) and forms stable complexes. These can efficiently be disaggregated by Hsp70/Hsp100 chaperones *in vivo* and *in vitro* (Cashikar et al., 2006; Haslbeck et al., 2005). In addition, a previous study showed that Hsp26 is able to antagonize polyglutamine aggregation thereby partially suppressing toxicity (Cashikar et al., 2006).

Hsp26 in its native form exists as a heterogeneous mixture of oligomers, with the 24mer representing the most populated state (Benesch et al., 2010; Bentley et al., 1992; Bossier et al., 1989; Tuite et al., 1990). As observed for other sHsps, dimers constitute the basic building units (Haslbeck et al., 2005; White et al., 2006). Each monomer of Hsp26 consists of an α-crystallin domain, a rather long N-terminal extension and a short C-terminal tail (Bagnéris et al., 2009; Haslbeck et al., 2005; Kim et al., 1998; van Montfort et al., 2001a; White et al., 2006) (Figure 4a). The N-terminal region can be subdivided into the N-terminal domain (NTD) and the middle domain (MD) separated by a short glycine-rich part (aa 25-31) (Haslbeck et al., 2004; White et al., 2006). Dimerization of Hsp26 depends on presence of the conserved C-terminal motif (in Hsp26 IEV) as well as the middle domain (Chen et al., 2010). In addition, the latter was shown to be involved in the thermal activation of Hsp26 (described in more detail below) (Franzmann et al., 2008). The NTD was suggested to play a role in substrate interaction and stabilization of the oligomeric state. However, the main contributions for oligomerization seem to be provided by the MD and the CTE (Stromer et al., 2004).

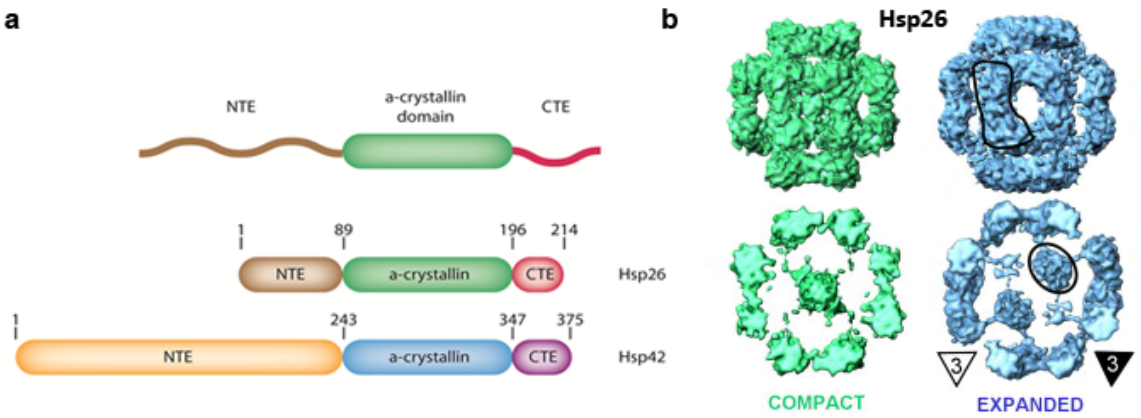

Figure 4: *Domain arrangement of sHsps and cryo-EM structures of oligomeric Hsp26 complexes.* ***(a)*** *Domain structure of sHsps in general and of yeast sHsps Hsp26 and Hsp42. NTE: N-terminal extension; CTE: C-terminal extension.* ***(b)*** *Cryo-EM images of Hsp26 oligomers reveal the coexistence of two distinct forms, a 'compact' form (left) and an 'expanded' form (right). The upper structures represent surface rendered views. One dimeric subunit is bordered (upper right structure). The bottom structures represent sliced open views, showing mass densities in the interior of the oligomer. One density is circled (bottom right structure) (White et al., 2006).*

Cryo-electron microscopy studies revealed two coexisting structures of Hsp26, each consisting of 24 monomers (White et al., 2006): a 'compact' and an 'expanded' form (Figure 4b). In both states elongated dimeric subunits assemble into a porous shell with tetrahedral symmetry. Domain fitting using homology models indicated that both termini and the MD mediate trimeric contacts between the dimers, and 12 C-termini penetrate inside the shell. In contrast to many other sHsps (see above), contacts between the conserved C-terminal IEV sequence and the α-crystallin of adjacent dimers seem impossible. However, the C-termini and the MD of nearby dimers are close enough to form interactions with each other, possibly mediating oligomerization.

A detailed study about the quaternary structure and dynamics of Hsp26 showed that at room temperature a variety of oligomeric states are present, ranging from 24 to 40mers (with 24mers being most abundant). Under heat shock conditions two shifts of the populations were detected: Additional dimers and monomers were formed by the dissociation of smaller oligomers (e.g. 24mers), and, higher-oligomeric species became more populated (predominantly 40mers) (Benesch et al., 2010). Dissociation of oligomers into dimers and monomers have previously been reported for other sHsps, and for some this is linked to chaperone activation (Benesch et al., 2003; Giese and Vierling, 2002; van Montfort et al., 2001a). For Hsp26, however, the heat-induced disassembly into dimers is not required for its activation (Franzmann et al., 2005). Thus, the changes in Hsp26 necessary to assume a high affinity state for binding non-native proteins do not depend on oligomer dissociation.

The basis for the temperature-regulated activation of Hsp26 was shown to be a heat-induced conformational rearrangement in the MD (Franzmann et al., 2008). This change is reversible and relies on alterations of the tertiary structure of Hsp26. The reorganization of the MD was suggested to control the accessibility to the substrate binding site, maybe by uncovering a buried substrate binding site (Franzmann et al., 2008). Thus, the Hsp26 MD acts as a 'thermoswitch' which can regulate its chaperone activity.

In addition, elevated temperature accelerates subunit exchange in Hsp26 in a biphasic process (Benesch et al., 2010). The first process was proposed to be a heat-induced conformational change in the CTE, which might lead to enhanced dissociation of oligomers representing the second phase (Benesch et al., 2010; Franzmann et al., 2005). The latest study on the mechanism of Hsp26 proposed that subunit exchange could be more dynamic in the active form of MD-conformers, resulting in higher chaperone activity (Benesch et al., 2010). This hypothesis is contradictory to previous findings demonstrating that subunit exchange in Hsp26 is significantly slower than substrate aggregation, and, Hsp26 is still active when subunit dissociation is inhibited (by crosslinking) (Franzmann et al., 2005).

An alternative model takes into account that the heat-induced activation of Hsp26 is a fast, biphasic process. The two processes could comprise the activation of two distinct populations (Franzmann et al., 2008). This is in good agreement with the cryo-EM studies which revealed two oligomeric species exhibiting different structural states (see above) (White et al., 2006).

Hsp42

Hsp42 is the second sHsp in the cytosol of *S. cerevisiae*. In contrast to Hsp26, Hsp42 is active at physiological and heat shock temperatures (Haslbeck et al., 2004). As Hsp42 is abundantly present at low and high temperatures, it might be an important player in maintaining protein homeostasis in both, stressed and unstressed cells.

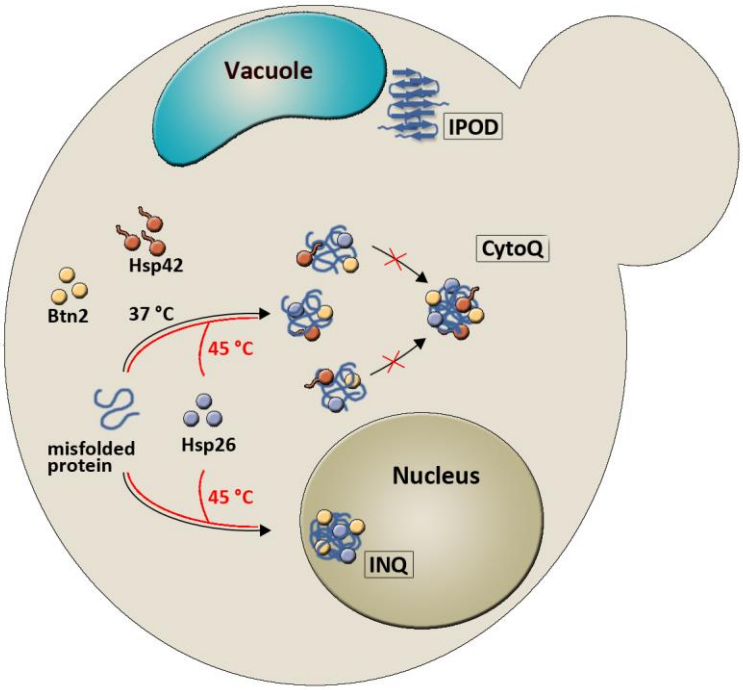

Figure 5: *Organized sequestration and deposition of misfolded proteins in S. cerevisiae. Misfolded polypeptide chains (dark blue) are either targeted to the CytoQ (cytosolic quality control compartment), the insoluble protein deposit (IPOD) close to the vacuole, or the intranuclear quality control compartment (INQ). Amyloidogenic substrates (dark blue β-sheets) accumulate at the IPOD. Under physiological folding stress (37°C) Hsp42 (orange) and Btn2 (yellow) co-aggregate with misfolded proteins, triggering the formation of CytoQ or INQ, respectively. In contrast, Hsp26 (light blue) only associates with misfolded polypeptides during severe heat stress (45°C) and is found in both compartments, CytoQ and INQ.*

Notably, compared to other sHsps, Hsp42 possesses an unusual elongated NTE (Figure 4a). The interaction with multiple substrate proteins and its tendency to aggregate hampers the purification of Hsp42. Thus, little is known about its mechanism and structure. However, size exclusion experiments showed that Hsp42 exists as a heterogeneous mixture of oligomers, consisting of 12-16 subunits, with a dimer as basic building block (Haslbeck et al., 2004). Moreover, the ACD seems to be involved in oligomerization (Wotton et al., 1996). Unlike Hsp26, CD and native polyacrylamide gel electrophoresis demonstrated that Hsp42 oligomers do not

dissociate at elevated temperature (Haslbeck et al., 2004). Negative stain EM pictures of Hsp42 followed by single-particle analysis revealed large, barrel-like complexes which are assembled of potentially dimeric building units (Haslbeck et al., 2004).

In vivo, Hsp42 was shown to play an important role during the organized sequestration and deposition of protein aggregates (Specht et al., 2011). Moreover, it has been implicated in the formation of stationary-phase granules in quiescent yeast (Liu et al., 2012). The organized deposition of protein aggregates is observed throughout all kingdoms of life. It is assumed to protect the cellular environment from misfolded protein species. Especially during stress conditions, the trapping of rapidly increasing amounts of unfolded or misfolded polypeptides seems to reduce the burden on the quality control system, and localization to distinct subcellular sites might help to coordinate the interplay between components of the proteastasis network. *S. cerevisiae* cells harbor three different types of protein aggregates (Figure 6). The IPOD (insoluble protein deposit) is located close to the vacuole and contains terminally aggregated proteins including amyloidogenic structures (Kaganovich et al., 2008). Physiological folding stress (37°C) leads to the formation of cytosolic aggregates (CytoQ: cytosolic quality control compartment) and the intranuclear quality control compartment (INQ), both harboring amorphously aggregated proteins (Miller et al., 2014; Specht et al., 2011). Recently, different factors have been shown to co-aggregate with CytoQ and INQ. Hsp26 was detected within CytoQ and INQ only upon severe heat shock (45°C) but seems to be dispensable for the organized sequestration of aggregates (Specht et al., 2011). Under mild heat stress (37°C) Btn2 is located to cytosolic and particularly nuclear aggregates whereas Hsp42 has exclusively been observed in the CytoQ. In this connection Btn2 has been shown to trigger the formation of INQ, whereas Hsp42 is required for the sequestration of misfolded proteins at CytoQ (Malinovska et al., 2012; Specht et al., 2011). Hence, both proteins were suggested to act as compartment-specific aggregases.

1.2.2 Disassembly of protein aggregates by ATP-dependent chaperones

In order to assure survival under stress, a network of various chaperone classes is active, in which the components are tightly working together. They prevent the aggregation of misfolded species and can reactivate proteins that are trapped in aggregates. During stress, sHsps seem to be the first responders, optimized to efficiently bind to non-native proteins and keep them in are more soluble, refolding-competent state. In bacteria, fungi and plants, further processing and reactivation of misfolded proteins is performed by a bi-chaperone system, consisting of the Hsp70-Hsp40 system (DnaK-DnaJ in *E. coli*; Ssa1-Ydj1/Sis1 in *S. cerevisiae*) and Hsp100 proteins (ClpB in *E. coli*; Hsp104 in *S. cerevisiae*) (Glover and Lindquist, 1998;

Goloubinoff et al., 1999; Parsell et al., 1994; Tessarz et al., 2008; Weibezahn et al., 2004).

Hsp70 chaperones can bind and release client proteins, regulated by ATP binding and hydrolysis, switching between low- or high substrate affinity states (Beissinger and Buchner, 1998; Bukau and Horwich, 1998; Walter and Buchner, 2002). ATPase cycling is usually controlled by cochaperones and nucleotide exchange factors. The largest class of Hsp70 cochaperones is the Hsp40/J-protein family (Kampinga and Craig, 2010). They bind non-native polypeptides, exerting holdase function (suppression of aggregation) and transfer substrates to Hsp70s. The J-domain of Hsp40s interacts with the ATPase domain of Hsp70s, thereby stimulating ATP-hydrolysis. Release of ADP and substrate is accelerated by nucleotide exchange factors (GrpE in *E. coli* and Sse1/Sse2, Fes1, Bag1 in *S. cerevisiae*). These ATPase cycles are able to drive an unfolding force, extracting trapped polypeptides from aggregates. For instance, Hsp70 unfolding activity has been demonstrated for a soluble misfolded form of firefly luciferase (Sharma et al., 2010).

1.2.2.1 Disassembly of amorphous aggregates

The disaggregation of small amorphous aggregates can be managed by the Hsp70 system alone (Deloche et al., 1997; Liberek et al., 2008; Skowyra et al., 1990). In contrast, the disassembly of larger, strongly misfolded aggregates requires the collaboration with Hsp100 chaperones (Ben-Zvi et al., 2004; Diamant et al., 2000; Goloubinoff et al., 1999). Hsp100 chaperones exhibit ATP-dependent unfolding activity and are part of the AAA+ protein superfamily (Neuwald et al., 1999). AAA+ proteins contain the AAA domain, which exerts ATPase activity and mediates oligomerization, mostly into hexameric rings. Through direct contacts at substrate termini or internal sites substrates are translocated through the central pore of the hexamer by an ATP-dependent pulling force (Burton et al., 2001; Haslberger et al., 2008).

During the disaggregation reaction Hsp70 first binds to hydrophobic surfaces of protein aggregates (Figure 6). Via direct contact between the ATPase domain of Hsp70 and ClpB/Hsp104, the substrate is delivered to the central cavity of the Hsp100 protein (Rosenzweig et al., 2013; Seyffer et al., 2012; Weibezahn et al., 2004; Zietkiewicz et al., 2004). This interaction with the substrate induces the activation of Hsp100 (Seyffer et al., 2012). An ATP-fueled power-stroke pulls at a free substrate site, thereby disentangling single polypeptide chains from the aggregated protein. Concomitantly, contacts between substrate and Hsp70 are disrupted (Rosenzweig et al., 2013). Refolding of the unfolded polypeptide occurs either spontaneously or assisted by chaperones.

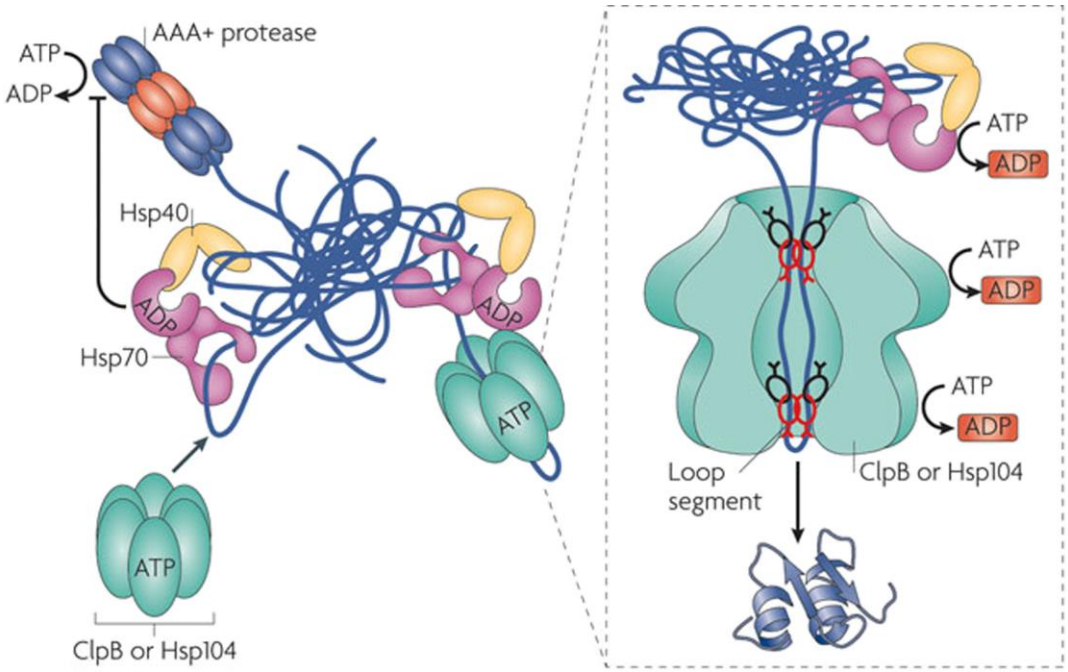

Figure 6: *Protein disaggregation by the cooperative action of the Hsp70-40 chaperone system and Hsp100 chaperones (ClpB in E. coli, Hsp104 in yeast). The Hsp40 cochaperone targets substrates to Hsp70 and stimulates its ATPase activity, leading to conformational changes that result in tight substrate binding by Hsp70. Via direct interaction between the ATPase domain of Hsp70 and ClpB/Hsp104 the substrate is transferred to the central cavity of the hexameric Hsp100 chaperone. Contacts to substrates are mediated by conserved aromatic residues in mobile loops at the openings of the central pore. An ATP-fueled power-stroke causes conformational changes of the loop segments and pulls the substrate through the pore, thereby dissolving non-native interactions. Refolding of the unfolded polypeptide occurs either spontaneously or assisted by chaperones (Tyedmers et al., 2010).*

Metazoan cells do not contain a ClpB/Hsp104 homolog in their cytosol or nucleus. Yet, cell extracts possess remarkable disaggregation activity and are able to disassemble amyloid aggregates (Murray et al., 2010). Previous studies suggest that Hsp110 cochaperones empower the metazoan Hsp70-Hsp40 system to perform efficient disaggregation (Rampelt et al., 2012; Shorter, 2011).

1.2.2.2 Disassembly of the native, dimeric replication initiator protein RepE

The Hsp70-chaperone system of *E. coli* does not only participate in the disaggregation and reactivation of amorphous protein aggregates. It is also involved in the disassembly of native protein complexes such as clathrin coats, viral capsids or replication initiation proteins (Mayer and Bukau, 2005). One example is the replication initiator protein RepE, which regulates the copy number of the mini-F plasmid in *E. coli*. The mini-F plasmid is a derivative of the F (fertility) factor, which is involved in sexual conjugation (Lovett and Helinksi, 1976). It is maintained to one to two copies per cell and its replication is strictly regulated on the level of initiation by the RepE protein (Ishiai et al., 1994). RepE exists predominantly as a dimer, but it can be monomerized by the concerted action of DnaK, DnaJ and GrpE (Ishiai et al., 1994; Kawasaki et al., 1990) (Figure 7a). Each oligomeric state performs a distinct function:

Dimeric RepE binds to inverted repeat operator DNA (IR-DNA), repressing its own transcription. Monomeric RepE binds to four direct repeats iteron DNA (DR-DNA) within the F plasmid replication origin *ori*2 and initiates plasmid replication (Masson and Ray, 1986; Wada et al., 1987). Iteron and operator DNA sequences share eight common base pairs. In addition, replication initiation is negatively controlled by pairing of the iterons in *ori*2 with a second set of iterons, called *Inc*C (Figure 7b). This results in DNA looping, inhibiting the formation of an open initiation complex. Previous findings suggest that the looping is mediated by RepE dimers that bridge iteron sequences bound to monomeric RepE. Therefore, efficient negative regulation requires both, monomeric and dimeric RepE (Zzaman and Bastia, 2005).

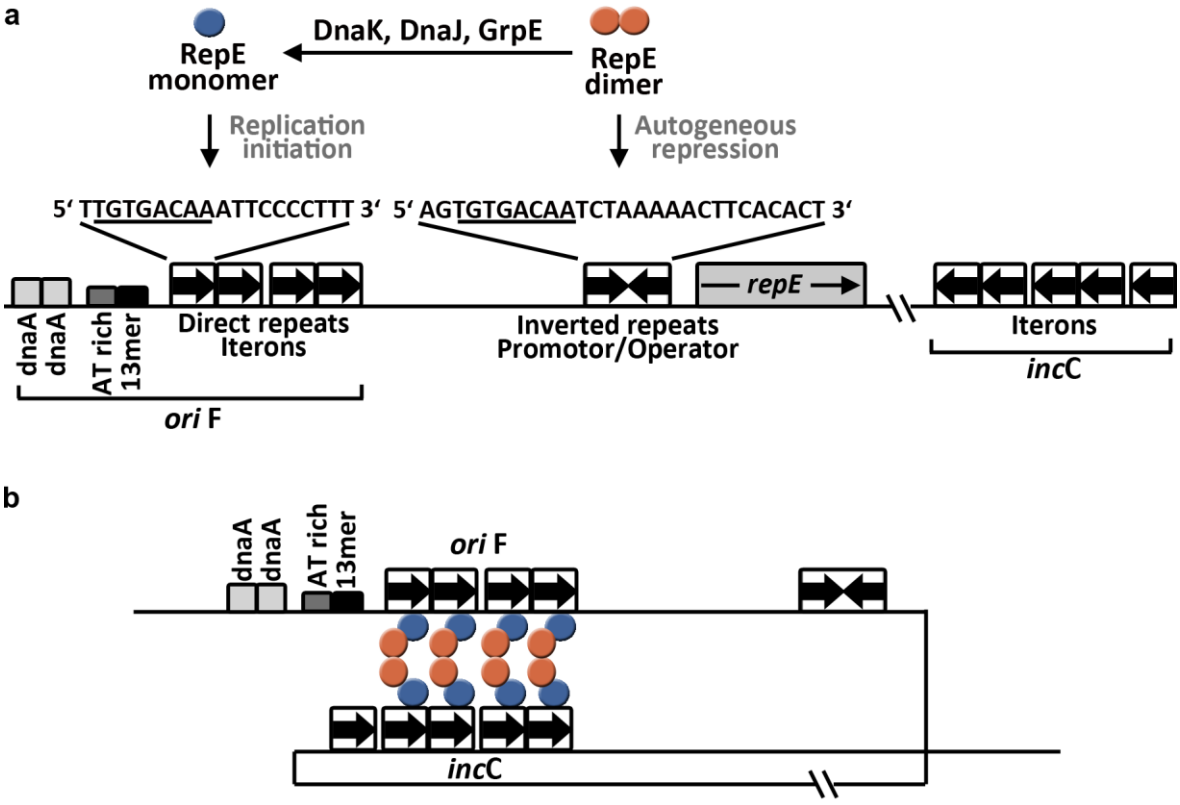

Figure 7: *Functions of dimeric and monomeric RepE.* ***(a)*** *RepE dimers bind to promotor inverted repeat DNA, repressing its own transcription. RepE monomers bind to four iteron direct repeats and initiate the replication of the mini-F plasmid in E. coli. Direct and inverted repeats share eight common base pairs (underlined).* ***(b)*** *Complete repression of repE transcription seems to involve the formation of a DNA-loop structure in which RepE monomers and dimers are bridging iterons of oriF and incC (Zzaman and Bastia, 2005)(modified).*

RepE54 is a constitutively monomeric variant, which carries a point mutation in the RepE dimer interface region (R118P) (Ishiai et al., 1992; Ishiai et al., 1994). *In vivo* experiments as well as studies with a reconstituted *in vitro* replication system demonstrated that this mutant has enhanced initiator and lower repressor activity and that a plasmid carrying this mutation can replicate in absence of the DnaK machinery (Ishiai et al., 1994; Matsunaga et al., 1997). In contrast to dimeric RepE wt, which tends to aggregate easily, monomeric RepE54 stays soluble even at high

concentrations and binds to iteron DNA with great efficiency. Therefore, first structural information about RepE was obtained from the crystallized RepE54-iteron DNA complex, whose preparation and crystallization appeared easier than for RepE wt (Komori et al., 1999). The crystal structure showed that the RepE monomer consists of topologically similar N- and C-terminal domains related to each other by internal pseudo two-fold symmetry. Moreover, both domains bind to the two major grooves of the iteron DNA but with strikingly different affinities. The N-terminal domain mostly contacts the phosphate backbone resulting in weak binding, whereas contacts between the C-terminal domain and the DNA bases mediate stronger main interactions with iteron DNA (Komori et al., 1999). Modelling of dimeric RepE to operator DNA, in a similar manner as observed for RepE54, resulted in a large sterical hindrance in the N-terminal domains. This implied that monomerization of RepE is accompanied by a marked structural change and that a different conformation of the RepE dimer is necessary to accommodate it to operator DNA. A few years later, the crystal structure of the complex between dimeric RepE wt and operator DNA was determined (Nakamura et al., 2007). It revealed differences in the relative orientations of the N- and C-terminal domains in RepE wt compared to RepE54, accompanied by secondary structural changes in the linker connecting the two domains. The observed alterations explain how the conformation of dimeric RepE wt adapts, enabling the binding to operator DNA. A recent study characterized the RepE-DnaJ complex using EM, crosslinking and gel retardation experiments (Cuéllar et al., 2013). The authors suggested a DnaJ-induced conformational change in the RepE dimer, which increases the intermolecular distance thereby enhancing its affinity for DNA. Still, the mechanism of chaperone-mediated monomerization of RepE remains elusive.

RepA is a replication initiator protein in *Pseudomonas syringae* and shows sequence and structural similarities to RepE. When using low DnaK/DnaJ/GrpE concentrations, the disassembly of the RepA dimer was shown to be much more efficient in presence of the ClpB chaperone (Doyle et al., 2007). This is similar for the chaperone-driven dissolution of amorphous protein aggregates, indicating that the disassembly of native protein oligomers might be mechanistically related to the disaggregation process.

2 Aims

In their native state, proteins perform the bulk of vital functions. However, especially under stress conditions, proteins can misfold and associate into large, amorphous aggregates. In such assemblies, some studies detected a relatively high β-sheet content, which might even assume amyloid-like organization. However, only few studies were performed using techniques with high structural resolution. Therefore, the structure of amorphous aggregates remains poorly defined.
In cells, the first reaction to the appearance of harmful, misfolded polypeptides is their association with sHsps. sHsps thereby modify aggregation, and the resulting sHsp-substrate complexes facilitate the reactivation of the bound non-native polypeptides by the Hsp70-Hsp100 machinery. The underlying sHsp-caused structural changes that facilitate disaggregation are still unclear.
The yeast sHsps, Hsp26 and Hsp42, were shown to localize to defined aggregate deposition sites. Hsp42, but not Hsp26, was found to be required for CytoQ formation (Specht et al., 2011). Which special feature of Hsp42 drives the sequestration of misfolded proteins in CytoQ is unknown.
The chaperone-mediated disassembly of native, oligomeric substrates seems to be mechanistically related to the disaggregation process. Examples of those native chaperone substrates are many replication initiator proteins for plasmids and phages. In their ground state, these proteins are dimers. Only upon monomerization by the Hsp70-system the proteins can bind to the replication origin initiating the replication of the plasmid- or phage-DNA (Del Solar et al., 1998). This Hsp70-mediated monomerization process is poorly understood. A suitable model substrate for studying the underlying mechanisms is RepE, the replication initiator protein for the mini-F plasmid in *E. coli*.

One major goal of this thesis was to elucidate why sHsps facilitate the disaggregation of amorphous aggregates. To be able to answer this question, I studied the structure of heat-induced protein aggregates formed in absence and presence of Hsp26 and Hsp42. A more detailed analysis of Hsp42 should reveal which part of the NTE is required for its chaperone activity *in vitro* (complementing *in vivo* results by Stephanie Miller, unpublished data). In addition, I wanted to determine the structural basis underlying the facilitated chaperone-mediated disassembly of sHsp-substrate complexes.
FRET approaches and amide hydrogen exchange experiments (HX) combined with mass spectrometry (MS) were used to investigate the structure of aggregates and to study how sHsps influence the aggregate architecture. Moreover, I performed HX-MS

as well as crosslinking between sHsps and substrate in heat-induced complexes in order to identify the interaction sites and to detect substrate-induced effects within sHsps. The roles of specific parts in the Hsp42 NTE were studied *in vitro* by aggregation and disaggregation assays, negative stain EM and HX-MS.
The experimental handling of native proteins is considerably easier than working with aggregates. Therefore, the chaperone-mediated disassembly of protein aggregates has been addressed by studying the monomerization of the RepE dimer as an example of a minimal model aggregate. Mainly HX-MS of RepE in presence and absence of DnaK and DnaJ chaperones as well as crosslinking approaches were used to study interactions and effects of chaperone binding to dimeric RepE wt or the constitutively monomeric variant RepE54.

To be more specific, in my PhD thesis I addressed the following questions:

Molecular analysis of heat-induced protein aggregates and interactions between substrate and yeast sHsps Hsp26 and Hsp42:

- Are proteins mostly unfolded in aggregates or does some native structure remain?
- How do sHsps alter the structure of aggregated proteins?
- Are there any functional differences between Hsp26 and Hsp42?
- Where are the chaperone binding sites within protein aggregates?
- Are there substrate-induced conformational changes within Hsp26 or Hsp42?
- Where are the substrate binding sites within Hsp26 and Hsp42?
- Which part of the Hsp42 NTE is required for the aggregase function of Hsp42?

Disassembly of the dimeric DnaK substrate RepE:

- Does DnaJ or DnaK bind to monomeric and dimeric RepE?
- Where are the DnaK and DnaJ binding sites in RepE?
- Does DnaJ or/and DnaK binding result in conformational changes of the RepE dimer?

Combining the results of biochemical and biophysical approaches should help to elucidate the architecture of protein aggregates and how sHsps influence the structure, thereby facilitating the disaggregation by the Hsp70/Hsp100-bi-chaperone-system. In particular, the role of the NTE for Hsp42 functionality was examined, and the findings were combined with unpublished *in vivo* data. Moreover, effects of chaperone binding on the RepE dimer combined with the known structures should contribute to elucidate the chaperone-mediated mechanism of the RepE monomerization process.

3 Results

3.1 Heat-induced MDH aggregates consist of largely unfolded conformers

In order to study the structure of heat-induced protein aggregates and the influence of sHsps on the aggregate architecture (chapter 3.2), I performed amide hydrogen exchange (HX) experiments combined with mass spectrometry (MS) analysis. HX is a powerful technique that can be used to study the structure and dynamics of proteins. It is based on the exchange of backbone amide protons against deuterons. The involvement of backbone amide hydrogens in the formation of hydrogen bonds protects them from HX. Therefore, HX analysis provides information about both: The tertiary structure, which determines general solvent accessibility to backbone hydrogens, as well as changes in the secondary structure of proteins.

In HX-MS experiments, proteins are incubated with D_2O-based buffer at physiological conditions. After a defined time the exchange reaction is quenched by lowering the pH to 2.2 and the temperature to 0°C. The number of incorporated deuterons is determined by HPLC (High Performance Liquid Chromatography)-coupled MS. The analysis of the full length protein is called 'global' exchange. Pepsin digest of the deuterated substrates (under quench conditions) and the subsequent analysis of the generated peptides ('local' exchange) allow for determining differences of the HX in short peptides, providing detailed structural information on molecular level. The resulting spectra are compared with those of the unexchanged proteins. The differences in deuteron incorporation, and thus in the solvent accessibility of the amide protons, reveal conformational changes.

To determine the structure of heat-induced protein aggregates by HX, thermolabile malate dehydrogenase (MDH) was chosen. MDH, which forms dimers in its native state, misfolds and aggregates at 47°C (Veinger et al., 1998) and, is a widely used model substrate in the chaperone field. However, employing protein aggregates in HX-MS bears multiple experimental challenges, which had to be managed, and a suitable setup had to be established. Firstly, aggregates must be solubilized before injection into the HPLC-coupled measuring setup. Secondly, the concentration of the model substrates used in aggregation-disaggregation reactions is usually strikingly lower than the concentrations which are necessary for the detection in the mass spectrometer. Thus, aggregates would either have to be formed at higher protein concentrations, or the aggregates have to be concentrated after their formation. The first procedure would create much larger aggregate species, which are not

disaggregated efficiently by chaperones. Concentrating aggregates by centrifugation is possible, could, however, alter the aggregate structure. Thus, both approaches were not suitable for the planned experiments. Instead, a His_6-tag was introduced at the N-terminus of MDH. After the formation of heat-induced aggregates, the protein was concentrated by binding to Ni-magnetic beads. The HX was performed on the bead-bound material. Attempts to elute and solubilize the aggregates with quench buffer containing 6 M guanidinium chloride were unsuccessful. Therefore, the determination of the global exchange of aggregates was not possible. Finally, the use of pepsin-containing quench buffer enabled simultaneous elution and digestion of the protein aggregates, circumventing the solubilization problem. After optimizing the conditions (amounts of MDH, Ni-magnetic beads and pepsin, as well as the duration for the incubation with pepsin) the time for pepsin digestion was restricted to 1 min at 0°C, as back-exchange of the deuterated protein had to be minimized.

By using the established settings, pepsin digested all of the bead-bound native MDH and more than 50% of MDH aggregates (Figure 8a). Larger degradation products were not detected, indicating that the majority of aggregated MDH species was accessible to HX analysis at the peptide level. For native MDH the sequence coverage was 83% (i.e. the percentage of the sequence, which is covered by the identified peptic peptides), for aggregated MDH 76%. In each HX experiment, three replicates were measured, with standard deviations for the deuteron incorporation between 5 and 15% for the aggregate (Figure 8b). Although different sets of experiments showed some variability for the HX of aggregate derived peptides (10-20% deviation of total HX), the trend always remained the same for all peptides. Aggregated MDH shows a high degree of deuterium incorporation up to 60%, indicating that most regions are largely unfolded (Figure 8b and c). Remaining protection could either be due to residual native structure or due to the formation of new, unspecific interactions during aggregation. A comparison to the HX pattern of native MDH illustrates considerable deprotection in the aggregated state, with deprotected peptides being distributed throughout the sequence and structure (Figure 8). Peptides Tyr32-Ala41 and Val213-Met227, which show only minor increase in HX, already strongly exchange in the native state. Phe90-Leu100 displays moderate HX in both, native and aggregated state. As this peptide is part of a surface exposed α-helix, protection against HX could arise from unfolding and subsequent hydrophobic interactions, rather than from residual native structure. The only peptide, keeping low HX in the aggregated state (Ala228-Phe236), is located in an α-helix at the MDH dimer interface. Further peptides at or near the dimer interface (e.g. Leu20-Leu31), however, display high exchange rates, arguing against a remaining dimer core structure in the aggregate.

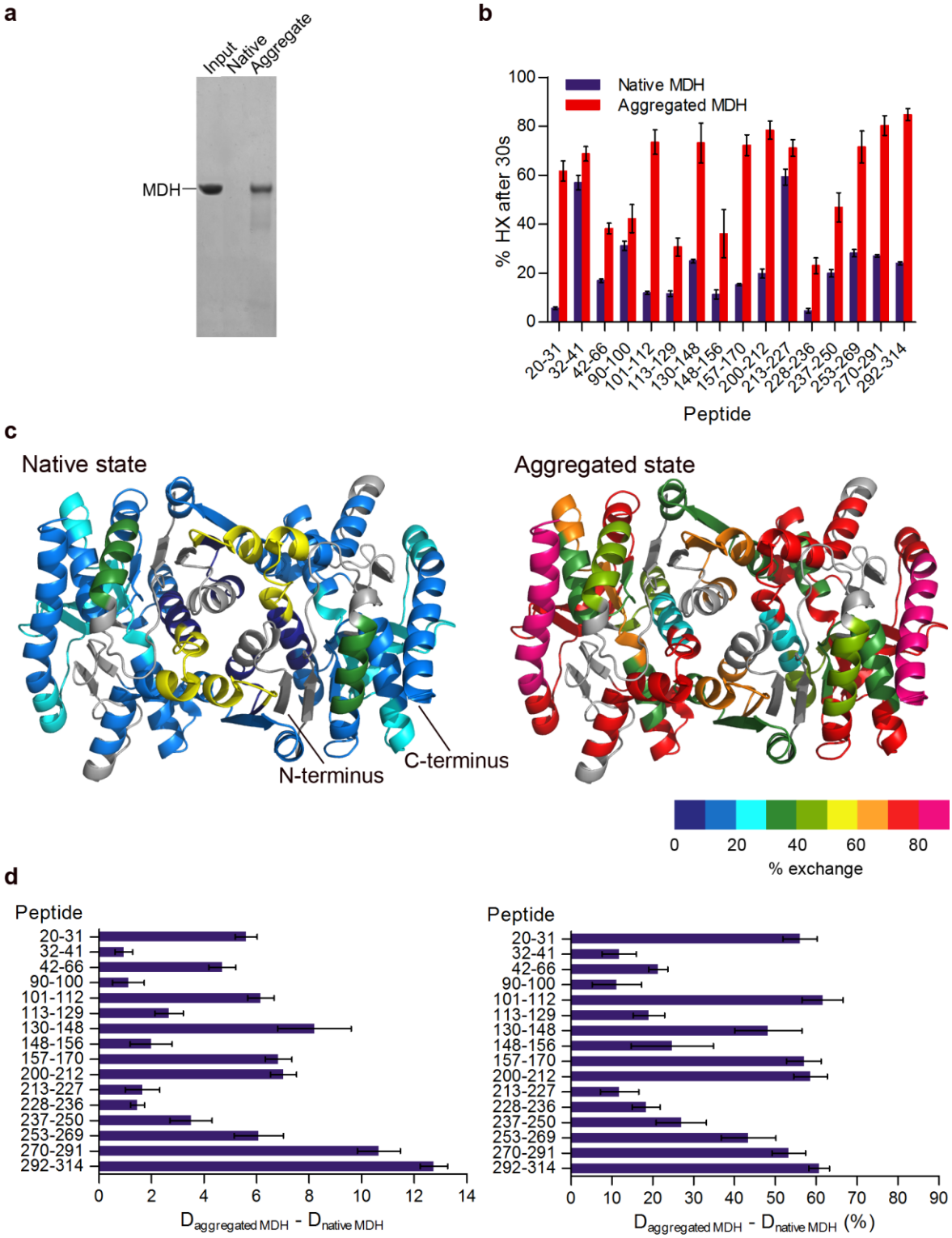

Figure 8: *Heat-induced aggregates of MDH are largely deprotected in HX.* ***(a)*** *In HX experiments resin-bound native or heat-aggregated His_6-MDH was digested by pepsin. Afterwards, undigested protein was analyzed by SDS-PAGE and Coomassie staining.* ***(b)*** *Relative proton/deuteron exchange in native and heat-aggregated MDH after 30 s incubation in D_2O. The data were corrected for deuteron losses due to back-exchange using a 100% deuterated control (i.e. protein in which all exchangeable protons have been replaced by deuterons).* ***(c)*** *HX-heat map of native and aggregated states of the MDH dimer structure (PDB ID 1MLD). Peptic peptides are colored according to their exchange behavior. Gray regions could not be detected.* ***(d)*** *Difference in deuteron incorporation of peptic peptides between native and aggregated MDH (left: absolute number of deuterons; right: number of deuterons relative to the total number of exchangeable deuterons in the respective peptide).*

In summary, the HX results indicate that MDH aggregates are composed of largely unfolded conformers and do not possess substantial secondary structures. In accordance, FTIR spectroscopy measurements of heat-denaturing MDH (at 47°C) did not result in pronounced increase of β-sheets (data not shown).

3.2 Impact of sHsp incorporation on heat-induced aggregation

The rapid association of sHsps with heat-denaturing polypeptides results in the formation of stable sHsp-substrate complexes. Those are smaller than heat-induced amorphous aggregates (lacking sHsps), and they keep the bound substrates in a refolding-competent state, facilitating their reactivation by Hsp70 and Hsp100 chaperones. To figure out how sHsps influence the heat-induced aggregation of MDH I used Hsp42 and Hsp26 as models for constitutively active and stress-activated sHsps, respectively.

3.2.1 Hsp26 and Hsp42 prevent the formation of large heat-induced aggregates and facilitate chaperone-mediated disaggregation

First, the chaperone functions of Hsp26 and Hsp42 were tested and compared in aggregation and disaggregation assays. In addition to MDH, thermolabile firefly luciferase was used as a second model substrate. MDH or luciferase was mixed with various ratios of sHsps and heat-denatured at 47°C or 43°C, respectively. This results in the formation of differently sized sHsp-substrate complexes.

Centrifugation and subsequent SDS-PAGE analysis of heat-induced MDH/sHsp complexes revealed that substoichiometric levels of Hsp26 and Hsp42 were not sufficient to prevent aggregation (Figure 9a). Consistently, turbid complexes were formed at this ratio, as demonstrated in light scattering measurements (Figure 9b). In contrast, excess amounts of sHsps resulted in soluble, non-turbid aggregates (Figure 9a and b). For MDH, prevention of heat-induced aggregation appears to be similarly efficient for both sHsps. However, when using luciferase, Hsp42 completely prevented the formation of turbid complexes already at equimolar ratios, whereas excess amounts of Hsp26 were necessary to keep MDH soluble.

For the disaggregation/refolding assay substrate and different levels of sHsps were mixed and complexes were formed by incubation for 30 min at 47°C or 15 min at 43°C for MDH or luciferase, respectively. The disaggregation and refolding was initiated by adding the yeast Hsp70/Hsp100 bi-chaperone system (Figure 10). In case of MDH, the GroEL/GroES chaperone machinery was included to accelerate efficient refolding.

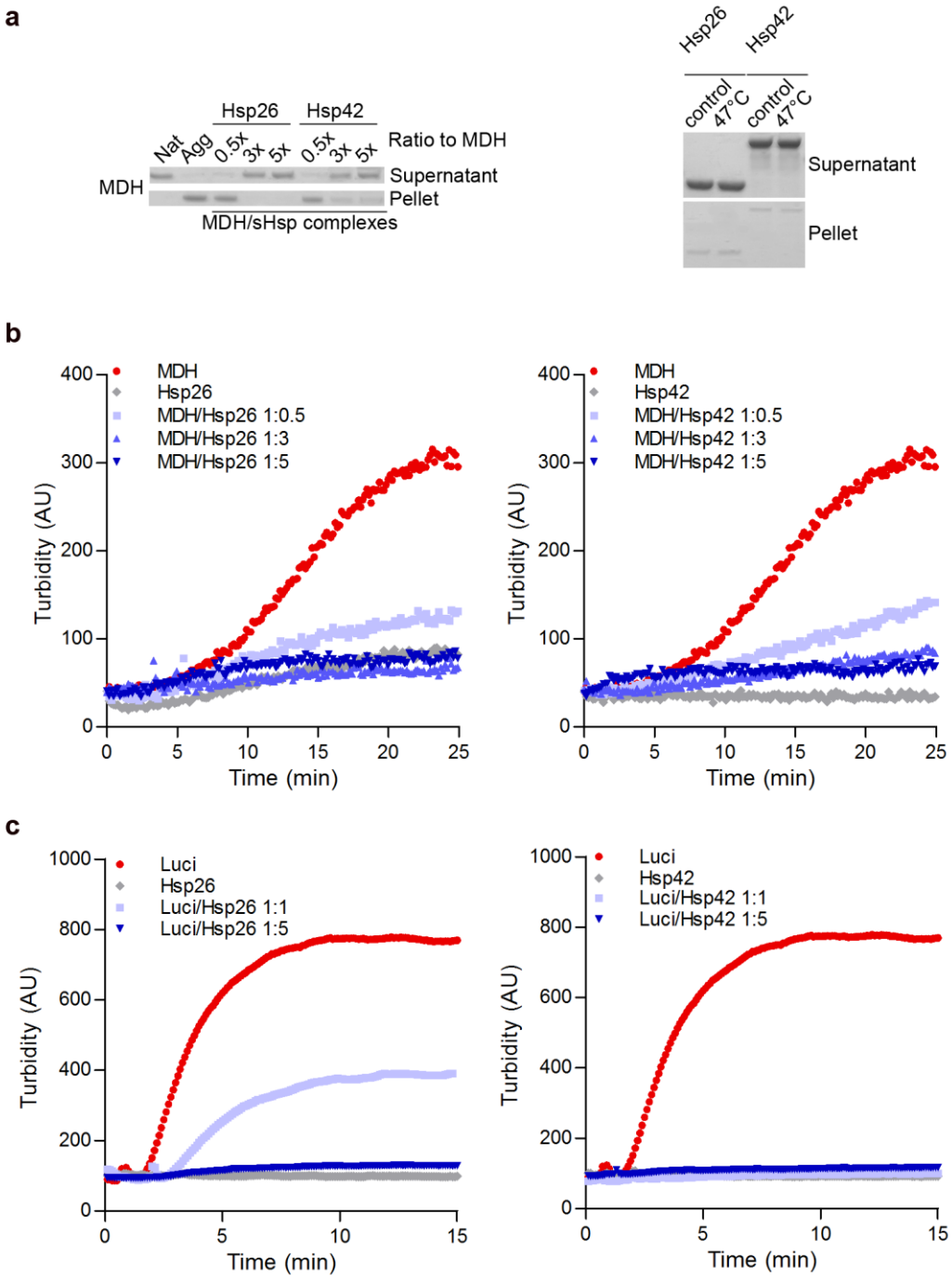

Figure 9: *Hsp26 and Hsp42 prevent the formation of turbid, insoluble MDH and luciferase aggregates.* ***(a)*** *MDH (0.5 µM) was denatured for 30 min at 47°C in absence or presence of sHsps at various ratios (0.25–2.5 µM). As a control 2.5 µM sHsps were heated alone. Samples were centrifuged (30 min, 13 000 rpm, 4°C). Equal amounts of supernatants and pellets were analyzed by SDS-PAGE and Coomassie-staining.* ***(b)*** *Samples were prepared as described in* ***(a)*** *and the formation of turbid MDH aggregates was followed at 550 nm.* ***(c)*** *Luciferase (0.1 µM) was denatured at 43°C in absence or presence of sHsps (0.1 µM or 0.5 µM) and the formation of turbid aggregates was followed at 600 nm. As a control 0.5 µM sHsps were heated alone. Luci: luciferase.*

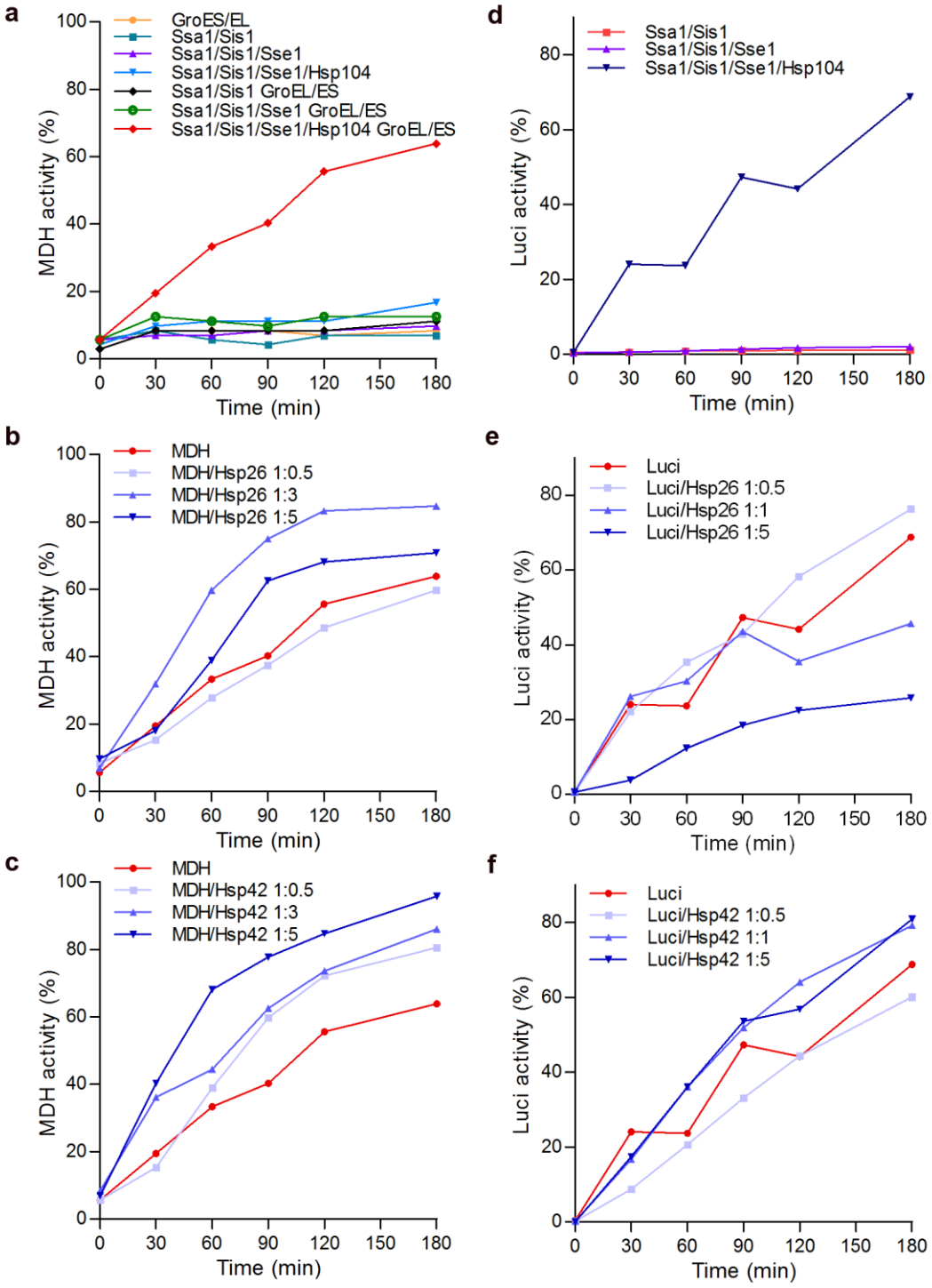

Figure 10: *Hsp26 and Hsp42 facilitate the chaperone-mediated refolding of heat-induced MDH and luciferase aggregates.* ***(a)-(c)*** *MDH (0.5 µM) was denatured for 30 min at 47°C in absence or presence of sHsps at various ratios (0.25–2.5 µM). MDH refolding from aggregated or sHsp-complexed states was initiated at 30°C by addition of the S. cerevisiae bi-chaperone system (2 µM Ssa1, 1 µM Sis1, 0.1 µM Sse1, 1 µM Hsp104) and 1 µM GroEL/GroES.* ***(d)-(f)*** *Luciferase (0.1 µM) was denatured for 15 min at 43°C in absence or presence of sHsps at various ratios (0.05–0.5 µM). Luciferase refolding from aggregated or sHsp-complexed states was initiated at 30°C by addition of the S. cerevisiae bichaperone system (2 µM Ssa1, 1 µM Sis1, 0.1 µM Sse1, 1 µM Hsp104). MDH and luciferase activities were determined at the indicated time points. The enzymatic activity of native MDH and luciferase was set at 100%.*

The renaturation was followed by observing the regain of enzymatic activity. The sHsp-bound substrates were inactive, but soluble complexes with sHsps facilitated chaperone-mediated MDH and luciferase reactivation. Hsp26 and Hsp42 caused a pronounced acceleration of MDH disaggregation and increased the levels of renatured protein by up to 30% (Figure 10b and c). High concentrations of Hsp26 seem to interfere with disaggregation/refolding, resulting in optimal efficiencies for a 1:3 MDH/Hsp26 ratio. In case of luciferase, even stronger inhibiting effects for Hsp26 were observed, and Hsp42 only slightly enhanced the final amounts of reactivated protein (Figure 10e and f). Thus, the consequences on refolding by ATP-dependent chaperones seem to be substrate-dependent.

Earlier findings showed that the dissolution of small aggregates and of aggregates with high content of non-native secondary structure (especially β-sheets) can occur by the Hsp70 system alone, without the need of Hsp100 chaperones (Ben-Zvi et al., 2004; Diamant et al., 2000; Lewandowska et al., 2007; Skowyra et al., 1990). However, MDH reactivation experiments omitting Hsp104 proved that the disaggregation of sHsp-substrate complexes containing Hsp26 or Hsp42 is still Hsp104-dependent (Figure 11).

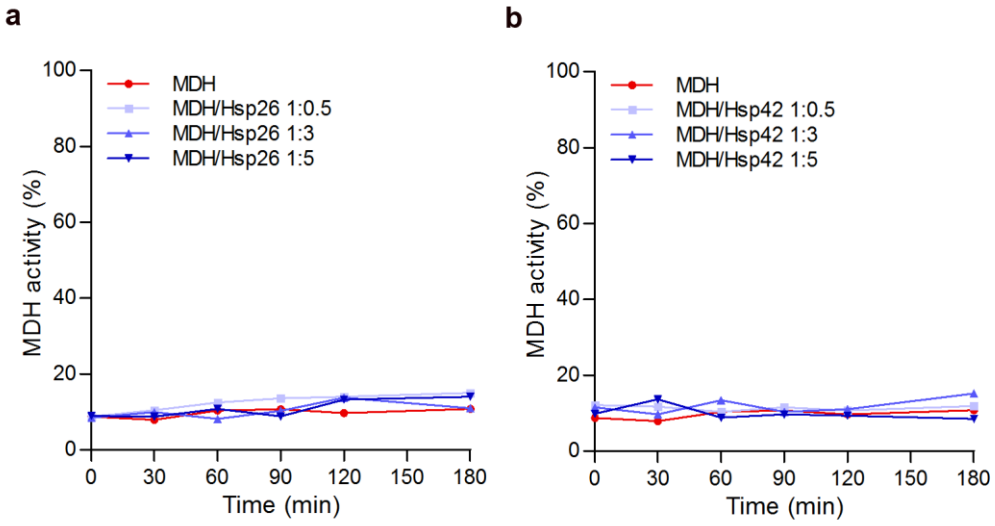

Figure 11: *The disaggregation of heat-induced complexes between MDH and Hsp26* ***(a)*** *or Hsp42* ***(b)*** *is still Hsp104-dependent. MDH (0.5 µM) was denatured for 30 min at 47°C in absence or presence of sHsps at various ratios (0.25–2.5 µM). MDH refolding from aggregated or sHsp-complexed states was initiated at 30°C by addition of the S. cerevisiae bi-chaperone system (2 µM Ssa1, 1 µM Sis1, 0.1 µM Sse1) and 1 µM GroEL/GroES. MDH activities were determined at the indicated time points. The enzymatic activity of native MDH was set at 100%.*

Summarized, Hsp26 and Hsp42 were both active in preventing the formation of large heat-induced aggregates. Moreover, complexes with either sHsp allowed for faster and more efficient chaperone-mediated reactivation of heat-denatured MDH in an Hsp104-dependent manner.

3.2.2 Hsp26 and Hsp42 increase the distance of sequestered misfolded proteins

Although yeast sHsps suppress the formation of large amorphous aggregates *in vitro*, Hsp42 was found to be required for the generation of CytoQ deposits in yeast cells. During severe heat stress cytosolic aggregates can, however, even be formed in *hsp42Δ* cells, albeit with reduced size. This observation brought us to consider that sHsps, especially Hsp42, might act as a protein aggregase, triggering and/or accelerating the formation of protein aggregates. Initiating aggregate formation might have important cytoprotective functions as potentially toxic misfolded proteins would become rapidly sequestered. To test for such a role of sHsps *in vitro*, I performed fluorescence resonance energy transfer (FRET) experiments using MDH-YFP and MDH labeled with 7-diethylcoumarin-3-carboxylic acid as FRET pair. Equimolar amounts of both FRET partners were mixed. An increase in donor fluorescence was detected at 47°C, but not at 30°C, indicating that the FRET signal reports on the heat-induced co-aggregation of MDH donor and acceptor molecules (Figure 12a). Compared to turbidity experiments (Figure 9) the signal increase occurred much earlier, indicating a higher sensitivity of this approach. When including Hsp26 or Hsp42, no acceleration of protein aggregation could be detected. Instead, a decrease of FRET efficiencies was observed in a concentration-dependent manner (Figure 12b). This could be explained by co-aggregation of denatured MDH molecules and Hsp26 or Hsp42, increasing the spacing between misfolded protein conformers and preventing the formation of hydrophobic interactions between denatured parts of MDH. In contrast to turbidity experiments, a stronger effect was detected for Hsp42 as compared to Hsp26. At substoichiometric ratio, Hsp26 did not change the donor fluorescence, whereas Hsp42 clearly reduced FRET intensity (Figure 12b), indicating a more efficient spacing of misfolded MDH by Hsp42. For Hsp42, similar experiments were performed using luciferase-YFP and luciferase-CFP, resulting in the same effects as observed for the MDH FRET pair (data not shown).

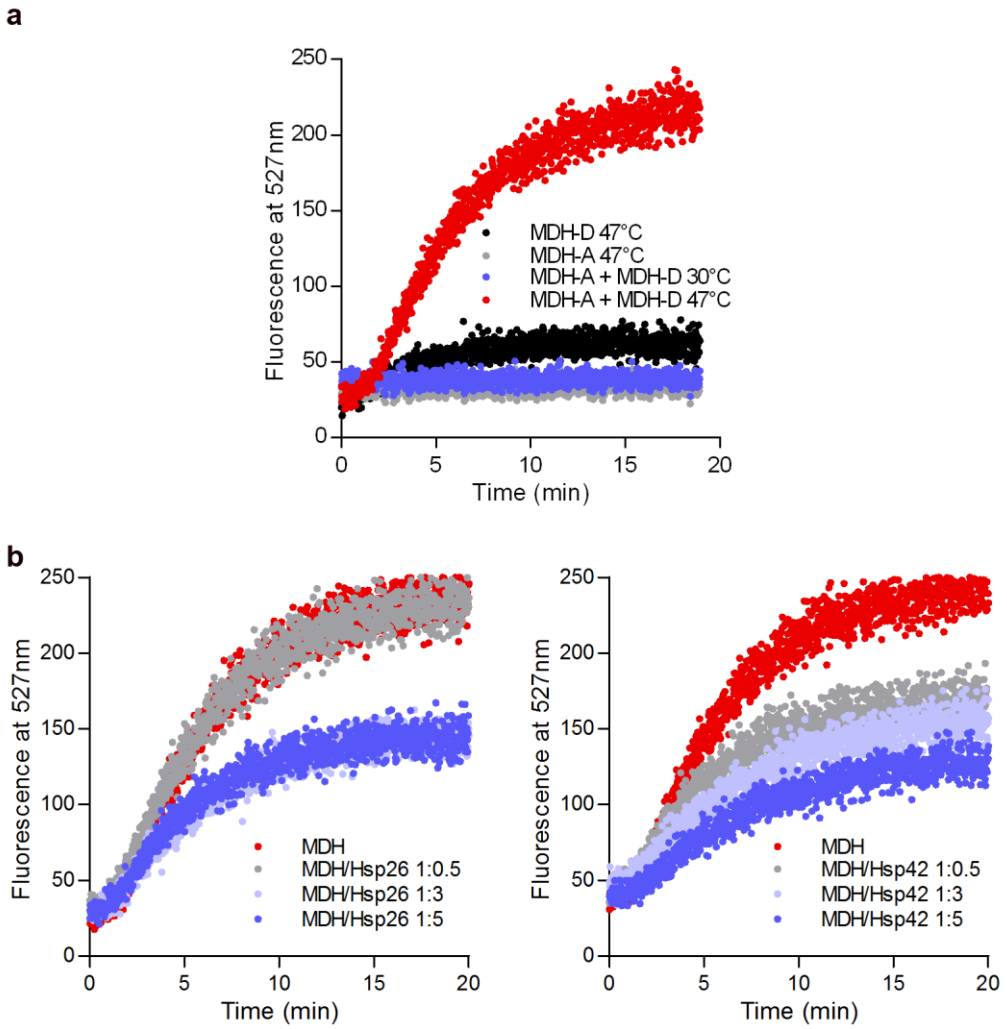

Figure 12: *Hsp26 and Hsp42 keep misfolded MDH molecules apart.* ***(a)*** *Co-aggregation of MDH-YFP (FRET donor, MDH-D) and MDH labeled with 7-diethylcoumarin-3-carboxylic acid (FRET acceptor, MDH-A) at 47°C causes specific FRET increase. A mixture of FRET donor and acceptor at 30°C or acceptor- or donor-only controls at 47°C do not result in FRET. Presence of Hsp26* ***(b)*** *or Hsp42* ***(c)*** *reduces FRET efficiencies between MDH-YFP and 7-diethylcoumarin-3-carboxylic acid-labeled MDH in a concentration-dependent manner.*

3.2.3 Hsp26 and Hsp42 globally reduce HX in sHsp-bound MDH

After having studied the effects of sHsps on the overall organization of amorphous aggregates, I wanted to investigate how sHsps change the structure of heat-induced aggregates at the molecular level. To analyze this, I performed HX of complexes generated with MDH and various ratios of yeast sHsps upon unfolding stress for 30 min at 47°C. Less peptic peptides could be identified from MDH/sHsp complexes compared to aggregated MDH (sequence coverages of 37% for Hsp26 and 52% for Hsp42). Analysis of the Ni-particles after pepsin treatment showed that reduced recovery was not due to less efficient digest (Figure 13). Rather, competing and overlapping signals from sHsp peptic peptides disturbed the MS analysis.

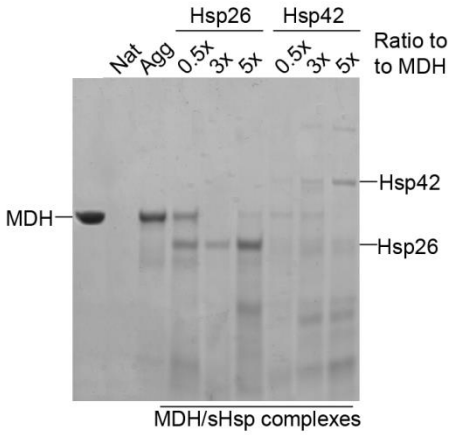

Figure 13: *Most of the sHsp-complexed MDH used in HX experiments was digested by pepsin. For HX experiments native, heat-aggregated or sHsp-complexed His_6-MDH were bound to MagneHis™ Ni-particles. After incubation in D_2O, the samples were digested by pepsin. Afterwards undigested protein was analyzed by SDS-PAGE and Coomassie staining.*

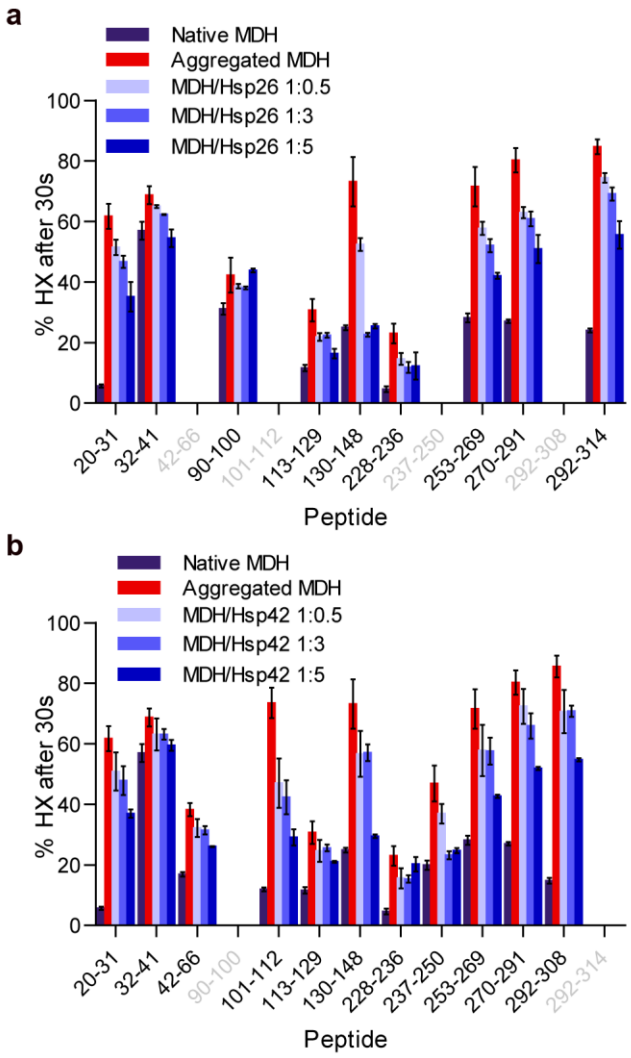

Figure 14: *Hsp26 and Hsp42 protect unfolded regions of aggregated MDH from HX. Relative proton/deuteron exchange in MDH co-aggregated with either Hsp26* ***(a)*** *or Hsp42* ***(b)*** *was determined after 30 s labeling. The data were corrected for deuteron losses due to back-exchange using a 100% deuterated control (i.e. protein in which all exchangeable protons have been replaced by deuterons). MDH/sHsp complexes were formed by incubation for 30 min at 47°C.*

MS analysis after HX revealed that mass spectra of many MDH peptides derived from MDH/sHsp complexes exist as a mixture of two populations ('bimodal distribution'), as will be explained in more detail below. First, the overall change of deuterium incorporation was determined by averaging over both populations. For both sHsps, rising concentrations during complex formation gradually increased the protection of most identified MDH peptides (Figure 14, Figure 15 and Figure 16).

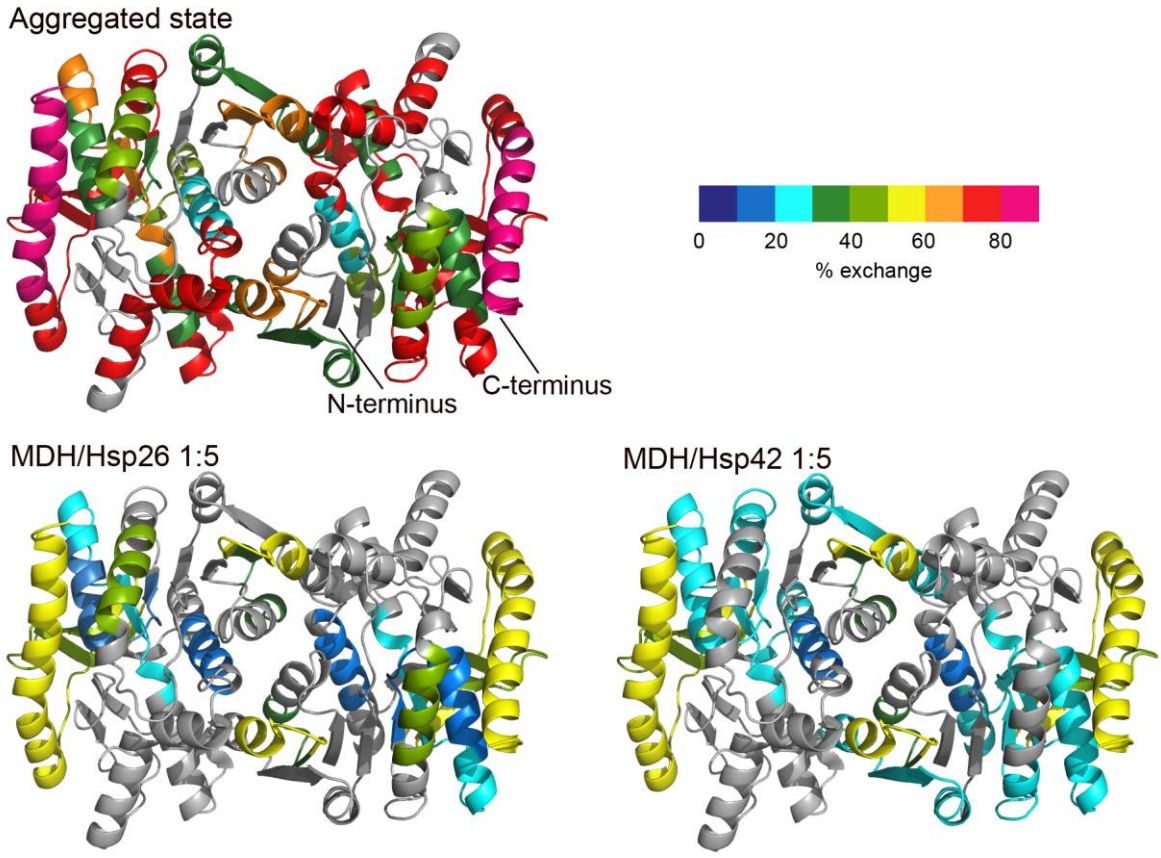

Figure 15: *HX-heat map of MDH in heat-induced MDH/sHsp complexes. Peptic peptides are colored according to their exchange behavior. Gray regions could not be identified. The ratio of sHsps vs. MDH during substrate denaturation is given.*

The degree of protection by Hsp26 and Hsp42 was similar and the effects were not locally restricted, but protected MDH peptides were distributed throughout sequence and structure. Peptide Val130-Leu148, which showed strongest protection upon complex formation, and Ser237-Glu250 are largely buried inside the hydrophobic core of native MDH (Figure 16c). A five-fold excess of sHsps resulted in native-like HX patterns of both peptides (Figure 16). There was no correlation between the hydrophobicity of a peptide and the degree of sHsp-caused protection. Some peptides (in Hsp26: Leu270-Met291, Ile292-Lys314; in Hsp42: Val130-Leu148, Phe253-Leu269, Leu270-Met291, Ile292-Glu308) showed strongly enhanced protective effects when increasing sHsp concentration from a three- to a five-fold excess during complex formation. These differences were not obvious in solubility or turbidity

experiments (Figure 8), demonstrating the potential of HX to sense conformational changes on molecular level.

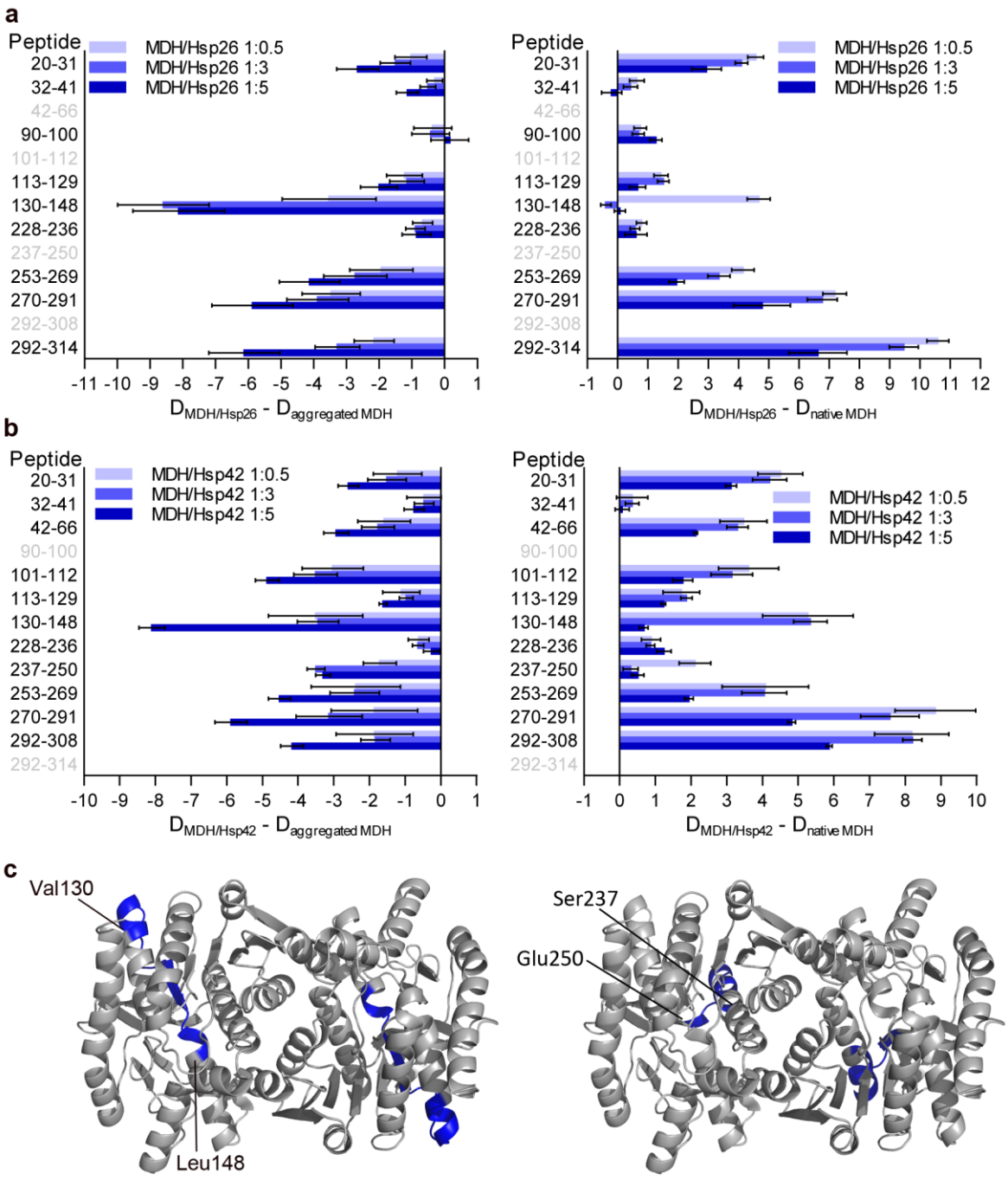

Figure 16: *Hsp26 and Hsp42 globally reduce HX in sHsp-complexed MDH.* ***(a)*** *Difference in deuteron incorporation between heat-induced MDH/Hsp26 complexes and aggregated (left panel) or native (right panel) MDH.* ***(b)*** *Difference in deuteron incorporation between heat-induced MDH/Hsp42 complexes and aggregated (left panel) or native (right panel) MDH.* ***(c)*** *Peptide Val130-Leu148, which showed strongest protection upon complex formation, and Ser237-Glu250 (both blue) are largely buried inside the hydrophobic core of native MDH. Peptides whose numbers are gray could not be detected.*

In conclusion, the association with sHsps globally protects unfolded MDH from HX. Protection could arise from both: Binding of sHsps to strongly exchanging unfolded regions in denatured MDH and from preservation of native conformation due to the

influence of sHsps. However, HX was still faster compared to native MDH, suggesting that sHsp-bound MDH is partially folded and more flexible (Figure 16).

3.2.4 sHsp-bound MDH displays native-like structures

As suggested above, protection of sHsp-complexed MDH might indicate preserved native conformation. Intriguingly, HX analysis revealed evidence for residual native structure: Bimodal peak distributions were found for many peptic peptides derived from sHsp-complexed MDH, reflecting the existence of two different structural states. We observed a low exchanging population, whose position was similar to the peak positions of the peptide from native MDH ('native-like'), and a high exchanging population, which resembled the aggregated state ('aggregate-like') (Figure 17). Bimodal distributions were not detected for peptides derived from native MDH and only to a minor extent for few peptides of aggregated MDH (Leu20-Leu31, Ala42-His66). With increasing concentrations of sHsps present during denaturation, there is a shift of peptides from the aggregate-like to the native-like population (Figure 18). This trend was found to a varying degree for all identified peptides exhibiting a bimodal distribution (see Appendix Figure 54). Therefore, the native-like HX pattern can be attributed to the promotion of native-like structures in MDH caused by association with sHsps upon heat-stress. MDH peptides Val130-Leu148 (bound to Hsp26 or Hsp42) and Ile113-Glu129 (bound to Hsp26) were almost completely shifted to native-like states, when using a five-fold excess of sHsps. Notably, these peptides are largely buried in the interior of native MDH, suggesting that MDH retains substantial tertiary structure in complex with sHsps (Figure 19).

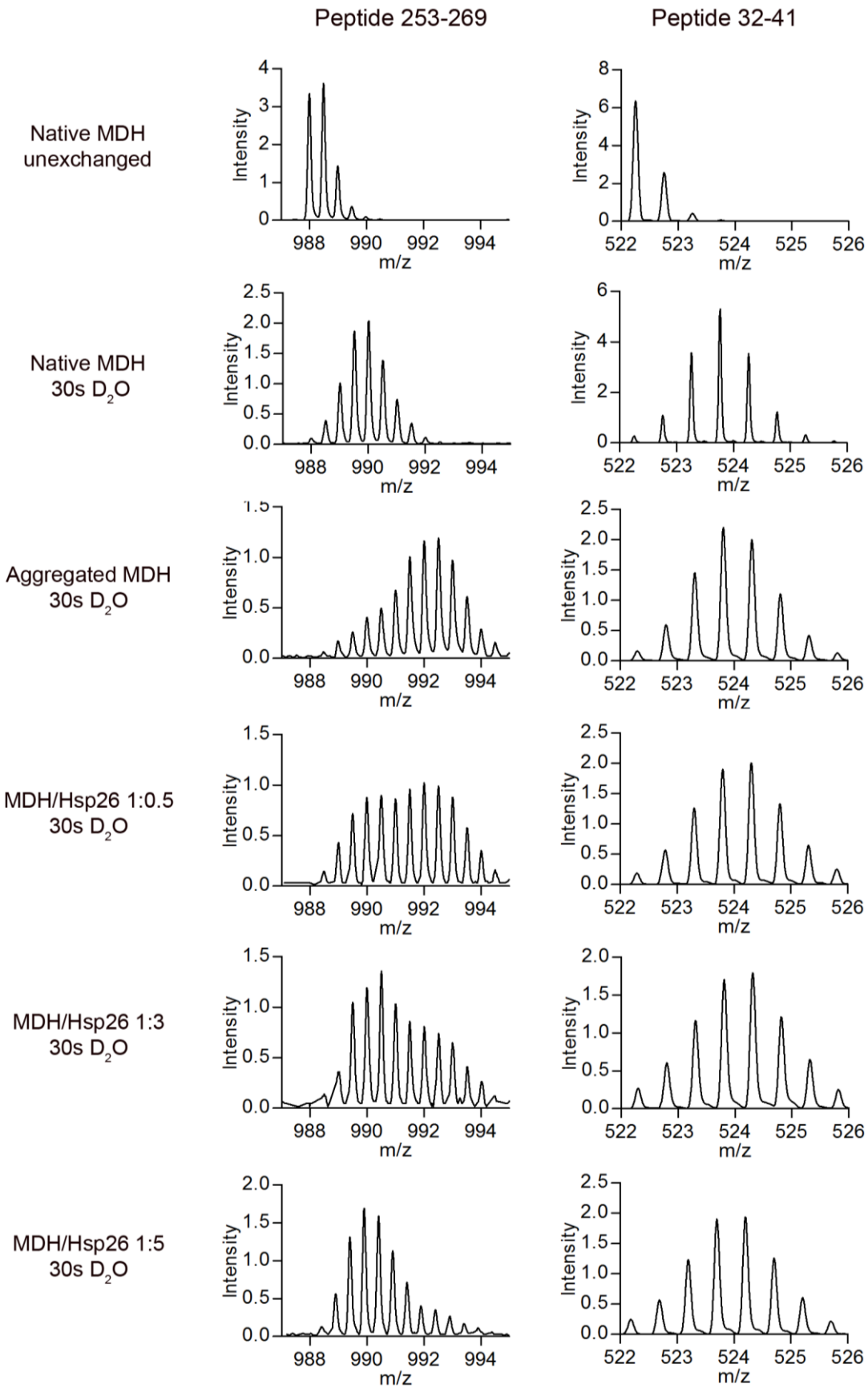

Figure 17: *sHsps stabilize segments of bound MDH in a native-like state. Mass spectra of MDH peptides in the native, aggregated or Hsp26-complexed state after 30 s D_2O incubation at 30°C. The left panels show a representative peptide displaying a bimodal distribution after HX when complexed with sHsps, whereas the peptide shown in the right panels exists as a single population.*

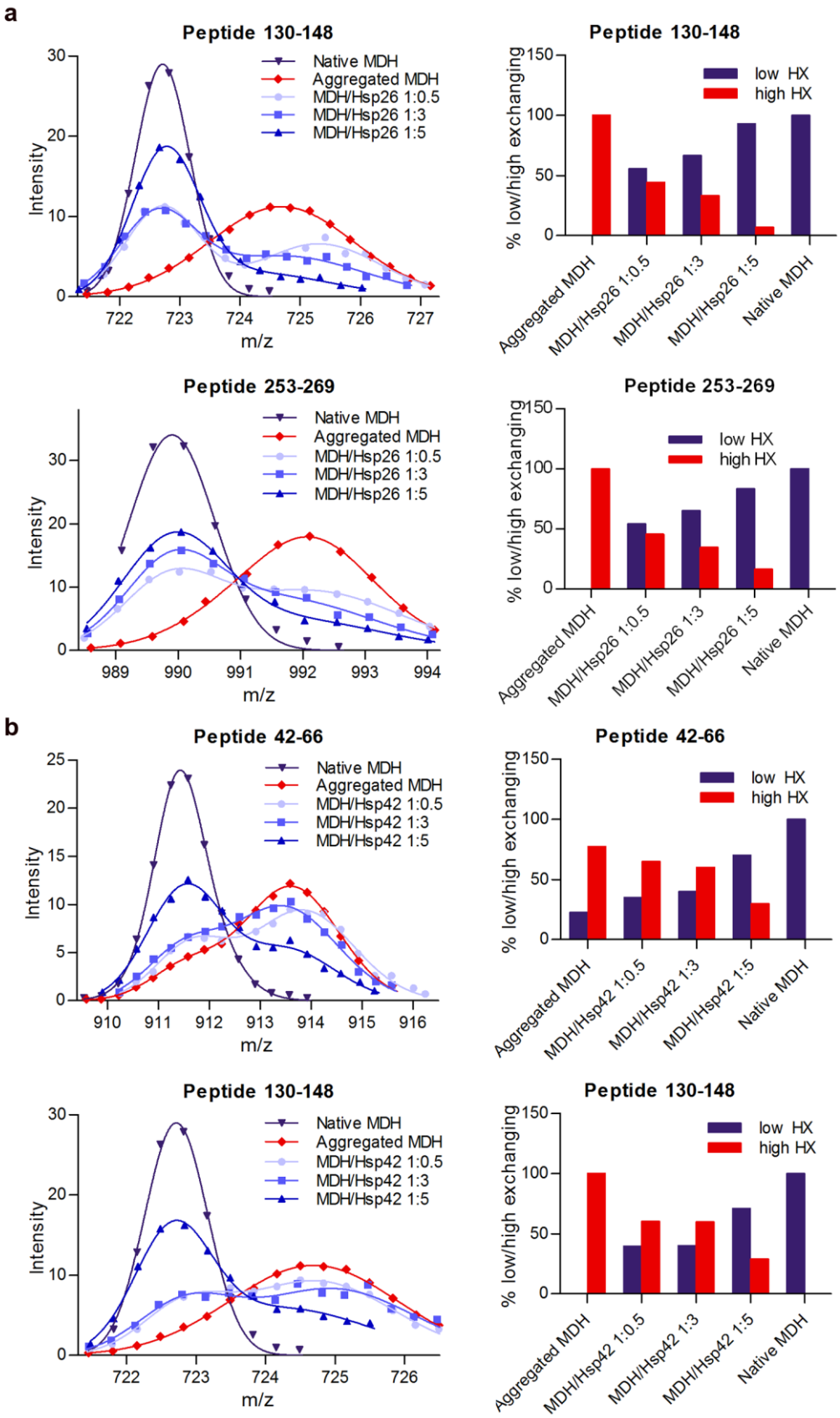

Figure 18: *Concentration-dependent stabilization of native-like structures in sHsp-complexed MDH. Bimodal distribution of isotope peaks of indicated MDH peptides derived from MDH/Hsp26* ***(a)*** *and MDH/Hsp42* ***(b)*** *complexes. Left panels: Intensity versus m/z diagrams for different peptic MDH peptides after 30 s HX at 30°C. Right panels: Fractions of native-like and aggregate-like populations calculated for respective peptides. For each sHsp two representative spectra are shown.*

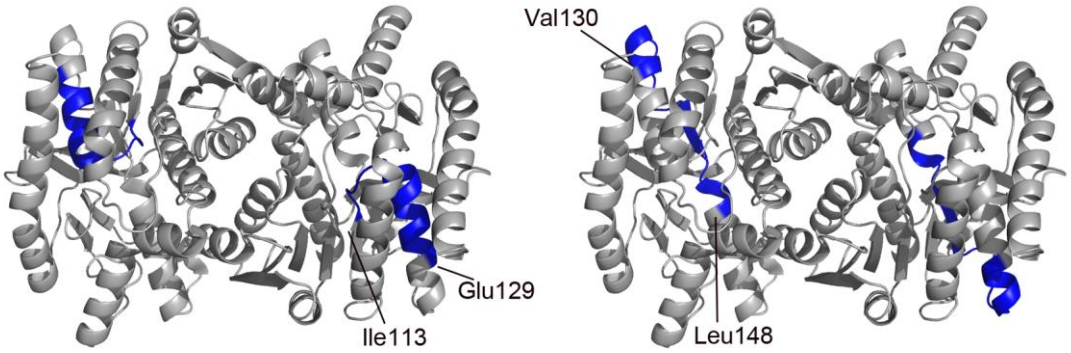

Figure 19: *Localization of peptides Ile113-Glu129 and Val130-Leu148 (blue) in the native MDH dimer structure. Both peptides show almost exclusively native-like HX pattern when complexed with sHsps.*

An alternative explanation for native-like HX patterns would be partial MDH refolding after spontaneous release from MDH/sHsp complexes. In order to test for this possibility, GroEL-D87K (GroEL-trap) was used. This is an ATPase-deficient variant, which traps misfolded proteins (Weber-Ban et al., 1999). Tritium-labeled MDH was heat-denatured in presence or absence of sHsps, incubated with GroEL-trap and separated by size exclusion chromatography (Figure 20). MDH was not transferred from MDH/sHsp complexes to GroEL-trap, excluding spontaneous dissociation of misfolded MDH conformers.

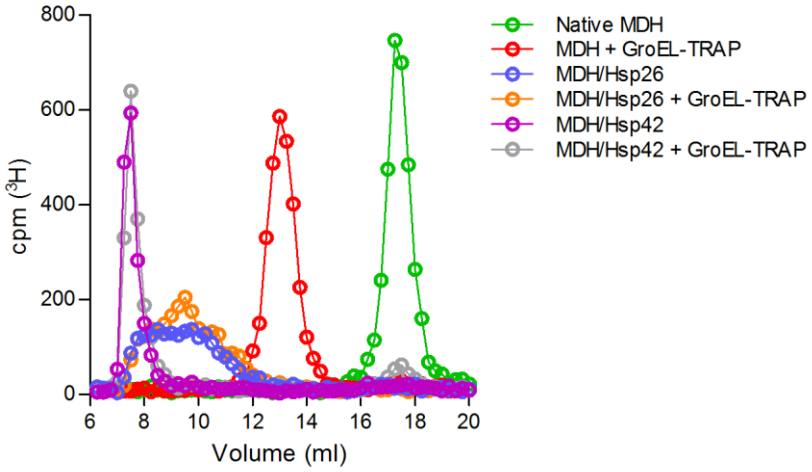

Figure 20: *MDH does not spontaneously dissociate from MDH/Hsp26 and MDH/Hsp42 complexes. 1 µM ^{3}H-MDH and 5 µM sHsps were heat treated for 30 min at 47°C. The formed sHsp/protein complexes were incubated for 10 min at 30°C with 2 mM ATP in presence or absence of 14 µM GroEL-D87K (GroEL-trap). As control ^{3}H-MDH was denatured in presence of 2 mM ATP and 14 µM GroEL trap (30 min at 47°C). All samples were separated by size exclusion chromatography and collected fractions were quantified by scintillation counting (open circles).*

Taken together, these findings demonstrate that Hsp26 and Hsp42 form stable complexes with heat-denatured MDH and the association with sHsps keeps parts of MDH in a native-like state.

3.2.5 Hsp42 suppresses the formation of tight aggregates and promotes native-like folds

Another, completely independent technique that is suitable for testing the effects of chaperones on protein aggregation is the optical-tweezer single-molecule technology.

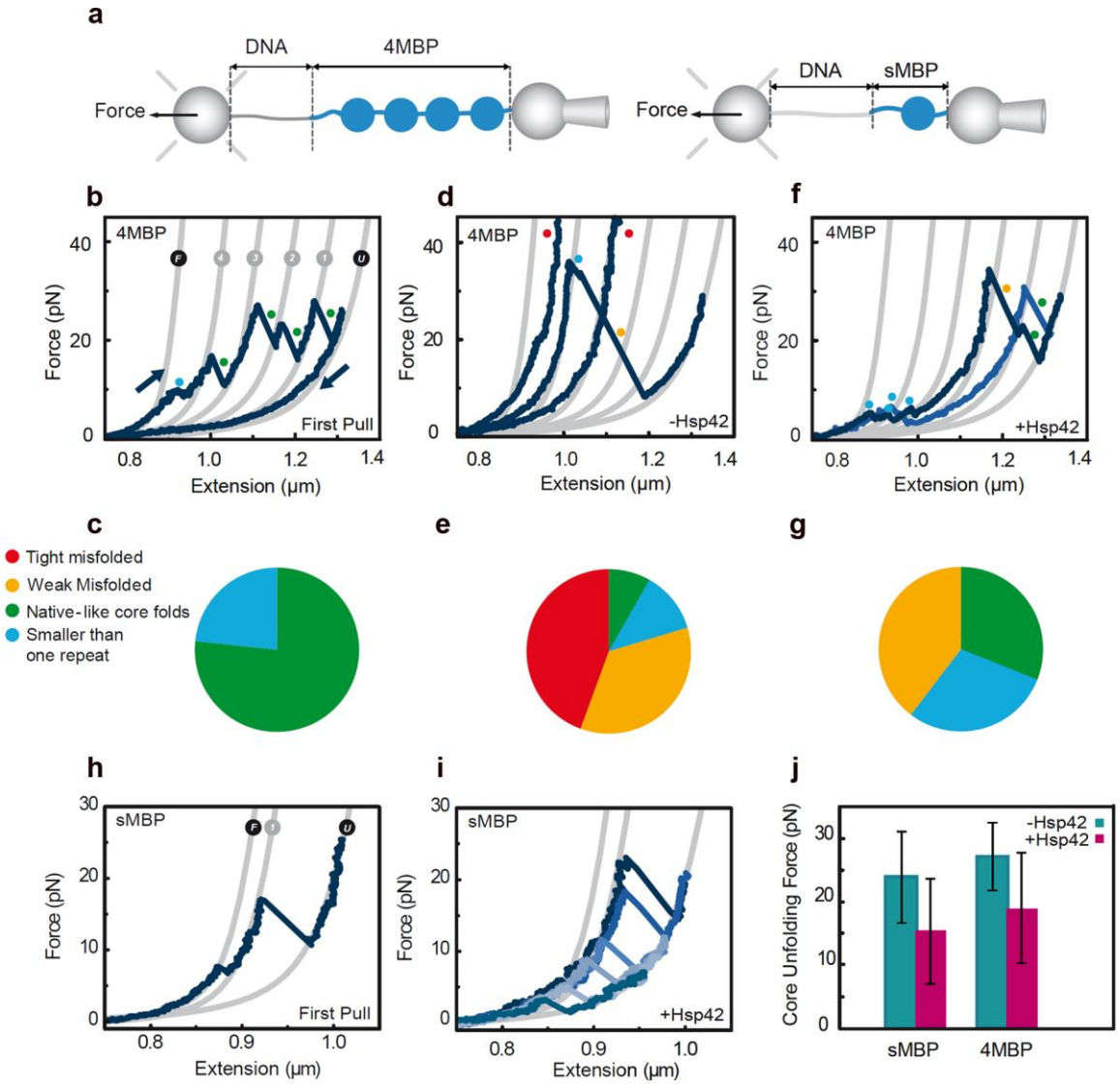

Figure 21: *Hsp42 suppresses the formation of tight aggregates and promotes native-like folds.* ***(a)*** *Setup for single-molecule experiments: MBP constructs are tethered between two beads by using a DNA spacer.* ***(c)***, ***(e)*** *and* ***(g)*** *show statistics on the unfolding events.* ***(b)*** *Force-extension curves for the first stretching-relaxation of natively-folded 4MBP. Gray lines represent the unfolding stages predicted by molecular dynamics simulations from the folded (F) to the unfolded (U) state. During stretching four native-like core unfolding events (green) (4→3→2→1→U) are observed.* ***(d)*** *After relaxation, subsequent pulling predominantly shows no unfolding (red) which indicates tight misfolding between domains. Sometimes also weak misfolding (yellow) or the unfolding of structures which are smaller than one repeat (blue) is observed.* ***(f)*** *In presence of Hsp42 (5μM), second or subsequent stretching mostly showed native-like unfolding, but no tight misfolds.* ***(h)-(i)*** *Stretching-relaxation experiments for sMBP.* ***(h)*** *Unfolding curve for natively-folded sMBP.* ***(i)*** *Repetitions of second pulls in presence of Hsp42 shows either native-like unfolding events or the unfolded sMBP remained in the unfolded state (curve not shown).* ***(j)*** *Statistics on core unfolding force show that presence of Hsp42 decreases the core unfolding force for both 4MBP and sMBP. Fatemeh Moayed (AMOLF institute, Amsterdam) performed the single-molecule experiments and prepared this figure.*

In this approach, four repeats of Maltose Binding Protein (4MBP) are tethered between two spheres by using a DNA spacer to prevent bead-bead interactions. Stretching the 4MBP-construct by pulling on one bead results in a force which is measured on the second bead (Figure 21a). The first stretching of the folded 4MBP construct starts with a gradual unfolding transition. This is followed by the distinct unfolding of the four remaining core structures, which is apparent by sudden changes in extension in the force-extension curves (Figure 21b and c). After relaxation to low force, predominantly tightly aggregated or weakly misfolded structures are formed. This becomes obvious during subsequent pulling during which the constructs either cannot be unfolded (tightly misfolded species) or only by applying high forces (weakly misfolded species) (Figure 21d and e). Fatemeh Moayed (AMOLF institute, Amsterdam) did single-molecule experiments in presence of Hsp42 to study its influence on MBP aggregation. Testing Hsp26 would require heat-induced activation, which is not possible in this setup. The first stretching curve was similar in presence and absence of Hsp42. Thus, Hsp42 does not bind to native MBP, or, if it does, it cannot stabilize MBP against forced unfolding. Subsequent pulls, however, show two important effects of Hsp42 (Figure 21f and g). Firstly, although weak misfolds were still present, tight aggregates were not detected any more, showing that Hsp42 prevents the formation of non-native contacts. Secondly, the portion of structures with native-like unfolding features increased substantially. Thus, interactions with Hsp42 promote native-like structures.

To further investigate the nature of the Hsp42-client interaction, the experiment was repeated using a single-MBP construct, which can refold but cannot aggregate during relaxation. After the first stretching, 1MBP is allowed to relax, and either the core structure of MBP refolds fully or it stays unfolded, while its carboxyterminal part (core terminus) does not refold at all (transition from folded (F) to (1)) (Figure 21h). The second pull reports on which of those two options has occurred (termed as ‘native-like unfolding’ when 1MBP fully refolded). Similarly, in presence of Hsp42, the second pull after unfolding and relaxation of 1MBP indicated either no refolding or a native core fold (Figure 21i).

Interestingly, for both, the 4MBP- and the 1MBP-construct, less unfolding force was required to unfold the refolded core states in presence of Hsp42 (Figure 21j). This observation suggests that Hsp42 bound to and destabilized the core structure, possibly by binding to small unfolded peptide segments at the core termini, or by interfering with the core fold in a different manner.

Altogether, these findings provide further evidence that Hsp42 binds near-native folded structures.

3.3 The NTE of Hsp26 or Hsp42 and the unfolded C-terminus of heat-aggregated MDH represent the major interaction sites

In order to further specify the interactions between Hsp26 or Hsp42 and heat-misfolded substrates, I employed HX and crosslinking approaches. In addition, HX might reveal conformational changes within sHsps upon substrate binding.

3.3.1 HX of Hsp26 and Hsp42 upon substrate binding

In HX experiments I analyzed Hsp26 and Hsp42 in their free states and complexed with MDH substrate.

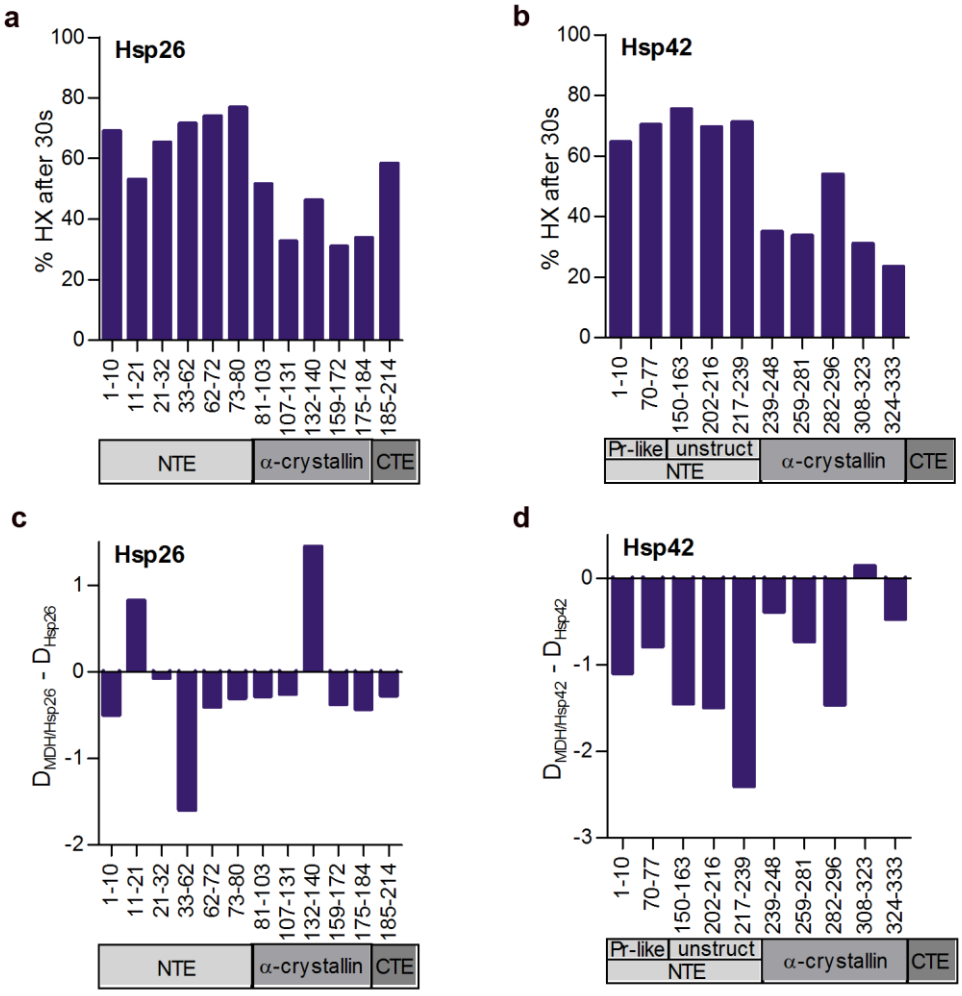

Figure 22: *Deuteron incorporation into sHsps after 30 s incubation in D_2O at 30°C. HX patterns of free Hsp26* ***(a)*** *or Hsp42* ***(b)*** *and difference in deuteron incorporation between MDH-complexed and free Hsp26* ***(c)*** *or Hsp42* ***(d)*** *are shown. The data were corrected for deuteron losses due to back-exchange using a 100% deuterated control (i.e. protein in which all exchangeable protons have been replaced by deuterons). NTE: N-terminal extension, CTE: C-terminal extension, Pr-like: Prion-like domain, unstr: unstructured domain.*

During complex formation an excess of sHsps was used yielding soluble complexes. Free sHsps were separated via size exclusion chromatography. Fractions containing

MDH/sHsp complexes were combined, incubated with MagneHis™ Ni-Particles and HX was performed at 30°C using the bead-bound material. After 30 s the D_2O-buffer was removed, low pH quench buffer containing pepsin was added and the tubes were transferred to ice. After 1 min pepsin digest, the peptides were injected into the mass spectrometer coupled HPLC setup.

For both sHsps N- and C-terminal extensions (CTE was only detected for Hsp26) displayed stronger proton/deuteron exchange than the α-crystallin domains, indicating high flexibility of those regions (Figure 22a and b). Upon substrate interaction, changes in HX profiles were noticed for both sHsps (Figure 22c and d). In Hsp26 two peptides became deprotected, indicating changed conformational states with increased flexibility. This is Phe11-Phe21 within the NTE and Val132-Leu140, a segment partially comprising the loop connecting β-strands 5 and 7 in the ACD (Figure 22 and Figure 23).

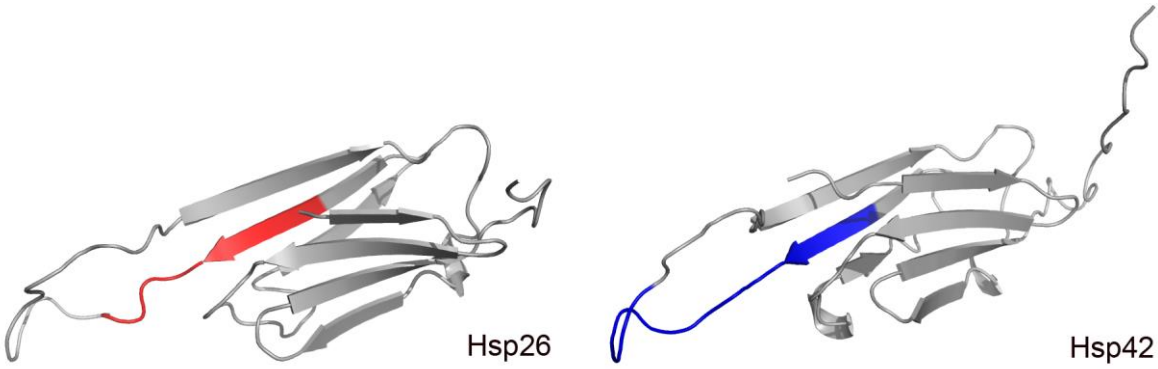

Figure 23: *Differences in HX exchange in sHsps upon substrate binding. Homology model for the α-crystallin domain of Hsp26 and Hsp42 based on the structure of wheat Hsp16.9 (PDB ID 1GME). Upon MDH binding Val132-Leu140 of Hsp26 is substantially deprotected (red), whereas Ile282-Phe296 of Hsp42 showed increased HX protection (blue).*

Increased HX protection was detected for Tyr33-Leu62 in the NTE, caused either by conformational changes or direct substrate interaction. For Hsp42 increased HX protection was noticed throughout the NTE and parts of the ACD with Ala217-Asp239 and Ile282-Phe296 showing the strongest effects for the respective domains (Figure 22d). Remarkably, this ACD segment corresponds to the one of Hsp26 showing increased HX (Val132-Leu140), suggesting that this loop of the ACD is particularly sensitive to substrate complexation (Figure 23).

In conclusion, the NTEs of Hsp26 and Hsp42 seem primarily involved in substrate interaction.

3.3.2 DSS-crosslinking of heat-induced MDH/sHsp complexes

HX of MDH/sHsp complexes suggested that the NTE is the major substrate binding site in Hsp26 and Hsp42. To more precisely identify the interaction sites between

MDH and sHsps, DSS-crosslinking experiments were performed and MDH-sHsp crosslinks were analyzed by MS (Appendix Table 6). The use of a mixture of deuterated and undeuterated DSS facilitated the identification of crosslinked peptides. DSS crosslinks lysine residues with maximal Cα-Cα-distances of less than 30 Å.

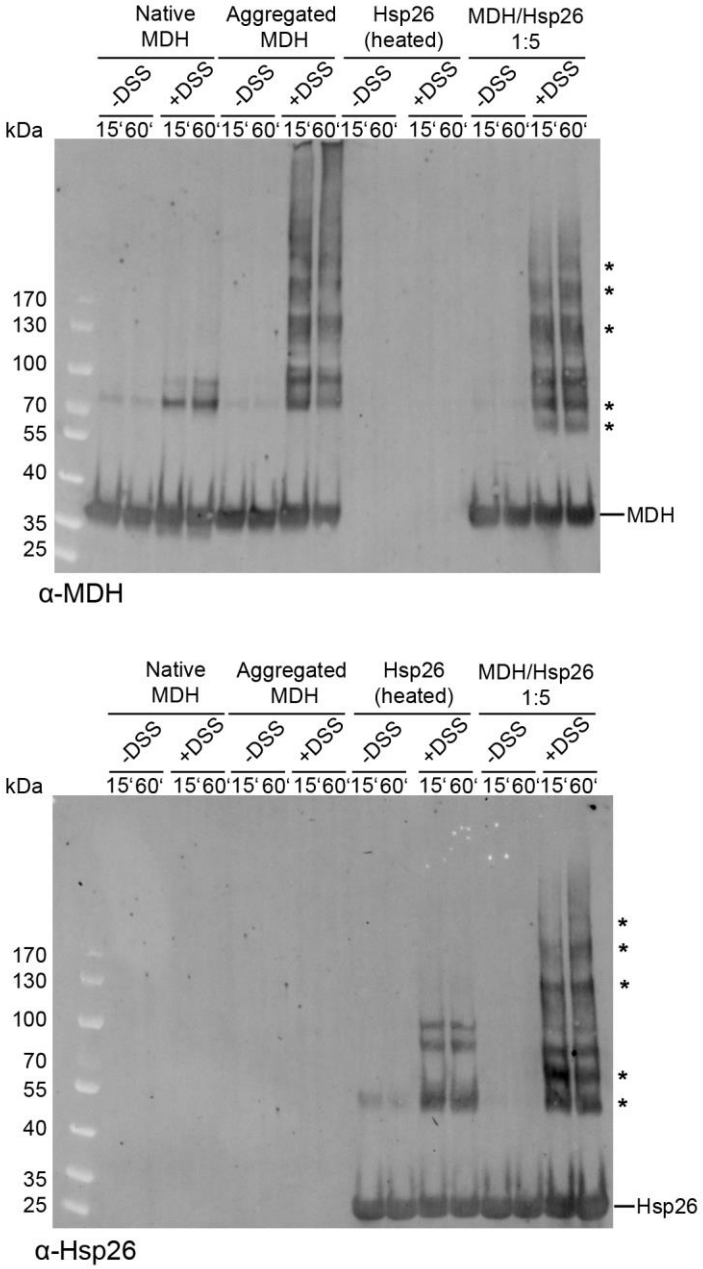

Figure 24: *DSS-crosslinking of native MDH, MDH aggregates and MDH/sHsp complexes. MDH (native or aggregated) and MDH/Hsp26 1:5 complexes were incubated with or without DSS at 30°C for 15 or 60 min. Crosslink products were analyzed by western blotting using MDH and Hsp26 specific antibodies. Crosslinks between MDH and Hsp26 are indicated by asterisks.*

In pre-experiments DSS crosslinking followed by western blot analysis revealed multiple crosslinked products for complexes between MDH and Hsp26 (Figure 24).

Accordingly, MS analysis could identify various MDH-Hsp26 crosslinks (Figure 25 and Appendix Table 6).

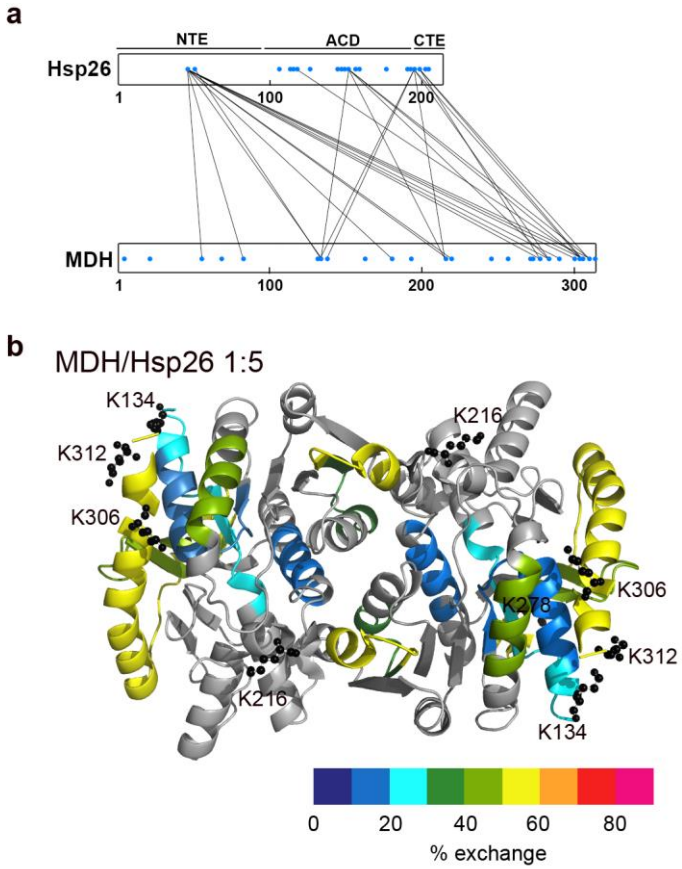

Figure 25: *Specific interactions of Hsp26 with exposed, flexible MDH segments. MDH-Hsp26 interaction sites were determined by DSS crosslinking and MS analysis.* ***(a)*** *Linear representation of crosslinks between lysine residues (blue dots) of Hsp26 and MDH. NTE: N-terminal extension, ACD: α-crystallin domain, CTE: C-terminal extension.* ***(b)*** *HX-heat map of MDH from the heat-induced MDH/Hsp26 (1:5 ratio) complex. Peptic peptides are colored according to their exchange behavior. Gray regions could not be detected. Lysine residues of MDH that were crosslinked to two or more lysines of Hsp26 are presented as balls and sticks.*

Involved residues comprised only a subset of theoretically available lysines (indicated by blue dots in Figure 25a), demonstrating specificity of detected interaction sites. Hsp26 crosslinked to specific lysines within MDH (Lys134, Lys 216, Lys278, Lys306 and Lys312), with lysine residues 134, 306, 312 clustered in close proximity in the structure of native MDH. All crosslinked lysines are located in regions which showed strong deprotection in the aggregated state, and thus large unfolding. HX of those peptides was strongly decreased upon sHsp binding, but still stayed high compared to other MDH peptides (Figure 25b). This holds in particular true for Ile292-Met314, located in an exposed C-terminal α-helix, which contains two major Hsp26 crosslink sites. In Hsp26 lysine residues of all three domains were crosslinked to MDH (Figure 25a). Both lysines of the NTE, two out of twelve and two out of six lysines of the ACD and the CTE were crosslinked to MDH substrate, respectively. ACD-MDH crosslinks were only observed at higher excess of Hsp26, suggesting that the ACD offers

additional substrate binding sites (Appendix Table 6). Most crosslinks were formed to the NTE, with Lys45 as a major substrate binding site, and Lys50.

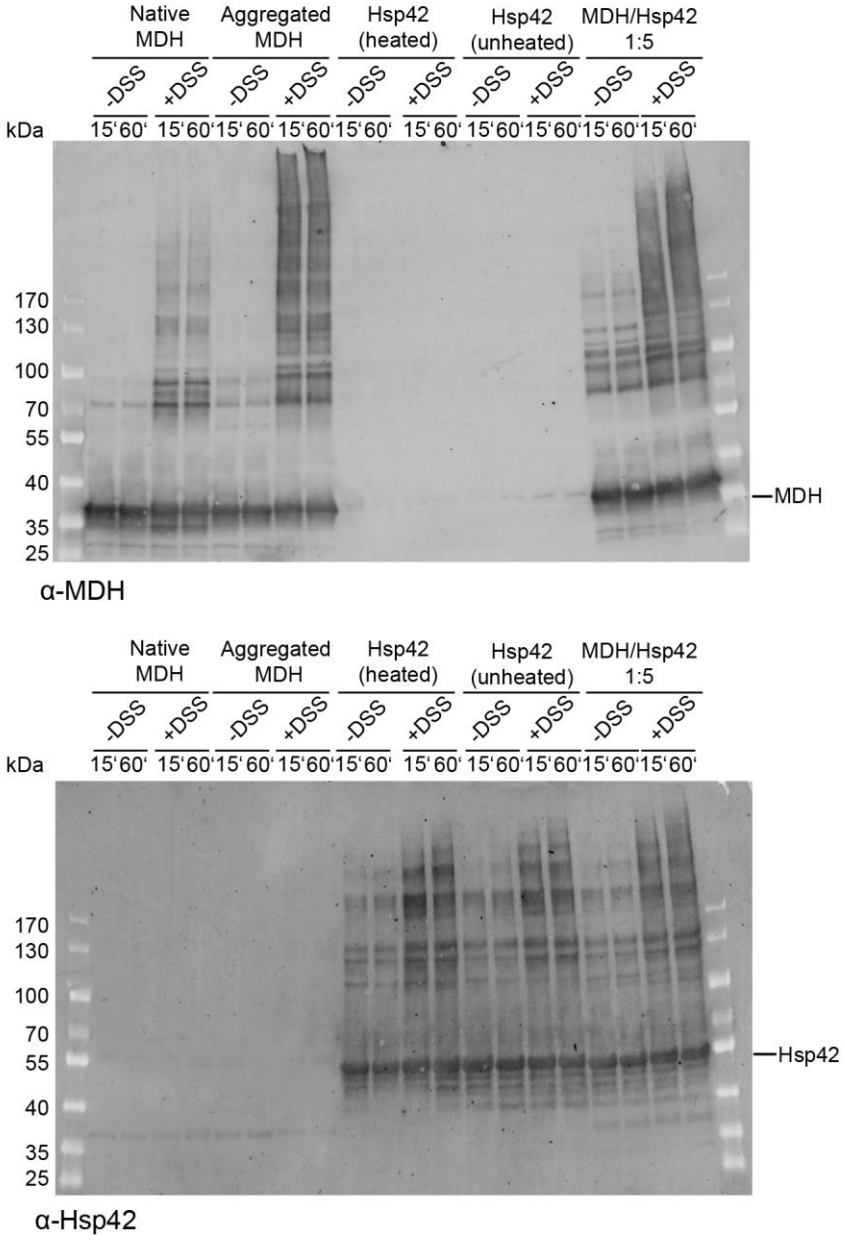

Figure 26: *DSS-crosslinking of native MDH, MDH aggregates and MDH/sHsp complexes. MDH (native or aggregated) and MDH/Hsp42 1:5 complexes were incubated with or without DSS at 30°C for 15 and 60 min. Crosslink products were analyzed by western blotting using MDH and Hsp42 specific antibodies.*

Notably, Lys45 is located in the central thermosensor region of Hsp26 NTE, which undergoes heat-shock induced conformational changes thereby activating Hsp26 (Franzmann et al., 2008). Other major crosslink sites to substrates include Lys151, located in a loop connecting β5 and β7 in the ACD and Lys195 and Lys198 in the CTE (Appendix Table 6).

For Hsp42, DSS-crosslinking with MDH in heat-induced complexes followed by western blot analysis did not show distinct crosslink bands, but only a slightly

changed smear of crosslink products compared to aggregated MDH or Hsp42 alone (Figure 26). MS determination identified multiple MDH-MDH and Hsp42-Hsp42 crosslink products but no single MDH-Hsp42 crosslink. Considering that the N-terminal 171 aa of Hsp42 do not contain lysine residues, it appears likely that this region is primarily involved in substrate interaction.

3.4 The prion-like domain of Hsp42 couples substrate binding and CytoQ formation

Previously described HX and crosslinking experiments indicated that Hsp42 binds substrates predominantly via its N-terminal region. Notably, compared to all known sHsps the NTE of Hsp42 is unusually elongated. The finding, that this region is crucial for the formation of cytosolic aggregates (CytoQ) *in vivo* (Specht et al., 2011) (see chapter 1.2.1.7), prompted us to further explore the features of this unique domain.

3.4.1 Hsp42 NTE harbors two intrinsically disordered subdomains

Interestingly, based on bioinformatic prediction the NTE of Hsp42 comprises two types of so-called intrinsically disordered domains (IDD) (Figure 27).

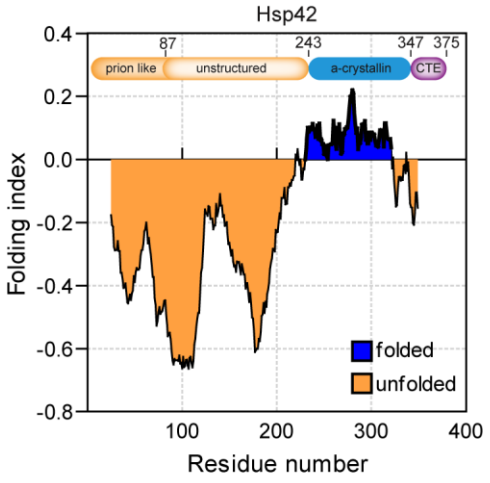

	Prion-like	unstruct.	ACD	CTE
% Y,F	20	3	10	4
% I,L,V	8	10	27	18
% Q,N	17	12	6	11
% K,R	7	12	14	14
% D,E	2	25	15	32

Figure 27: *Folding index of Hsp42 according to its primary sequence. According to its sequence features, Hsp42 harbors two intrinsically disordered domains (IDD): an N-terminal 'prion-like domain' (aa 1-86), which is enriched in Gln/Asn and Tyr residues, and an 'unstructured domain' (aa 87-242), containing mainly acidic aa and few large hydrophobic and aromatic residues. unstruct: unstructured domain; ACD: α-crystallin domain; CTE: C-terminal extension.*

IDDs are characterized by low hydrophobicity, high mean charge and often low sequence complexity (Malinovska et al., 2012), and they are able to self-interact and undergo multiple weak interactions with other cellular factors.
The first type of IDD within Hsp42 is called a 'prion-like domain' and includes the first 86 aa. This is followed by a region that I termed as 'unstructured domain', the second type of IDD (aa 87-242) (Figure 27). The prion-like domain is enriched in Gln/Asn and Tyr residues, whereas the unstructured domain is enriched for acidic amino acids and hardly contains hydrophobic and aromatic residues (Alberti et al., 2009). Which of both subdomains is crucial for CytoQ formation, and if this is directly linked to substrate binding remained unexplored.

3.4.2 The prion-like domain of Hsp42 mediates substrate interaction and CytoQ formation

We set out to dissect the functions of the prion-like and the unstructured subdomain of Hsp42 NTE. For this purpose two Hsp42 deletion variants were generated, lacking either subdomain. The effects on CytoQ formation and Hsp42 localization were studied *in vivo* (Stephanie Miller, unpublished data). I purified Hsp42 wt and both deletion variants and characterized them *in vitro* (chapters 3.4.3-3.4.7).

The results of the *in vivo* experiments performed by Stephanie Miller are summarized in Table 1. Deletion of the first 86 residues, corresponding to the predicted length of the prion-like domain, produced an Hsp42 variant which was unstable upon expression in yeast cells. Hence, we expressed an Hsp42Δ1-99 variant, omitting a C-terminal highly acidic peptide, and an Hsp42Δ100-242 variant, lacking almost the entire unstructured domain. As described in the introduction chapter, proteotoxic stress leads to the appearance of cytosolic (CytoQ) and nuclear (INQ) aggregates in yeast cells.

Table 1: *Overview of the effects on CytoQ formation, localization of Hsp42 and substrate binding caused by deleting the prion-like or the unstructured subdomain of Hsp42 NTE.*

	CytoQ	**Co-localization with**		**Substrate binding**
		INQ	**CytoQ**	
Hsp42 wt	yes	no	yes	yes
Hsp42Δ1-99	no	no	no	no
Hsp42Δ100-242	yes, but smaller and more	yes	yes	yes, increased binding capacity

Live cell imaging, using mCherry-VHL as aggregation-prone reporter, showed, that the deletion of Hsp42 abrogates CytoQ formation, only producing a single INQ inside

the nucleus (Specht et al., 2011). Expression of Hsp42Δ1-99 in *hsp42Δ* cells did not restore CytoQ formation and exclusive INQ formation was detected. Accordingly, Hsp42Δ1-99 did not co-aggregate or change cellular localization during heat stress but remained diffusely distributed. The Hsp42Δ100-242 variant was able to restore the generation of cytosolic aggregates. However, smaller and more cytosolic aggregates were observed compared to Hsp42 wt, suggesting defects in aggregate coalescence or differences in substrate interaction. In contrast to Hsp42 wt, Hsp42Δ100-242 co-localized with both, CytoQ (as for Hsp42 wt) and INQ. In addition, this deletion variant was already present in the nucleus at non stress conditions, whereas Hsp42 wt is excluded from the nucleus. In order to test substrate binding capacities of Hsp42 variants, *in vivo* co-precipitations were performed (Stephanie Miller, unpublished data). Hsp42Δ1-99 could not bind any substrate, explaining the loss of the ability to form CytoQ. In contrast, increased amounts of misfolded mCherry-VHL co-precipitated with Hsp42Δ100-242 compared to Hsp42 wt, indicating a higher substrate binding capacity.

In summary, the results showed that the prion-like domain of Hsp42 couples substrate binding and CytoQ formation, whereas the unstructured domain seems to have regulatory functions, controlling Hsp42 localization and the substrate binding capacity.

3.4.3 Hsp42 oligomerization depends on the prion-like domain

To better understand how the deletions of either subdomain affect the structure of oligomeric Hsp42 and to study their influence on chaperone activity, Hsp42 wt and both deletion variants were purified. Oligomer sizes were determined by static light scattering (Figure 28a). Hsp42 wt was a mixture of 8-14mers (325-575 kDa), with 10mers representing the most populated state. This oligomer size is in agreement with previous reports (12-16mers) in which the molecular weight was determined by size exclusion chromatography (Haslbeck et al., 2004). Hsp42Δ100-242 formed higher oligomers consisting of 28-38 subunits with 36mer as most populated state, while Hsp42Δ1-99 contained 4-6mers (4mers as most populated state). Negative stain electron microscopy confirmed that Hsp42Δ100-242 oligomers (20-25 nm diameter) are bigger and also more regularly shaped than Hsp42 wt oligomers (15-20 nm diameter) (Figure 28b).

Thus, deletion of the prion-like domain strongly reduces oligomer size, suggesting a major function in oligomerization. In contrast, the deletion of the unstructured domain promotes self-interactions, possibly mediated by the prion-like domain.

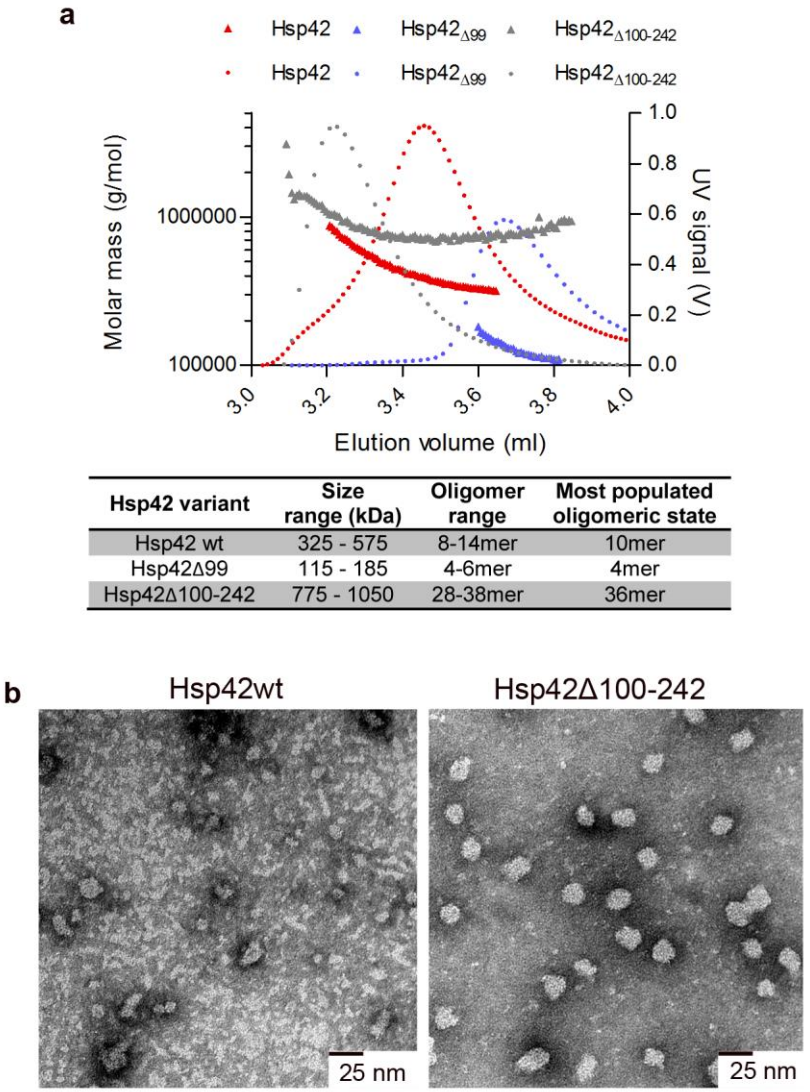

Hsp42 variant	Size range (kDa)	Oligomer range	Most populated oligomeric state
Hsp42 wt	325 - 575	8-14mer	10mer
Hsp42Δ99	115 - 185	4-6mer	4mer
Hsp42Δ100-242	775 - 1050	28-38mer	36mer

Figure 28: *The prion-like domain is involved in Hsp42 oligomerization.* ***(a)*** *The oligomeric states of Hsp42 wt and Hsp42 deletion constructs were determined by static light scattering measurements.* ***(b)*** *Negative stain electron microscopy. Hsp42Δ100-242 forms more regular and bigger oligomers compared to Hsp42 wt.*

Differences in the oligomeric states could result from conformational changes within Hsp42 variants. To test for structural properties, HX experiments were performed. Similar HX patterns were observed for all identified peptides in Hsp42 wt and Hsp42 variants (Figure 29), indicating that deletion of the N-terminal subdomains did not change the conformational state of Hsp42.

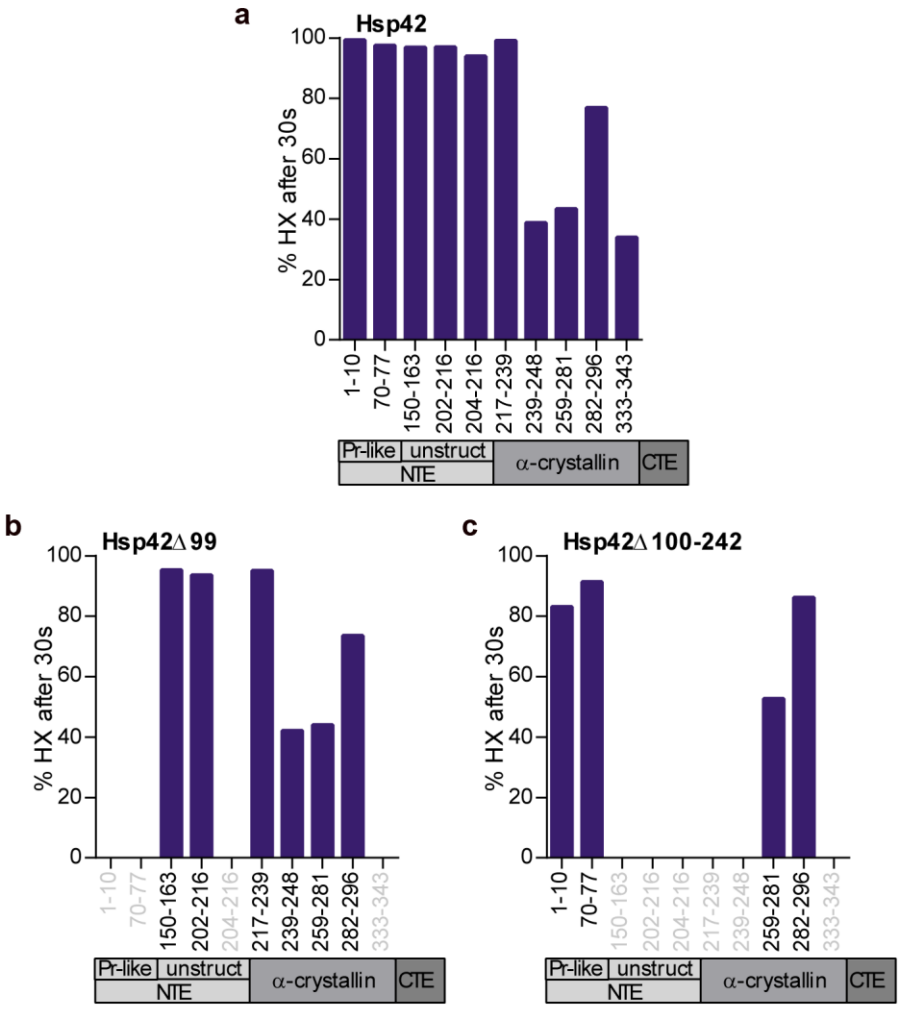

Figure 29: *The HX pattern is similar for all Hsp42 variants. Relative proton/deuteron exchange in Hsp42 wt and Hsp42 deletion constructs after 30 s of incubation in D_2O at 30°C. The data were corrected for deuteron losses due to back-exchange using a 100% deuterated control (i.e. protein in which all exchangeable protons have been replaced by deuterons).*

3.4.4 Surface-exposed hydrophobic patches are presented by the prion-like domain

We further characterized Hsp42 wt and deletion variants by incubation with 8-Anilinonaphthalene-1-sulfonic acid (ANS), a fluorescent probe, which binds to hydrophobic surfaces leading to increased ANS fluorescence. While Hsp42 wt and Hsp42Δ100-242 enhanced fluorescence to a similar extent, Hsp42Δ1-99 showed much reduced fluorescent signal indicating a great loss of hydrophobic surfaces (Figure 30). Since hydrophobic surfaces are supposed to bind misfolded proteins, these results are consistent with the suggestion that the prion-like domain is the major site for substrate interaction and triggers aggregate assembly.

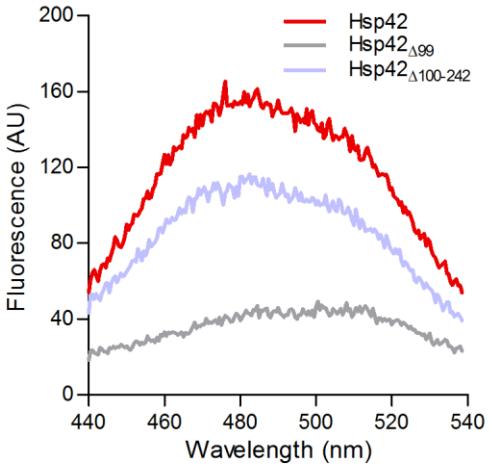

Figure 30: *Overall surface hydrophobicity of Hsp42 variants probed by ANS fluorescence. The surface hydrophobicity of Hsp42Δ1-99 is strongly reduced compared to Hsp42 wt.*

3.4.5 The prion-like domain is crucial for Hsp42 chaperone activity and the unstructured domain has regulatory functions

The chaperone activity of Hsp42 variants was determined by measuring their ability to suppress the formation of large aggregates. Turbidity measurements showed that Hsp42Δ1-99 was not able to prevent the formation of large MDH or luciferase aggregates at 47°C or 43°C, respectively (Figure 31). In contrast, Hsp42Δ100-242 could efficiently reduce aggregate formation, similar to Hsp42 wt.

In addition, I used the FRET approach, described in chapter 3.2.2, to monitor heat-induced MDH aggregation in presence and absence of Hsp42 variants (Figure 32). In this approach signal increase indicated the appearance of aggregates a few minutes earlier than in turbidity measurements, illustrating a higher sensitivity of this assay. The measurements revealed that Hsp42Δ100-242 is more efficient than Hsp42 wt since already substoichiometric Hsp42:MDH ratios resulted in maximal suppression of aggregation. The higher chaperone activity of Hsp42Δ100-242 might be linked to changes in the organization of MDH/Hsp42 complexes. Indeed, negative stain electron microscopy showed that heat-induced complexes between MDH and Hsp42Δ100-242 (20-25 nm) appeared smaller and more regular than with Hsp42 wt (35-40 nm) (Figure 33). This observation is consistent with *in vivo* findings, since expression of Hsp42Δ100-242 in *hsp42Δ* cells generated more and smaller cytosolic aggregates compared to Hsp42 wt (see chapter 3.4.2).

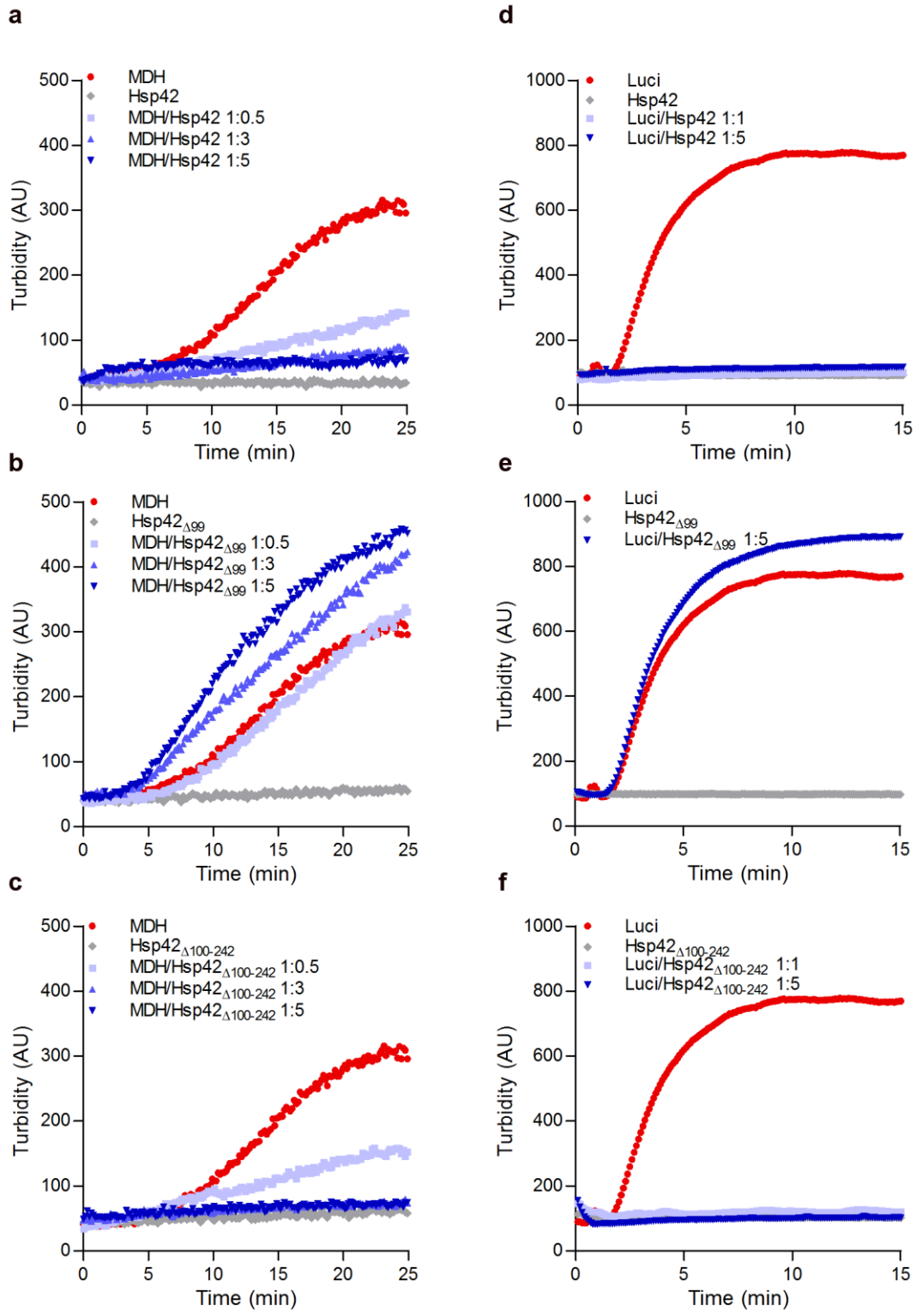

Figure 31: *Hsp42Δ1-99 cannot prevent the formation of turbid, insoluble MDH and luciferase aggregates.* ***(a)-(c)*** *MDH (0.5 µM) was denatured for 30 min at 47°C in absence or presence of Hsp42 variants at various ratios (0.25–2.5 µM). As a control 2.5 µM sHsps were heated alone. The formation of turbid MDH aggregates was followed at 550 nm.* ***(d)-(f)*** *Luciferase (0.1 µM) was denatured at 43°C in absence or presence of Hsp42 variants (0.1 µM or 0.5 µM) and the formation of turbid aggregates was followed at 600 nm. As a control 0.5 µM sHsps were heated alone. Luci: luciferase. For comparison with Hsp42 wt graphs previously shown in Figure 9a and d are included.*

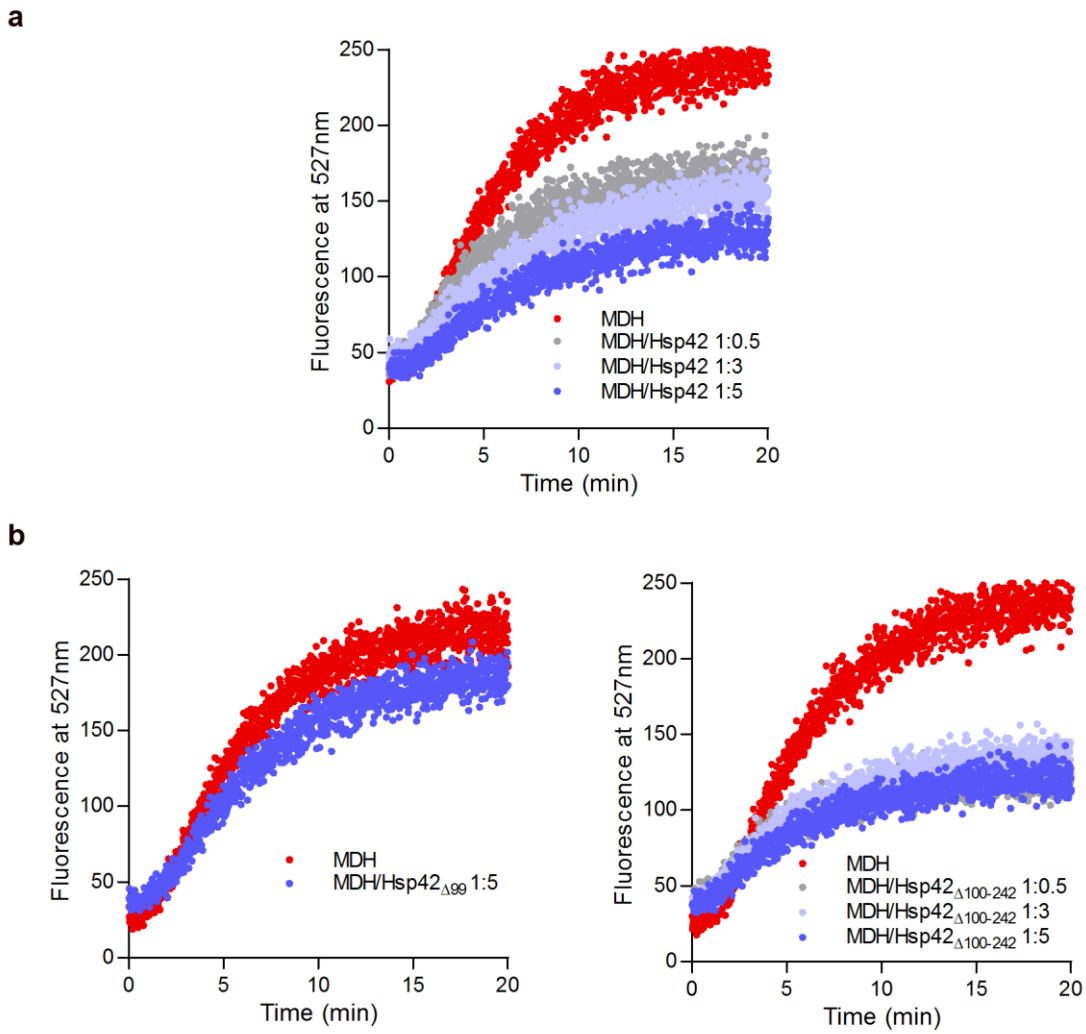

Figure 32: *Hsp42Δ1-99 is inactive, whereas Hsp42Δ100-242 is highly active in keeping misfolded proteins apart. Co-aggregation of MDH-YFP (FRET donor) and MDH labeled with 7-diethylcoumarin-3-carboxylic acid (FRET acceptor) at 47°C causes specific FRET increase. Presence of Hsp42Δ1-99* ***(b)*** *hardly affects FRET efficiencies, whereas Hsp42Δ100-242* ***(c)*** *reduces the FRET signal already at lower concentrations compared to Hsp42 wt* ***(a)****. The Hsp42 wt graph shown in Figure 12b is included.*

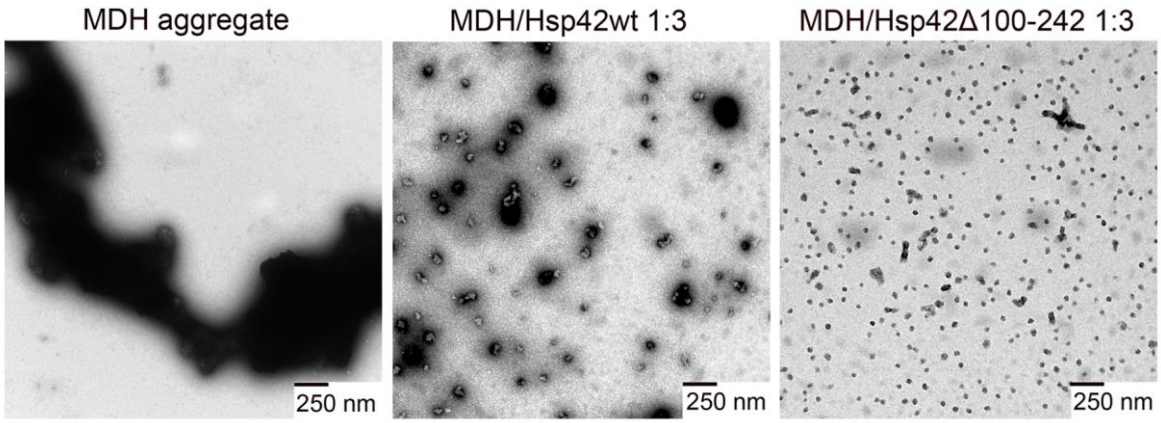

Figure 33: *Complexes of MDH with Hsp42Δ100-242 are smaller and more regular than with Hsp42 wt. Negative stain electron microscopy pictures of MDH (0.5 µM), which was aggregated alone (left) or in presence of a 3-fold excess of Hsp42 wt (middle) or Hsp42Δ100-242 (right) for 30 min at 47°C.*

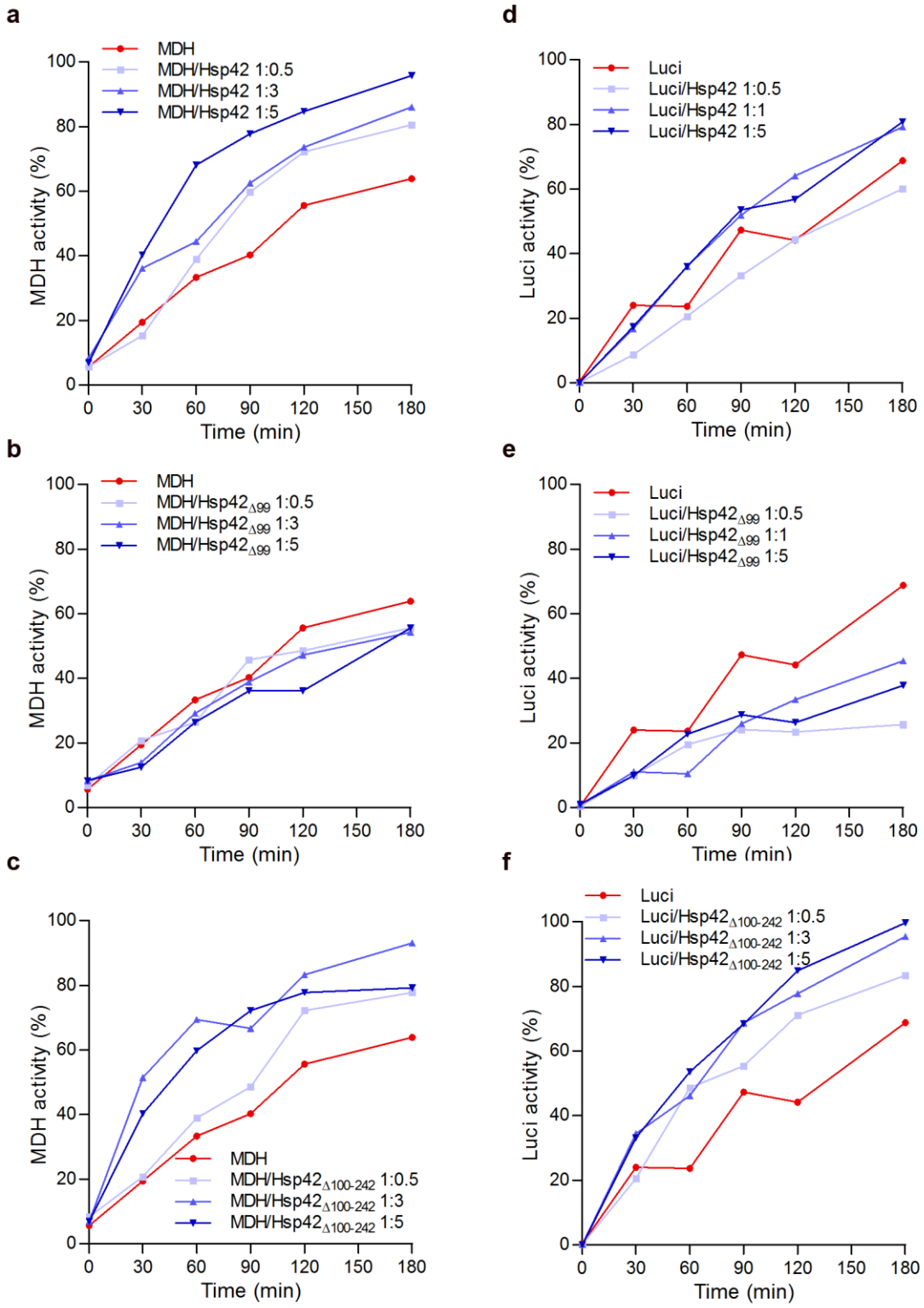

Figure 34: *Hsp42Δ1-99 cannot facilitate the chaperone-mediated refolding of heat-induced MDH and luciferase aggregates.* ***(a)-(c)*** *MDH (0.5 µM) was denatured for 30 min at 47°C in absence or presence of Hsp42 variants at various ratios (0.25 – 2.5 µM). MDH refolding from aggregated or sHsp-complexed states was initiated at 30°C by addition of the S. cerevisiae bi-chaperone system (2 µM Ssa1, 1 µM Sis1, 0.1 µM Sse1, 1 µM Hsp104) and 1 µM GroEL/GroES.* ***(d)-(f)*** *Luciferase (0.1 µM) was denatured for 15 min at 43°C in absence or presence of Hsp42 variants at various ratios (0.05 – 0.5 µM). Luciferase refolding from aggregated or sHsp-complexed states was initiated at 30°C by addition of the S. cerevisiae bi-chaperone system (2 µM Ssa1, 1 µM Sis1, 0.1 µM Sse1, 1 µM Hsp104) and 1 µM GroEL/GroES. MDH and luciferase activities were determined at the indicated time points. The enzymatic activity of native MDH and luciferase was set at 100%. The Hsp42 wt graphs previously shown in Figure 10a and d are included.*

Accordingly, chaperone-mediated disaggregation and refolding showed that Hsp42Δ1-99 did not facilitate the reactivation of heat-induced MDH or luciferase aggregates (Figure 34). The latter was even slightly inhibited when Hsp42Δ1-99 was included. In contrast, Hsp42Δ100-242 could promote MDH disaggregation similar to Hsp42 wt. Reactivation of luciferase was more efficient when heat-induced complexes were formed with Hsp42Δ100-242 (Figure 34). Despite higher chaperone activity of Hsp42Δ100-242 and smaller complex sizes, disaggregation and refolding of heat-induced complexes with MDH was still Hsp104-dependent (Figure 35).

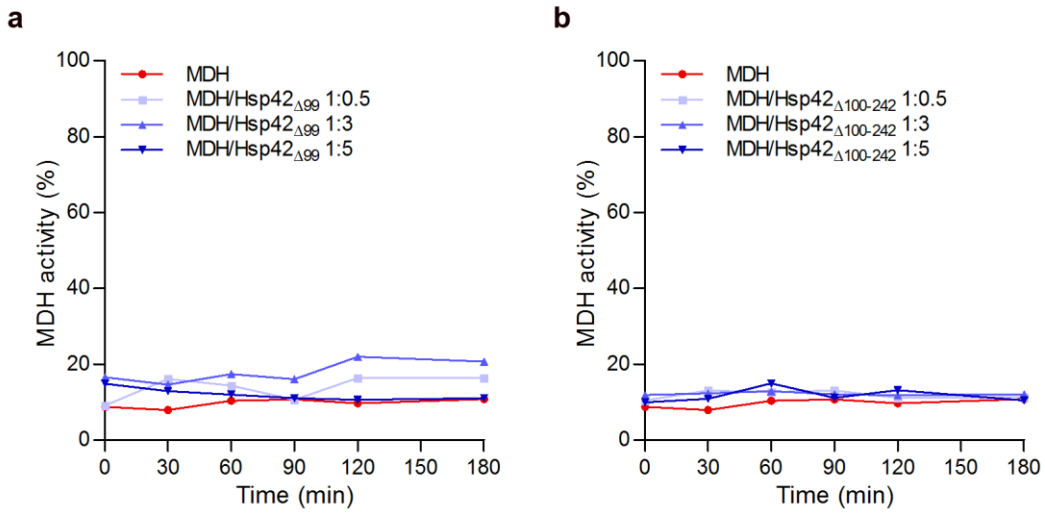

Figure 35: *The disaggregation of heat-induced complexes between MDH and Hsp42Δ1-99* ***(a)*** *or Hsp42Δ100-242* ***(b)*** *is still Hsp104-dependent. MDH (0.5 µM) was denatured for 30 min at 47°C in absence or presence of sHsps at various ratios (0.25 – 2.5 µM). MDH refolding from aggregated or sHsp-complexed states was initiated at 30°C by addition of the S. cerevisiae bi-chaperone system (2 µM Ssa1, 1 µM Sis1, 0.1 µM Sse1) and 1 µM GroEL/GroES. MDH activities were determined at the indicated time points. The enzymatic activity of native MDH was set at 100%.*

Together, these results indicate that the prion-like domain is also crucial for the chaperone activity *in vitro*, whereas the unstructured domain seems to be involved in negative regulation of Hsp42 activity. Attempts to purify and characterize the isolated prion-like domain failed due to a high aggregation tendency of this subdomain (data not shown).

3.4.6 Hsp42 lacking the unstructured domain is more efficient in stabilizing native-like structures in heat-denatured MDH

In chapter 3.2 I performed HX-MS to study heat-induced MDH/sHsp complexes. Hsp26 and Hsp42 were shown to protect denatured MDH from HX. MDH peptides derived from complexes with sHsps often exhibit two populations after HX: a native-like (low exchanging) and an aggregate-like (high exchanging) population. Increasing amounts of sHsps present during complex formation caused a shift of the populations towards the native-like state (Figure 18).

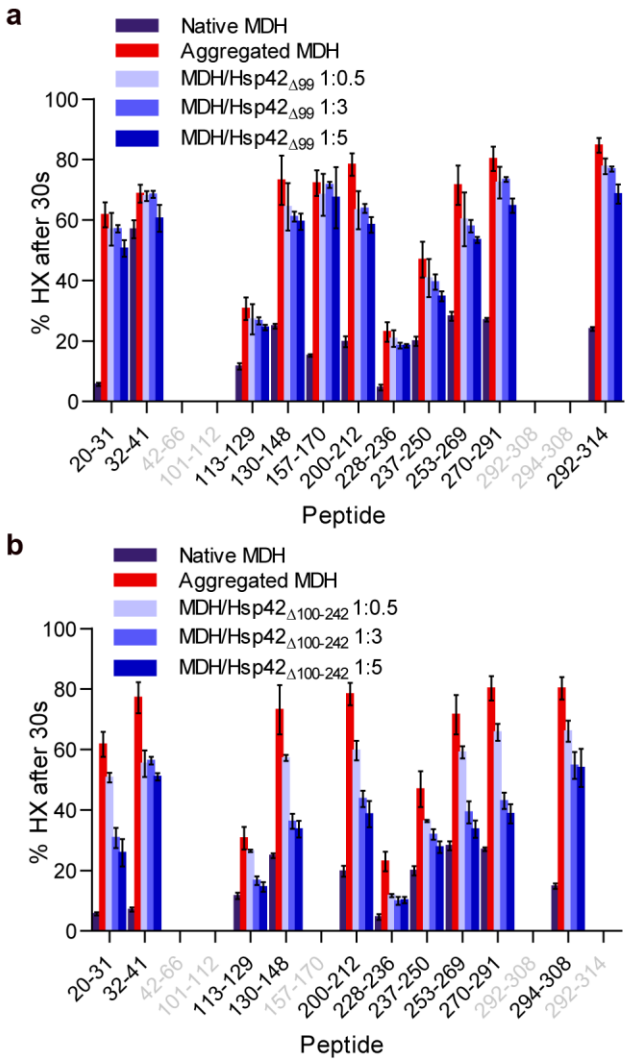

Figure 36: *Hsp42Δ100-242 efficiently protects unfolded regions of aggregated MDH from HX. Relative proton/deuteron exchange in MDH co-aggregated with either Hsp42Δ1-99* ***(a)*** *or Hsp42Δ100-242* ***(b)*** *was determined after 30 s labeling. The data were corrected for deuteron losses due to back-exchange using a 100% deuterated control (i.e. protein in which all exchangeable protons have been replaced by deuterons). MDH/sHsp complexes were formed by incubation for 30 min at 47°C.*

Now, HX was used to compare the chaperone activities of Hsp42 wt and Hsp42Δ100-242 at highest resolution possible. Heat-induced complexes between MDH and Hsp42 deletion constructs at different ratios were formed, and HX patterns were compared to those of aggregated and Hsp42 wt-complexed MDH (Figure 36 and Figure 37). Hsp42Δ1-99 hardly protected denatured MDH from HX and there were only minor effects regarding shifts of bimodal populations (Figure 38). This is in agreement with the observed loss of chaperone activity of this mutant. In contrast, Hsp42Δ100-242 very efficiently protected MDH from HX. A three-fold excess of Hsp42Δ100-242 was sufficient to find all bimodal peptides in the native-like state, whereas for Hsp42 wt a five-fold excess was necessary to see a similar trend. In addition, a substantial fraction of MDH peptides (113-129, 270-291, 292-308) still exhibited aggregate-like HX even at high excess of Hsp42 wt (Figure 38).

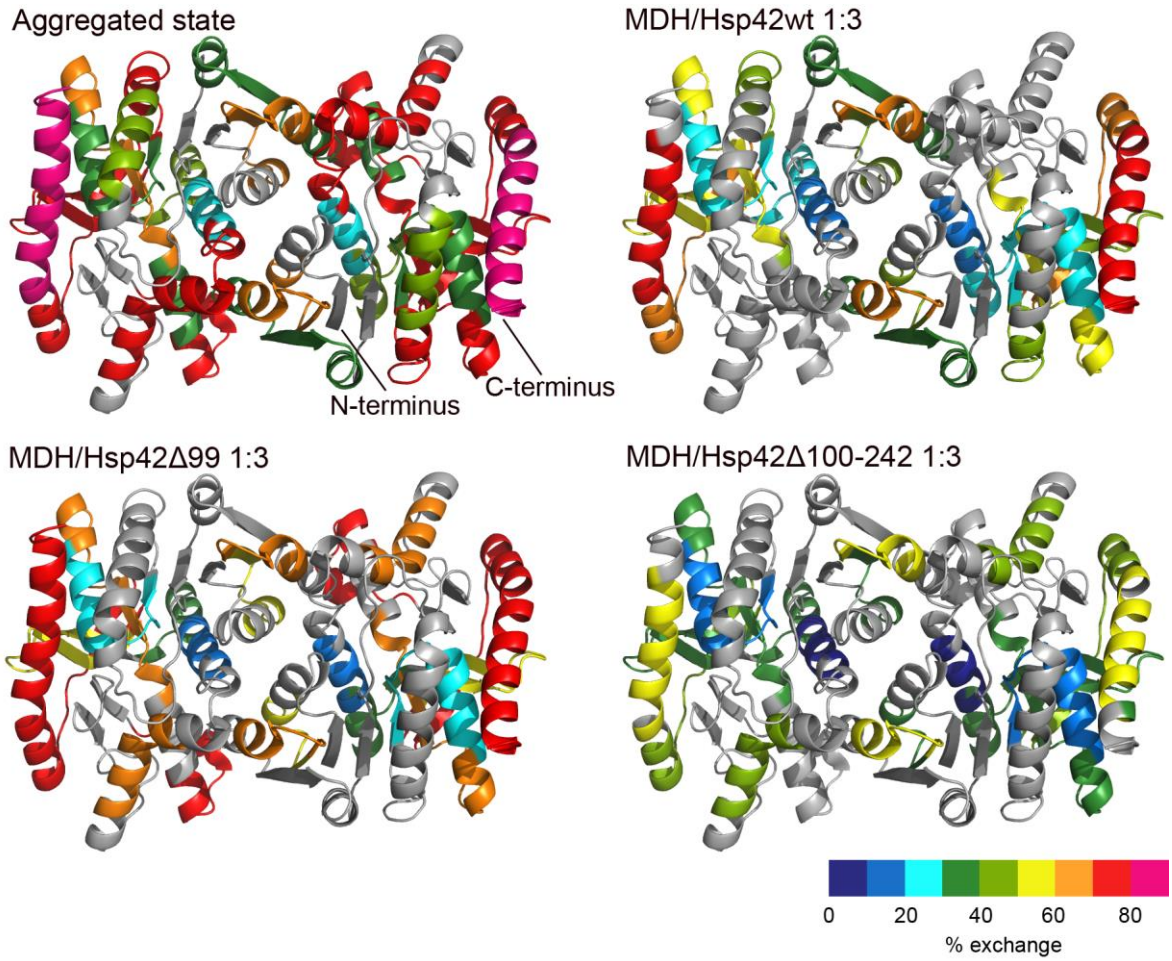

Figure 37: *HX-heat map of MDH in heat-induced MDH/sHsp complexes. Peptic peptides are colored according to their exchange behavior. Gray regions could not be identified. The ratio of sHsps vs. MDH during substrate denaturation is given.*

Thus, these data confirm our previous findings that the deletion of the unstructured domain leads to increased activity compared to Hsp42 wt, while deletion of the prion-like domain abolishes Hsp42 chaperone function.

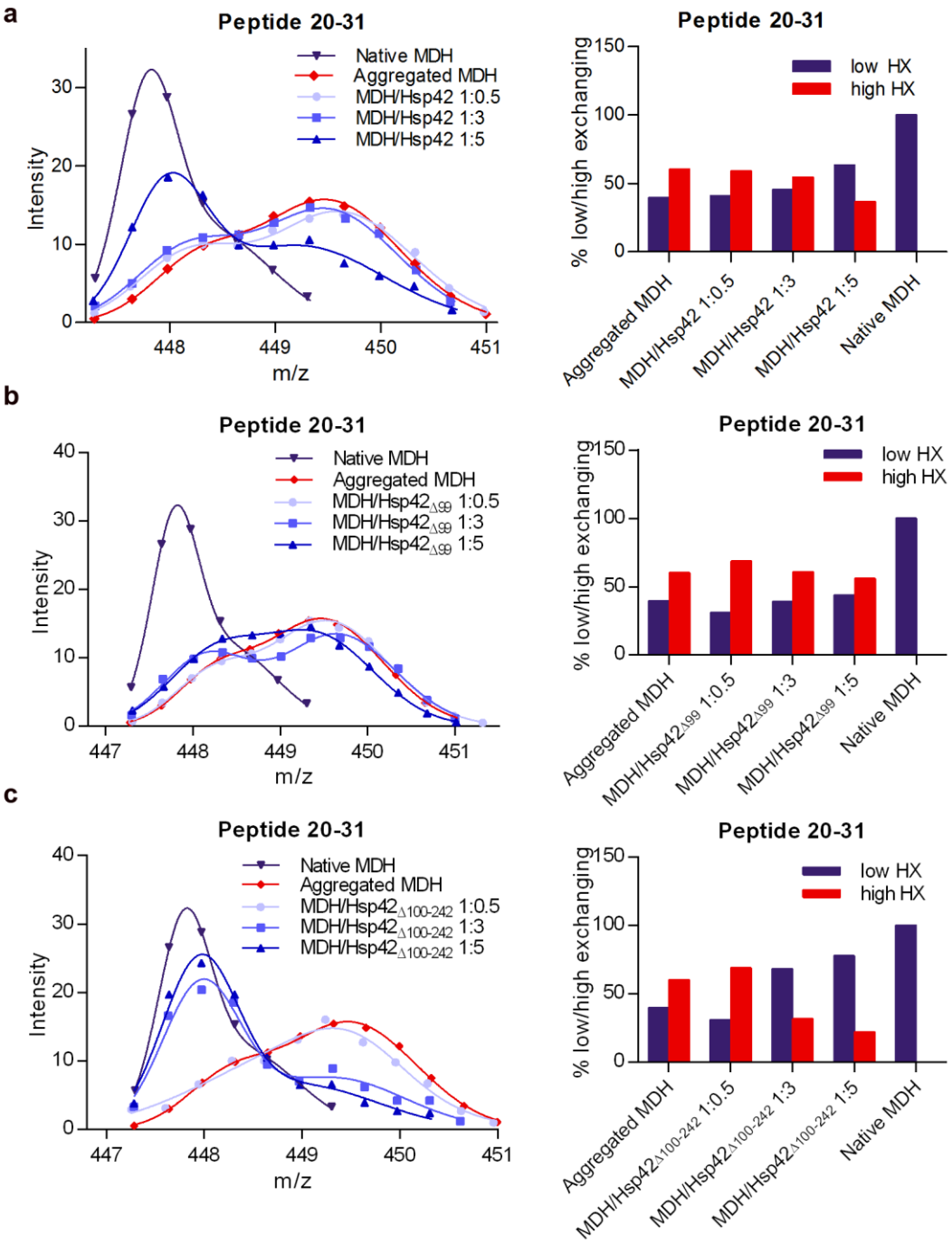

Figure 38: *Hsp42Δ100-242 stabilizes segments of bound MDH in a native-like state. Bimodal distribution of isotope peaks of indicated MDH peptides derived from MDH/Hsp42 wt* ***(a)****, MDH/Hsp42Δ1-99* ***(b)*** *and MDH/Hsp42Δ100-242 complexes. Left panels: Intensity versus m/z diagrams for different peptic MDH fragments after 30 s HX at 30°C. Right panels: Fractions of native-like and aggregate-like populations calculated for respective peptides. The spectra of one representative peptide are shown.*

3.4.7 Higher chaperone activity of Hsp42Δ100-242 is not due to higher subunit exchange

Previous studies showed that increased chaperone activity of sHsps can be caused by enhanced quaternary dynamics (Ahmad et al., 2008; Peschek et al., 2013). Therefore, a FRET approach was used to test if increased subunit exchange is the molecular basis for the higher chaperone activity of the Hsp42Δ100-242 deletion mutant.

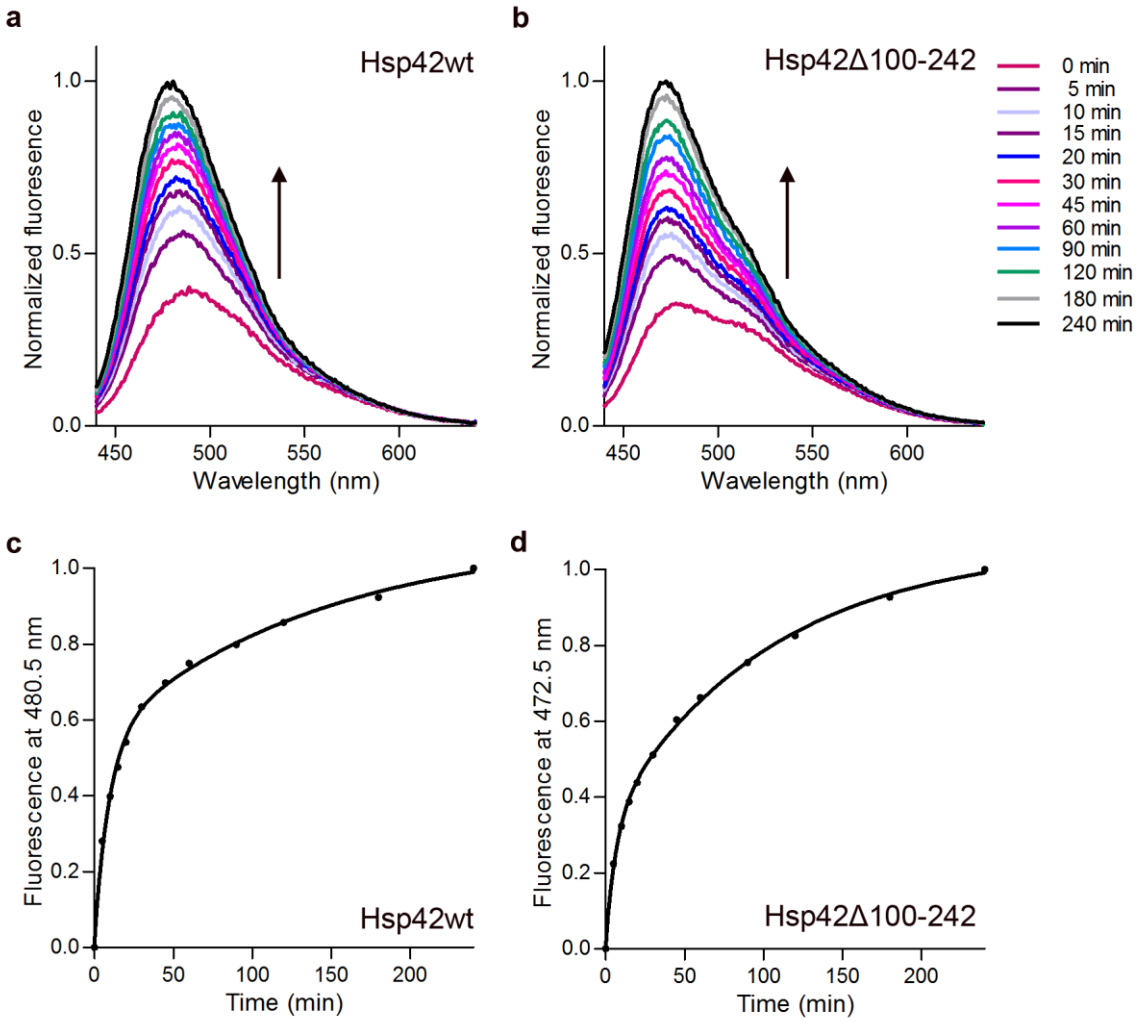

Figure 39: *Subunit exchange kinetics of Hsp42 wt and Hsp42Δ100-242. Shown are the temporal changes in the donor fluorescence intensities due to reversal FRET upon adding an excess of unlabeled Hsp42 wt* ***(a)*** *or Hsp42Δ100-242* ***(b)*** *to FRET-equilibrated oligomers of both variants labeled with 7-diethylaminocoumarin-3-carboxylic acid and NBD-X. Fitting to an exponential two-phase association equation yielded two rates each. For Hsp42 wt: k_{fast} 0.1066 min^{-1}; k_{slow}: 0.007129 min^{-1}; for Hsp42Δ100-242: k_{fast} 0.1514 min^{-1}; k_{slow}: 0.009707 min^{-1}.*

Hsp42 wt and Hsp42Δ100-242 were labeled with the amine-reactive dyes 7-diethylaminocoumarin-3-carboxylic acid and succinimidyl 6-(N-(7-nitrobenz-2-oxa-1,3-diazol-4-yl)amino) hexanoate (NBD-X). The donor- and acceptor-labeled proteins were mixed and incubated at 25°C over night. Addition of a ten-fold excess of unlabeled protein caused an increase of donor fluorescence with time (Figure 38).

Using an exponential two-phase association equation, two rate constants were obtained. The fast rate might originate from dissociation of dimeric subunits, whereas the slow rate might be caused by dimer to monomer conversion. With a fast rate of 0.1514 min^{-1} for Hsp42Δ100-242, subunit exchange seems somewhat faster than for Hsp42 wt (0.1066 min^{-1}). It remains unclear, if this difference is sufficient to explain the higher chaperone activity of the deletion mutant, or if subunit exchange is decisive at all.

3.5 Disassembly of the dimeric replication initiator protein RepE by the DnaK chaperone system

As already described, the Hsp70-mediated disassembly of the native, oligomeric substrates seems mechanistically related to the disaggregation process. An example for such a native Hsp70 substrate is the replication initiation protein RepE, which initiates the replication of the mini-F-plasmid in *E. coli*. In the dimeric state, RepE binds to the promotor of its gene repressing its own transcription (negative feedback). As a monomer RepE binds to a segment within the F plasmid replication origin *ori*2 and initiates plasmid replication (Masson and Ray, 1986; Wada et al., 1987). As its monomerization strictly depends on DnaK and DnaJ (Ishiai et al., 1994; Kawasaki et al., 1990), RepE is a suitable substrate for studying chaperone-mediated disassembly. Using a genetic screen, a RepE mutant (RepE54) was isolated that is independent of DnaK/DnaJ in replication initiation. In addition, crystal structures for RepE54 and RepE wt in complex with their respective DNA-segment containing the RepE binding sites were solved (Komori et al., 1999; Nakamura et al., 2007). Comparing the two structures showed that there are striking differences of the relative orientation of the N- and of the C-terminal domains between the RepE monomer and the dimer.

In previous work from this laboratory (done by Wolfgang Rist and Fernanda Rodriguez) RepE wt and RepE54 were studied by HX-MS. The proteins were diluted 1:50 into D_2O-buffer. At certain time points an aliquot was drawn, quenched by lowering the pH to 2.2 and the temperature to 0°C, and immediately injected into the rapid-desalting HPLC-setup, which was connected to a MS. Higher deuteron incorporation into RepE wt as well as partial proteolysis showed that monomeric RepE54 is more stable and more tightly packed than the dimer (data not shown). In addition, HX on peptide level revealed protection of region 96-128 in RepE wt compared to RepE54 (Figure 40), indicating that this might be the dimer interface.

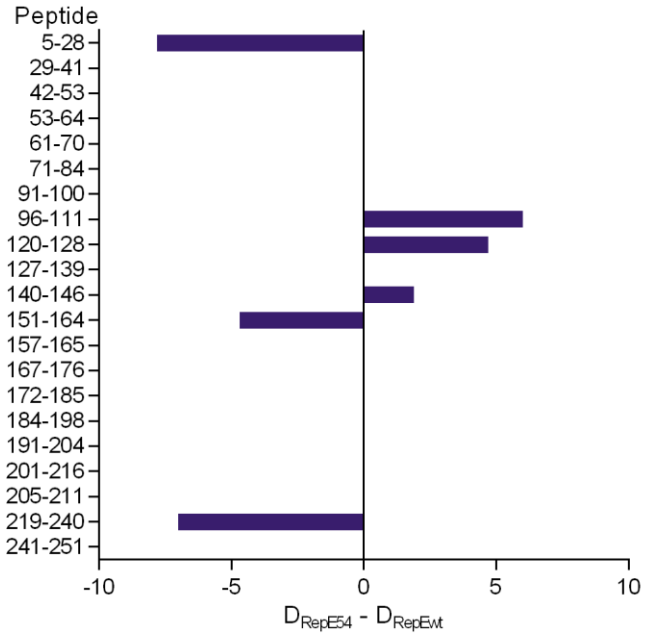

Figure 40: *Lower deuteron incorporation in some regions of RepE54 indicates conformational rearrangements during the monomerization process. Shown is the difference of deuteron incorporation into RepE54 (monomer) and RepE wt (dimer). Negative values indicate segments of the protein that exchange less in the monomer, whereas positive values indicate regions that exchange more in the monomer. This experiment was performed by Fernanda Rodriguez.*

This suggestion was confirmed in later studies when the crystal structure of dimeric RepE wt was solved (Nakamura et al., 2007) (dimer interface: aa 97-111, 121-128, 141-146) (Figure 41). There were also some peptides (aa 5-28, 151-164, 219-240) which exchanged more in the RepE dimer, indicating conformational changes that led to higher flexibility in those regions (Figure 40). The enhanced flexibility of dimeric RepE wt might be necessary for binding to inverted repeat operator DNA, since modelling of two RepE monomers on IR-DNA revealed a large sterical hindrance which excludes simultaneous binding (Komori et al., 1999). Two helix-turn-helix motifs in RepE54, namely α3-turn-α4 (aa 64-92) and α3'-turn-α4' (aa 168-242) are critical for binding to iteron DNA (Komori et al., 1999). However, HX did not show any differences in those regions when comparing RepE wt and RepE54. This indicates similar binding to DNA. In agreement, iteron and operator DNA possess 8 common base pairs and the α3'-turn-α4' (aa 168-242) motif is also critical for dimeric RepE wt to bind to IR-DNA (Matsunaga et al., 1995). The crystal structure of dimeric RepE wt in complex with IR-DNA revealed differences in the relative orientation of the N- and the C-terminal domain enabling the binding of dimeric RepE wt to operator DNA (Nakamura et al., 2007). During the reorientation an interdomain β-sheet in RepE54, comprising β1 (aa 17-20) and β1' (aa 146-149), is disrupted. This is consistent with the deprotection of peptide 5-28, which contains β1 (Figure 40 and Figure 41). A peptide including β1' was not found in HX experiments. Concomitantly, the linker connecting the two domains (aa 133-159) undergoes secondary structure alterations:

The long α5 helix found in the linker of dimeric RepE is changed to a shorter α5 helix, a loop structure, and a β1' strand. Peptide 140-146 is located in the loop region of the linker. Thus, the slight deprotection of aa 140-146 in monomeric RepE54 (Figure 41) could be attributed to the described structural alterations in the linker. The protection observed in region 152-164 might also arise from changes in the linker region.

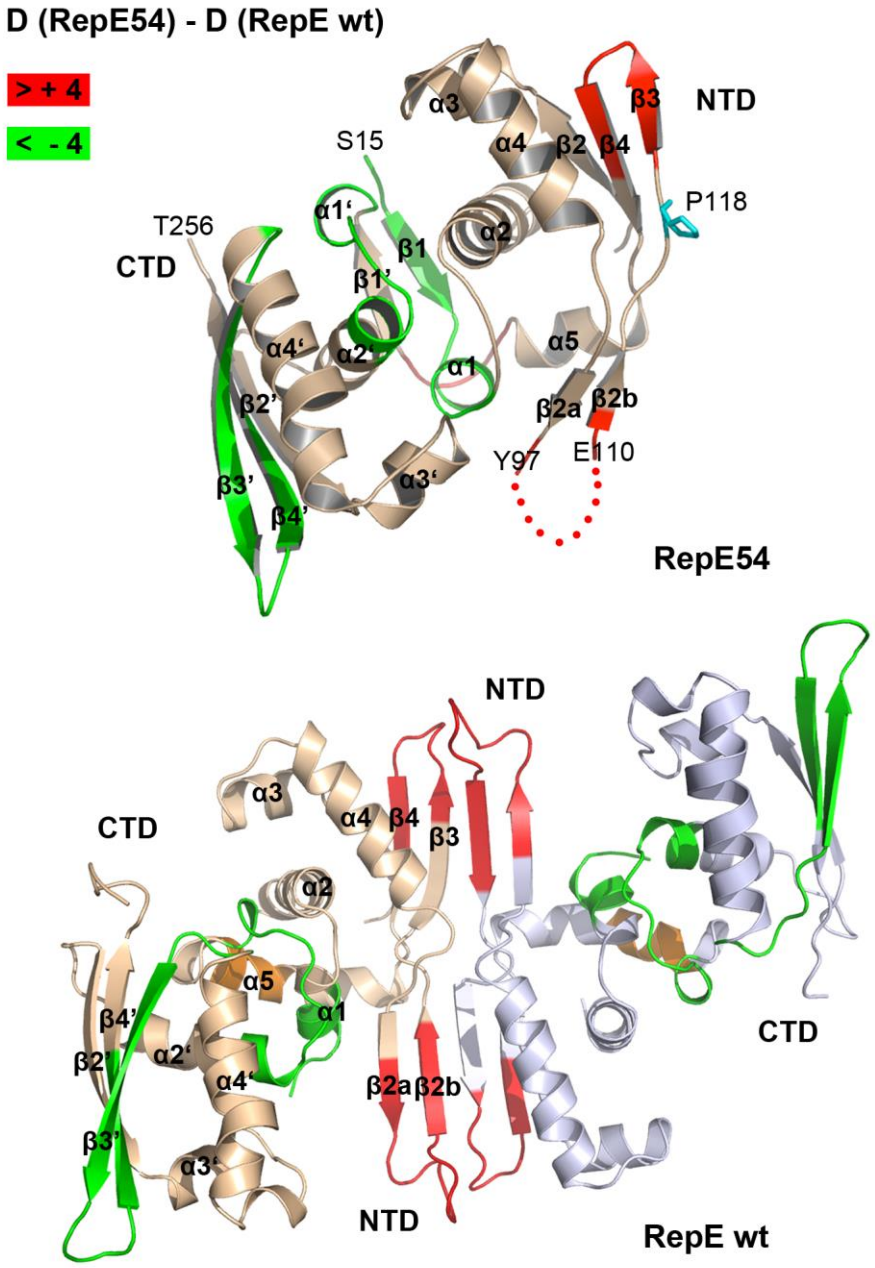

Figure 41: *Structure of monomeric RepE54 (upper panel, PDB ID 1REP) and dimeric RepE wt (lower panel, PDB ID 2Z90) (Komori et al., 1999; Nakamura et al., 2007). The coloring is according to the HX behavior. Regions that exchange significantly more deuterons in RepE54 are colored red, whereas regions that exchange significantly less deuterons are colored green.*

Additionally, the RepE dimer structure revealed the partial unfolding of α1 (aa 22-26) in the monomer. Since peptide 5-28 comprises both, β1' and α1, the lower

accessibility of β1' in monomeric RepE54 (see above) could compensate for the increased accessibility of α1 due to partial unfolding. This explains why peptide 5-28 appears protected in RepE54 during HX. Except for the conformational changes mentioned above, there were no obvious differences between the crystal structures of monomeric RepE54 and dimeric RepE wt. In HX, however, peptide 219-240 was markedly deprotected in RepE wt.

Overall, the HX data are consistent with changes observed in the RepE X-ray structures, and together this provides good information about structural differences of dimeric RepE wt and monomeric RepE54. Moreover, HX revealed increased flexibility at the C-terminus of RepE wt, indicating additional conformational changes during dimer disassembly. In the present study, we wanted to figure out how the DnaK-chaperone system acts on RepE, finally causing monomerization. For this purpose the interaction of DnaK and DnaJ with RepE were studied.

3.5.1 DnaK cannot bind to RepE wt or RepE54 in presence of their DNA-binding elements

In the first experiment, performed by Fernanda Rodriguez, specific crosslinking was used to study the binding of DnaK to RepE wt or RepE54. For this purpose a DnaK Q424C variant was utilized, in which glutamine 424, located close to the substrate binding pocket of DnaK, was replaced by cysteine. DnaK Q424C was labeled with a cysteine-specific UV-activatable heterobifunctional crosslinker (BPIA) and the activity of this variant was attested in luciferase disaggregation assays (data not shown). When RepE monomer or dimer was incubated with DnaK Q424C and irradiated with UV light, new specific bands appeared running at the expected height of a RepE-DnaK complex (Figure 42). Western blot analysis proved that the bands contained both, RepE and DnaK. However, when incubating RepE wt or RepE54 and DnaK Q424C in presence of IR- or DR-DNA, respectively, RepE-DnaK complex formation was not observed any more.

In previous work from our laboratory (done by Stefan Rüdiger), peptide library scanning revealed four potential DnaK binding sites in RepE (aa 39-42, 126-142, 224-227, 238-242). Two possible regions are located in the N-terminus of RepE and two in the C-terminus. Binding of DNA occurs via residues 200-219 in RepE wt and via residues 75-87 and 200-219 in RepE54 (Komori et al., 1999; Nakamura et al., 2007). Thus, both C-terminal putative DnaK binding sites (224-227, 238-242) are located close to the DNA binding residues. DNA bound to RepE might therefore sterically hinder the binding of DnaK.

Together, these experiments showed that dimeric RepE wt as well as monomeric RepE54 can bind DnaK, but that binding is prevented in presence of IR- or DR-DNA, respectively.

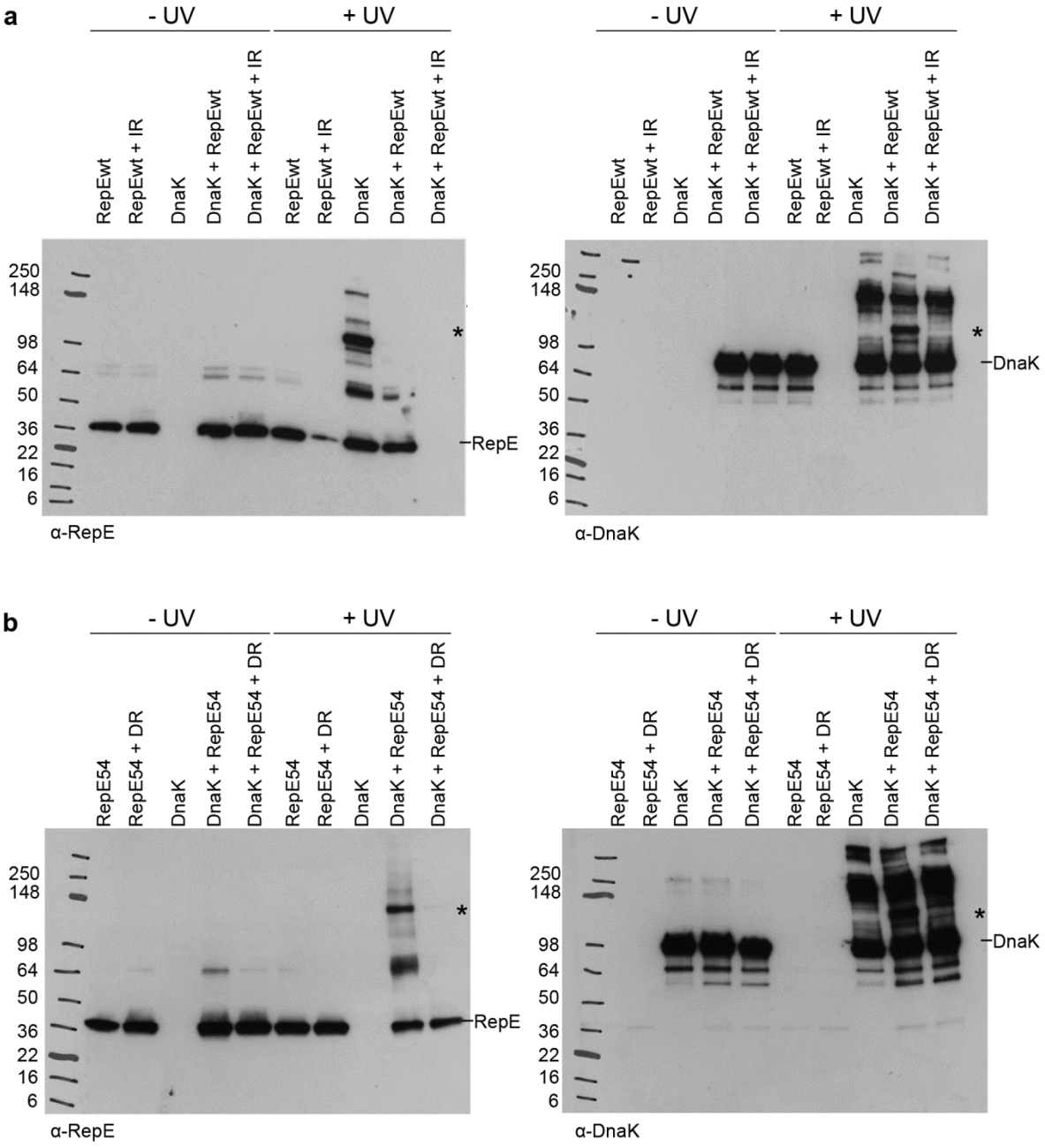

Figure 42: *BPIA-labeled DnaK Q424C crosslinks to RepE wt and RepE54 in absence of IR-DNA or DR-DNA, respectively. RepE wt (**a**) or RepE54 (**b**) were incubated with BPIA-labeled DnaK-Q424C for 1 h at 30°C in presence or absence of IR- or DR-DNA. Crosslinked products were separated by SDS-PAGE and analyzed by western blotting using RepE and DnaK specific antibodies. The crosslinked RepE-DnaK product is indicated by asterisks. This experiment was performed by Fernanda Rodriguez.*

3.5.2 Only dimeric RepE wt but not monomeric RepE54 binds DnaJ

Next, the ability of RepE wt or RepE54 to bind DnaJ was determined indirectly, by using single-turnover ATPase experiments (Figure 43). This assay was performed by

Fernanda Rodriguez. We exploited that ATP hydrolysis by DnaK is synergistically stimulated by DnaJ and substrate binding. Besides RepE, the native DnaK substrate σ^{32} was tested as a positive control (Rodriguez et al., 2008). Together with DnaJ, RepE wt stimulated ATP hydrolysis of DnaK similar to σ^{32} (Figure 43a). This is in agreement with previous results from steady-state ATPase measurements (Cuéllar et al., 2013). In contrast, RepE54 hardly increased ATPase rates, indicating that the affinity of monomeric RepE to bind DnaJ is drastically reduced. In addition, a deletion construct of RepE only harboring the first 144 residues was tested. This variant did not stimulate ATP hydrolysis (Figure 43b), which can be explained by a loss of the ability to bind to DnaJ, DnaK or to both.

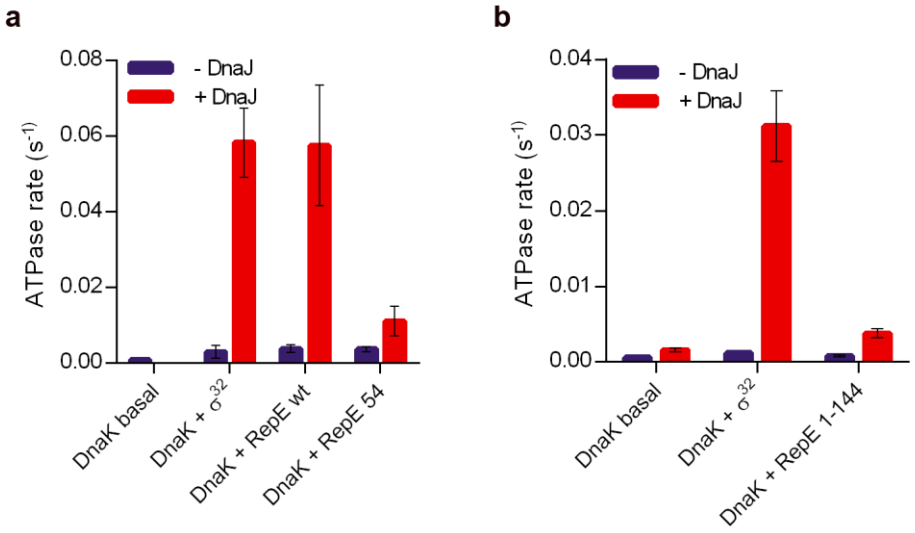

Figure 43: *Only dimeric RepE wt binds DnaJ. Single turnover experiments of DnaK ATPase activity in presence of σ^{32}, dimeric RepE wt, monomeric RepE54* ***(a)*** *or RepE 1-144* ***(b)*** *in presence or absence of DnaJ. This experiment was performed by Fernanda Rodriguez.*

In summary, these results suggest that only dimeric RepE wt can bind DnaJ, whereas monomeric RepE54 cannot. Lacking ATPase stimulation by RepE 1-144 indicates that the binding site for DnaJ and/or DnaK might be located in the C-terminal part of RepE.

3.5.3 Binding of DnaJ induces conformational changes within the DNA-binding region in RepE wt

In order to determine the binding site of DnaJ in RepE wt, I performed footprinting HX MS analysis. RepE wt was incubated for 10 s at 30°C in D_2O-based buffer in presence or absence of DnaJ. The exchange was quenched by lowering the pH to 2.2 and the temperature to 0°C, and the protein was injected into the MS-coupled HPLC-setup. Presence of DnaJ did not lead to pronounced protection of any RepE peptide (Figure 44a). Yet, complete sequence coverage was only obtained for the C-terminal part of RepE wt. For the N-terminal part many peptides could not be detected mainly due to disturbing signals from DnaJ derived peptides. Binding of DnaJ in the N-

terminal region would therefore not be obvious in this HX analysis. Instead, higher deuteron incorporation was detected in the C-terminal part of RepE, mainly for peptide 184-204 (Figure 44a). The increased HX indicates DnaJ-induced conformational changes. These changes could not be observed when using RepE54, confirming that DnaJ can only bind to dimeric RepE wt but not to monomeric RepE54 (Figure 44b).

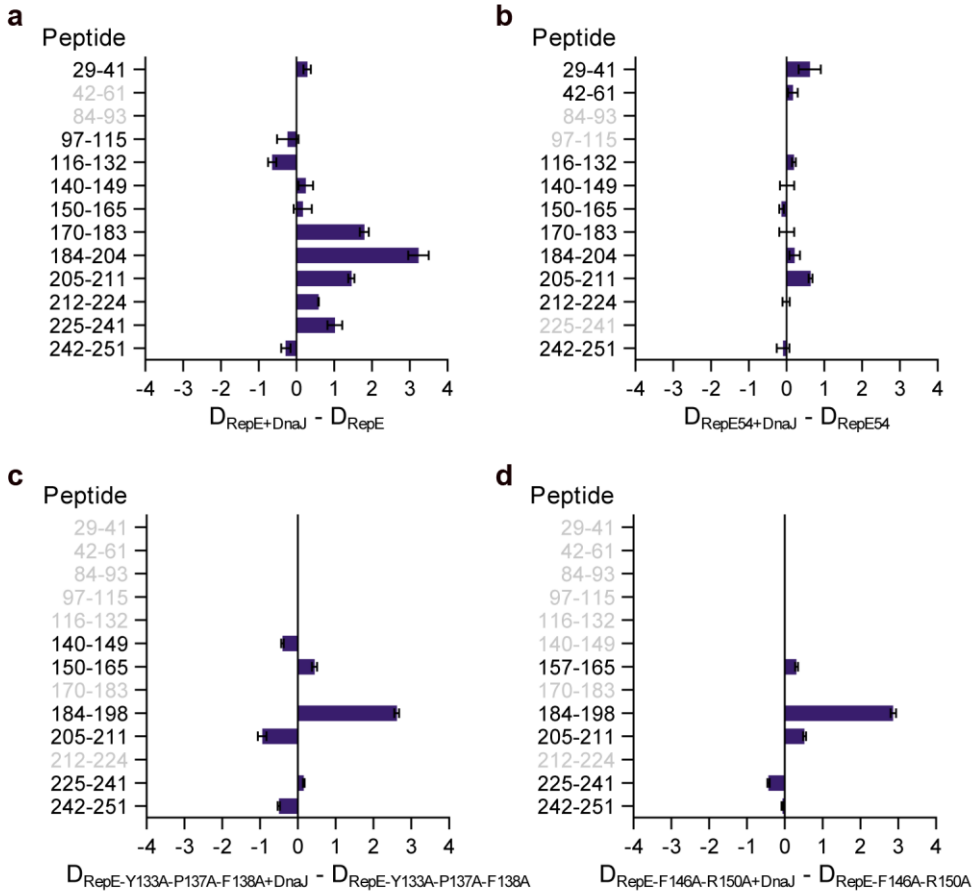

Figure 44: *Binding of DnaJ resulted in deprotection in a DNA-binding region of RepE wt. Difference in deuteron incorporation of RepE wt* ***(a)****, RepE54* ***(b)****, RepE-Y133A-P137A-F138A* ***(c)*** *or RepE-F146A-F150A* ***(d)*** *in presence and absence of DnaJ. Peptides in gray could not be detected.*

Using peptide library scanning (performed by Stefan Rüdiger), four putative DnaJ binding sites were identified in RepE wt (aa 96-116, 133-138, 146-150, 200-206). Three RepE variants were generated (by Fernanda Rodriguez), which possessed point mutations in one of the potential DnaJ binding sites: RepE-Y133A-P137A-F138A, RepE-F146A-F150A, RepE-R200A-P202A-R205A-R206A. The first two variants could be purified, the latter was degraded upon expression in *E. coli*. HX analysis of RepE-Y133A-P137A-F138A and RepE-F146A-F150A in presence of DnaJ revealed a similar deprotection in peptide 184-204 as observed for RepE wt, suggesting that both variants were still able to bind DnaJ. This is in agreement with previous studies (Cuéllar et al., 2013), which demonstrated that the deletion construct RepE 1-139 is capable of binding DnaJ. Region 96-116 is the only potential

DnaJ binding site which is included in RepE 1-139. Although peptide 97-115 is not markedly protected in HX (Figure 44a) the other results suggest that aa 96-116 could represent the DnaJ binding site in RepE wt.

Interestingly, the region which is deprotected in RepE wt upon binding of DnaJ comprises parts of the DNA-binding site. Accordingly, HX of RepE wt in presence of IR-DNA caused some protection throughout RepE, with highest protection in peptide 184-204 (Figure 45) (this HX experiment was performed by Fernanda Rodriguez).

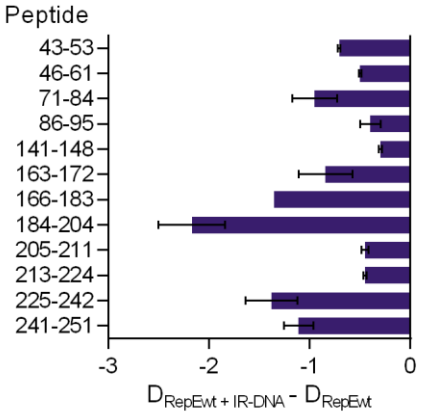

Figure 45: *Binding of IR-DNA mostly protects peptide 184-204. RepE wt was incubated in D_2O-based buffer for 30 s at 30°C in presence or absence of IR-DNA. The difference in deuteron incorporation between both conditions is shown.This experiment was performed by Fernanda Rodriguez.*

The observed DnaJ-induced changes might influence the DNA binding affinitiy of RepE. To test possible effects of DnaJ binding on the binding affinity of RepE to promotor DNA, gel retardation assays were performed in which RepE wt and Cy3-labeled IR-DNA were incubated in presence or absence of DnaJ (Figure 46).

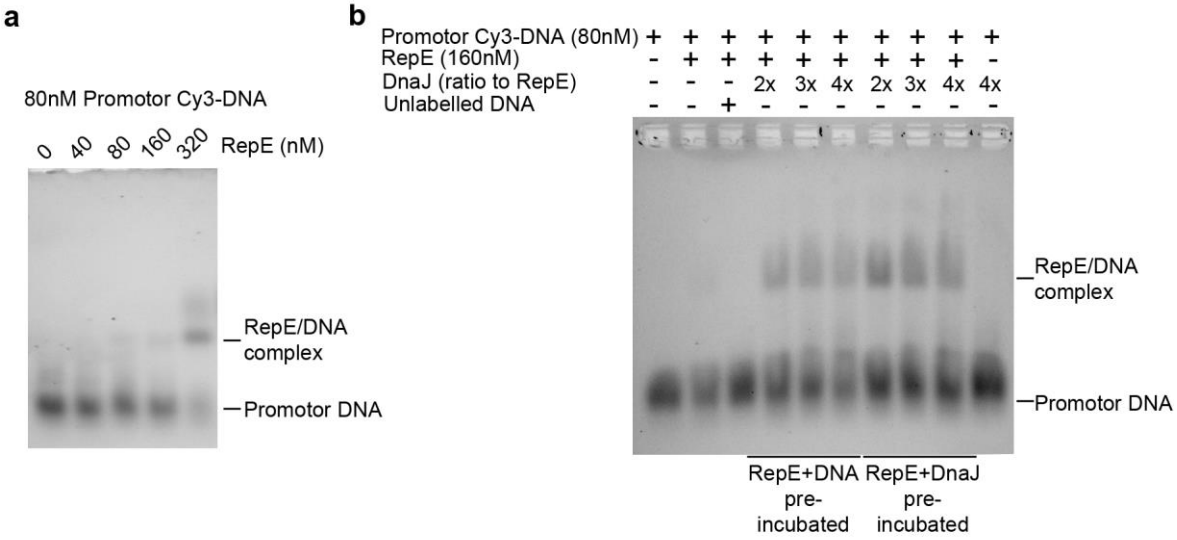

Figure 46: *DnaJ enhances the binding of RepE wt to promotor DNA. Gel retardation assay of Cy3-labeled RepE promotor-DNA mixed with RepE wt alone or together with increasing amounts of DnaJ. Either RepE wt and Cy3-labeled promotor-DNA were pre-incubated before adding DnaJ or RepE wt and DnaJ were pre-incubated before adding the promotor-DNA.*

In absence of DnaJ, RepE-DNA complexes were detected when using a four-fold excess of RepE wt over IR-DNA (Figure 46a). In presence of DnaJ, RepE-DNA complex formation was observed already at lower RepE concentrations and increasing amounts of DnaJ enhanced substrate binding (Figure 46b). This is consistent with previous findings (Kawasaki et al., 1992). When RepE and DnaJ were pre-incubated before adding DNA, the observed effects were greater compared to pre-incubation of RepE and DNA and subsequent addition of DnaJ (Figure 46b). These results exclude that DnaJ-induced changes lead to reduced affinity of RepE for DNA. In fact, binding of DnaJ to RepE even enhances its binding to IR promotor DNA.

Taken together, DnaJ binding seems to induce conformational changes in parts of the DNA-binding region of RepE. These changes might be needed to enable the binding of DnaK to RepE. Gel retardation assays indicated DnaJ-promoted binding of RepE wt to DNA. In addition, the results indirectly suggest that region 96-116 might include the DnaJ binding site in RepE wt.

3.5.4 Concerted DnaJ and DnaK binding induces major structural changes in dimeric RepE wt

Next, I performed HX footprinting trying to identify the DnaK binding site in RepE wt. In these experiments DnaK was immobilized on POROS 20 AL medium to avoid that overlapping DnaK peptides would reduce the number of detected RepE peptides. The immobilized DnaK was packed in a column, pre-incubated with ATP and loaded with His_{10}-RepE. After incubation for 30 min, D_2O-buffer was injected into the column. After 60 s at 30°C, HX was quenched and the protein was simultaneously eluted by using ice-cold, low pH quench buffer. To have a comparable reference, HX with His_{10}-RepE alone was performed using a Ni-NTA column (for details see Material and Methods). Presence of DnaK and ATP did not lead to prominent changes in the HX pattern of RepE wt. However, some protection in C-terminal peptide 227-241, which contains a putative DnaK binding site (aa 238-242; based on peptide library scanning), was observed (Figure 47a).

Subsequently, the effects on RepE wt by the combined binding of DnaJ and DnaK were studied using HX. For this experiment the complex between His_{10}-RepE and DnaJ was formed by incubation for 10 min at 30°C. Then the same procedure was followed as described for the experiment with DnaK alone. The HX pattern in presence of chaperones was strikingly different compared to RepE wt alone. The DnaJ-induced deprotection of peptide 184-204 (Figure 44) could not be observed when DnaK was included (Figure 47b). Consistently, there was no difference observed for this peptide when comparing dimeric and monomeric RepE (Figure 41).

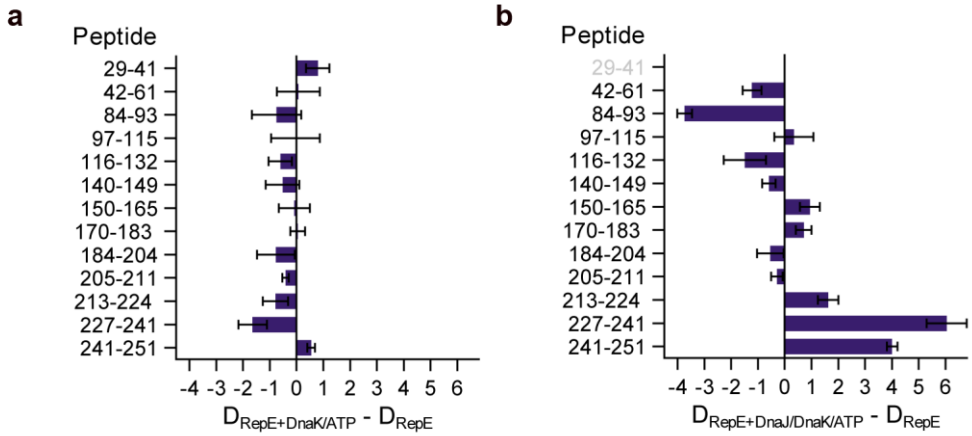

Figure 47: *Concerted binding of DnaJ and DnaK leads to pronounced conformational changes in RepE wt. Difference in deuteron incorporation of RepE wt in presence and absence of DnaK* ***(a)*** *or DnaJ and DnaK* ***(b)****. Both experiments were performed in presence of ATP. Peptides in gray could not be detected.*

The regions including the dimer interface (aa 97-115, 116-132, 140-149) remained basically unchanged. However, aa 84-93, located in helix α4 very close to the dimer interface, exchanged considerably less deuterons. Peptide 6-28, which was strongly protected in RepE54 compared to the dimer, could not be detected in this set of experiments. However, binding of DnaK and DnaJ caused strong deprotection in the C-terminal region (aa 213-224, 227-241, 241-251), indicating marked conformational changes (Figure 47b). This was unexpected, since monomeric RepE54 displayed a strong protection of peptide 220-240 (Figure 41). These differences imply that presence of the nucleotide exchange factor GrpE and possibly of iteron DNA is required to induce further conformational changes, causing monomerization of dimeric RepE wt.

In summary, HX footprinting experiments indicate that DnaK binding could occur in aa 238-242 in RepE wt, a putative binding site for DnaK identified by peptide library scanning. Simultaneous binding of DnaK and DnaJ resulted in major conformational changes, including the protection of α4 near the dimer interface and deprotection of wide C-terminal parts in RepE wt. Yet, HX patterns of the chaperone-bound RepE wt and RepE54 still considerably differed.

3.5.5 DnaK can bind to promotor DNA-complexed RepE wt when DnaJ and GrpE are present

In order to test if presence of DnaJ alone or together with GrpE enables the binding of DnaK to IR-DNA-bound RepE wt, I performed BPIA-crosslinking experiments using DnaK Q424C (as described in chapter 3.5.1).

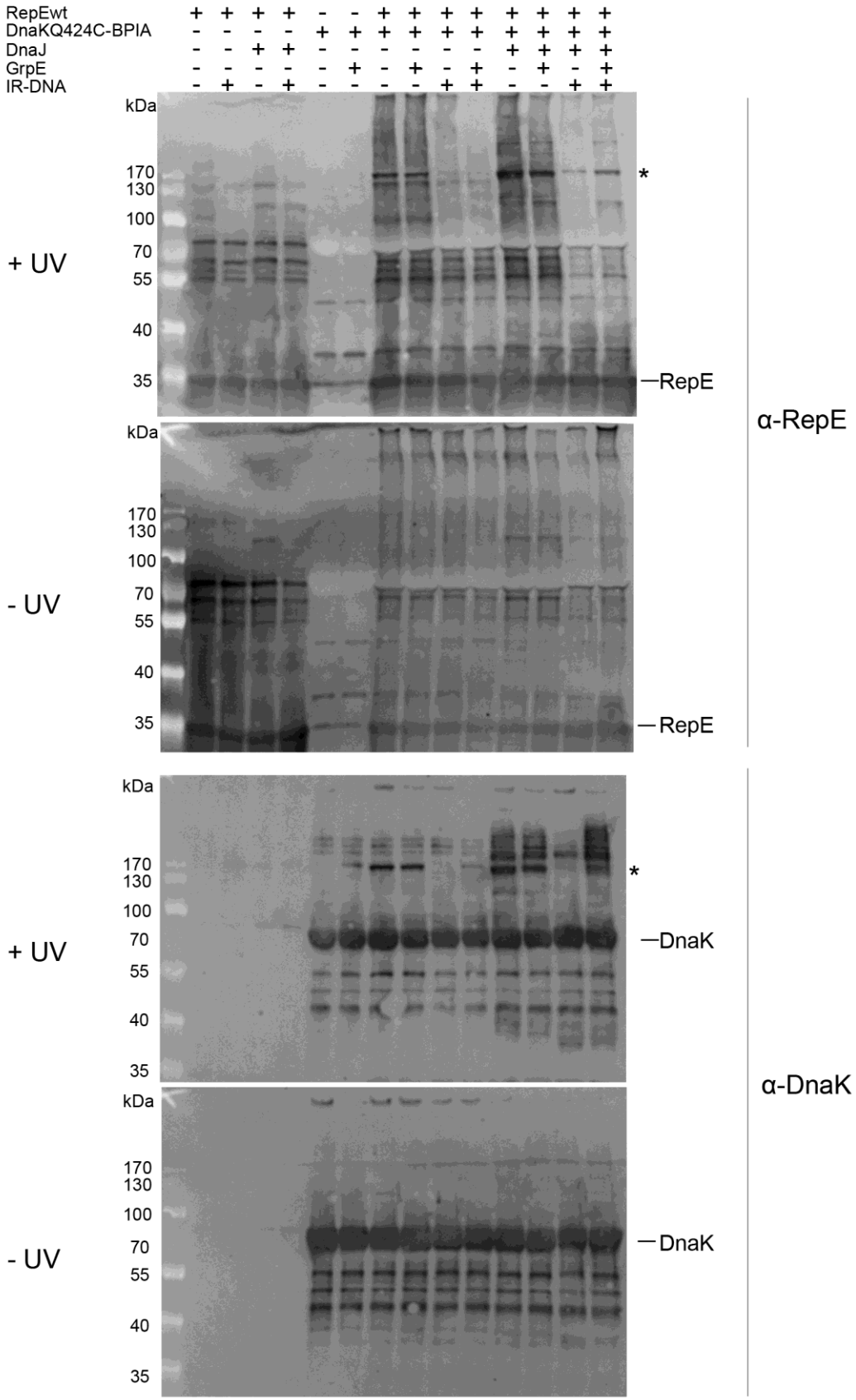

Figure 48: *BPIA-labeled DnaK-Q424C can crosslink to promotor DNA-complexed RepE wt when DnaJ and GrpE are present. RepE wt was incubated with different combinations of BPIA-labeled DnaK-Q424C, DnaJ, GrpE and RepE promotor DNA for 1 h at 30°C. Crosslinked products were separated by SDS-PAGE and analyzed by western blotting using RepE and DnaK specific antibodies. The crosslinked RepE-DnaK product is indicated by asterisks.*

RepE wt and DnaJ were pre-incubated for 10 min at 30°C, before the complex was mixed with different combinations of DnaK Q424C, GrpE and IR-DNA. The protein solutions were irradiated with UV light. As observed in chapter 3.5.1, the incubation of DnaK Q424C and RepE wt alone resulted in the formation of a DnaK-RepE wt crosslinking product (Figure 48, asterisk), which was strongly reduced in presence of IR-DNA. The addition of either DnaJ or GrpE could not restore the formation of the DnaK-RepE wt crosslinking product when promotor DNA was present. Only the concomitant presence of DnaJ and GrpE re-established crosslinking between IR-DNA-complexed RepE wt and DnaK Q424C (last lane in Figure 48). Thus, the concerted action of DnaJ and GrpE seems to allow the binding of DnaK to dimeric RepE wt during it is bound to promotor DNA.

4 Discussion and Outlook

In this thesis, the structure of heat-induced amorphous aggregates was studied using MDH as thermolabile model protein. The influence of yeast sHsps Hsp26 and Hsp42 on aggregation and on the architecture of heat-aggregates was determined. Moreover, with respect to its role in CytoQ formation, the structure-function relationship of Hsp42 was further explored. The chaperone-mediated disaggregation of protein assemblies was addressed by investigating the monomerization of the RepE dimer, representing a minimal model aggregate.

4.1 Structural analysis of heat-induced protein aggregates and interactions between yeast sHsps and aggregating proteins

How does the structure of heat-induced aggregates look like? So far, predominantly methods like electron microscopy, CD or FTIR spectroscopy and dye binding were used to address this question. To obtain more detailed insights, I performed HX to examine the structure of heat-induced MDH aggregates. Substantial, global deprotection of amide protons of the peptide backbone was observed in heat-induced MDH aggregates. This finding indicates that most regions were largely unfolded, providing potential binding sites for chaperones. A remaining core structure was not detected. Only Ala228-Phe236, located at the MDH dimer interface, displayed low HX even in the aggregated state. However, deprotection of other dimer interface peptides reason against the maintenance of the entire interface region. Segments exhibiting reduced deuteron incorporation were not detected. Thus, enhanced β-sheet structures, as often observed in other amorphous aggregates (Chang et al., 2009; Kendrick et al., 1998; Okuno et al., 2007), were likely not present. In addition, peptides that are involved in tight hydrophobic interactions in the aggregate would be expected to protect those regions from HX. Possibly, such segments are very sticky and might have gone lost during experimental procedures, or they were not detected due to impaired ionization.

In vivo, sHsps are among the first chaperones that associate with misfolded polypeptides, modulating their aggregation. As reported for other sHsps (Haslbeck et al., 2005; Mogk et al., 2003), Hsp26 and Hsp42 were found to form stable complexes with heat-denatured substrates (Figure 20), creating a reservoir of refolding-competent misfolded species (Ehrnsperger et al., 1997; Lee et al., 1997; Veinger et al., 1998). Substrate release requires downstream processing by ATP-

dependent Hsp70 and Hsp100 chaperones (Haslbeck et al., 2005; Mogk et al., 2003). Compared to pure aggregates, the co-aggregation of sHsps increases the distance between substrate molecules and keeps misfolded regions apart (Figure 12). This is in agreement with a better susceptibility of sHsp-substrate complexes to proteolysis (Basha et al., 2012). The enhanced spacing of misfolded conformers might improve the accessibility for chaperones, sustaining efficient disaggregation and refolding. In addition, it might reduce the force that Hsp100 chaperones need to extract misfolded species from the aggregate or enable Hsp70 to act alone (Mogk et al., 2003).

How do sHsps influence the structure of aggregates at the molecular level? HX showed that Hsp26 and Hsp42 globally protect heat-induced MDH aggregates from HX in a concentration-dependent manner. Binding of sHsps to unfolded MDH segments is one reason for reduced deuteron incorporation. In addition, the detailed analysis of HX data revealed that many regions of sHsp-complexed MDH exist as a mixture of two populations: a low exchanging and a high exchanging population. In the low exchanging population the degree of deuteron incorporation (indicated by the position of the mass/charge isotope peaks; Figure 17) corresponds quite precisely to the one in the native state (referred to as ‘native-like’). The HX of the high-exchanging population is similar to that of the aggregated state. This structural heterogeneity was observed for most of the detected peptides and has not been reported in a previous study in which sHsp-substrate complexes were studied by HX (Cheng et al., 2008). The high similarity between the HX of the low exchanging population and of the same peptide from native MDH renders the possibility unlikely that this particular HX pattern originates from sHsp binding to the respective MDH regions. Thus, these observations indicate that sHsps retain native-like structure in bound MDH substrate molecules. This is in agreement with earlier findings suggesting that two core regions in MDH are preserved by pea sHsp PsHsp18.1, and wheat sHsp TaHsp16.9 (Cheng et al., 2008). In the present study, the comparison of sHsp-complexed and aggregated MDH showed that the degree of MDH protection by sHsps is larger and more global than previously noticed. The appearance of a mixture of the two populations might be explained by different scenarios: At substoichiometric MDH:sHsp ratio, not all MDH molecules are bound by sHsps and thus this portion aggregates. Additionally, interactions with sHsps might be insufficient to preserve native-like structures. When using an excess of sHsps over MDH, binding of sHsps to different substrate segments might occasionally fail to efficiently retain native-like states. The latter suggestion would assume that productive preservation of native-like structures requires binding of sHsps to specific parts of denaturing MDH.

The findings from HX were substantiated by single-molecule measurements on MBP, which revealed that binding of Hsp42 suppresses tight interactions between

misfolded moieties and promotes native-like substrate folds. Similar to SecB (Bechtluft et al., 2007) and Trigger Factor (Mashaghi et al., 2013), Hsp42 does not seem to interact with completely folded native structures. Or, if any of those chaperones would interact, they would at least not significantly stabilize native MBP against forced unfolding. In presence of Hsp42 tight misfolds between misfolded MBP repeats were absent, which is consistent with observations from turbidity and FRET experiments. Though, weak misfolds were still measured, indicating that the suppression is not complete, possibly because client monomers have a very high effective local concentration in this approach. Prevention of the formation of tight aggregates has also been observed with SecB and Trigger Factor by using this assay. SecB was shown to keep MBP in an extended state, whereas Trigger Factor (Bechtluft et al., 2007; Mashaghi et al., 2013) promotes partially folded states, in which segments smaller than one MBP repeat retained some structural elements. In contrast, Hsp42 was observed to bind and stabilize only the near-native core structure of MBP, confirming results from HX.
Remaining native-like structures could additionally increase the distance between misfolded conformers in presence of sHsps (as observed by FRET). The enhanced spacing together with preserved native-like folds might be the reason for increased solubility of sHsp-substrate complexes and their improved reactivation by ATP-dependent chaperones.

Where are the preferred sHsp binding sites in heat-denaturing substrates? Based on HX, binding sites cannot be unambiguously assigned. DSS crosslinking experiments identified the C-terminal region of MDH as a major site for sHsp interaction. This region is located at the periphery of the MDH dimer and is surface-exposed. Corresponding peptides show highest HX in the aggregated state and remained partially deprotected upon sHsp binding. One could imagine that these MDH sites unfold early upon heat treatment and are immediately bound by sHsps. This allows sHsps to capture early unfolding MDH intermediates, protecting the remaining part of complexed substrates from further unfolding and keeping parts of the substrate in a native-like state. This hypothesis is in agreement with previous findings, in which MS studies of pea Hsp18.1/substrate complexes revealed that the native quaternary structure of bound substrate proteins is at least partially retained (Stengel et al., 2012).

The co-aggregation of Hsp26 and Hsp42 with denaturing substrates was shown to differ *in vivo*: Hsp42 associates with misfolded species at physiological mild heat stress (37°C), whereas Hsp26 only binds to unfolded polypeptides upon severe heat shock (45°C) (Specht et al., 2011). Accordingly, in *in vitro* assays, Hsp42 is constitutively active, but Hsp26 requires temperature-induced activation (Haslbeck

et al., 1999). Concerning MDH, no major differences were detected between Hsp26 and Hsp42. Both sHsps similarly suppressed the formation of big aggregates in turbidity and centrifugation assays, and the degree of MDH protection was comparable for Hsp26 and Hsp42. Only the FRET approach revealed that lower Hsp42 concentrations were needed to reduce the aggregation-caused FRET signal, suggesting a higher efficiency (Figure 12). When luciferase was used, clearly varying efficiencies were observed: Higher amounts of Hsp26 were required to suppress the formation of large turbid aggregates compared to Hsp42. In accordance, a previous study suggested that Hsp42 is the more efficient chaperone (Haslbeck et al., 2004). Furthermore, this is in agreement with observations that sHsps are less efficient with larger proteins, as they roughly bind equal amounts of their own weight (Basha et al., 2012), and luciferase has a higher molecular weight than MDH.

sHsp-bound MDH molecules did not exhibit enzyme activity, but smaller and more soluble complexes allowed for faster and more efficient MDH reactivation by ATP-dependent yeast chaperones. This is in agreement with earlier findings for other model substrates (Cashikar et al., 2005; Haslbeck et al., 2005). Despite facilitated reactivation, MDH disaggregation from sHsp-substrate complexes remained Hsp104-dependent. This contrasts with observations for *E. coli* chaperones. Here, the DnaK machinery alone was shown to reactivate proteins from small, soluble sHsp-substrate complexes. Only large, insoluble aggregates with incorporated sHsps required the complete DnaK-ClpB bi-chaperone system (Mogk et al., 2003).

Where are the substrate binding sites within Hsp26 and Hsp42 and does substrate binding induce conformational changes in sHsps? In absence of substrate, HX of Hsp26 and Hsp42 revealed highly flexible N- and C-terminal extensions, displaying high deuteron incorporation. This is in accordance with HX profiles determined for other sHsp family members (Basha et al., 2013; Cheng et al., 2008; Wintrode et al., 2003) and it explains the inability to resolve NTEs in X-ray crystallography (Basha et al., 2012). Interestingly, substrate binding induced the deprotection of two peptides located in the NTE and the ACD of Hsp26 (Figure 22). In how far these conformational changes might be functionally relevant, remains to be solved in further experiments. Upon substrate interaction, protection was mainly observed in N-terminal regions of the yeast sHsps, suggesting that these are the major binding sites. More specifically, DSS crosslinking revealed that Lys45 of Hsp26 formed most interactions with bound substrate. Remarkably, this residue is part of the thermosensor region in the middle domain of Hsp26 which undergoes a conformational change upon heat-activation (Franzmann et al., 2008). Consistently, deletion of N-terminal residues in Hsp26 was shown to affect substrate interaction (Haslbeck et al., 2004). DSS crosslinks between MDH and Hsp42 were not detected.

This might be explained by the absence of lysine residues (required for DSS-crosslinking) in the N-terminal 171 aa of Hsp42, implying that this region is primarily involved in substrate interaction. This suggestion was confirmed by co-immunoprecipitation experiments *in vivo* (done by Stephanie Miller; see below). Two more crosslinking approaches were tried to specify the Hsp42 substrate binding sites: Two Hsp42 mutants were generated, in which Gln20 or Arg35 of the Hsp42 prion-like domain were replaced by lysines, as respective changes exist in Hsp42 homologs. Still, no MDH-Hsp42 DSS-crosslinks could be detected. Furthermore, the use of acidic-specific crosslinkers did not reveal MDH-Hsp42 interaction sites.
Altogether, these findings are in agreement with previous studies, reporting that the N-terminal arm is the major, but not exclusive player in substrate recognition (Ahrman et al., 2007; Jaya et al., 2009; McHaourab et al., 2009).

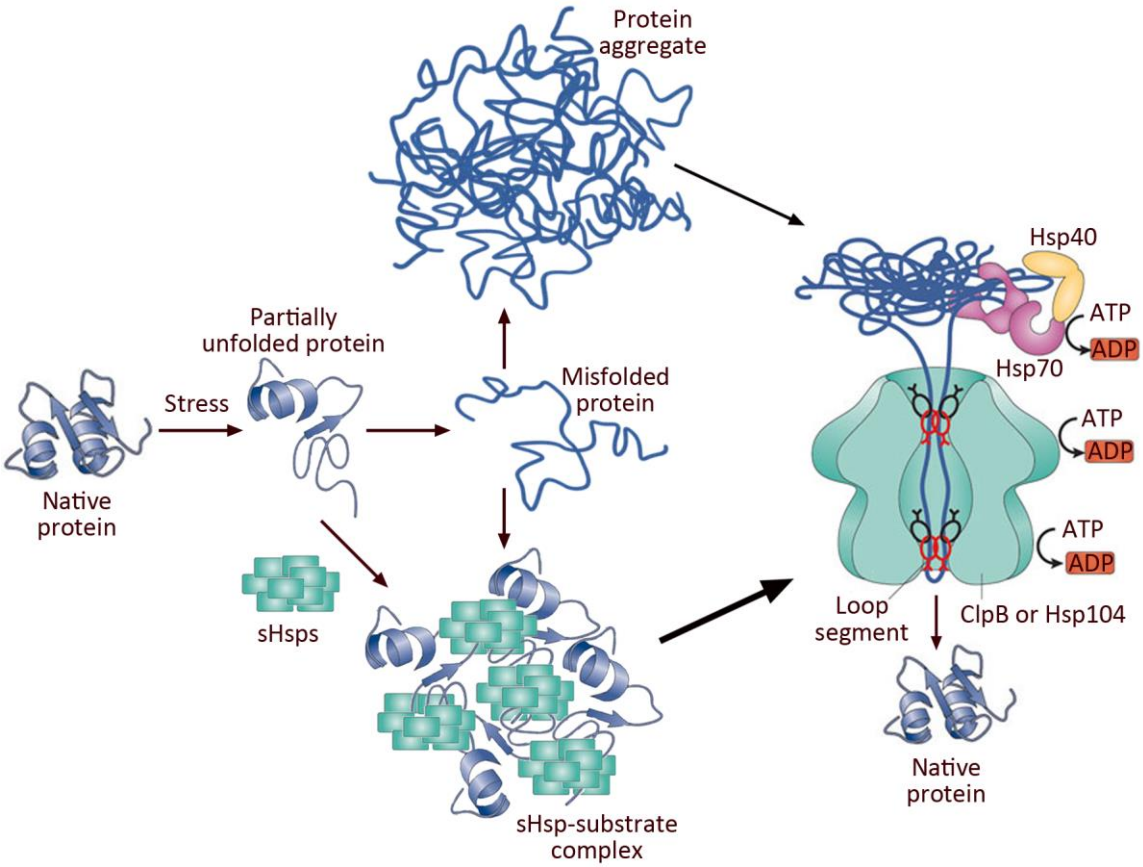

***Figure 49**: Hsp26 and Hsp42 sequester proteins early during aggregation. Thereby they preserve native-like structure of bound substrates and increase the distance between misfolded protein molecules, suppressing the formation of tight, large aggregates. These features contribute to facilitate chaperone-mediated disaggregation.*

Summarized, the results show that sHsps do not simply suppress the formation of large aggregates. They associate fast with denaturing proteins by interacting with exposed, unfolded segments and protect the substrate from global unfolding preserving native-like substrate fold, or allow the refolding of denatured misfolded proteins back to native-like structures (Figure 49). Retained or regained native-like

structure and sHsp-caused spacing of misfolded proteins should contribute to facilitate chaperone-mediated disaggregation.

4.2 The prion-like domain of Hsp42 couples substrate binding and phase transition of misfolded proteins

Strikingly, Hsp42 is an outstanding sHsp as it exhibits two highly remarkable features: Firstly, Hsp42 contains an unusually long N-terminal domain. Secondly, via this domain, Hsp42 participates in the organized deposition of protein aggregates in yeast. More precisely, the NTE of Hsp42 was shown to be required for the sequestration of misfolded proteins in cytosolic aggregates (CytoQ) (Miller et al., 2014). This process has cytoprotective functions, since *hsp42Δ* cells show severe growth disadvantage to wt cells during repetitive stress. So far, the molecular basis promoting CytoQ formation was unknown. Intriguingly, based on bioinformatic prediction, Hsp42 NTE can be divided into two prototypes of intrinsically disordered domains (IDD): A prion-like domain (enriched in Gln/Asn and Tyr) and an unstructured domain (high net charge, low hydrophobicity) (Alberti et al., 2009). IDDs are able to mediate self-interaction of proteins and interactions with other cellular factors. In so-called 'phase transitions', these properties allow the formation of self-organizing compartments, in which components can associate and dissociate. In addition to membrane-surrounded compartments, such self-organizing assemblies enable the clustering and orchestration of distinct cellular processes, and are thus crucial for homeostasis. In recent years, a number of those membrane-free compartments were described that are formed upon environmental stresses including heat, starvation and oxidative stress (Han et al., 2012; Kato et al., 2012; Narayanaswamy et al., 2009; Weber and Brangwynne, 2012). Often, these represent RNA granules, in which RNA-binding proteins mediate self-interaction via prion-like domains as well as the binding of mRNAs (Buchan, 2014). Similarly, Hsp42 acts as cytosolic protein aggregase, promoting the controlled phase separation during heat shock induced CytoQ formation. In this study, we dissected the roles of each of the IDDs of the Hsp42 NTE in this process. We found that the prion-like domain mediates substrate binding and triggers the generation of cytosolic aggregates, while the unstructured domain has regulatory function. Counter-intuitively, *in vitro*, Hsp42 shows normal chaperone activity, suppressing the formation of large aggregates when present at sufficiently high levels. I found that this function is also mediated by the prion-like domain.

Initially, the analysis of Hsp42 deletion constructs revealed that the prion-like subdomain of Hsp42 NTE is essential for generating cytosolic aggregates (Stephanie

Miller, unpublished data). But is the prion-like domain also sufficient for triggering CytoQ formation? Domain swapping experiments showed that replacing the NTE of Hsp26 by the prion-like domain of Hsp42 could not restore CytoQ formation in *hsp42Δ* cells, suggesting for an additional role of the unstructured domain (Stephanie Miller, unpublished data). However, an Hsp42 deletion mutant lacking the unstructured domain was still able to generate cytosolic aggregates (Figure 50a). Thus, the prion-like domain is required, but not necessarily sufficient for CytoQ formation. Accordingly, *in vitro*, Hsp42Δ1-99 was not able to perform its chaperone functions, i.e. it did not suppress the formation of large aggregates or facilitate disaggregation. Lacking activity of Hsp42Δ1-99 is due to the fact that the prion-like domain is needed for substrate interaction, as shown in co-precipitation experiments (Stephanie Miller, unpublished data). In agreement, ANS binding indicated the exposure of hydrophobic surfaces by the prion-like domain.

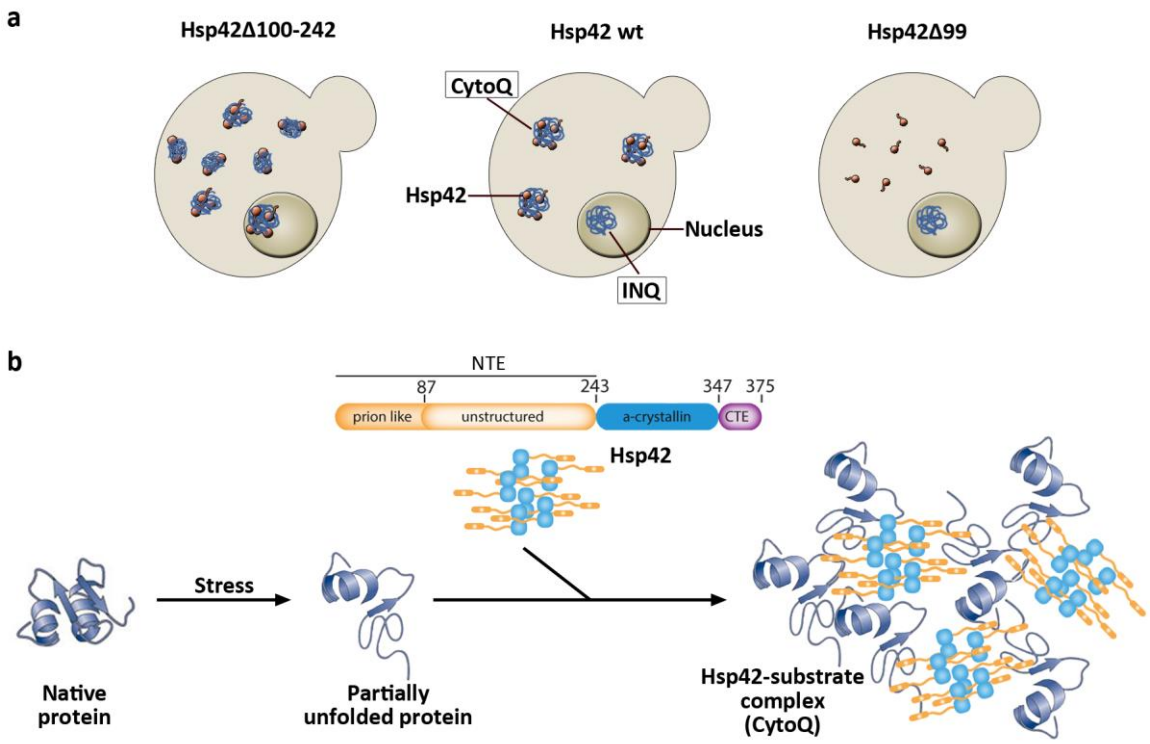

Figure 50: *The prion-like domain of Hsp42 couples substrate binding and phase transition of unfolded protein substrates resulting in CytoQ formation.* ***(a)*** *Phenotypic effects and subcellular localization at heat shock conditions are shown for all Hsp42 variants. Hsp42 is colored dark red and the aggregates blue.* ***(b)*** *Domain organization of Hsp42 with the NTE subdomains (prion-like and unstructured domain) shown in yellow, the ACD in blue and the CTE in violet. Numbers of aa residues at domain boundaries are indicated. The prion-like domain (rod-shaped) mediates self-interaction of Hsp42 (oligomerization), binds unfolded protein substrates and promotes their sequestration at CytoQ.*

More detailed investigation of the isolated prion-like domain was not possible, since its high aggregation propensity hampered the purification. Surprisingly, deletion of the unstructured domain resulted in enhanced Hsp42 activity: In HX, increased protection of bound MDH substrate was observed. Furthermore, Hsp42Δ100-242

efficiently reduced the aggregation-caused FRET signal of substrates *in vitro*, and the formation of smaller substrate complexes was detected by EM. Consistently, *in vivo*, Hsp42Δ100-242 generated more, though smaller, aggregates, which persisted for longer times after stress release (Figure 50a). In addition, deletion of the unstructured domain resulted in increased substrate binding capacity of Hsp42. The reason for the prolonged existence of the aggregates generated by Hsp42Δ100-242 remains to be investigated, since Hsp70/Hsp100-mediated substrate reactivation kinetics *in vitro* seems to be unaffected (Figure 34 and *in vivo* luciferase refolding assays by Stephanie Miller, unpublished data).
In conclusion, these results indicate that the prion-like domain is required for Hsp42 activity, whereas the unstructured domain has a negative regulatory function.

How does the unstructured domain of the NTE modulate Hsp42 activity? Given the enhanced substrate binding capacity of Hsp42Δ100-242, the unstructured domain could act as a spacer restricting substrate access. Furthermore, it is required to localize Hsp42 to the cytosol, as Hsp42Δ100-242 was shown to accumulate inside the nucleus, in contrast to Hsp42 wt which is cytosolic (Stephanie Miller, unpublished data). Deletion of the unstructured domain results in higher oligomers, whereas deleting the prion-like domain yields smaller Hsp42 oligomers. Thus, besides the ACD (Wotton et al., 1996) the prion-like domain is involved in the oligomerization of Hsp42. The oligomer state of sHsps *per se* does, however, not report on its activity. For human HSPB1 (Hsp27), the dissociation of bigger oligomers into dimers results in enhanced activity (Shashidharamurthy et al., 2005). In other cases, as for wheat Hsp16.9, pea Hsp18.1, and the αB-crystallin, sHsp activation is accompanied by an increase of the oligomeric state (Benesch et al., 2003; Stengel et al., 2010; Sun and Liang, 1998). HX did not reveal any differences between the Hsp42 deletion variants, but the number of detected peptides is limited, which prevents to draw conclusions. Also, ANS binding to Hsp42Δ100-242 did not increase, excluding the possibility that enhanced substrate binding could arise from exposure of more hydrophobic surfaces, as seen during the activation of other sHsps (Peschek et al., 2013). Finally, quite similar rates for subunit exchange have been determined for Hsp42Δ100-242 and Hsp42 wt. Thus, the molecular basis for increased substrate binding and chaperone activity remains elusive and requires further investigation. For the human sHsp HspB6, an internal deletion of the NTE also increases chaperone activity (Heirbaut et al., 2014), suggesting a more widespread role of internal NTE segments in sHsp activity control. Regarding its negative regulatory function, the unstructured domain of Hsp42 might also provide a binding site for the prion-like domain, which could be displaced upon substrate binding.

Interestingly, other factors that interact with protein aggregates in yeast, Mca1 and Ubp2, also contain prion-like domains (Alberti et al., 2009; Hill et al., 2014; Lee et al., 2010; Oling et al., 2014). These factors do not promote aggregate assembly, but facilitate protein disaggregation. The prion-like domain of Mca1 (Yca1) is essential for binding to aggregates (Lee et al., 2010). This might either occur by direct interactions with the misfolded proteins or by contacts with the prion-like or the unstructured domain of Hsp42 in Hsp42-substrate complexes.

Which are the common features of CytoQ and RNA granules? Similar to the formation of RNA granules, it is a prion-like domain mediating the Hsp42-dependent sequestration of misfolded proteins in CytoQ. It becomes more and more obvious that prion-like domains play a crucial role in phase transitions: This is not only true for the formation of RNA granules but also - as demonstrated in this study - for protein aggregates. In further agreement with RNA granule formation, the accumulation of misfolded substrates, mainly originating from newly synthesized proteins, is needed for CytoQ formation (Stephanie Miller, unpublished data). In RNA granules, the prion-like domains exclusively mediate self-association, while mRNA is bound via separate RNA binding domains. In contrast, in Hsp42 the prion-like domain couples both activities, binding of substrate and their organized sequestration in cytosolic aggregates. The prion-like domain of Hsp42 should not exhibit highly ordered cross-β-structure, due to the lack of expanded Gln/Asn stretches and presence of structure-interfering proline residues (Toombs et al., 2010). These sequence features might enable the dual activity of the prion-like domain during CytoQ formation: Efficient self-assembly, but still allowing the interaction with a variety of misfolded protein substrates (Figure 50b). This assumption is supported by the finding that replacing the Hsp42 NTE by the prion-forming NM-domains of Sup35 does not restore CytoQ formation in *hsp42Δ* cells (Stephanie Miller, unpublished data). One could speculate that substrate binding might induce conformational changes in the prion-like domain, facilitating self-assembly and triggering CytoQ formation.

In summary, these results suggest that the prion-like domain of Hsp42 mediates substrate binding and promotes the aggregation of misfolded proteins into CytoQ compartments, whereas the unstructured domain has some regulatory function. The stimulated organized sequestration of deleterious polypeptide species protects the cellular environment and might coordinate protein quality control factors acting on and clearing aggregates. The search for further potential factors involved in this process and a deeper study of the unstructured domain, might reveal more details about the mechanisms that control CytoQ formation and its regulation.

4.3 Chaperone-mediated disassembly of the native, dimeric DnaK substrate RepE

The disassembly of protein aggregates by ATP-dependent chaperones was studied using the native Hsp70-substrate RepE. As a dimer RepE represses its own transcription, as a monomer it initiates the replication of the mini-F plasmid in *E. coli*. Monomerization of RepE is mediated by the concerted action of DnaK, DnaJ and GrpE. HX was used to study RepE wt and RepE54, a constitutively monomeric variant. Increased deuteron incorporation into RepE wt indicated that dimeric RepE is less compact than monomeric RepE54. This is in accordance with the determined crystal structures of RepE54 and RepE wt in complex with their respective DNA-binding elements (Komori et al., 1999; Nakamura et al., 2007). In dimeric RepE wt the N- and C-terminal domains are reoriented relative to each other, which is accompanied by the disruption of an interdomain β-sheet (comprising β1 and β1') and secondary structural changes in the linker connecting both domains (Figure 41). These changes are reflected in HX (see chapter 3.5.1, Figure 40). In addition, HX revealed a strong deprotection of C-terminal peptide 219-240 in RepE wt compared to RepE54. Structural differences in this region were however not obvious in the crystal structures of both RepE variants. This discrepancy might be explained by the fact that the crystal structures were determined in complex with the respective DNA binding region, which might lead to further conformational rearrangements. In addition, HX is performed in solution, whereas crystal structure determination is not. Thus, the environmental conditions differed.

Do DnaK and DnaJ interact with dimeric RepE wt and monomeric RepE54? Crosslinking experiments showed that DnaK can bind to both, dimeric and monomeric RepE, but only in absence of the respective DNA-binding element. Close proximity of the DNA binding site and a putative DnaK binding site suggests that bound DNA could hinder DnaK binding at the C-terminus of RepE. In contrast, DnaJ only binds to RepE dimers but not to RepE54 monomers as was demonstrated indirectly by measuring the synergistic stimulation of the ATPase activity of DnaK by DnaJ and substrate binding, and by HX experiments (see chapter 3.5.3). One explanation for this result could be that the stable binding by the DnaJ dimer requires two binding sites in RepE – one site per RepE monomer. This observation is contradictory to a previous work in which the authors claimed that DnaJ can bind two RepE54 monomers (Cuéllar et al., 2013). Specific crosslinking, similar to experiments with DnaK Q424C, could be performed to further attest the binding of DnaJ to monomeric or dimeric RepE.

Where are the DnaK and DnaJ binding sites in RepE and does chaperone binding induce conformational changes within the substrate? The binding site of DnaJ was not obvious in HX experiments, since none of the detected RepE peptides showed pronounced protection in presence of the cochaperone. DnaJ was shown to mainly bind substrates by interactions with aa side chains, and not by backbone contacts (Rüdiger et al., 2001). Therefore, DnaJ binding may not lead to alterations in HX. As observed for RepE wt, two RepE variants, carrying mutations in C-terminal putative DnaJ binding sites (RepE F146A-R150A and RepE R200A-P202A-R205A-R206A), caused the deprotection of peptide 184-204 in presence of DnaJ. They were thus able to interact with DnaJ. Binding of DnaJ might occur in the N-terminal part of RepE wt, which contains another putative DnaJ binding site (aa 96-116, identified by peptide library scanning). This is in agreement with previous findings showing that RepE 1-139 is able to bind DnaJ (Cuéllar et al., 2013). The DnaJ-induced deprotection of C-terminal peptide 184-204 in helix α3' indicates enhanced solvent accessibility due to structural alterations (Figure 51a). These results are consistent with findings of a previous study in which the authors speculated about a DnaJ-induced conformational change in the RepE dimer, increasing the intermolecular distance (Cuéllar et al., 2013). Interestingly, the deprotected region includes parts of the DNA binding site close to a putative DnaK binding site (Figure 51a). Consistently, peptide 184-204 is slightly protected in presence of operator DNA (IR-DNA).

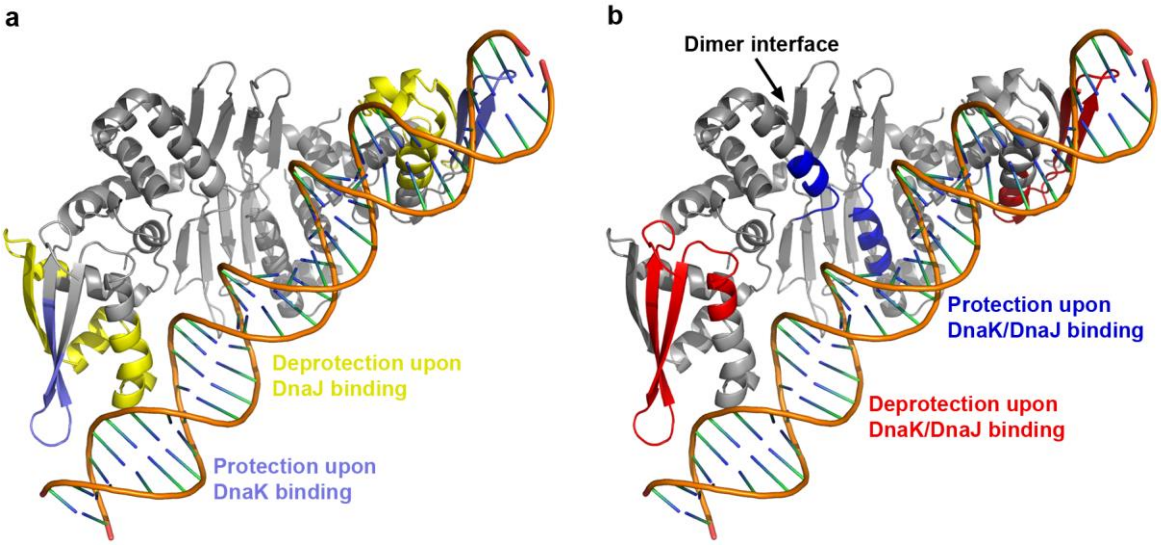

Figure 51: *Regions that are markedly protected or deprotected in dimeric RepE wt upon binding of DnaJ and DnaK. The structure of dimeric RepE wt bound to operator DNA is shown (PDB ID 2Z9O) (Nakamura et al., 2007). The coloring is according to the HX behavior.* ***(a)*** *Regions that exchange more deuterons upon DnaJ are colored yellow, regions that exchange less deuterons upon DnaK binding are colored light blue.* ***(b)*** *Regions that exchange more deuterons upon simultaneous DnaK/DnaJ binding are colored red, regions that exchange less are colored dark blue.*

Although the presence of DnaJ even enhances the binding of RepE to IR-DNA (Figure 46) (Cuéllar et al., 2013), one could speculate about a DnaJ-induced conformational

change, rendering the DnaK binding site more accessible in DNA-complexed RepE wt. HX of RepE wt in presence of DnaK resulted in slight protection of peptide 227-241, which includes parts of the presumable DnaK binding site (238-242)(Figure 51a). Concerted binding of DnaJ and DnaK induced pronounced conformational changes: While deuteron incorporation at the dimer interface was unchanged, parts of helix α4 close to the dimer interface became markedly protected (Figure 51b). This finding could indicate a stabilization of this helix, which might be implicated in the monomerization mechanism. In addition, a strong deprotection of the C-terminal part of RepE wt was observed (Figure 51b). In contrast, HX comparing RepE wt and RepE54, showed a marked protection in C-terminal peptide 220-240. These deviations might result from the fact that GrpE was not included though it is required for the monomerization of RepE (Kawasaki et al., 1990). Likely, we see a transition state, which might be passed on the way to monomerization. Also, presence of iteron DNA might cause additional conformational changes. This idea is consistent with a previous hypothesis suggesting that the RepE dimer could be remodeled to a premonomer by chaperones. Upon binding to iteron DNA it could further be modified to adapt a very similar or identical conformation as monomeric RepE54 (Zzaman and Bastia, 2005). Finally, crosslinking experiments demonstrated that the concomitant presence of DnaJ and GrpE enabled the binding of DnaK to DNA-complexed RepE wt.

In conclusion, I suggest the following mechanism (Figure 52):

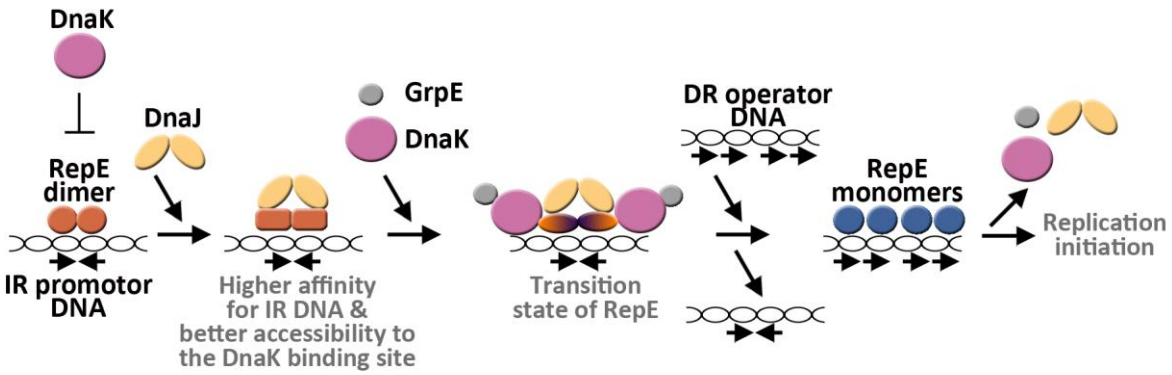

Figure 52: *Suggested interactions of dimeric RepE with components of the DnaK chaperone system during monomerization. DnaK cannot bind to IR-DNA-complexed RepE dimers. Binding of DnaJ leads to increased binding affinity of RepE for IR-DNA and might facilitate the access of DnaK to its binding site. Only concomitant presence of DnaJ and GrpE enables the binding of DnaK to RepE, which results in RepE monomerization. DnaK-bound RepE monomers represent transition states, which bind to DR iteron-DNA, thereby assuming their final monomeric conformation and releasing DnaK. IR: inverted repeat; DR: direct repeat.*

In absence of cochaperone and nucleotide exchange factor, DnaK is not able to bind DNA-complexed RepE wt, possibly due to blocking of the DnaK binding site by DNA. Binding of DnaJ, most likely to the N-terminal region (aa 96-116), leads to enhanced affinity of RepE wt for DNA. Simultaneously, a conformational change might be

induced in the C-terminal region (aa 184-204) comprising parts of the DNA binding site. Deprotection of this segment indicates increased flexibility, which could facilitate the access of DnaK to its binding site (maybe in aa 238-242). However, binding of DnaK to RepE seems only possible in presence of both, DnaJ and GrpE. Chaperone-mediated monomerization of the RepE dimer includes the reorientation of the N- and C-terminal domains resulting in sterical hindrance of the N-terminal domains. This conformational change causes the release of the RepE monomers from operator DNA. In order to avoid the reformation of the dimer, DnaK could remain bound to monomeric RepE. This hypothesis is supported by the fact that DnaK is able to bind monomeric RepE54. Subsequent binding of the RepE monomer to iteron DNA is accompanied by the release of DnaK and initiates the replication of the mini-F plasmid.

Confirmation of the suggested chaperone binding sites may be achievable by performing site-specific crosslinking with cysteines introduced close to the possible binding sites. Alternatively, RepE variants, mutated in the potential interaction sites, could be tested for their ability to bind to DnaJ or DnaK. Such experiments should allow an unambiguous identification of the binding sites. To gain better insights into the mechanism of RepE monomerization and to verify the assumptions above, further HX experiments with RepE wt are required. They should include the complete DnaK chaperone system (DnaK/DnaJ/GrpE) and the respective DNA binding elements.

Binding of DnaJ alone as well as the concerted binding of DnaJ and DnaK led to deprotection in RepE, which might indicate higher flexibility in these regions. If DnaJ would really bind in the N-terminal part of RepE wt, the induced conformational change would occur distant from the DnaJ binding site. Interestingly, similar observations were made for the heat shock transcription factor σ^{32}: DnaK and DnaJ are both able to induce local destabilization of secondary structure elements in parts of σ^{32} which are not close to the respective chaperone binding site (Rodriguez et al., 2008). One might speculate that this is a more general phenomenon and that DnaK and DnaJ have similar effects on other native or misfolded protein substrates or even protein aggregates.

5 Material and Methods

5.1 Material

5.1.1 Software and equipment

Computer software

Adobe Acrobat 9 Pro	Adobe Systems Inc.
Adobe Photoshop CS5	Adobe Systems Inc.
Adobe Illustrator CS3	Adobe Systems Inc.
Analyst QS with BioAnalyst extensions	Applied Biosystems/MDS SCIEX
Astra software	Wyatt Technology Co.
Image J	National Institutes of Health
ImageReader LAS-4000	FUJIFILM Co.
ImageReader LAS-3000	FUJIFILM Co.
Multi Gauge	FUJIFILM Co.
Prism 5	GraphPad Software, Inc.
PyMol	Delano Scientific
UltraVIEW ERS Imaging Suite	PerkinElmer

Equipment

Agarose gel chamber and trays	ZMBH workshop
ÄKTA purifier system	Amersham Pharmacia Biotech/GE Healthcare
ÄKTA purifier system micro	Amersham Pharmacia Biotech/GE Healthcare
Balances PG603-S and PB1502-S	Mettler-Toledo International, Inc.
Black-Ray B-100AP UV lamp	Ultraviolet Products
Centrifuges 5424 and 5424R	Eppendorf AG
Centrifuges Biofuge pico/ Multifuge 3SR	Heraeus Instruments GmbH
Centrifuge Sorval RC6	Thermo Scientific Inc.
Criterion™ Cell, electrophoresis chamber	Bio-Rad Laboratories, Inc.
EM900 microscope	Zeiss
FLA-3000 Fluorescent Image Analyzer	FUJIFILM Co.
French Pressure Cell	SLM/Aminco

GenoSmart gel documentation system	VWR
HPLC pumps: 1100 Series Capillary Pump and 1100 Series Binary Pump	Agilent Technologies, Inc.
Incubator MIR-254	SANYO Electric Biomedical Co. Ltd.
Intelli-Mixer	neolab
ImageQuant LAS-4000, biomolecular imager	FUJIFILM Co.
ISF1-X (Climo-Shaker)	Kuhner
LS 55 Fluorescence Spectrometer	PerkinElmer
LS6000 IC scintillation counter	Beckman
Lumat LB 9507	Berthold Technologies Gmbh & Co. KG
Magnetic stirrer MR 3001 K	Heidolph
Microwave KOR 6D07	Daewoo
MiniDawn instrument	Wyatt Technology Co.
Mini Trans-Blot® Cell	Bio-Rad Laboratories, Inc.
Mini-PROTEAN Cell, electrophoresis cell	Bio-Rad Laboratories, Inc.
NanoDrop ND-2000	Thermo Scientific Inc.
Novaspec Plus	GE Healthcare
Orbitryp Elite mass spectrometer	Thermo Scientific Inc.
pH-Meter FE20 and pH-electrode LE438	Metter-Toledo International, Inc.
Power supply ST 606 T	Gibco BRL Life technologies, Inc.
QSTAR Pulsar I Hybrid MS/MS System	Applied Biosystems/MDS SCIEX
Shaker 3018	GFL
Sonifier S-450	BRANSON
Spectrophotometer SPECORD 205	Analytik Jena AG
Spectrophotometer UV-1601	Shimadzu
Speed-Vac	Bachofer
Thermomixer comfort	Eppendorf AG
T-Gradient Thermocycler	Biometra GmbH
Tpersonal Thermocycler	Biometra Gmbh
Trans-Blot® Turbo™	Bio-Rad Laboratories, Inc.
UltiMate 3000 RSLCnano System	Thermo Scientific Inc.
Vortex-Genie 2	neoLab
Western blot apparatus midi/maxi	ZMBH workshop

Chromatography columns and materials

Amylose resin	New England Biolabs
BioBasic-8, 50 x 0.5 mm	Thermo Scientific Inc.

CNBr-activated Sepharose 4 Fast Flow	Amersham Pharmacia Biotech/GE Healthcare
MagneHis™ Ni-Particles	Promega
Ni-NTA agarose	Qiagen
PD-10 desalting columns	Amersham Pharmacia Biotech/GE Healthcare
POROS 10 R1	Applied Biosystems
POROS 20 AL	Applied Biosystems
Protino Ni-IDA sepharose	Macherey-Nagel
Sephacryl S-300 16/60	Amersham Pharmacia Biotech/GE Healthcare
SP-Sepharose	Amersham Pharmacia Biotech/GE Healthcare
Superdex 200 10/3000 GL	Amersham Pharmacia Biotech/GE Healthcare
Superdex 200 HiLoad 16/600	Amersham Pharmacia Biotech/GE Healthcare
Superose 6 10/300 GL	Amersham Pharmacia Biotech/GE Healthcare
WTC-0305N5	Wyatt Technology Co.

5.1.2 Expendable items

Amicon Concentrators	Millipore
Cellulose acetate filters, pore size 0.2 µm	Sartorius AG
Cellulose dialysis tubing	Fisherbrand
Costar 96 well plates	Corning Incorporated
Criterion™ TGX™ Precast Gels, various percentages, 18 and 26 wells	Bio-Rad Laboratories, Inc.
Cuvettes	Sarstedt AG & Co.
Low protein binding tubes, 1.5 ml	Sarstedt AG & Co.
Lumat PP tubes, 5 ml	Greiner Bio-One International AG
Microcentrifuge tubes, 1.5 ml, 2 ml	Sarstedt AG & Co.
PCR tubes, 200 ml	Sarstedt AG & Co.
Petri dishes	Greiner
Polypropylene conical centrifuge tubes, 15 ml, 50 ml	Sarstedt AG & Co.
PVDF membrane, Roti-PVDF	Carl Roth GmbH + Co. KG
RunBlue SDS-PAGE Precast Gels 8x10 cm, various percentages, 12 and 17 wells	Expedeon Ltd.

Scintillation vials	Zinsser Analytic
Slide-A-Lyzer dialysis cassettes	Thermo Scientific Inc.
Sterile filters Filtropur, 0.2 µM	Sarstedt AG & Co.
Sterile bottle filters	Sarstedt AG & Co.
Vivaspin concentrators	Sartorius AG
Whatman Paper, 3 mm	Schleicher & Schuell BioScience GmbH

5.1.3 Chemicals

If not stated otherwise, all chemicals were analytical grade and obtained from AppliChem, Fluka, Merck, Roth or Sigma-Aldrich. Only high purity solvents (HPLC grade) were used.

Enzymes and protease inhibitors

Aprotinin	AppliChem
DNase I	Sigma-Aldrich Co.
Leupeptin	AppliChem
Malate dehydrogenase	Roche
Apomyoglobin	Sigma-Aldrich Co.
Pepsin	Roche
Pepstatin A	AppliChem
Phenylmethylsulfonyl Fluoride (PMSF)	Thermo Scientific Inc.
Phusion®High-Fidelity DNA polymerase	New England Biolabs GmbH
PreScission protease	Sigma-Aldrich Co., Lab collection
Pyruvate kinase	Sigma-Aldrich Co.
Restriction enzymes	New England Biolabs, Thermo Scientific Inc.
T4 DNA Ligase	Thermo Scientific Inc.
Ulp1	Lab collection

Standards and kits

Bio-Rad Protein Assay Dye Reagent Concentrate (5 x Bradford reagent)	Bio-Rad Laboratories, Inc.
GenElute™ Gel Extraction Kit	Sigma-Aldrich Co.
GenElute™ Miniprep Kit	Sigma-Aldrich Co.
GenElute™ PCR purification Kit	Sigma-Aldrich Co.
GeneRuler 1 kb DNA Ladder (#SM0312)	Thermo Scientific Inc.

PageRuler Prestained Protein Ladder (#26616)	Thermo Scientific Inc.
QIAquick Gel Extraction Kit	QIAGEN GmbH
QIAprep Spin Miniprep Kit	QIAGEN Gmbh
QIAquick PCR Purification Kit	QIAGEN GmbH
Trans-Blot® Turbo™ 5x Transfer Buffer	Bio-Rad Laboratories, Inc.

Antibiotics

All antibiotic stock solutions were sterile-filtered. The final concentrations are indicated.

Ampicillin	100 µg/ml in water	Carl Roth GmbH
Chloramphenicol	20 µg/ml in 100% ethanol	Sigma-Aldrich Co.
Gentamycin	20 µg/ml in water	Carl Roth GmbH
Kanamycin	50 µg/ml in water	Carl Roth GmbH
Spectinomycin	50 µg/ml water	Abcam
Tetracyclin	25 µg/ml 50% ethanol	Merck

Other chemicals and reagents

Bromphenol Blue	Bio-Rad Laboratories, Inc.
D_2O (99.9%)	Carl Roth GmbH
ECF Substrate	GE Healthcare Life Sciences
Luciferin (sodium salt)	AppliChem GmbH

5.1.4 Media

All media were autoclaved. For the preparation of agar plates the medium was supplemented with 2% (w/v) agar prior to autoclaving.

LB (Luria-Bertani) medium	10 g/l tryptone 5 g/l yeast extract 5 g/l NaCl
2x YT medium	16 g/l tryptone 10 g/l yeast extract 5 g/l NaCl

5.1.5 Antibodies, primers, plasmids and strains

Antibodies

Table 2: *All antibodies are listed that were used in this study. The appropriate dilutions are indicated.*

Antibody	Generated in	Dilution	Source
α-Hsp42	rabbit	1 : 10 000	J. Buchner/M. Haslbeck
α-Hsp26	rabbit	1 : 4000	Lab collection
α-MDH	rabbit	1 : 1000	Lab collection
α-RepE	rabbit	1 : 10 000	Lab collection
α-DnaK	rabbit	1 : 10 000	Lab collection
Alkaline Phosphatase coupled anti-rabbit-IgG (H+L)	goat	1 : 20 000	Vector Laboratories, Inc.

Primers

All primers were custom synthesized by Sigma-Aldrich.

Table 3: *The nucleotide sequences of all primers that were used in this study are listed.*

Name	Sequence	Source
F_3 MDH-YFP-A	GGCCATCATATGGCGAAAGTGGCGGTGCTGGGTGCGAG C	This study
H_4 MDH-YFP-B	GGCCATCTCGAGCTTGTACAGCTCGTCCATGCCGAGAGT	This study
A2_MBP-Pre-Scission-Hsp42 fw	aacaacaacaacaataacaataacaacaacctcgggCTTGAGGTTCT CTTCGAGGGGCCCgtaccggaattcATGAGTTTTTATCAACC A	This study
B2_MBP-Pre-Scission-Hsp42 rev	TGGTTGATAAAAACTCATgaattccggtacGGGCCCCTCGAA GAGAACCTCAAGcccgaggttgttgttattgttattgttgttgttgtt	This study
13_Fw EcoRI HSP42	gcacGaattcATGAGTTTTTATCAACCATCCC	Stephanie Miller
49_Rv HSP42FLAG BamHI	gcacGgatccTCACTTGTCATCGTCGTCCTTGTAATCATTT TCTACCGTAGGGTTGGGA	Stephanie Miller
141_Fw_Hsp42_ ND99_EcoR1	gcacGaattcATGGTGGGTGACAGCGGCACT	Stephanie Miller
2 direct repeats of RepE iteron	ctgtCTGTGA CAAATTGCCC TTAAccCTGT GACAAATTGC CCTCAGatacTGAGGGCAATTTGTCACAG	This study

DNA, hairpin	ggTTAAGGGC AATTTGTCAC Agacag	
Inverted repeat of RepE iteron DNA, hairpin	ctgtCTGTGA CAAATTGCCC TTAAccCTGT GACAAATTGC CCTCAGatac CTGAGGGCAA TTTGTCACAG ggTTAAGGGC AATTTGTCAC Agacag	This study

Plasmids

Table 4: *All plasmids that were used in this study are listed. Their antibiotic resistances are indicated.*

Label	Name	Resistance	Source
pSU12	pET24a(+)	Kn	Lab collection
pSU61	pET24a(+)-MDH-YFP	Kn	This study
pSU33	pCA528-Hsp26	Kn	Sebastian Specht
pSM020	pMalE-Hsp42-FLAG	Amp	Stephanie Miller
pSU34	pMalE-Hsp42-FLAG (Pre-Scission cleavage site)	Amp	This study
pSM046	pRS303-pHsp42-Hsp42deltaUnstrucuturedDFLAG-Termhsp42	Amp	Stephanie Miller
pSU64	pMalE-Hsp42Δ1-99-FLAG (Pre-Scission cleavage site)	Amp	This study
pSU65	pMalE-Hsp42Δ100-242-FLAG (Pre-Scission cleavage site)	Amp	This study
pSU9	pCA528-RepEwt	Kn	Fernanda Rodriguez
pSU10	pMPM-A4-RepEwt-C10His	Amp	Fernanda Rodriguez
pSU5	pCA528-RepE54	Kn	Fernanda Rodriguez
pSU7	pCA528- RepEwt-Y133A-P137A-F138A	Kn	Fernanda Rodriguez
pSU8	pCA528- RepEwt-R200A-P202A-R205A-R206A	Kn	Fernanda Rodriguez
pSU6	pCA528-RepEwt-F146A-R150A	Kn	Fernanda Rodriguez

Strains

Table 5: *All strains that were used in this study are listed.*

Name	Genotype	Source
XL1-Blue	recA1 endA1 gyrA96 thi-1	Stratagene

	hsdR17 supE44 relA1 lac [F´ proAB lacIqZDM15 Tn10 (Tetr)]	
BL21 Rosetta	F- ompT lon hsdSB(rB m B) gal dcm pRARE (CmR) l(DE3)	Novagen
ArcticExpress™ (DE3)RIL strain	*E. coli* B F– ompT hsdS(rB– mB–) dcm+ Tetr gal λ(DE3) endA Hte [cpn10cpn60 Gentr] [argU ileY leuW Strr]	Stratagene

5.2 Methods

5.2.1 Molecular biology methods

Agarose gel electrophoresis

For the preparation of flat bed agarose gels, agarose powder was mixed with 0.5 x TBE buffer (0.8% or 1% w/v) and heated in the microwave until the agarose was completely dissolved. After cooling down to 50-60°C, ethidium bromide (3 µl of a 1% (w/v) stock solution per 50 ml) was added and the gels were poured in a flat bed tray with combs to generate loading pockets. When the gels were solid, DNA samples were mixed with DNA gel loading buffer, applied to the gel and DNA fragments were separated by electrophoresis at 180 V in 0.5 x TBE running buffer. The DNA fragments were visualized by using a UV documentation system. For size determination 1 µl of the GeneRuler 1 kb DNA ladder co-migrated next to the DNA samples.

TBE buffer	45 mM Tris 60 mM boric acid 1 mM EDTA
6 x DNA loading dye	40% (w/v) sucrose 0.2% (w/v) Orange G

Polymerase chain reaction (PCR)

The total volume of the PCR reaction mix was 50 µl and contained 1 x Phusion buffer, 2% (v/v) DMSO, 50-100 ng template DNA, 200 µM of dNTP mix, 10 pmol of each primer (forward and reverse) and 1 U DNA Phusion polymerase. For site-directed mutagenesis *E. coli* cells from a colony grown on a LB agar plate served as a template.

The temperature cycling steps are listed below. The PCR reaction product was purified by using the GenElute™ PCR purification or the QIAquick PCR Purification Kit. If needed, PCR products were separated by agarose gel electrophoresis and the appropriate DNA fragment was isolated by applying the GenElute™ Gel Extraction or the QIAquick Gel Extraction Kit according to the manufacturer's instructions. For site-directed mutagenesis the QuikChange® PCR protocol (Braman et al., 1996) was followed. Upon completion of the PCR reaction, the methylated template DNA was digested by 10 U DpnI for 1 h at 37°C and the reaction mix was transformed into *E. coli* XL1-Blue.

10 x Phusion buffer	200 mM Tris pH 8.8 100 mM $(NH_4)_2SO_4$ 500 mM KCl 1% (v/v) Triton X-100 20 mM $MgSO_4$

Step	**Temperature**	**Time**	**Cycles**
Denaturation	98°C	5 min	
Denaturation	98°C	40 s	
Annealing	50-60°C	40 s	30 x
Elongation	72°C	15 s/kb	
Elongation	72°C	5 min	

Restriction digest of DNA

The total volume of the restriction digest mixture was 80 µl, containing DNA fragments generated by PCR or vector DNA (maximal amounts of 3 µg). Buffer conditions and relative concentrations of restriction enzymes in a double digest were used according to the manufacturer's recommendation. The digest was performed for 1.5 h at 37°C. The restriction digested DNA fragments were separated by agarose gel electrophoresis and purified by the GenElute™ Gel Extraction or the QIAquick Gel Extraction Kit according to the manufacturer's instructions.

Ligation of DNA fragments

The ligation of restriction digested DNA fragments was carried out in a total volume of 20 µl using 1 x ligation buffer and 1 µl T4 DNA Ligase. At least a 5-fold molar excess of insert over vector DNA was used. The ligation was carried out for 30-60 min at RT.

As a religation control, only restricted vector was present during ligation. Subsequently, the ligation mixture was transformed into *E. coli* XL1-Blue.

2 x ligation buffer	132 mM Tris pH 7.6 20 mM $MgCl_2$ 2 mM DTT 2 mM ATP 15% PEG 6000

Preparation of competent cells and transformation of *E. coli*

For the preparation of $CaCl_2$-competent *E. coli* cells, cells were grown at 30°C in 50 ml LB-medium supplemented with the appropriate antibiotics. When the culture reached an OD600 of approximately 0.3, cells were incubated on ice for 10 min and centrifuged for 10 min at 4500 rpm and 4°C. The supernatant was discarded, cells were resuspended in 50 ml ice-cold, sterile 100 mM $CaCl_2$ solution and centrifuged for 10 min at 4500 rpm and 4°C. The supernatant was discarded and cells were resuspended in 1 ml ice-cold, sterile 100 mM $CaCl_2$ solution containing 15% glycerol. Cells were split into 50 µl or 100 µl aliquots and snap-frozen in liquid nitrogen.

For the transformation procedure, an aliquot of $CaCl_2$-competent *E. coli* cells were thawed on ice and 1 µl of plasmid DNA or 20 µl ligation mixture was added. Cells and DNA were gently mixed, incubated on ice for 30 min and transferred to 42°C for 90 s. After cooling on ice for 1 min, 500 µl of LB medium was added and cells were incubated at 37°C during shaking for 1.5 h. Subsequently, the cells were plated on LB-agar containing the appropriate antibiotics and incubated at 37°C over night.

Isolation of plasmid DNA from *E. coli*

Plasmid DNA was purified from *E. coli* cells using the GenElute™ Miniprep Kit or the QIAprep Spin Miniprep Kit according to the manufacturer's instructions. Plasmid DNA originating from a cloning experiment was sent to GATC Biotech AG for sequencing.

Plasmids constructed in this study

pSU61 was constructed by cloning MDH-YFP amplified by PCR from pDS56-MDH-YFP into pET24a(+) via NdeI (5') and XhoI (3') restriction sites.

In order to build pSU34, the Enterokinase cleavage site in pSM020 was changed to a PreScission cleavage site by QuikChange® PCR using primers A2_MBP-Pre-Scission-Hsp42 fw and B2_MBP-Pre-Scission-Hsp42 rev.

pSU64 was obtained by amplifying Hsp42Δ1-99 by PCR from pSU34 using primers 141_Fw_Hsp42_ND99_EcoR1 and 49_Rv HSP42FLAG BamHI. The PCR product was cloned into pSU34 via EcoRI (5') and BamHI (3') restriction sites, replacing Hsp42 wt-FLAG.

To generate pSU65, Hsp42Δ100-242FLAG was amplified by PCR from pSM046 using primers 13_Fw EcoRI HSP42 and 49_Rv HSP42FLAG BamHI. The PCR product was cloned into pSU34 via EcoRI (5') and BamHI (3') restriction sites, replacing Hsp42 wt-FLAG.

5.2.2 Protein purification

If not stated otherwise, all proteins were purified from *E. coli* BL21 STAR [DE3] rosetta. After cell harvest, cells were resuspended in the appropriate buffer and DNase I and protease inhibitors (PMSF, Aprotinin, Leupeptin and Pepstatin A) were added. Cells were lysed via French press and centrifuged 2 x at 17 000 rpm for 30 min at 4°C. Proteins whose purification is not described here were either taken from the stock of the lab or were purified according to existing protocols.

Purification of His_6-MDH

His_6-MDH was expressed from pDS56-MDH (lab collection) in *E. coli* XL1 blue placIq. Cells were grown at 37°C in 2 x YT containing ampicillin and spectinomycin. At OD600 0.6, protein production was induced by adding 0.1 mM IPTG. After incubation at 20°C over night, cells were resuspended in MDH buffer, lysed and centrifuged. The supernatant was incubated with Ni-IDA for 1 h at 4°C, washed with 4 CV MDH buffer, with 2 CV of high salt MDH buffer and eluted with 200 mM imidazole in MDH buffer. MDH containing fractions were dialysed against MDH buffer containing 10% glycerol.

MDH buffer	50 mM Tris-HCl pH 7.6 150 mM KCl 20 mM $MgCl_2$ 2 mM DTT
High salt MDH buffer	50 mM Tris-HCl pH 7.6 1 M KCl 20 mM $MgCl_2$ 2 mM DTT

MDH-YFP-His$_6$

MDH-YFP was expressed from pSU61 with a C-terminal His$_6$-tag. Protein production and Ni-IDA chromatography was done as described for His$_6$-MDH, followed by size exclusion using a Superdex75 16/60 column equilibrated in MDH buffer.

Purification of Hsp26

pCA528-Hsp26 was transformed into *E. coli* BL21 STAR [DE3] rosetta. Cells grew at 37°C in 2 x YT medium containing kanamycin and chloramphenicol. When the cell culture reached OD600 0.6, Hsp26 production was induced by adding 0.5 mM IPTG at 30°C. After 3.5 h, cells were harvested, resuspended in lysis buffer, lysed and centrifuged. The supernatant was removed and the pellet was resuspended in denaturing buffer. After stirring for 2 h at RT the sample was centrifuged (17 000 rpm, 30 min, 4°C) to remove insoluble compounds. The supernatant was incubated with Ni-IDA for 1 h at 4°C, washed with 10 CV of denaturing buffer, and with 2 CV of 2 M urea buffer. Protein was eluted with 250 mM imidazole in 2 M urea buffer and Hsp26 containing fractions were pooled. Ulp1 was added to cleave the SUMO-tag during dialysis against lysis buffer at 4°C over night. Then, the protein was incubated with Ni-IDA for 1 h at 4°C to remove the cleaved tag and loaded onto a Sephacryl S-300 HR 16/60 column equilibrated with lysis buffer. Hsp26 containing fractions were pooled and concentrated using a Vivaspin concentrator (cut-off 10 kDa).

Lysis buffer	40 mM HEPES-KOH pH 7.5 150 mM KCl 5% glycerol 5 mM β-mercaptoethanol
Denaturing buffer	40 mM HEPES-KOH pH 7.5 150 mM KCl 8 M urea 5 mM β-mercaptoethanol
2 M urea buffer	40 mM HEPES-KOH pH 7.5 150 mM KCl 2 M urea 5 mM β-mercaptoethanol

Purification of Hsp42 wt, Hsp42Δ1-99 and Hsp42Δ100-242

C-terminally FLAG-tagged Hsp42 and its deletion variants were cloned into pMal-c2E creating a C-terminal fused Maltose binding protein (MBP)-tag. The Enterokinase cleavage site in pMal-c2E was changed to a PreScission cleavage site by site-directed mutagenesis. The resulting plasmids, pSU34, pSU64 and pSU65, were each transformed into ArcticExpress™. Cells were grown in 2 x YT medium supplemented with ampicillin and gentamycin at 37°C to OD600 0.9. Cell cultures were cooled down to 13°C, 0.5 mM IPTG was added and protein was expressed at 13°C over night. Cells were resuspended in Hsp42 buffer, lysed and centrifuged. The soluble extract was incubated with amylose resin and the manufacturer's protocol was followed. In brief, the resin was washed with water and equilibrated with Hsp42 buffer. Soluble cell extract was incubated with the amylose resin for 1 h at 4°C, unbound protein was washed using Hsp42 buffer and protein was eluted with 20 mM maltose. Hsp42 containing fractions were pooled and the MBP-tag was cleaved at 4°C over night by PreScission protease, followed by size exclusion using a Sephacryl S-300 HR 16/60 column equilibrated in Hsp42 buffer. Fractions containing Hsp42 were unified and concentrated by dialysis against Hsp42 buffer containing 10% (w/v) PEG 20 000 using a dialysis tube with the pore size 3500 MWCO.

Hsp42 buffer	50 mM Tris-HCl pH 7.5
	200 mM NaCl
	2 mM DTT
	10% glycerol

Purification of RepE wt, RepE54 and RepE point mutants

pCA528 carrying RepE wt, RepE54, RepE-F146A-R150A, RepE- Y133A-P137A-F138A or RepE-R200A-P202A-R205A-R206A (pSU5, pSU6, pSU7, pSU8 and pSU9) were transformed into *E. coli* BL21 STAR [DE3] rosetta. Cells were grown at 37°C in 2 x YT supplemented with kanamycin and chloramphenicol. When the cell culture reached OD600 0.7, 1 mM IPTG was added at 30°C. After 4 h, cells were harvested, resuspended in lysis buffer, lysed and centrifuged. Soluble cell extract was incubated with Ni-NTA for 1 h at 4°C and washed with 20 CV wash buffer containing 20 mM imidazole, 20 CV high salt buffer and 20 CV ATP buffer. Protein was eluted with 200 mM imidazole in wash buffer. Subsequently, RepE containing fractions were pooled, diluted 5-fold using dilution buffer, incubated with Ulp1 for 2 h at 4°C and loaded onto a 10 ml SP-Sepharose (self-packed) equilibrated with buffer A. RepE was eluted with a 15 CV gradient from 100 mM to 1 M NaCl by mixing buffer A and B. RepE-Y133A-P137A-F138A was strongly degraded, so that purification was not

possible for this construct. His_{10}-RepE was purified from pSU10 similar to the other RepE variants. However, the addition of Ulp1 was omitted.

Lysis buffer	40 mM Na_2HPO_4/NaH_2PO_4 pH 7.9 450 mM NaCl 0.1 mM EDTA 7 mM β-mercaptoethanol 10% glycerol
Wash buffer	40 mM Na_2HPO_4/NaH_2PO_4 pH 7.9 100 mM NaCl 10% glycerol
High salt buffer	40 mM Na_2HPO_4/NaH_2PO_4 pH 7.9 1 M KCl 10% glycerol
ATP buffer	40 mM Na_2HPO_4/NaH_2PO_4 pH 7.9 100 mM NaCl 10% glycerol 10 mM ATP 25 mM $MgCl_2$
Dilution buffer	40 mM Na_2HPO_4/NaH_2PO_4 pH 7.9 100 mM NaCl 10% glycerol
Buffer A	40 mM HEPES-KOH pH 6.6 100 mM NaCl 0.1 mM EDTA 7 mM β-mercaptoethanol 10% glycerol
Buffer B:	Buffer A but 1 M NaCl

5.2.3 Protein analysis

Determination of protein concentrations

Protein concentrations were determined by using Bradford reagent (Bio-Rad Laboratories, Inc.) following the manufacturer's instructions. BSA was used to create a standard curve (Bradford, 1976).

SDS polyacrylamide gel electrophoresis (SDS-PAGE)

Sodium dodecyl sulfate polyacrylamide gel electrophoresis (SDS-PAGE) was used to separate and analyze proteins based on their ability to move within an electrical current, which is a function of the length of their polypeptide chains or of their molecular weight (Laemmli, 1970). Criterion™TGX™Precast Gels (Bio-Rad Laboratories, Inc.) or RunBlue SDS-PAGE Precast Gels 8x10 cm (Expedeon) of different percentages were used, depending on the size of the proteins to be separated. If not stated differently, protein samples were mixed with sample buffer and incubated for 5 min at 95°C. Samples were applied onto the gel and separated at constant voltage of 150-180 V SDS running buffer (for Expedeon gels) or RunBlue Rapid buffer (for RunBlue gels).

4 x SDS sample buffer	200 mM Tris-HCl pH 6.8 8% (w/v) SDS 0.4% (w/v) bromphenole blue 40% (v/v) glycerol 7% (v/v) β-mercaptoethanol
SDS running buffer	193 mM glycine 25 mM Tris 0.1% (w/v) SDS
RunBlue Rapid buffer	30 mM MOPS pH 8.2 60 mM Tris 0.1% (w/v) SDS 6.5 mM sodium bisulfite

Visualization and analysis of proteins separated by SDS-PAGE

Coomassie staining

For visualizing of all proteins after a SDS-PAGE, the SDS gel was incubated in Coomassie staining solution for at least 30 min at RT on the shaker. Unbound dye was removed by incubation and shaking in destaining solution at RT.

Coomassie staining solution	40% (v/v) methanol 0.25% (w/v) Coomassie Brilliant Blue R-250 10% (v/v) acetic acid
Destaining solution	40% (v/v) methanol 10% (v/v) acetic acid

Western blot analysis

Western blot analysis was performed to specifically visualize a distinct protein in a protein mixture or at low concentrations (Renart et al., 1979; Towbin et al., 1979). After separation by SDS-PAGE, proteins were transferred from the SDS gel onto a PVDF membrane using the Trans-Blot Turbo system from Bio-Rad according to the manufacturer's protocol. To reduce unspecific binding of primary and secondary antibodies, the membrane was incubated with TBS-T containing 3% (w/v) BSA for 1 h at RT or at 4°C over night on the shaker. The primary antibody was diluted in TBS-T containing 3% (w/v) BSA to the appropriate concentration and added to the membrane. After incubation for 1-2 h at RT or at 4°C over night on the shaker, the membrane was washed 3 x for 10 min with TBS-T. Then the membrane was incubated with the appropriate dilution of the secondary antibody in TBS-T for at least 1 h. After washing the membrane 3 x for 10 min with TBS-T, the membrane was transferred onto a clean glass plate and coated with ECF solution (GE Healthcare) in order to visualize the desired protein. After 10 min, the reaction was stopped by drying the membrane within two layers of whatman paper. The fluorescent product was detected using the FLA-3000 Fluoroimager or LAS-4000 imaging system (both FUJIFILM Co.).

TBS-T	10 mM Tris 150 mM NaCl pH adjusted to 8.0 with HCl 0.5% (v/v) Tween-20

5.2.4 Biochemical methods

HKM buffer	50 mM HEPES-KOH pH 7.6 50 mM KCl 5 mM $MgCl_2$ 2 mM DTT

Aggregation assays

Heat-induced protein aggregation was either detected by observing the light scattering signal or by centrifugation of the heat-treated sample and analysis of the supernatant and pellet fractions.

For light scattering measurements 0.5 µM His_6-MDH or 0.1 µM luciferase in HKM buffer was denatured at 47°C or 43°C, respectively, in absence or presence of various sHsp concentrations. Turbidity was measured at an excitation and emission wavelength of 550 nm or 600 nm for His_6-MDH or luciferase, respectively (PerkinElmer fluorescence spectrometer).

For centrifugation assays His_6-MDH (2 µM) in HKM buffer was denatured for 30 min at 47°C in presence or absence of sHsps followed by 30 min centrifugation (14 000 rpm, 4°C). Supernatants and pellets were analyzed by SDS-PAGE followed by Coomassie staining.

Disaggregation and refolding of thermally aggregated MDH

His_6-MDH (0.5 µM) was denatured at 47°C for 30 min in HKM buffer in presence or absence of sHsps. Protein disaggregation and refolding were started by diluting aggregated protein or sHsp-substrate complexes and chaperones 1:1 in HKM buffer containing 0.1 mg/ml BSA (final concentrations: 2 µM Ssa1, 1 µM Sis1, 0.1 µM Sse1, 1 µM Hsp104, 1 µM GroEL, 1 µM GroES). The reactivation occurred at 30°C in presence of an ATP-regenerating system (3 mM phosphoenolpyruvate; 20 µg/ml pyruvate kinase; 2 mM ATP) and was monitored as published previously (Mogk et al., 2003) using an Amersham Biosciences Novaspec Plus™ spectrophotometer.

Disaggregation and refolding of thermally aggregated luciferase

Luciferase (0.1 µM) was dentured at 43°C for 15 min in HKM buffer in presence or absence of sHsps. Protein disaggregation and refolding were started by diluting aggregated protein or sHsp-substrate complexes and chaperones 1:1 in HKM buffer (final concentrations: 2 µM Ssa1, 1 µM Sis1, 0.1 µM Sse1, 1 µM Hsp104). The

reactivation occurred at 30°C in presence of an ATP-regenerating system (3 mM phosphoenolpyruvate; 20 µg/ml pyruvate kinase; 2 mM ATP) and was monitored as published previously (Goloubinoff et al., 1999) using a spectrophotometer (Analytik Jena AG, Shimadzu).

^{3}H labeling of His$_{6}$-MDH and size exclusion chromatography of sHsp-substrate complexes after incubation with GroEL-trap

Radioactive labeling was performed by incubating His$_{6}$-MDH in HKM buffer with N-Succinimidyl [2,3-^{3}H] propionate (Amersham; 40 Ci/mmol) for 3 h at RT. Free unreacted N-Succinimidyl [2,3-^{3}H] propionate was removed by dialysis against HKM buffer. 1 µM ^{3}H-MDH and 5 µM of sHsps were heat treated for 30 min at 47°C. The formed sHsp-substrate complexes were incubated for 10 min at 30°C with 2 mM ATP in presence or absence of 14 µM GroEL-trap. As a control ^{3}H-MDH was aggregated in presence of 2 mM ATP and 14 µM GroEL-trap for 30 min at 47°C. All samples were separated at RT by Superose™ 6 10/300 GL size exclusion chromatography in HKM buffer containing 5% (v/v) glycerol. Collected fractions were quantified by scintillation counting (LS6000 IC scintillation counter, Beckman).

Förster energy resonance transfer during thermal aggregation of MDH

MDH (Roche) was labeled with 7-diethylcoumarin-3-carboxylic acid succinimidyl ester (Molecular Probes) according to the manufacturer's protocol. The labeled MDH and a C-terminally YFP-tagged MDH variant (each 0.25 µM) were mixed in pre-heated HKM buffer and the FRET signal was recorded at 527 nm in a PerkinElmer fluorescence spectrometer at 47°C.

Static light scattering

Static light scattering measurements were performed at RT by use of a miniDawn instrument coupled to WTC-0305N5 (both Wyatt Technology Co.) size exclusion chromatography runs in HKM buffer. 50 µM solutions of Hsp42 wt or variants were injected and molar masses were determined by Astra software (Wyatt Technology Co.).

Subunit exchange of Hsp42 wt and Hsp42Δ100-242

Hsp42 wt and Hsp42Δ100-242 in HKM buffer were labeled with 7-diethylaminocoumarin-3-carboxylic acid succinimidyl ester and Succinimidyl 6-(N-(7-Nitrobenz-2-oxa-1,3-diazol-4-yl)amino)hexanoate (NBD-X, SE) (both Thermo Fisher Sci.) for 2 h at RT according to the manufacturer's protocol. Unreacted dye was

separated by PD10 columns and subsequent dialysis against HKM buffer. The donor- and acceptor-labeled proteins (each 1 µM in HKM buffer) were mixed and incubated at 25°C over night. A 10-fold excess of unlabeled protein was added and fluorescence spectra were recorded at 30°C in the range 440-640 nm at an excitation of 420 nm using a PerkinElmer fluorescence spectrometer. The observed increase of donor fluorescence with time was fitted using an exponential two phase association equation in Prism 5 (Graphpad Software).

Binding of 1-Anilino-8-napthalene-sulfonate (ANS)

The stock of 100 mM ANS was dissolved in DMSO. 10 µM of Hsp42 wt or deletion variants in PBS buffer were mixed with 1 mM ANS and incubated for 15 min at 30°C. Fluorescence spectra were recorded using PerkinElmer fluorescence spectrometer at 30°C in the range of 440 to 540 nm with an excitation at 424 nm.

Electrophoretic mobility shift assay (EMSA)

The EMSAs were performed in HKM buffer in a total volume of 15 µl. 80 nM Cy3-labeled hairpin DNA (either 2 direct repeats of RepE operator DNA or inverted repeats of RepE promotor DNA, both as hairpin structure), 160 or 320 nM RepE wt or RepE54, 640 nM DnaK/1 mM ATP, 160 nM DnaJ and 320 nM GrpE were mixed as indicated and incubated for 30 min at 30°C. The samples were run on a 1% agarose gel (without ethidium bromide) at 150 V and the fluorescent DNA was detected using the LAS-3000 Fluoroimager.

Crosslinking experiments using benzophenone-4-iodoacetamide (BPIA)

The labeling of DnaKQ424C with BPIA crosslinker was performed according to the manufacturer's protocol. DnaKQ424C was dialyzed against HKM buffer lacking DTT, a 20-fold excess of a 100 mM BPIA stock in DMSO was added during vortexing. After incubation for 2.5 h at RT, unreacted BPIA was removed by dialysis against HKM buffer. Crosslinking experiments were performed in 25 mM HEPES-KOH pH 7.6, 50 mM KCl, 5 mM $MgCl_2$ in a total volume of 25 µl. 6 µM DnaKQ424C-BPIA, 6 µM RepE wt, 6 µM DnaJ, 6 µM GrpE, 12 µM RepE promotor DNA and 5 mM ATP were mixed in the indicated combinations and incubated for 1 h at 30°C. When RepE and DnaJ were present, RepE and DnaJ were mixed and pre-incubated for 10 min at 30°C. Subsequently, the proteins were crosslinked by irradiating with UV light (365 nm, 100 W) at a distance of 3 cm for 10 min on ice.

Transmission negative stain electron microscopy

Heat-induced aggregates or sHsp/protein complexes were formed as described in the aggregation assays. Images were recorded using a Zeiss EM900 microscope.

5.2.5 Amide hydrogen exchange

Immobilization of proteins

Immobilization of pepsin on POROS 20 AL

160 mg pepsin (Roche) was dissolved in 4 ml 50 mM sodium citrate pH 4.4, mixed with 0.5 g POROS 20 AL medium and incubated for 5 min at RT in the overhead shaker. Two crumbs of $NaBH_3CN$ were added. Then, 4 ml of 2 M Na_2SO_4 were slowly (distributed over 2 h) pipetted into the suspension and the mixture was incubated at 4°C over night. The addition of 160 µl 2 M Tris-HCl pH 7.6 was followed by 4 h of incubation at 4°C in the overhead shaker. The medium with immobilized pepsin was washed 6-8 times with 0.1% HCO_2H by centrifugation for 3 min at 700 rpm and stored in 0.1% HCO_2H with 0.05% NaN_3 at 4°C.

Immobilization of DnaK on CNBr-activated sepharose

DnaK was immobilized on CNBr-activated Sepharose 4 Fast Flow (Amersham Pharmacia) according to the manufacturer's instructions. In short, DnaK was dialyzed against coupling buffer (200 mM $NaHCO_3$, pH 8.3, 500 mM NaCl). 250 mg CNBr-activated Sepharose was suspended in cold 1 mM HCl, incubated for 30 min, washed with 15 volumes cold 1 mM HCl and equilibrated with coupling buffer. The pre-activated gel was then mixed with DnaK and incubated for 4 h at RT in the overhead shaker. The reaction was stopped by washing with 1 M ethanolamine for 2 h at RT. The medium with immobilized DnaK was washed with HKM buffer, HKM buffer with 1 M NaCl and HKM buffer with 0.05% NaN_3 and stored at 4°C.

Column packing

In this study the trap column and the pepsin column were self-packed according to a procedure similar to published protocols (Southan et al., 1999). Tubing, HPLC fittings, unions, filters, and screens were obtained from Upchurch. The analytical column was a BioBasic-8 (50x0.5 mm) column from Thermo Scientific.

For the trap column POROS 50 R1 bulk material (Applied Biosystems) was packed into a 2x20 mm column body. For the pepsin column POROS AL 20 material with

immobilized pepsin was packed into four 2x20 mm column bodies, which were connected after the packing procedure.

Preparation of D_2O-based buffers and fully deuterated protein controls

For the preparation of D_2O-based buffers, 500 µl of the 10 x concentrated buffer was prepared using H_2O. The buffer was frozen in liquid nitrogen and lyophilized using a vacuum centrifuge. The dried buffer was dissolved in 500 µl of D_2O and dried in the vacuum centrifuge. The procedure was repeated three times. Prior to use, the 10 x buffer stocks were diluted using D_2O.

Fully deuterated controls were obtained by denaturing the protein in 6 M GdmCl in the usual buffer for 1 h at 30°C. Then the prodecure was followed as described for D_2O-based buffers. The final volume in which the protein was dissolved was similar to the starting volume.

In-line peptic digestion/Rapid-desalting HPLC setup

The setup consisted of two HPLC pumps (Agilent 1100 Series), a Theodyne injection valve (Model 7725i) with a 200 µl steel sample loop and a 2-position/10-port valve with microelectric actuator (Valco C2-1000EP6) as published (Rist et al., 2003). For sample loading and desalting 0.05% TFA was pumped with 400 µl/min by pump A. For eluting proteins, pump B pumped 90% ACN containing 0.05% TFA with 17.5 µl/min. Deuterated, quenched samples were loaded via the injection valve and passed through the pepsin column by pump A. The resulting peptic fragments were then trapped on a reversed-phase trap column. After 3 min of desalting, the 10-port valve was switched to elute the peptides with organic solvent from pump B. The peptides were further separated by the analytical column and transferred into the electrospray ion source of the quadrupole time-of-flight mass spectrometer (QSTAR Pulsar, Applied Biosystems) using the following gradient: 0-10 min: 15-55% B, 10-11 min: 55-100% B, 11-12 min: 100-15% B (with A: 0.05% TFA and B: 90% ACN with 0.05% TFA). The whole setup was immersed in an ice bath to minimize back exchange.

Amide hydrogen exchange experiments

Setup for amide hydrogen exchange experiments with RepE

The amide hydrogen exchange reactions were initiated by a 20 to 50-fold dilution of 100 pmol protein into D_2O-based HKM buffer and incubation at 30°C. After a certain time, the reaction was quenched by decreasing the temperature to 0°C and the pH to

2.2 using quench buffer (500 mM K-phosphate buffer, pH 2.2). The quenched sample was injected into the MS-coupled HPLC setup.

For HX of RepE wt or RepE variants in presence of DnaJ, 100 pmol RepE and 200 pmol DnaJ were pre-incubated for 10 min at 30°C before performing the HX for 30 s at 30°C.

For HX of RepE wt and DnaK, immobilized DnaK packed in a column and RepE-His_{10} were used. In each experiment, the column packed with DnaK was washed with HKM buffer alone and then with HKM buffer containing 1 mM ATP. After incubation for 5 min at 30°C and another wash with HKM buffer, 300 pMol RepE-His_{10} was loaded and the column was incubated for 30 min at 30°C. Unbound protein was removed by washing with HKM buffer and D_2O-based buffer was loaded onto the column. After a certain time, the HX was quenched and the protein was simultaneously eluted with ice-cold, low pH quench buffer (500 mM K-phosphate buffer, pH 2.2). The eluted protein was injected into the mass spectrometer-coupled HPLC setup.
Here, HX of His_{10}-RepE alone was done by using a Ni-NTA column. The procedure was similar as described for immobilized DnaK, but incubation with ATP was omitted. After the experiment, the Ni-NTA was regenerated by washing the column with 0.1 M $NiCl_2$.

Setup for amide hydrogen exchange experiments with heat-induced aggregates

Native His_6-MDH (2 µM, 400 µl), thermally aggregated His_6-MDH or sHsp-MDH complexes (both formed for 30 min at 47°C) in HKM buffer were incubated with 50 µl MagneHis™ Ni-Particles (Promega) for 15 min at RT in the overhead shaker. The supernatant was removed and the beads were washed with HKM buffer. D_2O-based HKM buffer was added to initiate amide proton-deuteron exchange at 30°C. After 30 s the exchange reaction was quenched by adding ice-cold low pH quench buffer (500 mM K-phosphate buffer, pH 2.2) containing pepsin (25 µg/ml, Roche). Protein was digested from the Ni-Particles for 1 min on ice. Quenched, digested samples were injected into the HPLC setup with online peptic digest and analyzed on an electrospray ionization quadrupole time-of-flight mass spectrometer as described above. For HX experiments in which changes within sHsps upon substrate binding were determined, the sHsp-MDH complexes were formed at a ratio of 1 to 2.5 or 2 for Hsp26 or Hsp42, respectively. Before binding to the Ni-Particles, the excess of free sHsps was separated by Superose™ 6 10/300 GL size exclusion chromatography.

Data analysis of amide hydrogen exchange experiments

Analysis of deuteron incorporation into peptides was performed by using AnalystQS software (Applied Biosystems) as described (Rist et al., 2003). For the calibration of the mass spectrometer apomyoglobin was used (Sigma-Aldrich Co.). The deuterium content of the peptides was obtained by calculating the average mass difference between the isotopic envelopes of the deuterated and the undeuterated peptides. In order to correct for deuterium losses due to back-exchange, a 0% deuterium control (i.e. peptides of the unexchanged protein) and a 100% deuterium control (i.e. peptides of the fully deuterated protein) were used according to the following formula (Zhang and Smith, 1993):

$$D = \frac{< m > - < m_{0\%} >}{< m_{100\%} > - < m_{0\%} >} \cdot N$$

Here, D is the number of deuterons present in a particular peptic peptide after incubation of the protein in D_2O, N is the total number of exchangeable amide hydrogens in this peptide and <m> is the experimentally determined average mass. <$m_{0\%}$> and <$m_{100\%}$> are the average molecular masses of the same peptide obtained by analysis of the non-deuterated and the fully deuterated controls, respectively.

5.2.6 Crosslinking mass spectrometry

DSS crosslinking

Native His_6-MDH (5 µM, 200 µl), thermally aggregated His_6-MDH or sHsp-MDH complexes (both formed for 30 min at 47°C) in HKM buffer were mixed with 2.7 µl DSS stock solution (1.25 mM each of DSS-d0 and 1.25 mM DSS-d12 in DMF; Creative Molecules, Canada). Samples were incubated for 30 min at 30°C in an Eppendorf Thermomixer mixing at 300 rpm. Remaining crosslinker was quenched by adding aqueous NH_4HCO_3 to a final concentration of 90 mM and incubation for 10 min at 35°C and 600 rpm. RapiGest™ SF Surfactant (Waters), urea and NH_4HCO_3 were added to final concentrations of 1 µg/µl, 8 M and 300 mM, respectively. Samples were sonicated for 1 min, DTT was added (10 mM final concentration) followed by 30 min incubation at 37°C and 600 rpm. Aqueous iodacetamide (GE Healthcare) solution was added to a final concentration of 15 mM. After incubation for 30 min at RT in the dark, DTT was added (final concentration 10 mM) for 5 min at RT. Subsequently, lysyl endopeptidase (mass spectrometry grade; Wako Chemicals) was added at an enzyme-to-substrate ratio of 1:100, followed by incubation for 6 h at 37°C and 600 rpm. The solution was adjusted to 2 M urea and trypsin (Thermo Scientific Inc.) was included at a 1:50 enzyme-to-substrate-ratio. After incubation over night at 37°C and 600 rpm, samples were acidified to 2% formic acid and purified by solid-phase extraction using

50 mg Sep-Pak tC18 cartridges (Waters) according to the manufacturer's protocol. The eluate was evaporated to dryness in a vacuum centrifuge.

Fractionation of crosslinked peptides by size exclusion chromatography

Samples were solved in 50 µl of SEC mobile phase (water/acetonitrile/trifluoroacetic acid, 70:30:0.1) and size exclusion chromatography was performed as previously described (Leitner et al., 2012). Briefly, crosslinked peptides were separated on a Superdex Peptide PC 3.2/30 column using a GE ÄKTA micro system. The flow rate was set to 50 µl/min using the SEC mobile phase (water/acetonitrile/trifluoroacetic acid 70:30:0.1). UV absorption at 215 nm and 280 nm was recorded and 100 µl fractions were collected. Crosslinked peptides eluted at retention volumes 0.9-1.4 ml and were evaporated to dryness using a vacuum centrifuge.

Liquid Chromatography-Tandem Mass Spectrometry (LC-MS/MS)

Peptides were reconstituted in 0.1% TFA and analyzed by an Orbitrap Elite mass spectrometer coupled to an UltiMate 3000 RSLCnano System (both Thermo Scientific Inc.). After trapping, samples were loaded on a 75 µm x 250 mm Acclaim PepMap (Thermo Scientific Inc.) column with buffer A (0.1% formic acid (FA), 1% acetonitrile (ACN), 98.9% H_2O) and eluted with buffer B (0.1% FA, 10% H_2O, 89.9% ACN). Peptide separation was achieved with a 300 nl/min flow rate using the following gradient: 0-3 min: 4% B, 3-90 min: 4-45% B, 90-95 min: 45-95% B, 95-101 min 95% B. The mass spectrometer was operated in data dependent mode with the top 20 most intense ions (resolution: 60 000) selected for fragmentation in the range of m/z 350-1600 by collision induced dissociation at 40%. Singly and doubly charged peptides as well as unassigned were excluded and dynamic exclusion duration was set to 60 s, list size of 500 and a mass window of 20 ppm.

Data analysis of crosslinked peptides

Resulting Thermo Xcalibur . raw files were converted to mzXML format using MSConvert (ProteoWizard version 3.0). Crosslinked peptides were analyzed using xQuest and xProphet as previously described (Leitner et al., 2014). In brief, masses of 12.07531 Da difference for DSS-d0 and DSS-d12 were paired requiring a charge state of 3-7 within a 1 min retention time window of triggering. Spectra were searched against a database containing the UniProt entries of the target proteins as well as the reverse sequence. For xQuest the following search parameters were used: Two maximal missed cleavages, peptide length: 4-50 amino acids, fixed modifications: carbamidomethylated Cys, variable modification: oxidized Met, number of variable modification: 1, mass shift of the light crosslinker: 138.0680796, mass shift of mono-

links: 156.0786442 and 155.0964278 Da, MS1 tolerance: 10 ppm, MS2 tolerance: 0.2 Da for common and 0.3 Da for crosslink ions. For filtering the search results a target/decoy false discovery rate of 5% was estimated using xProphet as described (Walzthoeni et al., 2012); the following filtering criteria were used: MS1 mass tolerance window: -4 to 7 ppm, ld score > 20, min delta score of 0.95.

Bibliography

Ahmad, M. F., Raman, B., Ramakrishna, T. and Rao, C. M. (2008). Effect of phosphorylation on alpha B-crystallin: Differences in stability, subunit exchange and chaperone activity of homo and mixed oligomers of alpha B-crystallin and its phosphorylation-mimicking mutant. J Mol Biol *375*, 1040–1051.

Ahrman, E., Lambert, W., Aquilina, J., Robinson, C. and Emanuelsson, C. (2007). Chemical cross-linking of the chloroplast localized small heat-shock protein, Hsp21, and the model substrate citrate synthase. Protein Sci *16*, 1464–1478.

Alberti, S., Halfmann, R., King, O., Kapila, A. and Lindquist, S. (2009). A systematic survey identifies prions and illuminates sequence features of prionogenic proteins. Cell *137*, 146–158.

Aquilina, J., Benesch, J., Ding, L., Yaron, O., Horwitz, J. and Robinson, C. (2004). Phosphorylation of alphaB-crystallin alters chaperone function through loss of dimeric substructure. J Biol Chem *279*, 28675–28680.

Aquilina, J., Benesch, J., Ding, L., Yaron, O., Horwitz, J. and Robinson, C. (2005). Subunit exchange of polydisperse proteins: mass spectrometry reveals consequences of alphaA-crystallin truncation. J Biol Chem *280*, 14485–14491.

Bagnéris, C., Bateman, O., Naylor, C., Cronin, N., Boelens, W., Keep, N. and Slingsby, C. (2009). Crystal structures of alpha-crystallin domain dimers of alphaB-crystallin and Hsp20. J Mol Biol *392*, 1242–1252.

Baldwin, A., Hilton, G., Lioe, H., Bagnéris, C., Benesch, J. and Kay, L. (2011). Quaternary dynamics of aB-crystallin as a direct consequence of localised tertiary fluctuations in the C-terminus. J Mol Biol *413*, 310–320.

Bardwell, J. and Jakob, U. (2012). Conditional disorder in chaperone action. Trends Biochem Sci *37*, 517–525.

Basha, E., Jones, C., Blackwell, A. E., Cheng, G., Waters, E. R., Samsel, K. A., Siddique, M., Pett, V., Wysocki, V. and Vierling, E. (2013). An unusual dimeric small heat shock protein provides insight into the mechanism of this class of chaperones. J Mol Biol *425*, 1683–1696.

Basha, E., Lee, G., Breci, L., Hausrath, A., Buan, N., Giese, K. and Vierling, E. (2004). The identity of proteins associated with a small heat shock protein during heat stress *in*

vivo indicates that these chaperones protect a wide range of cellular functions. J Biol Chem *279*, 7566–7575.

Basha, E., O'Neill, H. and Vierling, E. (2012). Small heat shock proteins and alpha-crystallins: dynamic proteins with flexible functions. Trends Biochem Sci *37*, 206–227.

Bechtluft, P., Leeuwen, R., Tyreman, M., Tomkiewicz, D., Nouwen, N., Tepper, H., Driessen, A. and Tans, S. (2007). Direct observation of chaperone-induced changes in a protein folding pathway. Science *318*, 1458–1461.

Beissinger, M. and Buchner, J. (1998). How chaperones fold proteins. Biol Chem *379*, 245–259.

Ben-Zvi, A., De Los Rios, P., Dietler, G. and Goloubinoff, P. (2004). Active solubilization and refolding of stable protein aggregates by cooperative unfolding action of individual Hsp70 chaperones. J Biol Chem *279*, 37298–37303.

Ben-Zvi, A. P. and Goloubinoff, P. (2002). Proteinaceous infectious behavior in non-pathogenic proteins is controlled by molecular chaperones. J Biol Chem *277*, 49422–49427.

Benesch, J., Aquilina, J., Baldwin, A., Rekas, A., Stengel, F., Lindner, R., Basha, E., Devlin, G., Horwitz, J., Vierling, E., Carver, J. and Robinson, C. (2010). The quaternary organization and dynamics of the molecular chaperone HSP26 are thermally regulated. Chem Biol *17*, 1008–1017.

Benesch, J., Sobott, F. and Robinson, C. (2003). Thermal dissociation of multimeric protein complexes by using nanoelectrospray mass spectrometry. Anal Chem *75*, 2208–2214.

Bentley, N. J., Fitch, I. T. and Tuite, M. F. (1992). The small heat-shock protein Hsp26 of *Saccharomyces cerevisiae* assembles into a high molecular weight aggregate. Yeast *8*, 95–106.

Bepperling, A., Alte, F., Kriehuber, T., Braun, N., Weinkauf, S., Groll, M., Haslbeck, M. and Buchner, J. (2012). Alternative bacterial two-component small heat shock protein systems. Proc Natl Acad Sci U S A *109*, 20407–20412.

Berlett, B. and Stadtman, E. (1997). Protein Oxidation in Aging, Disease, and Oxidative Stress. J Biol Chem *272*, 20313–20316.

Bernstein, S., Dupuis, N., Lazo, N., Wyttenbach, T., Condron, M., Bitan, G., Teplow, D., Shea, J., Ruotolo, B., Robinson, C. and Bowers, M. (2009). Amyloid-beta protein oligomerization and the importance of tetramers and dodecamers in the aetiology of Alzheimer's disease. Nature Chem *1*, 326–331.

Bolognesi, B., Kumita, J., Barros, T., Esbjorner, E., Luheshi, L., Crowther, D., Wilson, M., Dobson, C., Favrin, G. and Yerbury, J. (2010). ANS binding reveals common features of cytotoxic amyloid species. ACS Chem Biol *5*, 735–740.

Bosl, B., Grimminger, V. and Walter, S. (2006). The molecular chaperone Hsp104 - a molecular machine for protein disaggregation. J Struct Biol *156*, 139–148.

Bossier, P., Fitch, I., Boucherie, H. and Tuite, M. (1989). Structure and expression of a yeast gene encoding the small heat-shock protein Hsp26. Gene *78*, 323–330.

Bova, M., Ding, L., Horwitz, J. and Fung, B. (1997). Subunit exchange of alphaA-crystallin. J Biol Chem *272*, 29511–29517.

Bova, M., Huang, Q., Ding, L. and Horwitz, J. (2002). Subunit exchange, conformational stability, and chaperone-like function of the small heat shock protein 16.5 from *Methanococcus jannaschii*. J Biol Chem *277*, 38468–38475.

Bova, M., McHaourab, H., Han, Y. and Fung, B. (2000). Subunit exchange of small heat shock proteins: analysis of oligomer formation of alphaA-crystallin and Hsp27 by fluorescence resonance energy transfer and site-directed truncations. J Biol Chem *275*, 1035–1042.

Bowden, G., Paredes, A. and Georgiou, G. (1991). Structure and morphology of protein inclusion bodies in *Escherichia coli*. Biotechnology *9*, 725–730.

Bradford, M. (1976). A rapid and sensitive method for the quantitation of microgram quantities of protein utilizing the principle of protein-dye binding. Anal Biochem *72*, 248–254.

Brady, J., Garland, D., Duglas-Tabor, Y., Robison, W.G., J., Groome, A. and Wawrousek, E. (1997). Targeted disruption of the mouse alpha-A crystallin genes induces cataract and cytoplasmic inclusion bodies containing the small heat shock protein alpha-B crystallin. Proc Natl Acad Sci U S A *94*, 884–889.

Braman, J., Papworth, C. and Greener, A. (1996). Site-directed mutagenesis using double-stranded plasmid DNA templates. Methods in molecular biology (Clifton, NJ) *57*, 31–44.

Broome, B. and Hecht, M. (2000). Nature disfavors sequences of alternating polar and non-polar amino acids: Implications for amyloidogenesis. J Mol Biol *296*, 961–968.

Bruey, J., Ducasse, C., Bonniaud, P., Ravagnan, L., Susin, S., Diaz-Latoud, C., Gurbuxani, S., Arrigo, A., Kroemer, G., Solary, E. and Garrido, C. (2000). Hsp27 negatively regulates cell death by interacting with cytochrome c. Nat Cell Biol *2*, 645–652.

Brunet Simioni, M., De Thonel, A., Hammann, A., Joly, A., Bossis, G., Fourmaux, E., Bouchot, A., Landry, J., Piechaczyk, M. and Garrido, C. (2009). Heat shock protein 27 is involved in SUMO-2/3 modification of heat shock factor 1 and thereby modulates the transcription factor activity. Oncogene *28*, 3332–3344.

Buchan, J. (2014). mRNP granules. RNA Biol *11*, 1019–1030.

Bukau, B. and Horwich, A. (1998). The Hsp70 and Hsp60 chaperone machines. Cell *92*, 351–366.

Burton, R., Siddiqui, S., Kim, Y., Baker, T. and Sauer, R. (2001). Effects of protein stability and structure on substrate processing by the ClpXP unfolding and degradation machine. EMBO J *20*, 3092–3100.

Butt, E., Immler, D., Meyer, H., Kotlyarov, A., Laass, K. and Gaestel, M. (2001). Heat shock protein 27 is a substrate of cGMP-dependent protein kinase in intact human platelets: phosphorylation-induced actin polymerization caused by HSP27 mutants. J Biol Chem *276*, 7108–7113.

Buxbaum, J. N. and Linke, R. P. (2012). A molecular history of the amyloidoses. J Mol Biol *421*, 142–159.

Campioni, S., Mannini, B., Zampagni, M., Pensalfini, A., Parrini, C., Evangelisti, E., Relini, A., Stefani, M., Dobson, C. and Cecchi, C. amd Chiti, F. (2010). A causative link between the structure of aberrant protein oligomers and their toxicity. Nature Chem Biol *6*, 140–147.

Canet, D., Last, A., Tito, P., Sunde, M., Spencer, A., Archer, D., Redfield, C., Robinson, C. and Dobson, C. (2002). Local cooperativity in the unfolding of an amyloidogenic variant of human lysozyme. Nat Struct Biol *9*, 308–315.

Carra, S., Boncoraglio, A., Kanon, B., Brunsting, J., Minoia, M., Rana, A., Vos, M., Seidel, K., Sibon, O. and Kampinga, H. (2010). Identification of the *Drosophila* ortholog of HSPB8: implication of HSPB8 loss of function in protein folding diseases. J Biol Chem *285*, 37811–37822.

Cashikar, A., Duennwald, M. and Lindquist, S. (2005). A chaperone pathway in protein disaggregation. Hsp26 alters the nature of protein aggregates to facilitate reactivation by Hsp104. J Biol Chem *280*, 23869–23875.

Cashikar, A., Duennwald, M. and Lindquist, S. (2006). A Chaperone Pathway in Protein Disaggregation. J Biol Chem *280*, 23869–23875.

Chang, E., Liao, T. Y., Lim, T., Fann, W. and Chen, R. (2009). A new amyloid-like beta-aggregate with amyloid characteristics, except fibril morphology. J Mol Biol *385*, 1257–1265.

Charette, S., Lambert, H. and Landry, J. (2001). A kinase-independent function of Ask1 in caspase-independent cell death. J Biol Chem *276*, 36071–36074.

Chen, J., Feige, M., Franzmann, T., Bepperling, A. and Buchner, J. (2010). Regions outside the alpha-crystallin domain of the small heat shock protein Hsp26 are required for its dimerization. J Mol Biol *398*, 122–131.

Chen, L., Balabanidou, V., Remeta, D., Minetti, C., Portaliou, A., Economou, A. and Kalodimos, C. (2011). Structural instability tuning as a regulatory mechanism in protein- protein interactions. Mol Cell *44*, 734–744.

Cheng, G., Basha, E., Wysocki, V. and Vierling, E. (2008). Insights into small heat shock protein and substrate structure during chaperone action derived from hydrogen/deuterium exchange and mass spectrometry. J Biol Chem *238*, 26634–26642.

Cheon, M., Chang, I., Mohanty, S., Luheshi, L., Dobson, C., Vendruscolo, M. and Favrin, G. (2007). Structural reorganisation and potential toxicity of oligomeric species formed during the assembly of amyloid fibrils. PLoS Comp Biol *3*, 1727–1738.

Chiti, F. and Dobson, C. M. (2006). Protein misfolding, functional amyloid, and human disease. Annu Rev Biochem *75*, 333–366.

Christopeit, T., Hortschansky, P., Schroeckh, V., Guhrs, K., Zandomeneghi, G. and Fändrich, M. (2005). Mutagenic analysis of the nucleation propensity of oxidized Alzheimer's beta-amyloid peptide. Protein Sci *14*, 2125–2131.

Ciryam, P., Tartaglia, G., Morimoto, R., Dobson, C. and Vendruscolo, M. (2013). Widespread aggregation and neurodegenerative diseases are associated with supersaturated proteins. Cell Rep *5*, 781–790.

Clark, J. and Muchowski, P. (2000). Small heat-shock proteins and their potential role in human disease. Curr Opin Struct Biol *10*, 52–59.

Cohen, A. S. (1969). High resolution ultrastructure, immunology and biochemistry of amyloid. Amyloidosis. Proceedings of the Symposium on Amyloidosis*, 149–171.*

Cohen, S., Linse, S., Luheshi, L., Hellstrand, E., White, D., Rajah, L., Otzen, D., Vendruscolo, M., Dobson, C. and Knowles, T. (2013). Proliferation of amyloid-beta 42 aggregates occurs through a secondary nucleation mechanism. Proc Natl Acad Sci U S A *110*, 9758–9763.

Collinge, J. & Clarke, A. R. (2007). A general model of prion strains and their pathogenicity. Science *318*, 930–936.

Cremades, N., Cohen, S., Deas, E., Abramov, A., Chen, A., Orte, A., Sandal, M., Clarke, R., Dunne, P., Aprile, F., Bertoncini, C., Wood, N., Knowles, T., Dobson, C. and Klenerman, D. (2012). Direct observation of the interconversion of normal and toxic forms of alpha-synuclein. Cell *149*, 1048–1059.

Cuéllar, J., Perales-Calvo, J., Muga, A., Valpuesta, J. and Moro, F. (2013). Structural Insights into the Chaperone Activity of the 40-kDa Heat Shock Protein DnaJ. J Biol Chem *288*, 15065–15074.

David, D., Ollikainen, N., Trinidad, J., Cary, M., Burlingame, A. and Kenyon, C. (2010). Widespread protein aggregation as an inherent part of aging in *C. elegans*. PLoS Biol *8*, e1000450.

Del Solar, G., Giraldo, R., Ruiz-Echevarria, M., Espinosa, M. and Diaz-Orejas, R. (1998). Replication and control of circular bacterial plasmids. Microbiol. Mol. Biol. Rev. *62*, 434–464.

Deloche, O., Liberek, K., Zylicz, M. and Georgopoulos, C. (1997). Purification and biochemical properties of Saccharomyces cerevisiae Mdj1p, the mitochondrial DnaJ homologue. J Biol Chem *272*, 28539–28544.

den Engelsman, J., Bennink, E., Doerwald, L., Onnekink, C., Wunderink, L., Andley, U., Kato, K., de Jong, W. and Boelens, W. (2004). Mimicking phosphorylation of the small heat-shock protein alphaB-crystallin recruits the F-box protein FBX4 to nuclear SC35 speckles. Eur J Biochem *271*, 4195–4203.

Deng, M., Chen, P., Xie, S., Zhao, J., Gong, L., Liu, J., Zhang, L., Sun, S., Liu, J., Ma, H., Batra, S. and Li, D. (2010). The small heat shock protein alphaA-crystallin is expressed in

pancreas and acts as a negative regulator of carcinogenesis. Biochim Biophys Acta *1802*, 621–631.

Diamant, S., Ben-Zvi, A., Bukau, B. and Goloubinoff, P. (2000). Size-dependent disaggregation of stable protein aggregates by the DnaK chaperone machinery. J Biol Chem *275*, 21107–21113.

Dobson, C. (1999). Protein misfolding, evolution and disease. Trends Bioch Sci *24*, 329–332.

Dobson, C. (2003). Protein folding and misfolding. Nature *426*, 884–890.

Dobson, C. M. (2001). The structural basis of protein folding and its links with human disease. Philos Trans R Soc Lond B Biol Sci *356*, 133–145.

Doyle, S., Hoskins, J. and Wickner, S. (2007). Collaboration between the ClpB AAA+ remodeling protein and the DnaK chaperone system. Proc Natl Acad Sci U S A *104*, 11138–11144.

Drummond, D. A. and Wilke, C. O. (2008). Mistranslation-induced protein misfolding as a dominant constraint on coding-sequence evolution. Cell *134*, 341–352.

Dunker, A., Silman, I., Uversky, V. and Sussman, J. (2008). Function and structure of inherently disordered proteins. Curr Opin Struct Biol *18*, 756–764.

Ecroyd, H. and Carver, J. (2009). Crystallin proteins and amyloid fibrils. Cell Mol Life Sci *66*, 62–81.

Ecroyd, H., Meehan, S., Horwitz, J., Aquilina, J., Benesch, J., Robinson, C., Macphee, C. and Carver, J. (2007). Mimicking phosphorylation of alphaB-crystallin affects its chaperone activity. Biochem J *401*, 129–141.

Ehrnsperger, M., Graber, S., Gaestel, M. and Buchner, J. (1997). Binding of non-native protein to Hsp25 during heat shock creates a reservoir of folding intermediates for reactivation. EMBO J *16*, 221–229.

Eisenberg, D. and Jucker, M. (2012). The amyloid state of proteins in human diseases. Cell *148*, 1188–1203.

Ellis, R. and Minton, A. (2006). Protein aggregation in crowded environments. Biol Chem *387*, 485–497.

Fink, A. (1998). Protein aggregation: folding aggregates, inclusion bodies and amyloid. Fold Des *3*, R9–23.

Fitzpatrick, A., Debelouchina, G., Bayro, M., Clare, D., Caporini, M., Bajaj, V., Jaroniec, C., Wang, L., Ladizhansky, V., Müller, S., MacPhee, C., Waudby, C., Mott, H., De Simone, A., Knowles, T., Saibil, H., Vendruscolo, M., Orlova, E., Griffin, R. and Dobson, C. (2013). Atomic structure and hierarchical assembly of a cross-beta amyloid fibril. Proc Natl Acad Sci U S A *110*, 5468–5473.

Fändrich, M. (2007). On the structural definition of amyloid fibrils and other polypeptide aggregates. Cell Mol Life Sci *64*, 2066–2078.

Fändrich, M. and Dobson, C. (2002). The behaviour of polyamino acids reveals an inverse side chain effect in amyloid structure formation. EMBO J *21*, 5682–5690.

Fändrich, M., Fletcher, M. A. and Dobson, C. M. (2001). Amyloid fibrils from muscle myoglobin. Nature *410*, 165–166.

Fändrich, M., Forge, V., Buder, K., Kittler, M., Dobson, C. M. and Diekmann, S. (2003). Myoglobin forms amyloid fibrils by association of unfolded polypeptide segments. Proc Natl Acad Sci U S A *100*, 15463 – 15468.

Fändrich, M., Zandomeneghi, G., Krebs, M. R., Kittler, M., Buder, K., Rossner, A., Heinemann, S. H., Dobson, C. M. and Diekmann, S. (2006). Apomyoglobin reveals a randomnucleation mechanism in amyloid protofibril formation. Acta Histochem *108*, 215–219.

Franzmann, T., Menhorn, P., Walter, S. and Buchner, J. (2008). Activation of the chaperone Hsp26 is controlled by the rearrangement of its thermo sensor domain. Mol Cell *29*, 207–216.

Franzmann, T. M., Wühr, M., Richter, K., Walter, S. and Buchner, J. (2005). The activation mechanism of Hsp26 does not require dissociation of the oligomer. J Mol Biol *350*, 1083–1093.

García-Fruitós, E., González-Montalbán, N., Morell, M., Vera, A., Ferraz, R., Arís, A., Ventura, S. and Villaverde, A. (2005). Aggregation as bacterial inclusion bodies does not imply inactivation of enzymes and fluorescent proteins. Microb Cell Fact *4*, 27.

Garridoa, C., Paul, C., Seigneurica, R. and Kampinga, H. (2012). The small heat shock proteins family: The long forgotten chaperones. Int J Biochem Cell Biol *44*, 1588–1592.

Ghosh, J., Shenoy, A.K., J. and Clark, J. (2007). Interactions between important regulatory proteins and human alphaB crystallin. Biochemistry *46*, 6308–6317.

Giese, K., Basha, E., Catague, B. and Vierling, E. (2005). Evidence for an essential function of the N terminus of a small heat shock protein *in vivo*, independent of *in vitro* chaperone activity. Proc Natl Acad Sci U S A *102*, 18896–18901.

Giese, K. and Vierling, E. (2002). Changes in oligomerization are essential for the chaperone activity of a small heat shock protein *in vivo* and *in vitro*. J Biol Chem *277*, 46310–46318.

Giese, K. C. and Vierling, E. (2004). Mutants in a small heat shock protein that affect the oligomeric state. Analysis and allele-specific suppression. J Biol Chem *279*, 32674–32683.

Glover, J. and Lindquist, S. (1998). Hsp104, Hsp70, and Hsp40: a novel chaperone system that rescues previously aggregated proteins. Cell *94*, 73–82.

Gobbo, J., Gaucher-Di-Stasio, C., Weidmann, S., Guzzo, J. and Garrido, C. (2011). Quantification of HSP27 and HSP70 molecular chaperone activities. Methods Mol Biol *787*, 137–143.

Goldfarb, L. and Dalakas, M. (2009). Tragedy in a heartbeat: malfunctioning desmin causes skeletal and cardiac muscle disease. J Clin Invest *119*, 1806–1813.

Goldfarb, L., Olivé, M., Vicart, P. and Goebel, H. (2008). Intermediate filament diseases: desminopathy. Adv Exp Med Biol *642*, 131–164.

Goldsbury, C., Frey, P., Olivieri, V., Aebi, U. and Muller, S. A. (2005). Multiple assembly pathways underlie amyloid-beta fibril polymorphisms. J Mol Biol *352*, 282–298.

Goloubinoff, P., Mogk, A., Zvi, A., Tomoyasu, T. and Bukau, B. (1999). Sequential mechanism of solubilization and refolding of stable protein aggregates by a bichaperone network. Proc Natl Acad Sci U S A *96*, 13732–13737.

Gonzalez-Montalban, N., Carrio, M., Cuatrecasas, S., Aris, A. and Villaverde, A. (2005). Bacterial inclusion bodies are cytotoxic in vivo in absence of functional chaperones DnaK or GroEL. J Biotechnol *118*, 406–412.

Graw, J. (2009). Genetics of crystallins: cataract and beyond. Exp Eye Res *88*, 173–189.

Haass, C. and Selkoe, D. (2007). Soluble protein oligomers in neurodegeneration: lessons from the Alzheimer's amyloid beta-peptide. Nature Rev Mol Cell Biol *8*, 101–112.

Han, T., Kato, M., Xie, S., Wu, L., Mirzaei, H., Pei, J., Chen, M., Xie, Y., Allen, J., Xiao, G. and McKnight, S. (2012). Cell-free formation of RNA granules: bound RNAs identify features and components of cellular assemblies. Cell *149*, 768–779.

Haslbeck, M. (2003). sHsps and their role in the chaperone network. Cell Mol Life Sci *59*, 1649–1657.

Haslbeck, M., Braun, N., Stromer, T., Richter, B., Model, N., Weinkauf, S. and Buchner, J. (2004). Hsp42 is the general small heat shock protein in the cytosol of *Saccharomyces cerevisiae*. EMBO J *23*, 638–649.

Haslbeck, M., Franzmann, T., Weinfurtner, D. and Buchner, J. (2005). Some like it hot: the structure and function of small heat-shock proteins. Nat Struct Mol Biol *12*, 842–846.

Haslbeck, M., Ignatiou, A., Saibil, H., Helmich, S., Frenzl, E., Stromer, T. and Buchner, J. (2004). A domain in the N-terminal part of Hsp26 is essential for chaperone function and oligomerization. J Mol Biol *343*, 445–455.

Haslbeck, M., Kastenmüller, A., Buchner, J., Weinkauf, S. and Braun, N. (2008). Structural dynamics of archaeal small heat shock proteins. J Mol Biol *378*, 362–374.

Haslbeck, M., Miess, A., Stromer, T., Walter, S. and Buchner, J. (2005). Disassembling protein aggregates in the yeast cytosol. The cooperation of Hsp26 with Ssa1 and Hsp104. J Biol Chem *280*, 23861–23868.

Haslbeck, M., Walke, S., Stromer, T., Ehrnsperger, M., White, H., Chen, S., Saibil, H. and Buchner, J. (1999). Hsp26: a temperature-regulated chaperone. EMBO J *18*, 6744–6751.

Haslberger, T., Zdanowicz, A., Brand, I., Kirstein, J., Turgay, K., Mogk, A. and Bukau, B. (2008). Protein disaggregation by the AAA+ chaperone ClpB involves partial threading of looped polypeptide segments. Nat Struct Mol Biol *15*, 641–650.

Heirbaut, M., Beelen, S., Strelkov, S. and Weeks, S. (2014). Dissecting the Functional Role of the N-Terminal Domain of the Human Small Heat Shock Protein HSPB6. PLoS One *9*, e105892.

Heise, H., Hoyer, W., Becker, S., Andronesi, O., Riedel, D. and Baldus, M. (2005). Molecular-level secondary structure, polymorphism, and dynamics of full-length alpha-synuclein fibrils studied by solid-state NMR. Proc Natl Acad Sci U S A *102*, 15871–15876.

Hill, S., Hao, X., Liu, B. and Nystrom, T. (2014). Life-span extension by a metacaspase in the yeast *Saccharomyces cerevisiae*. Science *344*, 1389–1392.

Horwitz, J. (1992). Alpha-crystallin can function as a molecular chaperone. Proc Natl Acad Sci U S A *89*, 10449–10453.

Horwitz, J. (2003). Alpha-crystallin. Exp Eye Res *76*, 145–153.

Ishiai, M., Wada, C., Kawasaki, Y. and Yura, T. (1992). Mini-F plasmid mutants able to replicate in *Escherichia coli* deficient in the DnaJ heat shock protein. J Bacteriol *174*, 5597–5603.

Ishiai, M., Wada, C., Kawasaki, Y. and Yura, T. (1994). Replication initiator protein RepE of mini-F plasmid: Functional differentiation between monomers (initiator) and dimers (autogenous repressor). Proc Natl Acad Sci U S A *91*, 3839 – 3843.

Jackson, M. and Mantsch, H. H. (1991). Protein secondary structure from FT-IR spectroscopy: correlation with dihedral angles from three-dimensional Ramachandran plots. Can J Chem *69*, 1636–1642.

Jaenicke, R. (1998). Protein self-organization *in vitro* and *in vivo*: partitioning between physical biochemistry and cell biology. Biol Chem *379*, 237–243.

Jahn, T. and Radford, S. (2005). The yin and yang of protein folding. FEBS J *272*, 5962–5970.

Jahn, T. and Radford, S. (2008). Folding versus aggregation: polypeptide conformations on competing pathways. Arch Biochem Biophys *469*, 100–117.

Jaya, N., Garcia, V. and Vierling, E. (2009). Substrate binding site flexibility of the small heat shock protein molecular chaperones. Proc Natl Acad Sci U S A *106*, 15604–15609.

Jehle, S., van Rossum, B., Stout, J., Noguchi, S., Falber, K., Rehbein, K., Oschkinat, H., Klevit, R. and Rajagopal, P. (2009a). alphaB-crystallin: a hybrid solid-state/solutionstate NMR investigation reveals structural aspects of the heterogeneous oligomer. J Mol Biol *385*, 1481–1497.

Jehle, S., Vollmar, B., Bardiaux, B., Dove, K., Rajagopal, P., Gonen, T., Oschkinat, H. and Klevit, R. (2009b). N-terminal domain of aB-crystallin provides a conformational switch for multimerization and structural heterogeneity. Proc Natl Acad Sci U S A *108*, 6409–6414.

Jucker, M. and Walker, L. (2013). Self-propagation of pathogenic protein aggregates in neurodegenerative diseases. Nature *501*, 45–51.

Kaganovich, D., Kopito, R. and Frydman, J. (2008). Misfolded proteins partition between two distinct quality control compartments. Nature *454*, 1089–1096.

Kamada, M., So, A., Muramaki, M., Rocchi, P., Beraldi, E. and Gleave, M. (2007). Hsp27 knockdown using nucleotide-based therapies inhibit tumor growth and enhance chemotherapy in human bladder cancer cells. Mol Cancer Ther *6*, 299–308.

Kampinga, H. and Craig, E. (2010). The HSP70 chaperone machinery: J proteins as drivers of functional specificity. Nat Rev Mol Cell Biol *11*, 579–592.

Kampinga, H., Hageman, J., Vos, M., Kubota, H., Tanguay, R., Bruford, E., Cheetham, M., Chen, B. and Hightower, L. (2009). Guidelines for the nomenclature of the human heat shock proteins. Cell Stress Chaperones *14*, 105–111.

Karran, E., M. M. and De Strooper, B. (2011). The amyloid cascade hypothesis for Alzheimer's disease: an appraisal for the development of therapeutics. Nature Rev Drug Discov *10*, 698–712.

Kato, M., Han, T., Xie, S., Shi, K., Du, X., Wu, L., Mirzaei, H., Goldsmith, E., Longgood, J., Pei, J., Grishin, N., Frantz, D., Schneider, J., Chen, S., Li, L., Sawaya, M., Eisenberg, D., Tycko, R. and McKnight, S. (2012). Cell-free formation of RNA granules: low complexity sequence domains form dynamic fibers within hydrogels. Cell *149*, 753–767.

Kawasaki, Y., Wada, C. and Yura, T. (1990). Roles of *Escherichia coli* heat shock protein DnaK, DnaJ and GrpE in mini-F plasmid replication. Mol Gen Genet *220*, 277–282.

Kawasaki, Y., Wada, C. and Yura, T. (1992). Binding of RepE initiator protein to mini-F DNA origin (ori2). J Biol Chem *267*, 11520–11524.

Kayed, R., Head, E., Thompson, J., McIntire, T., Milton, S., Cotman, C. and Glabe, C. (2003). Common structure of soluble amyloid oligomers implies common mechanism of pathogenesis. Science *300*, 486–489.

Kayed, R., Pensalfini, A., Margol, L., Sokolov, Y., Sarsoza, F., Head, E., Hall, J. and Glabe, C. (2009). Annular protofibrils are a structurally and functionally distinct type of amyloid oligomer. J Biol Chem *284*, 4230–4237.

Kelly, J. (2005). Attacking amyloid. N Engl J Med *352*, 722–723.

Kendrick, B., Cleland, J., Lam, X., Nguyen, T., Randolph, T., Manning, M. and Carpenter, J. (1998). Aggregation of recombinant human interferon gamma: kinetics and structural transitions. J Pharm Sci *87*, 1069–1076.

Kennaway, C., Benesch, J., Gohlke, U., Wang, L., Robinson, C., Orlova, E., Saibil, H. and Keep, N. (2005). Dodecameric structure of the small heat shock protein Acr1 from *Mycobacterium tuberculosis*. J Biol Chem *280*, 33419–33425.

Kim, K., Kim, R. and Kim, S. (1998). Crystal structure of a small heat-shock protein. Nature *394*, 595–599.

Koga, H., Kaushik, S. and Cuervo, A. M. (2011). Protein homeostasis and aging: the importance of exquisite quality control. Ageing Res Rev *10*, 205–215.

Komori, H., Matsunaga, F., Higuchi, Y., Ishiai, M., Wada, C. and Miki, K. (1999). Crystal strcuture of a prokaryotic replication initiator protein bound to DNA at 2.6 Å resolution. EMBO J *18*, 4597–4607.

Kriehuber, T., Rattei, T., Weinmaier, T., Bepperling, A., Haslbeck, M. and Buchner, J. (2010). Independent evolution of the core domain and its flanking sequences in small heat shock proteins. FASEB J *24*, 3633–3642.

Krishnan, R. and Lindquist, S. (2005). Structural insights into a yeast prion illuminate nucleation and strain diversity. Nature *435*, 765–772.

Kurtz, S., Rossi, J., Petko, L. and Lindquist, S. (1986). An ancient developmental induction: heat shock proteins induced in sporulation and oogenesis. Science *231*, 1154–1157.

Laemmli, U. K. (1970). Cleavage of structural proteins during the assembly of the head of bacteriophage T4. Nature *227*, 680–685.

Laganowsky, A., Benesch, J., Landau, M., Ding, L., Sawaya, M., Cascio, D., Huang, Q., Robinson, C., Horwitz, J. and Eisenberg, D. (2010). Crystal structures of truncated alphaA and alphaB crystallins reveal structural mechanisms of polydispersity important for eye lens function. Protein Sci *19*, 1031–1043.

Lanneau, D., de Thonel, A., Maurel, S., Didelot, C. and Garrido, C. (2007). Apoptosis versus cell differentiation: role of heat shock proteins HSP90, HSP70 and HSP27. Prion *1*, 53–60.

Laskowska, E., Matuszewska, E. and Kuczy?ska-Wi?nik, D. (2010). Small heat shock proteins and protein-misfolding diseases. Curr Pharm Biotechnol *11*, 146–157.

Launay, N., Goudeau, B., Kato, K., Vicart, P. and Lilienbaum, A. (2006). Cell signaling pathways to alphaB-crystallin following stresses of the cytoskeleton. Exp Cell Res *312*, 3570–3584.

Lee, G., Roseman, A., Saibil, H. and Vierling, E. (1997). A small heat shock protein stably binds heat-denatured model substrates and can maintain a substrate in a folding-competent state. EMBO J *16*, 659–671.

Lee, R., Brunette, S., Puente, L. and Megeney, L. (2010). Metacaspase Yca1 is required for clearance of insoluble protein aggregates. Proc Natl Acad Sci U S A *107*, 13348–13353.

Leitner, A., Reisch, R., Walzthoeni, T., Herzog, F., Bohn, S., Förster, F. and Aebersold, R. (2012). Expanding the chemical cross-linking toolbox by the use of multiple proteases and enrichment by size exclusion chromatography. Mol Cell Proteomics *11*, M111.014126.

Leitner, A., Walzthoeni, T. and Aebersold, R. (2014). Lysine-specific chemical cross-linking of protein complexes and identification of cross-linking sites using LC-MS/MS and the xQuest/xProphet software pipeline. Nature protocols *9*, 120–137.

Lesné, S., Koh, M., Kotilinek, L., Kayed, R., Glabe, C., Yang, A., Gallagher, M. and Ashe, K. (2006). A specific amyloid-beta protein assembly in the brain impairs memory. Nature *440*, 352–357.

Lewandowska, A., Matuszewska, M. and Liberek, K. (2007). Conformational properties of aggregated polypeptides determine ClpB-dependence in the disaggregation process. J Mol Biol *371*, 800–811.

Lührs, T., Ritter, C., Adrian, M., Riek-Loher, D., Bohrmann, B., Döbeli, H., Schubert, D. and Riek, R. (2005). 3D structure of Alzheimer's amyloid-beta(1-42) fibrils. Proc Natl Acad Sci U S A *102*, 17342–17347.

Liberek, K., Lewandowska, A. and Zi?tkiewicz, S. (2008). Focus quality control. Chaperones in control of protein disaggregation. EMBO J *27*, 328–335.

Lindner, R., Carver, J., Ehrnsperger, M., Buchner, J., Esposito, G., Behlke, J., Lutsch, G., Kotlyarov, A. and Gaestel, M. (2000). Mouse Hsp25, a small shock protein. The role of its C-terminal extension in oligomerization and chaperone action. Eur J Biochem *267*, 1923–1932.

Liu, I.-C., Chiu, S.-W., Lee, H.-Y. and Leu, J.-Y. (2012). The histone deacetylase Hos2 forms an Hsp42-dependent cytoplasmic granule in quiescent yeast cells. Mol Biol Cell *23*, 1231–1242.

Lovett, M. and Helinksi, D. (1976). Method for the Isolation of the Replication Region of a Bacterial Replicon: Construction of a Mini-F'km Plasmid. J Bacteriol *127*, 982 – 987.

Lowe, J., McDermott, H., Pike, I., Spendlove, I., Landon, M. and Mayer, R. (1992). alphaB-crystallin expression in non-lenticular tissues and selective presence in ubiquitinated inclusion bodies in human disease. J Pathol *166*, 61–68.

Maji, S. K., W. L. G. J. and Riek, R. (2009). Structure-activity relationship of amyloid fibrils. FEBS Lett *583*, 2610–2617.

Malinovska, L., Kroschwald, S., Munder, M., Richter, D. and Alberti, S. (2012). Molecular chaperones and stress-inducible protein-sorting factors coordinate the spatiotemporal distribution of protein aggregates. Mol Biol Cell *23*, 3041–3056.

Mashaghi, A., Kramer, G., Bechtluft, P., Zachmann-Brand, B., Driessen, A., Bukau, B. and Tans, S. (2013). Reshaping of the conformational search of a protein by the chaperone trigger factor. Nature *500*, 98–101.

Masson, L. and Ray, D. (1986). Mechanism of autonomous control of the *Escherichia coli* F plasmid: different complexes of the initiator/repressor protein are boun to its operator and to an F plasmid replication origin. Nucleic Acids Res *14*, 5693–5711.

Matsunaga, F., Ishiai, M., Kobayashi, G., Uga, H., Yura, T. and Wada, C. (1997). The central region of RepE initiator protein of mini-F plasmid plays a crucial role in dimerization required for negative replication control. J Mol Biol *274*, 27–38.

Matsunaga, F., Kawasaki, Y., Ishiai, M., Nishikawa, K., Yura, T. and Wada, C. (1995). DNA-binding domain of the RepE initiator protein of mini-F plasmid: involvement of the carboxyl-terminal region. J Bacteriol *177*, 1994–2001.

Mayer, M. and Bukau, B. (2005). Hsp70 chaperones: Cellular functions and molecular mechanism. Cell Mol Life Sci *62*, 670 – 684.

McHaourab, H., Godar, J. and Stewart, P. (2009). Structure and mechanism of protein stability sensors: chaperone activity of small heat shock proteins. Biochemistry *48*, 3828–3837.

Michelitsch, M. and Weissman, J. (2000). A census of glutamine/asparagine-rich regions: Implications for their conserved function and the prediction of novel prions. Proc Natl Acad Sci U S A *97*, 11910–11915.

Miller, S., Ho, C.-T., Winkler, J., Khokhrina, M., Neuner, A., Mohamed, M., Guilbride, L., Richter, K., Lisby, M., Schiebel, E., Mogk, A. and Bukau, B. (2014). Compartment-specific aggregases direct distinct nuclear and cytoplasmic aggregate deposition. submitted .

Mogk, A., Schlieker, C., Friedrich, K., Schonfeld, H., Vierling, E. and Bukau, B. (2003). Refolding of substrates bound to small Hsps relies on a disaggregation reaction mediated most efficiently by ClpB/DnaK. J Biol Chem *278*, 31033–31042.

Murray, A., Solomon, J., Wang, Y., Balch, W. and Kelly, J. (2010). Discovery and characterization of a mammalian amyloid disaggregation activity. Protein Sci *19*, 836–846.

Nakamura, A., Wada, C. and Miki, K. (2007). Structural basis for regulation of bifunctional roles in replication initiator protein. Proc Natl Acad Sci U S A *104*, 18484–18489.

Narayan, P., Ganzinger, K., McColl, J., Weimann, L., Meehan, S., Qamar, S., Carver, J., Wilson, M., St George-Hyslop, P., Dobson, C. and Klenerman, D. (2013). Single molecule characterization of the interactions between amyloid-beta peptides and the membranes of hippocampal cells. J Am Chem Soc *135*, 1491–1498.

Narayanaswamy, R., Levy, M., Tsechansky, M., Stovall, G., O'Connell, J., Mirrielees, J., Ellington, A. and Marcotte, E. (2009). Widespread reorganization of metabolic enzymes into reversible assemblies upon nutrient starvation. Proc Natl Acad Sci U S A *106*, 10147–10152.

Narberhaus, F. (2002). Alpha-crystallin-type heat shock proteins: socializing minichaperones in the context of a multichaperone network. Microbiol Mol Biol Rev *62*, 64–93.

Nelson, R. and Eisenberg, D. (2006). Recent atomic models of amyloid fibril structure. Curr Opin Struct Biol *16*, 260–265.

Nelson, R., Sawaya, M., Balbirnie, M., Madsen, A., Riekel, C., Grothe, R. and Eisenberg, D. (2005). Structure of the cross-beta spine of amyloid-like fibrils. Nature *435*, 773–778.

Nettleton, E., Tito, P., Sunde, M., Bouchard, M., Dobson, C. and Robinson, C. (2000). Characterization of the oligomeric states of insulin in self-assembly and amyloid fibril formation by mass spectrometry. Bioph J *79*, 1053–1065.

Neuwald, A., Aravind, L., Spouge, J. and Koonin, E. (1999). AAA+: A class of chaperone-like ATPases associated with the assembly, operation, and disassembly of protein complexes. Genome Res *9*, 27–43.

O'Callaghan-Sunol, C., Gabai, V. and Sherman, M. (2007). Hsp27 modulates p53 signaling and suppresses cellular senescence. Cancer Res *67*, 11779–11788.

Okuno, A., Kato, M. and Taniguchi, Y. (2007). Pressure effects on the heat-induced aggregation of equine serum albumin by FT-IR spectroscopic study: Secondary structure, kinetic and thermodynamic properties. Biochim Biophys Acta *1774*, 652–660.

Oling, D., Eisele, F., Kvint, K. and Nystrom, T. (2014). Opposing roles of Ubp3-dependent deubiquitination regulate replicative life span and heat resistance. EMBO J *33*, 747–761.

Olzscha, H., Schermann, S., Woerner, A., Pinkert, S., Hecht, M., Tartaglia, G., Vendruscolo, M., Hayer-Hartl, M., Hartl, F. and Vabulas, R. (2011). Amyloid-like aggregates sequester numerous metastable proteins with essential cellular functions. Cell *144*, 67–78.

Otzen, D. and Oliveberg, M. (1999). Salt-induced detour through compact regions of the protein folding landscape. Proc Natl Acad Sci U S A *96*, 11746–11751.

Painter, A., Jaya, N., Basha, E., Vierling, E., Robinson, C. and Benesch, J. (2008). Real-time monitoring of protein complexes reveals their quaternary organization and dynamics. Chem Biol *15*, 246–253.

Parcellier, A., Schmitt, E., Brunet, M., Hammann, A., Solary, E. and Garrido, C. (2005). Small heat shock proteins HSP27 and alphaB-crystallin: cytoprotective and oncogenic functions. Antioxid Redox Signal *7*, 404–413.

Parsell, D., Kowal, A., Singer, M. and Lindquist, S. (1994). Protein disaggregation mediated by heat-shock protein Hsp104. Nature *372*, 475–478.

Paul, C., Manero, F., Gonin, S., Kretz-Remy, C., Virot, S. and Arrigo, A. (2002). Hsp27 as a negative regulator of cytochrome C release. Mol Cell Biol *22*, 816–834.

Perng, M., Cairns, L., van den IJssel, P., Prescott, A., Hutcheson, A. and Quinlan, R. (1999). Intermediate filament interactions can be altered by HSP27 and alphaB-crystallin. J Cell Sci *112*, 2099–20112.

Peschek, J., Braun, N., Franzmann, T., Georgalis, Y., Haslbeck, M., Weinkauf, S. and Buchner, J. (2009). The eye lens chaperone alpha-crystallin forms defined globular assemblies. Proc Natl Acad Sci U S A *106*, 13272–13277.

Peschek, J., Braun, N., Rohrberg, J., Back, K., Kriehuber, T., Kastenmüller, A., Weinkauf, S. and Buchner, J. (2013). Regulated structural transitions unleash the chaperone activity of alphaB-crystallin. Proc Natl Acad Sci U S A *110*, 3780–3789.

Petko, L. and Lindquist, S. (1986). Hsp26 is not required for growth at high temperatures, nor for thermotolerance, spore development, or germination. Cell *45*, 885–894.

Petkova, A., Leapman, R., Guo, Z., Yau, W., Mattson, M. and Tycko, R. (2005). Self-propagating, molecular-level polymorphism in Alzheimer's beta-amyloid fibrils. Science *307*, 262–265.

Pierre, P. (2005). Dendritic cells, DRiPs, and DALIS in the control of antigen processing. Immunol Rev *207*, 184–190.

Poulain, P., Gelly, J. and Flatters, D. (2010). Detection and architecture of small heat shock protein monomers. PLoS One *5*, e9990.

Powers, E. T., Morimoto, R. I., Dillin, A., Kelly, J. W. and Balch, W. E. (2009). Biological and chemical approaches to diseases of proteostasis deficiency. Annu Rev Biochem *78*, 959–991.

Préville, X., Salvemini, F., Giraud, S., Chaufour, S., Paul, C., Stepien, G., Ursini, M. and Arrigo, A. (1999). Mammalian small stress proteins protect against oxidative stress through their ability to increase glucose-6-phosphate dehydrogenase activity and by maintaining optimal cellular detoxifying machinery. Exp Cell Res *247*, 61–78.

Rajasekaran, N., Connell, P., Christians, E., Yan, L., Taylor, R., Orosz, A., Zhang, X., Stevenson, T., Peshock, R., Leopold, J., Barry, W., Loscalzo, J., Odelberg, S. and Benjamin, I. (2007). Human alpha B-crystallin mutation causes oxido-reductive stress and protein aggregation cardiomyopathy in mice. Cell *130*, 427–439.

Rampelt, H., Kirstein-Miles, J., Nillegoda, N., Chi, K., Scholz, S., Morimoto, R. and Bukau, B. (2012). Metazoan Hsp70 machines use Hsp110 to power protein disaggregation. EMBO J *31*, 4221–4235.

Rüdiger, S., Schneider-Mergener, J. and Bukau, B. (2001). Its substrate specificity characterizes the DnaJ co-chaperone as a scanning factor for the DnaK chaperone. EMBO J. *20*, 1042–1050.

Reichmann, D., Xu, Y., Cremers, C., Ilbert, M., Mittelman, R., Fitzgerald, M. and Jakob, U. (2012). Order out of disorder: Working cycle of an intrinsically unfolded chaperone. Cell *148*, 947–957.

Reis-Rodrigues, P., Czerwieniec, G., Peters, T., Evani, U., Alavez, S., Gaman, E., Vantipalli, M., Mooney, S., Gibson, B., Lithgow, G. and Hughes, R. (2012). Proteomic analysis of agedependent changes in protein solubility identifies genes that modulate lifespan. Aging Cell *11*, 120–127.

Renart, J., Reiser, J. and Stark, G. (1979). Transfer of proteins from gels to diazobenzyloxymethyl-paper and detection with antisera: a method for studying antibody specificity and antigen structure. Proc Natl Acad Sci U S A *76*, 3116–3120.

Rist, W., Jorgensen, T., Roepstorff, P., Bukau, B. and Mayer, M. (2003). Mapping temperature-induced conformational changes in the *Escherichia coli* heat shock transcription factor sigma32 by amide hydrogen exchange. J Biol Chem *278*, 51415–51421.

Ritter, C., Maddelein, M., Siemer, A., Lührs, T., Ernst, M., Meier, B., Saupe, S. and Riek, R. (2005). Correlation of structural elements and infectivity of the HET-s prion. Nature *435*, 844–848.

Robertson, A., Headey, S., Saunders, H., Ecroyd, H., Scanlon, M., Carver, J. and Bottomley, S. (2010). Small heat-shock proteins interact with a flanking domain to suppress polyglutamine aggregation. Proc Natl Acad Sci U S A *107*, 10424–10429.

Rodriguez, F., Arsène-Ploetze, F., Rist, W., Rüdiger, S., Schneider-Mergener, J., Mayer, M. and Bukau, B. (2008). Molecular basis for regulation of the heat shock transcription factor sigma32 by the DnaK and DnaJ chaperones. Mol Cell *32*, 347–358.

Rogalla, T., Ehrnsperger, M., Preville, X., Kotlyarov, A., Lutsch, G., Ducasse, C., Paul, C., Wieske, M., Arrigo, A., Buchner, J. and Gaestel, M. (1999). Regulation of Hsp27 oligomerization, chaperone function, and protective activity against oxidative stress/tumor necrosis factor alpha by phosphorylation. J Biol Chem *274*, 18947–18956.

Rosenzweig, R., Moradi, S., Zarrine-Afsar, A., Glover, J. and Kay, L. (2013). Unraveling the mechanism of protein disaggregation through a ClpB-DnaK interaction. Science *339*, 1080–1083.

Ross, C. A. and Poirier, M. A. (2004). Protein aggregation and neurodegenerative disease. Nature Med *10*, S10–S17.

Rousseau, F., Schymkowitz, J. and Serrano, L. (2006). Protein aggregation and amyloidosis: confusion of the kinds? Curr Opin Struct Biol *16*, 118–126.

Sambashivan, S., Liu, Y., Sawaya, M., Gingery, M. and Eisenberg, D. (2005). Amyloid-like fibrils of ribonuclease A with three-dimensional domain-swapped and native-like structure. Nature *437*, 266–269.

Sawaya, M., Sambashivan, S., Nelson, R., Ivanova, M., Sievers, S., Apostol, M., Thompson, M., Balbirnie, M., Wiltzius, J., McFarlane, H., Madsen, A. and Riekel, C. Eisenberg, D. (2007). Atomic structures of amyloid cross-beta spines reveal varied steric zippers. Nature *447*, 453–457.

Selkoe, D. (2003). Folding proteins in fatal ways. Nature *426*, 900–904.

Serio, T. R., Cashikar, A. G., Kowal, A. S., Sawicki, G. J., Moslehi, J. J., Serpell, L., Arnsdorf, M. F. and Lindquist, S. L. (2000). Nucleated conformational conversion and the replication of conformational information by a prion determinant. Science *289*, 1317–1321.

Seyffer, F., Kummer, E., Oguchi, Y., Winkler, J., Kumar, M., Zahn, R., Sourjik, V., Bukau, B. and Mogk, A. (2012). Hsp70 proteins bind Hsp100 regulatory M domains to activate AAA+ disaggregase at aggregate surfaces. Nat Struct Mol Biol *19*, 1347–1355.

Shammas, S., Waudby, C., Wang, S., Buell, A., Knowles, T., Ecroyd, H., Welland, M., Carver, J., Dobson, C. and Meehan, S. (2011). Binding of the molecular chaperone alphaB-crystallin to A-beta amyloid fibrils inhibits fibril elongation. Biophys J *101*, 1681–1689.

Sharma, S., De los Rios, P., Christen, P., Lustig, A. and Goloubinoff, P. (2010). The kinetic parameters and energy cost of the Hsp70 chaperone as a polypeptide unfoldase. Nat Chem Biol *6*, 914–920.

Shashidharamurthy, R., Koteiche, H., Dong, J. and McHaourab, H. (2005). Mechanism of chaperone function in small heat shock proteins: dissociation of the HSP27 oligomer is required for recognition and binding of destabilized T4 lysozyme. J Biol Chem *280*, 5281–5289.

Shemetov, A., Seit-Nebi, A., Bukach, O. and Gusev, N. (2008). Phosphorylation by cyclic AMP-dependent protein kinase inhibits chaperone-like activity of human HSP22 *in vitro*. Biochemistry *73*, 200–208.

Shorter, J. (2011). The mammalian disaggregase machinery: Hsp110 synergizes with Hsp70 and Hsp40 to catalyze protein disaggregation and reactivation in a cell-free system. PLoS One *6*, e26319.

Sipe, J. D. and Cohen, A. S. (2000). Review: History of the amyloid fibril. J Struct Biol *130*, 88–98.

Skowyra, D., Georgopoulos, C. and Zylicz, M. (1990). The *E. coli* dnaK gene product, the hsp70 homolog, can reactivate heat-inactivated RNA polymerase in an ATP hydrolysis-dependent manner. Cell *62*, 939–944.

Smeller, L., Rubens, P. and Heremans, K. (1999). Pressure effect on the temperature-induced unfolding and tendency to aggregate of myoglobin. Biochemistry *38*, 3816–3820.

Smith, D. P., Radford, S. E. and Ashcroft, A. E. (2010). Elongated oligomers in beta2-microglobulin amyloid assembly revealed by ion mobility spectrometry-mass spectrometry. Proc Natl Acad Sci U S A *107*, 6794–6798.

Sobott, F., Benesch, J., Vierling, E. and Robinson, C. (2002). Subunit exchange of multimeric protein complexes. Real-time monitoring of subunit exchange between small heat shock proteins by using electrospray mass spectrometry. J Biol Chem *277*, 38921–38929.

Southan, C., Lavery, P. and Fantom, K. (1999). Disposable microbore high-pressure liquid chromatography columns for protein and peptide separations. Anal Biochem *271*, 152–158.

Specht, S., Miller, S., Mogk, A. and Bukau, B. (2011). Hsp42 is required for sequestration of protein aggregates into deposition sites in *Saccharomyces cerevisiae*. J Cell Biol *195*, 617–629.

Stamler, R., Kappe, G., Boelens, W. and Slingsby, C. (2005). Wrapping the alpha-crystallin domain fold in a chaperone assembly. J Mol Biol *353*, 68–79.

Stengel, F., Baldwin, A., Bush, M., Hilton, G., Lioe, H., Basha, E., Jaya, N., Vierling, E. and Benesch, J. . (2012). Dissecting heterogeneous molecular chaperone complexes using a mass spectrum deconvolution approach. Chem Biol *19*, 599–607.

Stengel, F., Baldwin, A., Painter, A., Jaya, N., Basha, E., Kay, L., Vierling, E., Robinson, C. and Benesch, J. (2010). Quaternary dynamics and plasticity underlie small heat shock protein chaperone function. Proc Natl Acad Sci U S A *107*, 2007–2012.

Stromer, T., Ehrnsperger, M., Gaestel, M. and Buchner, J. (2003). Analysis of the interaction of small heat shock proteins with unfolding proteins. J Biol Chem *278*, 18015–18021.

Stromer, T., Fischer, E., Richter, K., Haslbeck, M. and Buchner, J. (2004). Analysis of the regulation of the molecular chaperone Hsp26 by temperature-induced dissociation: the N-terminal domail is important for oligomer assembly and the binding of unfolding proteins. J Biol Chem *279*, 11222–11228.

Sun, T. and Liang, J. (1998). Intermolecular exchange and stabilization of recombinant human alphaA- and alphaB-crystallin. J Biol Chem *273*, 286–290.

Sunde, M., Serpell, L., Bartlam, M., Fraser, P., Pepys, M. and Blake, C. (1997). Common core structure of amyloid fibrils by synchrotron X-ray diffraction. J Mol Biol *273*, 729–739.

Susek, R. and Lindquist, S. (1989). Hsp26 of *Saccharomyces cerevisiae* is related to the superfamily of small heat shock proteins but is without a demonstrable function. Mol Cell Biol *9*, 5265–5271.

Tanaka, M., Collins, S., Toyama, B. and Weissman, J. (2006). The physical basis of how prion conformations determine strain phenotypes. Nature *442*, 585–589.

Tapley, T., Körner, J., Barge, M., Hupfeld, J., Schauerte, J., Gafni, A., Jakob, U. and Bardwell, J. (2009). Structural plasticity of an acid-activated chaperone allows promiscuous substrate binding. Proc Natl Acad Sci U S A *106*, 5557–5562.

Tartaglia, G., Pawar, A., Campioni, S., Dobson, C., Chiti, F. and Vendruscolo, M. (2008). Prediction of aggregation-prone regions in structured proteins. J Mol Biol *380*, 425–436.

Tartaglia, G., Pechmann, S., Dobson, C. and Vendruscolo, M. (2007). Life on the edge: a link between gene expression levels and aggregation rates of human proteins. Trends Biochem Sci *32*, 204–206.

Tessarz, P., Mogk, A. and Bukau, B. (2008). Substrate threading through the central pore of the Hsp104 chaperone as a common mechanism for protein disaggregation and prion propagation. Mol Microbiol *68*, 87–97.

Tessier, D., Komalavilas, P., Panitch, A., Joshi, L. and Brophy, C. (2003). The small heat shock protein (HSP) 20 is dynamically associated with the actin cross-linking protein actinin. J Surg Res *111*, 152–157.

Tompa, P. and Csermely, P. (2004). The role of structural disorder in the function of RNA and protein chaperones. FASEB J *18*, 1169–1175.

Toombs, J., McCarty, B. and Ross, E. (2010). Compositional determinants of prion formation in yeast. Mol Cell Biol *30*, 319–332.

Towbin, H., Staehelin, T. and Gordon, J. (1979). Electrophoretic transfer of proteins from polyacrylamide gels to nitrocellulose sheets: procedure and some applications. Proc Natl Acad Sci U S A *76*, 4350–4354.

Tuite, M. F., Bentley, N. J., Bossier, P. and Fitch, I. T. (1990). The structure and function of small heat shock proteins: analysis of the *Saccharomyces cerevisiae* Hsp26 protein. Antonie Van Leeuwenhoek *58*, 147–154.

Tyedmers, J., Mogk, A. and Bukau, B. (2010). Cellular strategies for controlling protein aggregation. Nat Rev Mol Cell Biol *11*, 777–788.

Uversky, V. (2011). Intrinsically disordered proteins from A to Z. Int J Biochem Cell Biol *43*, 1090–1103.

van derWel, P., Lewandowski, J. and Griffin, R. (2007). Solid-state NMR study of amyloid nanocrystals and fibrils formed by the peptide GNNQQNY from yeast prion protein Sup35p. J Am Chem Soc *129*, 5117–5130.

van Montfort, R., Slingsby, C. and Vierling, E. (2001a). Structure and function of the small heat shock protein/alpha-crystallin family of molecular chaperones. Adv Protein Chem *59*, 105–156.

van Montfort, R. L., Basha, E., Friedrich, K. L., Slingsby, C. and Vierling, E. (2001b). Crystal structure and assembly of a eukaryotic small heat shock protein. Nat Struct Biol *8*, 1025–1030.

van Noort, J., Bsibsi, M., Gerritsen, W., van der Valk, P., Bajramovic, J., Steinman, L. and Amor, S. (2010). Alpha b-crystallin is a target for adaptive immune responses and a trigger of innate responses in preactive multiple sclerosis lesions. J Neuropathol Exp Neurol *69*, 694–703.

Varela, J., van Beekvelt, C., Planta, R. and Mager, W. (1992). Osmostress-induced changes in yeast gene expression. Mol Microbiol *6*, 2183–2190.

Veinger, L., Diamant, S., Buchner, J. and Goloubinoff, P. (1998). The small heat-shock protein IbpB from *Escherichia coli* stabilizes stress-denatured proteins for subsequent refolding by a multichaperone network. J Biol Chem *273*, 11032–11037.

Vendruscolo, M., K. T. P. J. . D. C. M. (2011). Protein solubility and protein homeostasis: A generic view of protein misfolding disorders. Cold Spring Harb. Perspect. Biol. *3*, a010454.

Ventura, S. (2005). Sequence determinants of protein aggregation: tools to increase protein solubility. Microb Cell Fact *4*, 11.

Ventura, S. and Villaverde, A. (2006). Protein quality in bacterial inclusion bodies. Trends Biotechnol *24*, 179–185.

Vos, M., Hageman, J., Carra, S. and Kampinga, H. (2008). Structural and functional diversities between members of the human HSPB, HSPH, HSPA, and DNAJ chaperone families. Biochemistry *47*, 7001–7011.

Vos, M., Zijlstra, M., Kanon, B., van Waarde-Verhagen, M., Brunt, E., Oosterveld-Hut, H., Carra, S., Sibon, O. and Kampinga, H. (2010). HSPB7 is the most potent polyQ aggregation suppressor within the HSPB family of molecular chaperones. Hum Mol Genet *19*, 4677–4693.

Wada, C., Imai, M. and Yura, T. (1987). Host control of plasmid replication: Requirement for the sigma factor sigma32 in transcription of mini-F replication initiator gene. Proc Natl Acad Sci U S A *84*, 8849–8853.

Wadhwa, R., Ryu, J., Gao, R., Choi, I., Morrow, G., Kaur, K., Kim, I., Kaul, S., Yun, C. and Tanguay, R. (2010). Proproliferative functions of *Drosophila* small mitochondrial heat shock protein 22 in human cells. J Biol Chem *285*, 3833–3839.

Walker, L., Diamond, M., Duff, K. and Hyman, B. (2013). Mechanisms of protein seeding in neurodegenerative diseases. JAMA Neurol *70*, 304–310.

Walsh, D., Klyubin, I., Fadeeva, J., Cullen, W., Anwyl, R., Wolfe, M., Rowan, M. and Selkoe, D. (2002). Naturally secreted oligomers of amyloid beta protein potently inhibit hippocampal longterm potentiation *in vivo*. Nature *416*, 535–539.

Walter, S. and Buchner, J. (2002). Molecular chaperones-cellular machines for protein folding. Angew Chem Int Ed Engl *41*, 1098–1113.

Walzthoeni, T., Claassen, M., Leitner, A., Herzog, F., Bohn, S., Förster, F., Beck, M. and Aebersold, R. (2012). False discovery rate estimation for crosslinked peptides identified by mass spectrometry. Nature Methods *9*, 901–903.

Wang, L., Maji, S., Sawaya, M., Eisenberg, D. and Riek, R. (2008). Bacterial inclusion bodies contain amyloid-like structure. PLoS Biol *6*, e195.

Wang, L., S. D. S. M. R. E. D. and Riek, R. (2010). Multidimensional structure-activity relationship of a protein in its aggregated states. Angew Chem Int Ed Engl *49*, 3904–3908.

Wasmer, C., Lange, A., Van Melckebeke, H., Siemer, A., Riek, R. and Meier, B. (2008). Amyloid fibrils of the HET-s(218-289) prion form a beta solenoid with a triangular hydrophobic core. Science *319*, 1523–1526.

Waudby, C., Knowles, T., Devlin, G., Skepper, J., Ecroyd, H., Carver, J., Welland, M., Christodoulou, J., Dobson, C. and Meehan, S. (2010). The interaction of alphaB-crystallin with mature alpha-synuclein amyloid fibrils inhibits their elongation. Biophys J *98*, 843–851.

Weber, S. and Brangwynne, C. (2012). Getting RNA and protein in phase. Cell *149*, 1188–1191.

Weibezahn, J., Tessarz, P., Schlieker, C., Zahn, R., Maglica, Z., Lee, S., Zentgraf, H., Weber-Ban, E., Dougan, D., Tsai, F., Mogk, A. and Bukau, B. (2004). Thermotolerance requires refolding of aggregated proteins by substrate translocation through the central pore of ClpB. Cell *119*, 653–665.

White, H., Orlova, E., Chen, S., Wang, L., Ignatiou, A., Gowen, B., Stromer, T., Franzmann, T., Haslbeck, M., Buchner, J. and Saibil, H. (2006). Multiple distinct assemblies reveal conformational flexibility in the small heat shock protein Hsp26. Structure *14*, 1197–1204.

Wintrode, P., Friedrich, K., Vierling, E., Smith, B. and Smith, D. (2003). Solution structure and dynamics of a heat shock protein assembly probed by hydrogen exchange and mass spectrometry. Biochemistry *42*, 10667–10673.

Wotton, D., Freeman, K. and Shore, D. (1996). Multimerization of Hsp42p, a novel heat shock protein of *Saccharomyces cerevisiae*, is dependent on a conserved carboxyl-terminal sequence. J Biol Chem *271*, 2717–2723.

Zhang, Z. and Smith, D. (1993). Determination of amide hydrogen exchange by mass spectrometry: a new tool for protein structure determination. Protein Sci *2*, 522–531.

Zietkiewicz, S., Krzewska, J. and Liberek, K. (2004). Successive and synergistic action of the Hsp70 and Hsp100 chaperones in protein disaggregation. J Biol Chem *279*, 44376–44383.

Zzaman, S. and Bastia, D. (2005). Oligomeric initiator protein-mediated DNA looping negatively regulates plasmid replication in vitro by preventing origin melting. Mol Cell *20*, 833–843.

Appendix

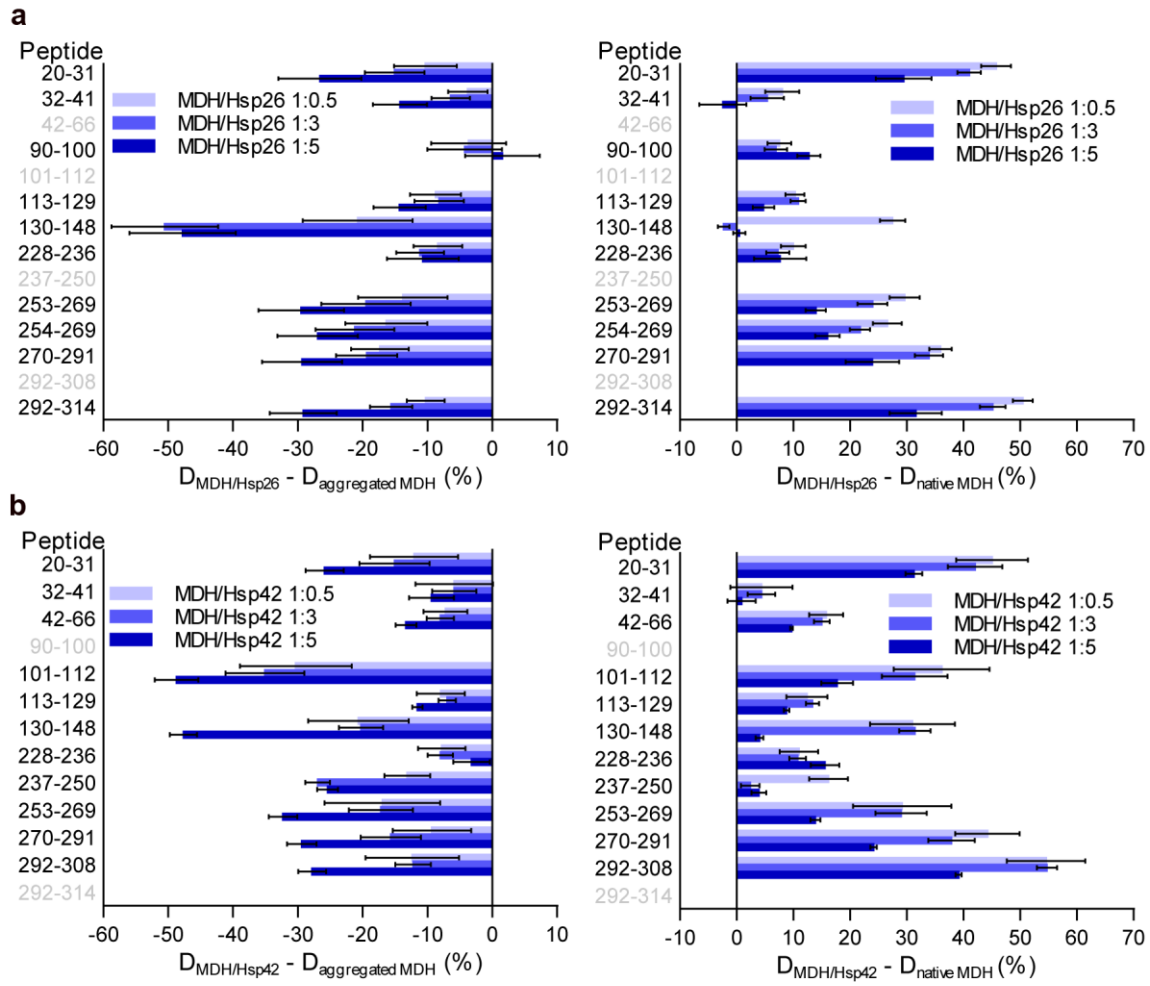

Figure 53: *Hsp26 and Hsp42 globally reduce HX in sHsp-complexed MDH.* ***(a)*** *Difference in deuteron incorporation between heat-induced MDH/Hsp26 complexes and aggregated (left panel) or native (right panel) MDH.* ***(b)*** *Difference in deuteron incorporation between heat-induced MDH/Hsp42 complexes and aggregated (left panel) or native (right panel) MDH. The number of deuterons relative to the total number of exchangeable deuterons in the respective peptide is shown. Peptides in gray could not be detected.*

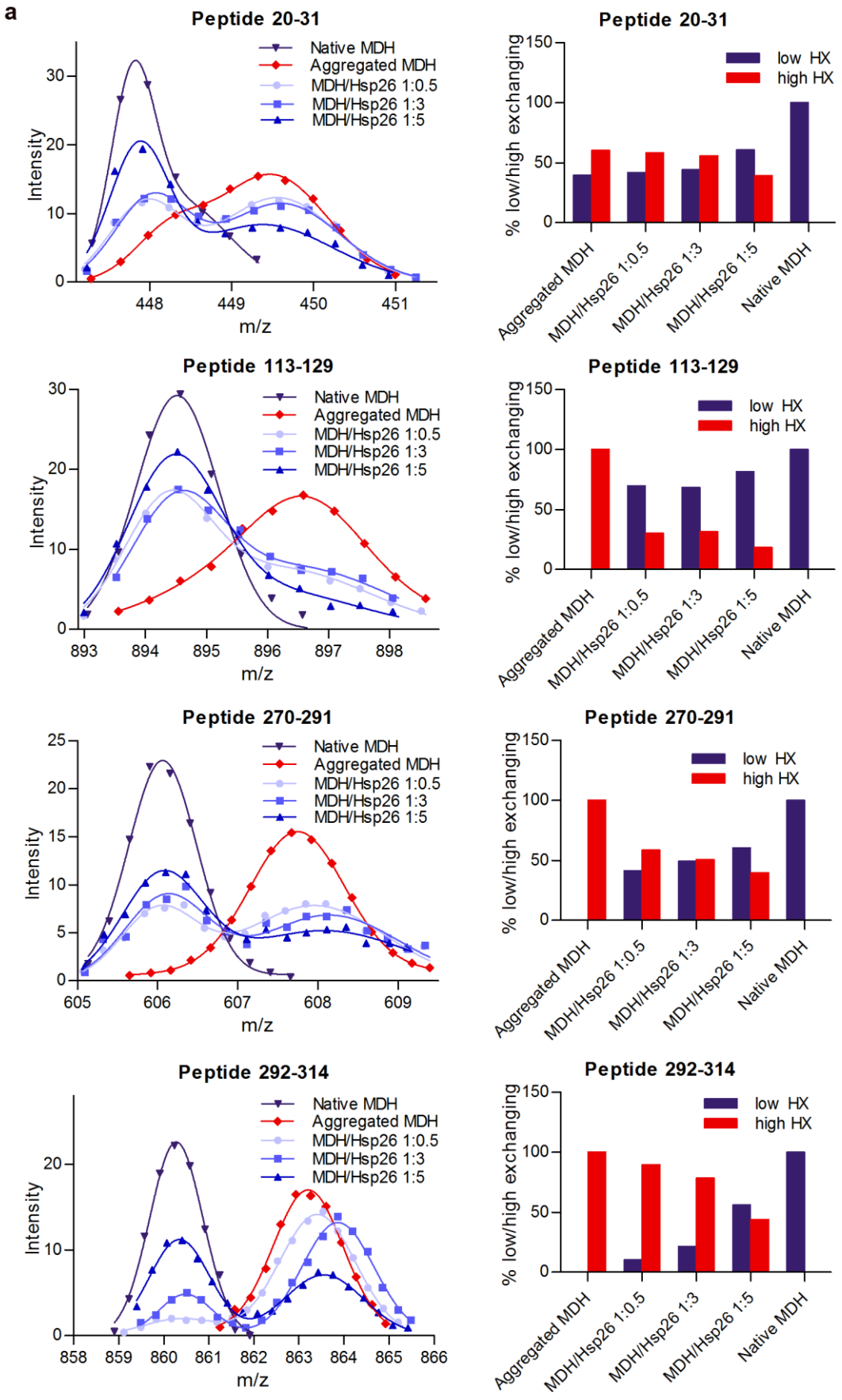
a
Peptide 20-31
Native MDH
Aggregated MDH
MDH/Hsp26 1:0.5
MDH/Hsp26 1:3
MDH/Hsp26 1:5
Intensity
m/z
Peptide 20-31
low HX
high HX
% low/high exchanging
Aggregated MDH
MDH/Hsp26 1:0.5
MDH/Hsp26 1:3
MDH/Hsp26 1:5
Native MDH
Peptide 113-129
Peptide 270-291
Peptide 292-314

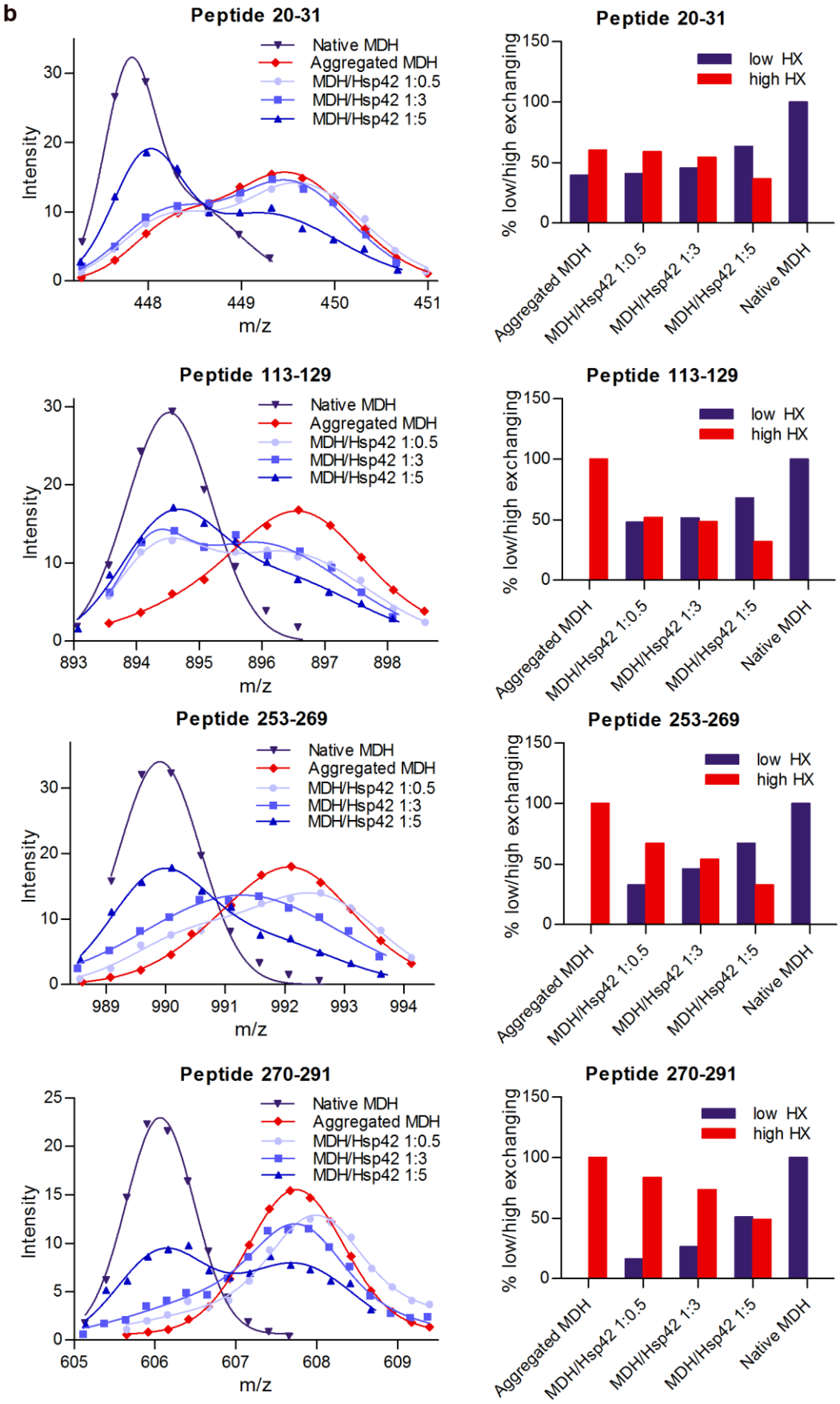
b
Peptide 20-31
Native MDH
Aggregated MDH
MDH/Hsp42 1:0.5
MDH/Hsp42 1:3
MDH/Hsp42 1:5
Intensity
m/z
Peptide 20-31
low HX
high HX
% low/high exchanging
Aggregated MDH
MDH/Hsp42 1:0.5
MDH/Hsp42 1:3
MDH/Hsp42 1:5
Native MDH
Peptide 113-129
Peptide 253-269
Peptide 270-291

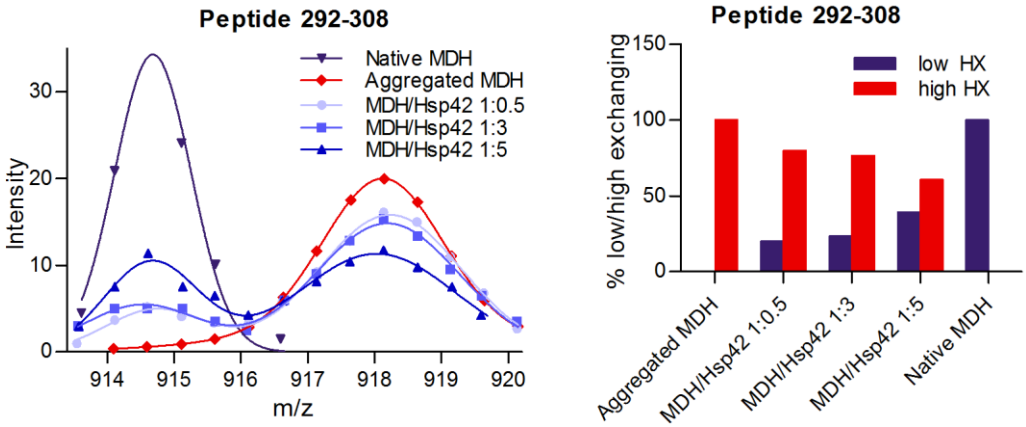

Figure 54: *sHsps stabilize segments of bound MDH in a native-like state. Bimodal distribution of isotope peaks of indicated MDH peptides derived from MDH/Hsp26* ***(a)*** *and MDH/Hsp42* ***(b)*** *complexes. Left panels: Intensity versus m/z diagrams for different peptic MDH fragments after 30 s HX at 30°C. Right panels: Fractions of native-like and aggregate-like populations calculated for respective peptides.*

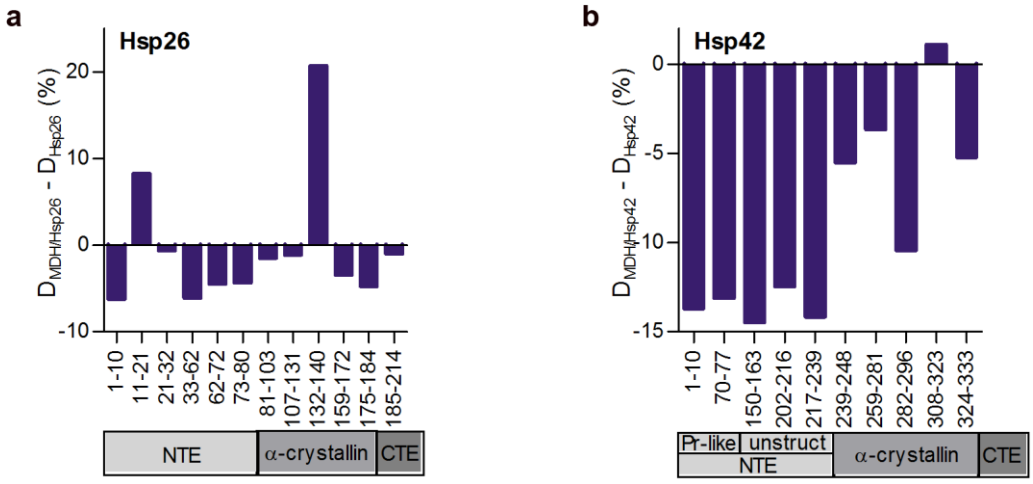

Figure 55: *Deuteron incorporation into sHsps after 30 s incubation in D_2O at 30°C. Difference in deuteron incorporation between MDH-complexed and free Hsp26* ***(a)*** *or Hsp42* ***(b)****. The data were corrected for deuteron losses due to back-exchange using a 100% deuterated control (i.e. protein in which all exchangeable protons have been replaced by deuterons). NTE: N-terminal extension, CTE: C-terminal extension, Pr-like: Prion-like domain, unstr: unstructured domain. The number of deuterons relative to the total number of exchangeable deuterons in the respective peptide is shown.*

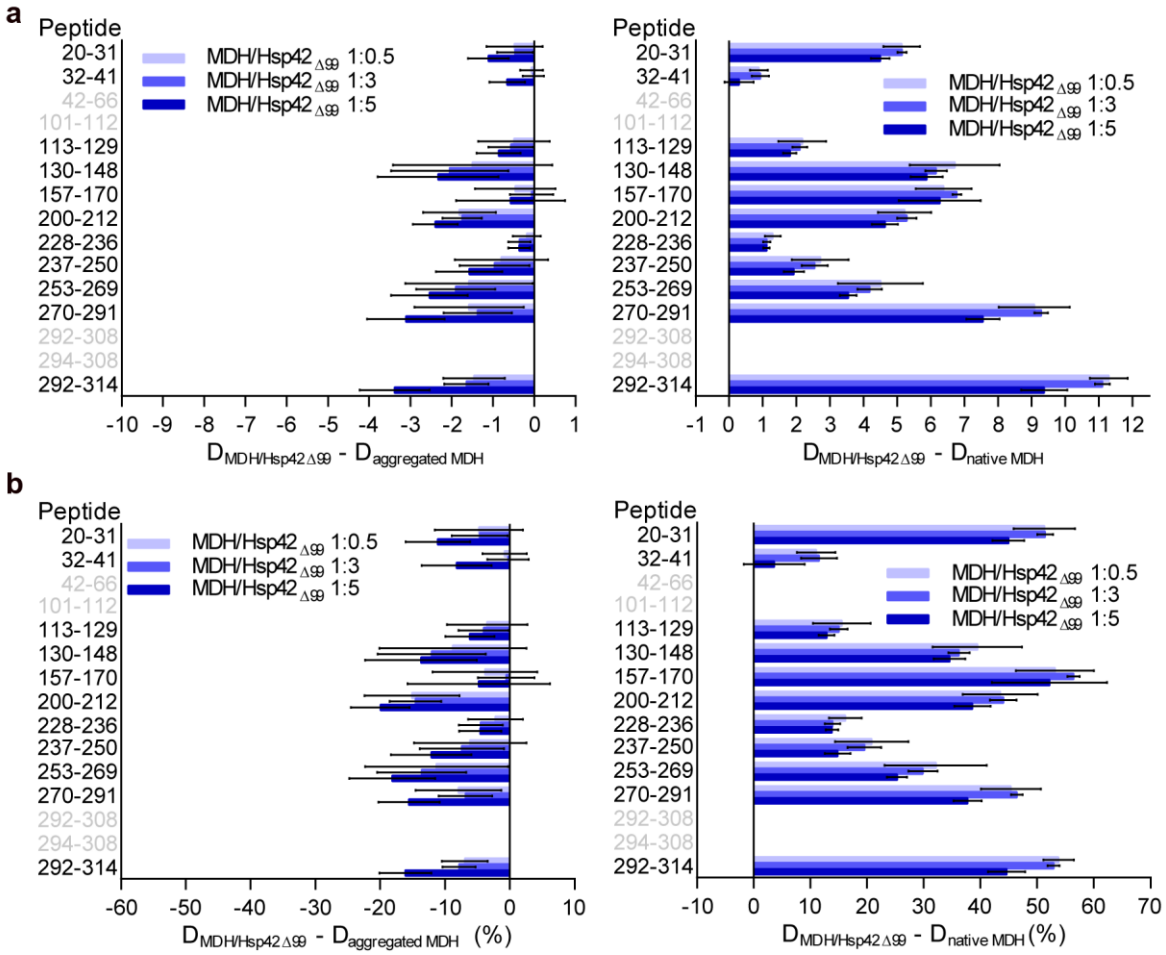

Figure 56: *Hsp42Δ1-99 hardly protects heat-induced MDH aggregates from HX. Difference in deuteron incorporation between heat-induced MDH/Hsp42Δ1-99 complexes and aggregated (left panel) or native (right panel) MDH in* ***(a)*** *absolute deuterons and* ***(b)*** *deuterons relative to the total number of exchangeable deuterons in the respective peptide. Peptides in gray could not be detected.*

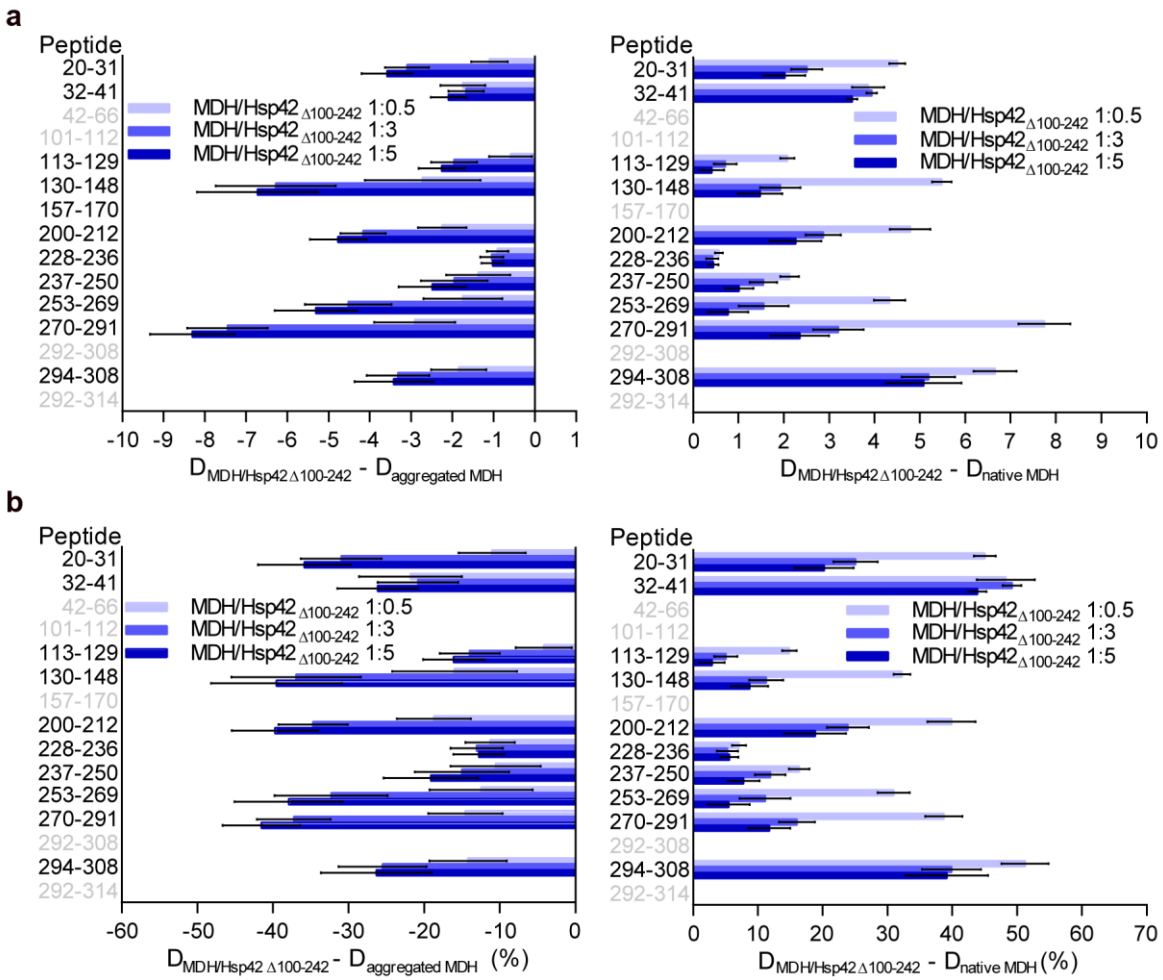

Figure 57: *Hsp42Δ100-242 efficiently reduces HX in sHsp-complexed MDH. Difference in deuteron incorporation between heat-induced MDH/Hsp42Δ100-242 complexes and aggregated (left panel) or native (right panel) MDH in* ***(a)*** *absolute deuterons and* ***(b)*** *deuterons relative to the total number of exchangeable deuterons in the respective peptide. Peptides in gray could not be detected.*

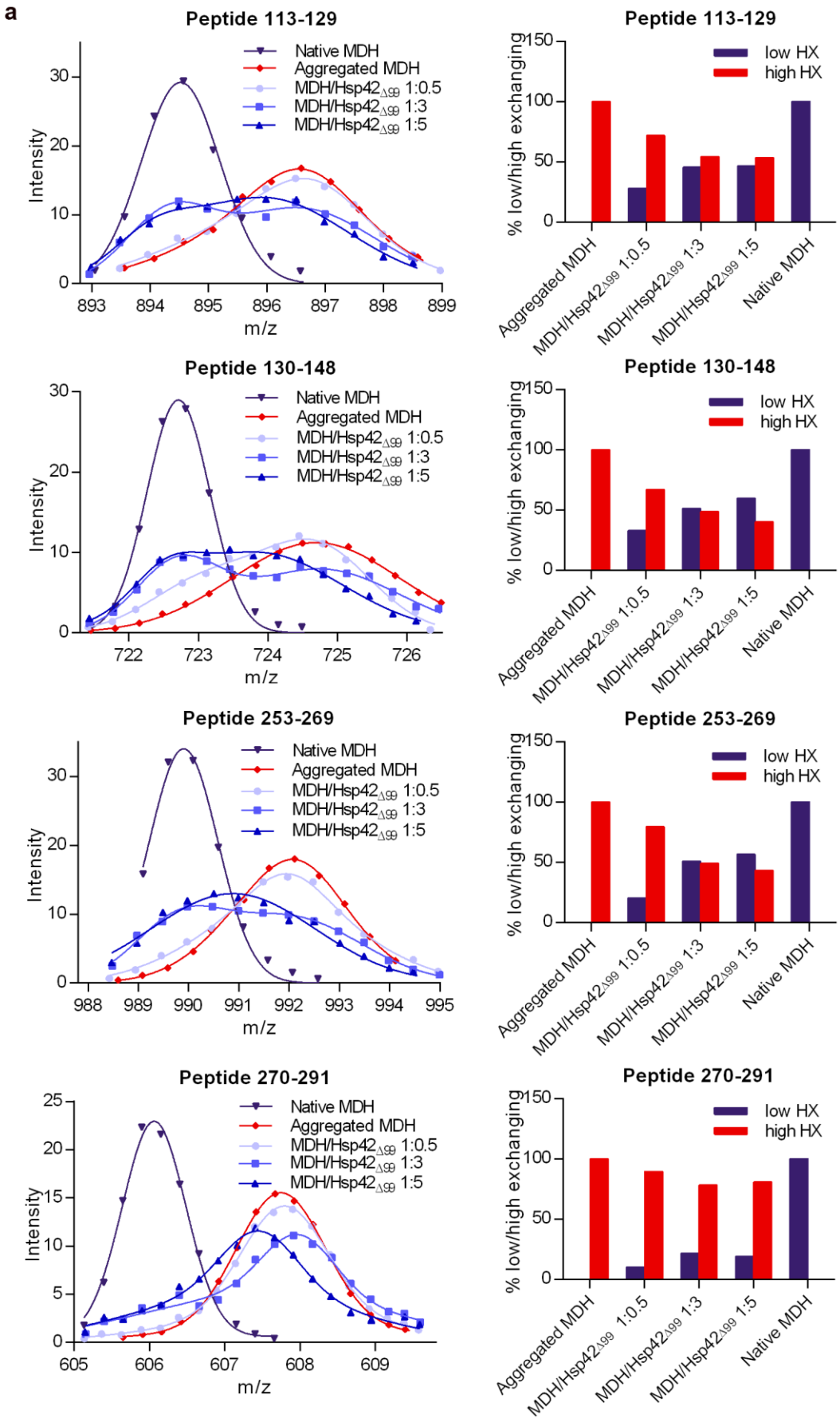
a
Peptide 113-129
Native MDH
Aggregated MDH
MDH/Hsp42Δ99 1:0.5
MDH/Hsp42Δ99 1:3
MDH/Hsp42Δ99 1:5
Intensity
m/z
% low/high exchanging
low HX
high HX
Aggregated MDH
MDH/Hsp42Δ99 1:0.5
MDH/Hsp42Δ99 1:3
MDH/Hsp42Δ99 1:5
Native MDH
Peptide 130-148
Peptide 253-269
Peptide 270-291

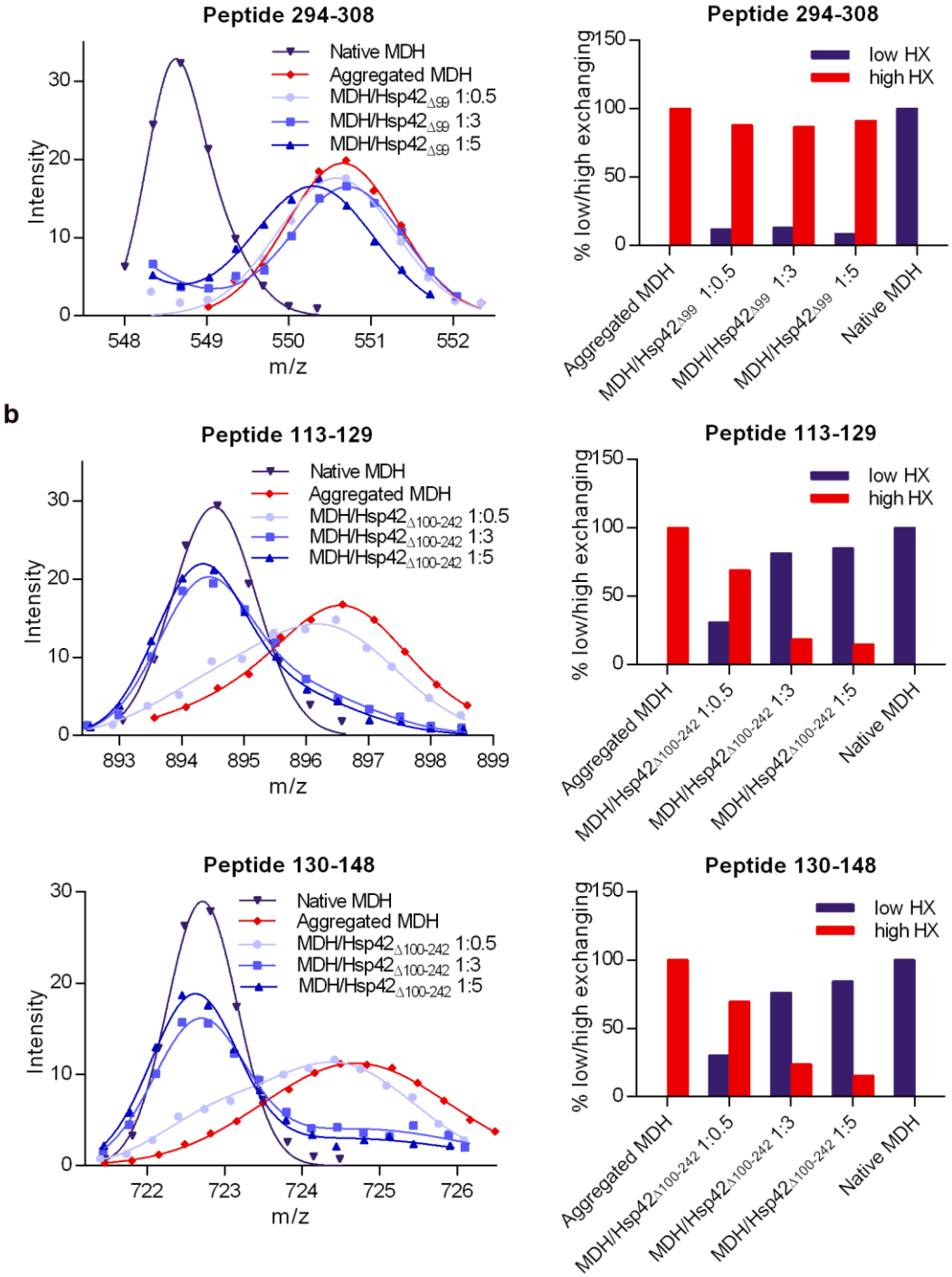
Peptide 294-308
Native MDH
Aggregated MDH
MDH/Hsp42Δ99 1:0.5
MDH/Hsp42Δ99 1:3
MDH/Hsp42Δ99 1:5
Intensity
m/z
Peptide 294-308
low HX
high HX
% low/high exchanging
Aggregated MDH
MDH/Hsp42Δ99 1:0.5
MDH/Hsp42Δ99 1:3
MDH/Hsp42Δ99 1:5
Native MDH
b
Peptide 113-129
Native MDH
Aggregated MDH
MDH/Hsp42Δ100-242 1:0.5
MDH/Hsp42Δ100-242 1:3
MDH/Hsp42Δ100-242 1:5
Intensity
m/z
Peptide 113-129
low HX
high HX
% low/high exchanging
Aggregated MDH
MDH/Hsp42Δ100-242 1:0.5
MDH/Hsp42Δ100-242 1:3
MDH/Hsp42Δ100-242 1:5
Native MDH
Peptide 130-148
Native MDH
Aggregated MDH
MDH/Hsp42Δ100-242 1:0.5
MDH/Hsp42Δ100-242 1:3
MDH/Hsp42Δ100-242 1:5
Intensity
m/z
Peptide 130-148
low HX
high HX
% low/high exchanging
Aggregated MDH
MDH/Hsp42Δ100-242 1:0.5
MDH/Hsp42Δ100-242 1:3
MDH/Hsp42Δ100-242 1:5
Native MDH

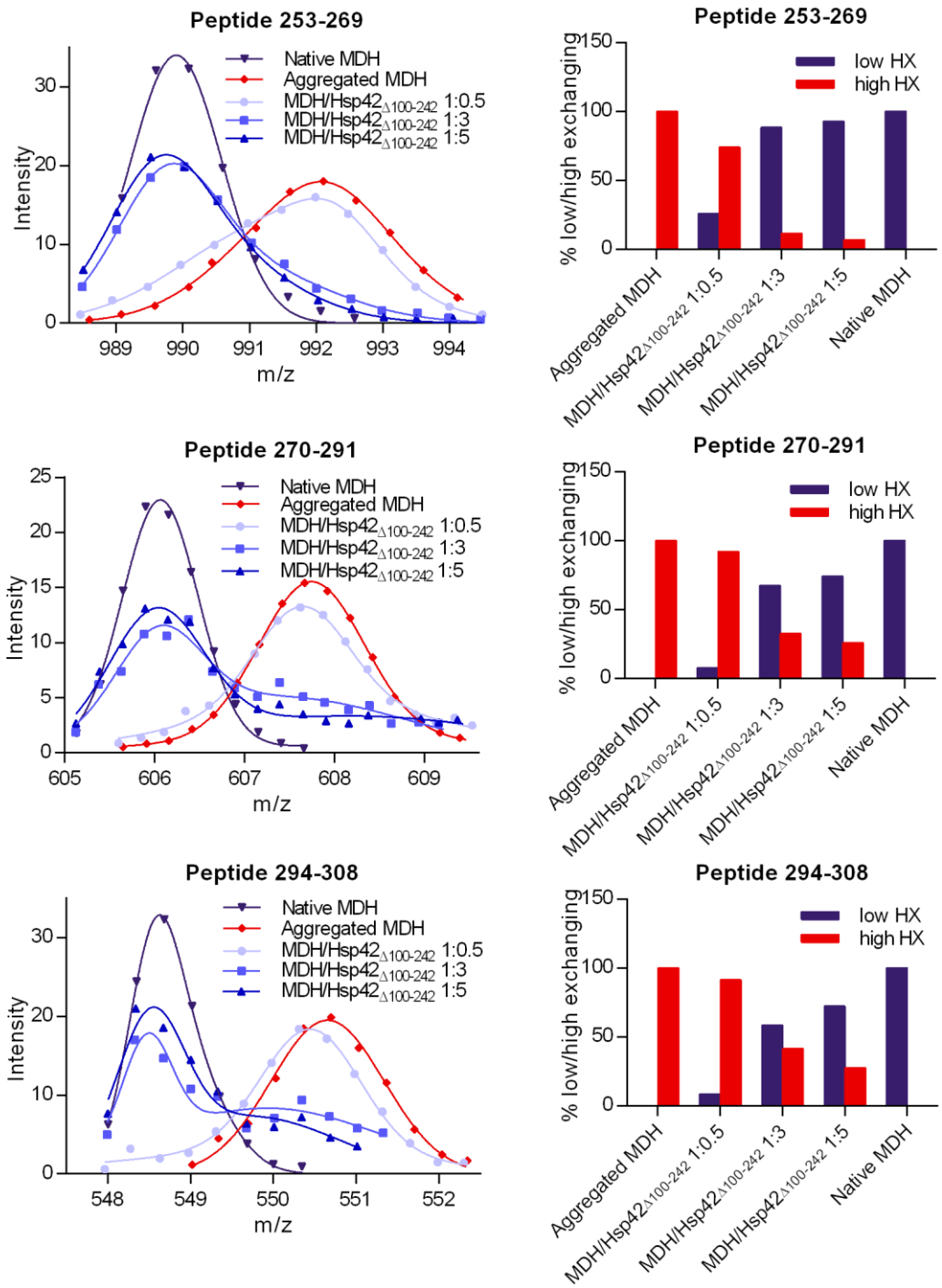

Figure 58: *Hsp42Δ100-242 stabilizes segments of bound MDH in a native-like state. Bimodal distribution of isotope peaks of indicated MDH peptides derived from MDH/Hsp42Δ1-99* ***(a)*** *and MDH/Hsp42Δ100-242* ***(b)*** *complexes. Left panels: Intensity versus m/z diagrams for different peptic MDH fragments after 30 s HX at 30°C. Right panels: Fractions of native-like and aggregate-like populations calculated for respective peptides.*

Table 6: *Crosslink products between MDH and Hsp26 after DSS crosslinking of MDH/Hsp26 complexes were identified by mass spectrometry.*

MDH-Hsp26-x-link	MDH/Hsp26 1/0.5	MDH/Hsp26 1/3	MDH/Hsp26 1/5	Id-score MDH/Hsp26 1/0.5	Id-score MDH/Hsp26 1/3	Id-score MDH/Hsp26 1/5	Hsp26 domain
K55-K45		x	x		28.59	32.12	NTE
K82-K45	x	x	x	28.02	32.17	31.32	NTE
K134-K45	x	x	x	32.06	23.79	33.44	NTE
K180-K45			x			20.16	NTE
K216-K45		x	x		20.64	29.48	NTE
K218-K45		x	x		34.29	32.56	NTE
K278-K45	x	x	x	36.74	29.41	33.86	NTE
K284-K45		x	x		39.93	29.43	NTE
K291-K45	x			30.24			NTE
K301-K45		x			20.97		NTE
K306-K45		x	x		35.01	36.7	NTE
K312-K45	x	x	x	20.76	24.53	29.11	NTE
K134-K50		x	x		40.61	32.07	NTE
K306-K117			x			39.57	NTE
K134-K151			x			30.19	ACD
K216-K151			x			22.62	ACD
K284-K151		x			27.84		ACD
K306-K151		x			23.4		ACD
K312-K151			x			20.91	ACD
K134-K195			x			27.13	CTE
K142-K195	x			23.72			CTE
K216-K195	x			20.77			CTE
K284-K195	x			32.42			CTE
K306-K195	x	x	x	35.24	33.72	25.92	CTE
K278-K198			x			33.62	CTE
K306-K198	x	x	x	35.37	38.26	47.47	CTE
K312-K198			x			24.5	CTE

List of Figures

List of Tables

List of Abbreviations

aa:	Amino acid
ACD:	α-crystallin domain
ACN:	Acetonitrile
ANS:	1-Anilino-8-napthalene-sulfonate
ATP:	Adenosine triphosphate
bp:	Base pair
BPIA:	Benzophenone-4-iodoacetamide
BSA:	Bovine serum albumin
CD spectroscopy:	Circular dichroism spectroscopy
CTE:	C-terminal extension
CV:	Column volumn
CytoQ:	Cytosolic quality control compartment
DMSO:	Demethyl sulfoxide
DNA:	Deoxyribonucleic acid
dNTP:	deoxynucleoside triphosphate
DR:	Direct repeat
DTT:	Dithiothreitol
E. coli:	*Escherichia coli*
EDTA:	Ethylenediaminetetraacetic acid
EM:	Electron microscopy
FRET:	Fluorescence resonance energy transfer
FTIR:	Fourier transform infrared spectroscopy
GdmCl:	Guanidinium chloride
h:	Hour
HPLC:	High performance liquid chromatography
Hsp:	Heat shock protein
HX:	Amide hydrogen exchange
INQ:	Intranuclear protein quality control compartment
IR:	Inverted repeat
IR spectroscopy:	Infrared spectroscopy
kDa:	Kilodalton
LB:	Luria Bertani
MD:	Middle domain
min:	Minute

MS:	Mass spectrometry
MWCO:	Molecular weight cut off
$NiCl_2$:	Nickel chloride
nm:	Nanometer
NTE:	N-terminal extension
OD:	Optical density
PAGE:	Polyacrylamide gel electrophoresis
PBS:	Phosphate buffered saline
PEG:	Polyethylene glycol
PMSF:	Phenylmethylsulphonyl fluoride
rpm:	Revolutions per minute
RT:	Room temperature
s:	second
S. cerevisiae:	*Saccharomyces cerevisiae*
SDS:	Sodium dodecylsulfate
sHsp:	Small heat shock protein
TBS:	Tris buffered saline
TFA:	Trifluoroacetic acid
Tris:	Tris(hydroxymethyl)aminomethane
U:	Unit
UV:	Ultraviolet
V:	Volt
VHL:	Van-Hippel-Lindau tumor suppressor protein
v/v:	Volume per volume
w/v:	Weight per volume
YFP:	Yellow fluorescent protein

Danksagung/Acknowledgement

Mein erster Dank geht an meinen Betreuer Bernd Bukau, der mir die Möglichkeit gegeben hat, meine Promotion in seiner renommierten und wissenschaftlich breit aufgestellten Arbeitsgruppe durchzuführen. Die ausgezeichnete Bereitstellung von Arbeitsmitteln und die erstklassige technische Ausstattung haben mir sehr gute Rahmenbedingungen für die erfolgreiche Durchführung meiner Promotion geboten. Bernd, ich danke Dir für die Unterstützung, den wissenschaftlichen Input sowie Deine Ermutigung und Motivation während der gesamten Promotion.

Ebenso möchte ich mich bei meinem Co-Betreuer Matthias Mayer bedanken. Insbesondere bei H/D-Experimenten, aber auch bei vielen anderen Experimenten oder Problemen habe ich von Deiner wissenschaftlichen Erfahrung und Deinem breiten Fachwissen profitieren können und Du hast mich hilfsbereit unterstützt.

Besonders bedanken möchte ich mich bei Axel Mogk, für die Anleitung bei der experimentellen Arbeit sowie für Verbesserungsvorschläge bei schriftlichen Arbeiten. Dein schnelles, zuverlässiges und konstruktives Feedback hat das Vorankommen meiner Projekte erleichtert.

Thomas Ruppert von der Massenspektrometrie Facility danke ich für die Hilfe bei der Lösung von häufig auftretenden, nervenaufreibenden und vielfältigen technischen Problemen am Massenspektrometer.

Ein großer Dank geht an Annette Scharf von der Massenspektrometrie Facility für die Etablierung der Durchführung von Isotopen-Crosslinking Experimenten am ZMBH für meine Doktorarbeit. Ihr und Nicole Lübbehusen danke ich auch für die Auswertung der Crosslinking-Experimente und die angenehme Zusammenarbeit.

Während der gesamten Doktorarbeit, besonders zu Beginn der Promotion als wir uns ein Labor teilten, hat mir Stephanie Miller bei Fragen oder der Durchführung von Experimenten wertvolle Tipps gegeben und mir immer engagiert weiter geholfen. Dafür möchte ich mich herzlich bedanken.

Ich danke der ganzen Bukau-Gruppe und der Mayer-Gruppe für eine entspannte Arbeitsatmosphäre und allgemeine Hilfsbereitschaft. Kristina Döring möchte ich besonders danken - für ihre offene und fröhliche Art und dafür, dass sie mir zahlreiche kleine Gefallen getan hat, die mir einige Wochenend-Fahrten nach Heidelberg erspart haben.

Bei Regina Zahn, Silke Druffel-Augustin und Beate Zachmann-Brand bedanke ich mich dafür, dass sie sich darum gekümmert haben, dass alle notwendigen Chemikalien und andere Arbeitsmittel stets zur Verfügung standen. Silke danke ich zudem für viele nette Gespräche und für eine sehr angenehme Zeit als Labornachbarinnen.

Ich bedanke mich bei den Damen aus der Spülküche. Dass das Spülen, Autoklavieren und LB-Platten gießen übernommen wird, schätze ich sehr und es hat viel Zeit gespart, die für Experimente oder anderweitig genutzt werden konnte.

Ein herzlicher Dank geht an Jutta Rami und Ina Baro, die sich immer engagiert und zuverlässig um alle Formalitäten gekümmert haben. Das konsequent nachgefüllte „Naschglas“ in ihrem Büro sicherte zudem die Versorgung mit Süßigkeiten – eine wichtige Einrichtung, wenn der Tag nicht enden wollte, der Hunger größer wurde und Unishop und Bäckerei schon geschlossen hatten.

Ich bedanke mich bei meinen Geschwistern Jan und Jochen Mende. Jan danke ich insbesondere für die Beratung und schnelle Hilfe bei computertechnischen Fragen und Problemen.

Meinen Eltern, Febronia und Rüdiger Mende, möchte ich von Herzen dafür danken, dass sie in jeder Situation hinter mir stehen und für die Gewissheit, dass sie weiterhin immer für mich da sein werden.

Meinem lieben Mann Jan danke ich für seine liebevolle Art und sein Verständnis während der letzten Jahre. Ich danke Dir für viele gemeinsame schöne und lustige Erlebnisse, Abende und Tage. Diese wertvollen Stunden mit Dir haben mir Kraft gegeben, auch schwierige Phasen gut zu überstehen und mit Zuversicht weiterzumachen.